Genetic studies in ulcerative colitis.

A thesis submitted for the degree of
Masters of Science by Research

University of Oxford
Hilary Term 2015

Robert Venning Bryant

Linacre College
Nuffield Department of Clinical Medicine

ABSTRACT

Genetic studies in ulcerative colitis.

Robert Venning Bryant, Linacre College and Nuffield Department of Clinical Medicine

Submitted for the degree of MScR in Clinical Medicine, Hilary Term 2015

Inflammatory bowel diseases (IBD), encompassing ulcerative colitis (UC) and Crohn's disease (CD), are lifelong inflammatory disorders of complex and multifactorial aetiology. Genetic studies have played an important role in the identification of immunological pathways involved in the pathogenesis of IBD. Genome wide association studies have revealed more than 160 genetic polymorphisms associated with IBD, although the expected heritability in UC is smaller than for CD, and the relationship between genotype and phenotype in UC is unclear. The source of the missing heritability in UC, may be at least accounted for by rare variants which carry a larger effect size. In this thesis, the influence of polygenic burden on disease phenotype in UC is investigated. In addition, functional characterisation of a rare genetic variant is performed, in order to investigate for a pathogenic association with a very early onset colitis phenotype.

Polygenic risk burden, as measured using genetic risk scores (GRS), is assessed amongst a well-phenotyped cohort of patients with UC. GRS are shown to be greater amongst patients diagnosed with UC before the age of 10 years, as compared to those diagnosed in adulthood. GRS are also shown to be greater amongst patients with a history of acute severe UC (ASUC), as compared to those with a mild UC disease course. Although lacking in power, variance analysis suggests enrichment of genetic polymorphisms within the IL-10 cytokine signalling pathway amongst patients with a history of ASUC.

Exploration of a possible causal relationship between a novel and rare mutation in the *NOX1* gene, encoding NADPH oxidase 1, and a clinical phenotype of very early onset colitis in a single patient is undertaken in this thesis. It is shown that NOX1 mRNA is highly expressed in colonic epithelial cells and that the *NOX1* p.N122H variant impairs function of the gene product. The findings implicate that the *NOX1* p.N122H variant contributes to development of severe and early onset colitis by attenuating colonic epithelial superoxide production.

ACKNOWLEDGEMENTS

I would like to thank my supervisor Holm Uhlig, for his support, endless time and enthusiasm, and tolerant teaching, which has allowed me to pursue an MScR degree. I am extremely grateful to Holm for providing me with the opportunity to explore a novel genetic mutation, as it is his discovery that has formed the basis of my research.

I would like to thank Simon Travis, for his steadfast mentoring, leadership, and guidance, not only throughout my degree, but during my entire time in Oxford. I am eternally grateful.

I would like to thank Fiona Powrie for showing faith in me and for so generously facilitating the opportunity for me to undertake this degree.

I would like to thank the talented laboratory colleagues with whom I have been lucky to work. To the NOX1 team, Jon Jung, Sumeet Pandey, and Tobias Schwerd; I am so grateful for your enduring patience, supervision, and teaching. You have each dedicated countless hours in support of a fumbling clinician's entry into the laboratory, and it is only through the work of our team, and upon the foundation that you built, that the project was able to progress. To the genetics team, Maria Quaranta and Davis McCarthy, I am so thankful for your collaborative efforts in generating the risk scores and integrating the genetics data. The genetics project was able to move forward with the benefit of your hard work and insight. To my collaborators at the National Institute of Medical Research, Laween Meran and Vivian Li, thank you for your help in culturing the organoids, which were a key component of our work. To James Chivenga and Priya Siddhanathi, thank you for all your help and energy in collecting specimens and facilitating the smooth-running of our ventures.

I would like to thank Lilly and the Nuffield Department of Medicine for their generous support, without which I would not have had the means to pursue this degree.

Lastly, I would like to thank my beautiful wife Maddie. Without her patient love and support, this degree would not have been possible. Thank you for bearing with me, pacifying my frustrations, and for tolerating a single-minded husband with eyes only for his computer. I love you dearly.

ABBREVIATIONS

$^{\bullet}OH$	Hydroxyl radical
$^{1}O_2$	Singlet oxygen
1^{O}FHx	First degree family history
5ASA	5-aminosalicylic acid
AIEC	Adherent invasive *Escherichia coli*
ANXA1	Annexin A1
APC	Antigen presenting cell
ASUC	Acute severe ulcerative colitis
AUC	Area under the curve
CD	Crohn's disease
cDNA	Complimentary DNA
CFU	Colony forming unit
CGD	Chronic granulomatous disease
CNV	Copy number variant
CRISPR-Cas9	Clustered regularly interspaced short palindromic repeats
CRP	C reactive protein
CYBB, $gp91^{phox}$	NADPH Oxidase 2
DNA	Deoxyribonucleic acid
DPI	Diphenyleneiodonium
DUOX	Dual oxidase
DUOXA1	Dual oxidase activator
DUOXA2	Dual oxidase organiser
DUSP3	Dual specificity protein phosphatase 3
EBV	Epstein Barr virus
EcN	*Escherichia coli* Nissle 1917
EDTA	Ethylenediaminetetracetic acid
EOIBD	Early onset inflammatory bowel disease
ER	Endoplasmic reticulum
ERK	Extracellular signal-related kinase
FAD	Flavin adenine dinucleotide
FAK	Focal adhesion kinases
FCS	Foetal calf serum
fMLP	Formyl-Methionyl-Leucyl-Phenylalanine
FPR	Formyl peptide receptor
GDP	Guanosine diphosphate
GRS	Genetic risk scores
GTP	Guanosine triphosphate
GWAS	Genome wide association studies
H&E	Haematoxylin and eosin stain
H_2O_2	Hydrogen peroxide
HLA	Human leucocyte antigen
HLH	Haemophagocytic lymphohistiocytosis

HOCl	Hypochlorous acid
HPL	Haemophagocytic lymphohistiocytosis
HT-29	HT-29 colon cancer cell-line
IBD	Inflammatory bowel disease
IBDu	Inflammatory bowel disease yet to be classified
ICHIP	Immunochip
IFN-γ	Interferon gamma
IL	Interleukin
IM	Immunomodulator
IPAA	Ileal pouch-anal anastomosis
IQR	Interquartile range
JAK	Janus kinase
LB	Luria Bertani broth
LC3	1A/1B-light chain 3
LPS	Lipopolysaccharide
MAPK	Mitogen activated protein kinases
MDP	Muramyl dipeptide
MHC	Major histocompatibility complex
MOI	Multiplicity of infection
MPO	Myeloperoxidase
MRS	De Man, Regosa, Sharpe broth
NADPH	Nicotinamide adenine dinucleotide phosphate
NBT	Nitroblue tetrazolium
NF-κB	Nuclear factor kappa beta
NK	Natural killer cells
NLR	NOD-like receptor
NOS	Nitric oxygen synthase
NOX	Nicotinamide adenine dinucleotide phosphate oxidase
NOXA1	NADPH oxidase 1 activator
NOXO1	NADPH oxidase 1 organiser
ns	Not significant (p value ≥ 0.05)
NSAID	Non-steroidal anti-inflammatory
$O_2^{-\bullet}$	Superoxide
O^3	Ozone
OD	Optical density
$ONOO^-$	Peroxynitrite
OR	Odds ratio
PAMP	Pathogen associated molecular pathogen
PAS	Periodic acid and Schiff's stain
PBS	Phosphate buffered saline
PKC	Protein kinase C
PMA	Phorbol 12-myristate 13-acetate
PMN	Polymorphonuclear leucocyte
PSC	Primary sclerosing cholangitis

PTEN	Phosphatase and tensin homolog
PTP	Protein tyrosine phosphatase
qRT-PCR	Quantitative reverse transcriptase polymerase chain reaction
RAC1	Ras-related C3 botulinum toxin substrate 1
RAF	Risk allele frequency
RLU	Relative light unit
RNA	Ribonucleic acid
ROC	Receiver operating characteristic
ROS	Reactive oxygen species
siRNA	Short-interfering RNA
SLE	Systemic lupus erythematosus
SNP	Single nucleotide polymorphism
SOD	Superoxide dismutase
STAT	signal transducer and activator of transcription
TGF-β	Transforming growth factor beta
TLR	Toll-like receptor
TNF-α	Tumour necrosis factor alpha
Treg	Regulatory T cells
UC	Ulcerative colitis
UCEIS	Ulcerative colitis endoscopic index of severity
UPR	Unfolded protein response
VEOIBD	Very early onset inflammatory bowel disease
WGS	Whole genome sequencing

TABLE OF CONTENTS

LIST OF FIGURES AND TABLES

FIGURES

TABLES

CHAPTER 1: INTRODUCTION

1.1 Introduction

Inflammatory bowel diseases (IBD), encompassing ulcerative colitis (UC) and Crohn's disease (CD), are lifelong inflammatory diseases. The prevalence of IBD has risen sharply over the past three decades, and is estimated to affect as many as 827 per 100,000 persons in Europe (1-3). The aetiology of IBD is complex, multifactorial and incompletely understood, although is purported to involve susceptible host genetics, immune dysregulation, intestinal dysbiosis, and environmental factors (4-6).

Genetic studies have played a key role in identifying putative immunological pathways in the pathogenesis of IBD (5, 7, 8). Meta-analyses of genome wide association studies (GWAS) and immunochip (ICHIP) studies have identified 163 IBD-associated risk loci, many of which are shared between both CD and UC phenotypes (7). However, the IBD-associated GWAS risk loci account for only a relatively small proportion of total disease variance; 13.6% in CD and 7.5% in UC (7). The source of the 'missing heritability' in IBD, may be at least partially accounted for by rare and private genetic variants, the functional study of which has facilitated deeper insights into the interaction between host immune cells and the microbiota at the intestinal epithelial interface (7, 9-12).

The available evidence points to a greater genetic contribution for CD than UC, however the broader application of whole genome sequencing (WGS) and ICHIP has led to an increasing recognition of the importance of genetic risk in susceptibility for UC (13). There are hints that burden of genetic risk in UC may also influence the natural history and severity, though such evidence is scarce and contradictory (14, 15).

1.2 Ulcerative colitis

1.2.1 Incidence and prevalence of UC

The incidence and prevalence of UC is increasing worldwide; systematic review suggests an annual incidence of 24.3 per 100,000 person-years and a prevalence of 505 per 100,000 persons in Europe (1-3). The risk of UC is highest in Western society, although prevalence is rising amongst migrant populations and in developing countries (16-18).

1.2.2 Diagnosis, classification, and natural history of UC

UC is a form of IBD that is characterised by chronic, non-granulomatous inflammation that is limited to the colonic mucosa, involving the rectum and a variable proximal extent of the colon in continuity (19, 20). The clinical presentation of UC is dependent on the extent of disease, although is typically one of bloody diarrhoea with associated urgency, tenesmus, and lower abdominal pain (19).

The diagnosis of UC is established on the basis of the clinical presentation, along with typical endoscopic and histological features (19). Laboratory studies typically reveal features of inflammation such as an elevated C reactive protein (CRP), anaemia, and hypoalbuminaemia, although can be normal in the setting of limited UC (21). Endoscopic features of UC are those of macroscopic colonic inflammation, characterised by a loss of vascular pattern, ulceration, and mucosal bleeding (22, 23). The effect of treatment in UC can also lead to discontinuous inflammation (24). Histological features of UC are those of crypt architectural abnormalities and an acute and chronic inflammatory infiltrate with cryptitis and crypt abscess formation (19).

UC may be classified according to the age of onset, natural history of disease, distribution of disease, severity of disease (both clinical and endoscopic), and response to therapy (*Table 1.1*).

Age of onset. UC typically presents in late adolescence or early adulthood, although there is a small peak in incidence later in life (1). Around 25% of UC is diagnosed in the paediatric age group, and epidemiological data suggests a rising incidence of paediatric-onset disease (25, 26). The Paediatric Paris modification of the Montreal Criteria, as well as the criteria proposed by Uhlig *et al*, provide classification criteria for IBD diagnosed in the paediatric age-group (9, 27, 28).

Distribution. The distribution of disease in UC is defined according to the Montreal criteria (20). The extent of disease is relevant to prognostication in UC, given that extensive disease is associated with a higher risk of acute severe colitis (ASUC), colectomy, and colorectal cancer (29, 30). Furthermore, the extent of disease in UC is an important factor in consideration of the appropriate treatment and colonoscopic surveillance regimen (31, 32). However, disease extent in UC is not stable, as in up to half of patients, disease either extends or regresses over time (33, 34).

Severity. Clinical disease activity in UC may be classified as mild, moderate, or severe according to Truelove and Witts' criteria (35). Endoscopic scoring systems also allow classification of UC disease activity, which have been shown correlation with outcomes (22, 23, 36). The presence of deep ulcers at colonoscopy predicts a poor prognosis in UC (37). Remission of UC is defined as complete resolution of symptoms and endoscopic mucosal healing (19, 32).

Response to therapy. The mainstay of therapy for UC are 5-aminosalicylic acid (5-ASA) preparations, which may be administered orally or topically (31, 32).

Corticosteroids are commonly used for induction of remission in UC, however for maintenance of severe UC immunomodulatory and biologic therapy may be required. Patients with UC may be classified according to their response to therapy, as having steroid-refractory, steroid-dependent, or immunomodulator refractory colitis (19, 32).

Natural history. The disease course of UC typically follows a relapsing and remitting pattern, although a small proportion of patients have an unremitting course from the outset (38). The heterogeneity of natural history in UC is influenced by multiple factors, including the extent and severity of disease, timely introduction and compliance with appropriate treatment modalities, and achievement of endoscopic and histological mucosal healing (39, 40).

Studies suggest that around 25% of patients with UC suffer from ASUC during their disease course, of whom, 30% require a colectomy (41, 42). The long-term risk of colectomy overall amongst patients with UC is around 10% (43, 44).

Disease-related factor	Classification System	Criteria
Age of onset	Montreal criteria (20)	-A1 <17 years -A2 17-40 years -A3 >40 years
	Paris Criteria (27) Muise/Uhlig (10, 28)	-Early onset IBD (A1a) <10 years -Very early onset IBD <6 years
Disease distribution	Montreal criteria (20)	-E1 proctitis -E2 left-sided colitis -E3 extensive disease
Disease severity	Truelove and Witts' Criteria (35)	-Clinical criteria based on bloody stools, pulse rate, fever, haemoglobin level and inflammatory markers. -Mild, moderate, or severe.
	Ulcerative colitis endoscopic index of severity (UCEIS) (22, 23)	-Endoscopic criteria based on colonic mucosal vascular pattern, mucosal blood, and presence of erosions and ulceration.

Table 1.1. Classification of UC. *UC may be classified according to established criteria on the basis of the age of onset, disease distribution, and disease severity.*

1.3 Genetics of UC

1.3.1 Family history and twin studies

Support for the role of genetics in IBD was first derived from studies of family history and twins (45). The heritability of UC has been consistently reported as lower than that of CD (45-47). Compared to the general population, the risk of UC in a first-degree relative of a patient with UC is 10-fold (48). The consequent life-time risk of developing UC in a first-degree relative of a patient with UC is thus around 2% (19, 49). If both parents are affected, the risk of IBD in the progeny is estimated to be around one in three (45, 50).

Twin studies have revealed that concordance rates for UC are 16% between monozygotic twins and around 4% in dizygotic twins, which is lower than the twin concordance observed for CD (30% and 10%, respectively) (51-54).

1.3.2 GWAS and ICHIP studies in UC

WGS and ICHIP studies in patients with IBD has led to a rapid expansion in the identification of IBD-associated risk alleles through GWAS meta-analyses (7, 55-59) (*Table 1.2*). The largest and most recent GWAS meta-analysis, included 6,333 cases and 15,056 controls for CD, and 6,687 cases and 19,718 controls for UC (7). In addition, ICHIP genotyping data from 14,763 patients with CD, 10,920 patients with UC, and 15,977 non-IBD controls was included in the analysis. Samples were derived from an ethnically European population.

The GWAS meta-analysis and ICHIP data identified 193 statistically significant independent signals of genome wide significance ($p<5 \times 10^{-8}$) for IBD, 71 of which were new associations (7). Given that some of the signals were likely representative of the same functional subunit of a gene, these were merged into 163 regions. The study identified 110 shared risk loci for IBD (both disease types), amongst which there was significant disease-specific heterogeneity of effect size (odds ratio, OR) observed for 60 genes. Of the 53 outstanding loci, 30 were CD-specific risk loci, and 23 were UC-specific risk loci. Amongst these 53 loci, 10 loci were protective for one disease whilst posing risk for the other, with notable such examples being NOD2 and PTPN22 (7).

Author, year	UC patients/Controls	UC risk loci	IBD Risk Loci
Franke *et al*, 2008 (59)	1,167 UC patients (1,855 replication) 777 European controls (3,091 replication)	4 risk loci	
Silverberg *et al*, 2009 (58)	1,052 UC patients 2,571 European controls	14 risk loci	
McGovern *et al*, 2010 (56)	2,693 UC patients 6,791 European controls	30 risk loci (50% shared with CD)	
Anderson *et al*, 2011 (55)	6687 UC patients 19,718 European controls	47 risk loci (28 shared with CD)	99 IBD risk loci
Jostins *et al*, 2012 (7)	17,607 UC patients 35,695 European controls	133 risk loci (110 shared with CD)	163 IBD risk loci

Table 1.2. GWAS and ICHIP studies in UC. *The table depicts the expansion of UC and IBD risk loci identified by GWAS and ICHIP studies.*

The cellular expression of IBD-risk loci has been shown to be enriched in immune cells (7). There is substantial overlap between the IBD-risk loci and other autoimmune diseases; in particular Type 1 diabetes mellitus, ankylosing spondylitis, systemic lupus erythematosus (SLE) and psoriasis (7). Furthermore, IBD loci are enriched for genes involved in primary immunodeficiencies, as well susceptibility to mycobacterial infection (7). The key risk alleles identified in UC and their cellular expression are described in *Table 1.3, Figure 1.1*.

1.4 Key molecular pathways in UC

GWAS and ICHIP IBD-risk loci have shed light on the genetic architecture and immunological pathways implicated in the pathogenesis of UC (4, 46, 60) (*Table 1.3*). The key pathways involve the interaction between the immune system and the intestinal microflora, including epithelial barrier function, microbial handling, and regulation of innate and adaptive immunity (4). Although there are multiple shared immunological pathways between UC and CD, there is distinct degree of heterogeneity in common risk loci, suggesting unique biological differences between the diseases (7).

Category	Role	UC Risk loci
Epithelial barrier function	Epithelial permeability Epithelial tight junctions	***GNA12***, *HNF4A, CDH1, ERRF1, PTPN2*
	Epithelial restitution and regeneration	***HNF4A***, *STAT3, NKX2*
	Mucus layer	*MUC2, MUC19*
	Epithelial stress	***ORMDL3***, ***XBP1***
Innate immune response	Phagocytosis and bacterial handling Pro-inflammatory signalling	*SCL11A1*, ***FCGR2A/B***, ***CARD9***, *CARD11*, ***NFKB1,*** *NOD2**
	Antigen presentation	***HLA-DQB1***, ***HLA-DRB1***, *HLA-DQA1, HLA-DRA*
	Autophagy	*IRGM, LRRK2, SMURF1,* ***DAP***, *RIPK2*
	IL-23/Th17 pathway	***IL23R, STAT3, JAK2,*** ***TYK2***, *TNFSF15, IL12RB, RORC, CCR6*
Adaptive immunity	Immune cell recruitment and chemotaxis	*CCL13, CCL2*, ***ITGAL,*** ***IL8RA, IL8RB***
	Immune regulation and tolerance	***IL10***, *IL27, IL1R1,* ***IL1R2,*** ***IFNG,*** *CREM,* ***STAT3***, *JAK2,* ***TYK2***
	T cell regulation	***TNFRSF14,*** *IL12B, TNFSF8, IL2,*
	B cell regulation	***IRF5,*** *IL7R*

Table 1.3. UC risk loci and associated immune pathways*. The risk loci are those from Jostins et al (7). In bold are key genes in the identified pathways for UC. *NOD2 is a protective locus in UC. The pathway analysis was derived from (4, 46, 60).*

1.4.1 Epithelial barrier function.

Tight junctions between intestinal epithelial cells maintain the integrity of the intestinal epithelial cell layer (61). GWAS studies in IBD have identified susceptibility loci in *HNF4A, CDH1*, and *GNA12* genes, which play a key role in the transcription and assembly of proteins involved in the tight junction formation (4, 55, 62). In addition to forming a physical barrier, intestinal epithelial cells produce anti-bacterial substances, such as β-defensins (4, 62). Paneth cells, residing in the small intestinal epithelial crypts, produce α-defensins, and are an important protagonist in the pathogenesis of CD, but do not seem to play a role in UC (63).

The colonic mucus layer, produced by epithelial goblet cells, plays an important role in intestinal barrier function. The inner mucus layer, shown to be largely impervious to microbes in the non-inflamed setting, is penetrated by bacteria that are in direct contact with the epithelium in UC (64). GWAS have identified *MUC19* as a shared risk loci for both UC and CD (7, 57). Epithelial stress is a term commonly used to describe endoplasmic reticulum (ER) stress and the associated unfolded protein response (UPR), which are closely associated with barrier function and innate immunity in UC (4, 65). Mutations in the *XBP1* gene involved in the UPR, have been shown to confer risk for both UC and CD (65).

1.4.2 Innate immune response.

The physical barrier in the gut is enhanced by innate immune responses, which must balance protection against pathogenic insults whilst dampening response to commensal intestinal flora (4). Pattern recognition receptors such as toll-like receptors (TLRs), NOD-like receptors (NLRs), harboured by both immune cells (macrophages and dendritic cells) as well as non-immune cells (epithelial cells), function to recognise pathogen associated molecular patterns (PAMPs) (66). Upon recognition of PAMPs, nuclear factor (NF-κB) is activated, the gene for which has been identified as a key UC-specific locus (*NFKB1),* generating a pro-inflammatory cascade to defend against the invading pathogen (7).

NOD2 was the first genetic variant to be discovered in IBD (67, 68), and remains the strongest genetic determinant of susceptibility to CD (7). However, *NOD2* polymorphisms have been shown to yield a protective effect in UC (7). NOD2 proteins directly bind to muramyl dipeptide (MDP), derived from peptidoglycans of the bacterial cell wall, and play a role in orchestrating the ensuing innate and adaptive immune

response, including promoting autophagy, Paneth cell activation, and T cell differentiation (69). The heterogeneity of effect for *NOD2* between UC and CD is likely to reflect differences in the pathogenesis of the IBD phenotypes. Yet, it is of note that in UC, genetic variants similarly associated with pathogen control and host immunity, such as *CARD9*, confer susceptibility (7, 46).

Autophagy, the process of lysosomal degradation of cytoplasmic contents in response to metabolic or infectious triggers, is an important pathway in the pathogenesis of IBD (70). Although *ATG16L1*, the key genetic protagonist in autophagy is specific for CD and does not confer risk for UC, other autophagy loci are implicated in UC susceptibility (*Table 1.3*) (7).

The IL-23/Th17 pathway is an important pro-inflammatory pathway in UC, and plays a role in orchestrating the interaction between the innate and adaptive immune systems (62, 66, 71). Single nucleotide polymorphisms (SNPs) in the IL-23 receptor (*IL23R*) gene have been shown to be important risk loci in both UC and CD (7). Further risk loci in the IL-23/Th17 pathway, include signal transducer and activator of transcription 3 (*STAT3*) and Janus kinase 2 (*JAK2*) (7).

1.4.3 Adaptive immune response.

The adaptive immune response in UC polarises CD4+ T cells toward Th2 differentiation, in contrast to Th1 as in CD (4). Th2 polarisation in UC is driven by IL-4 cytokine production by antigen presenting cells (APCs), which leads to generation of IL-4, IL-5, IL-9 and IL-13 (*Figure 2.1*) (72). In addition to the classical Th2 response in UC, there is also a role for Th17 cells, which are a population of RORγt-expressing inflammatory T cells that expand in response to the pro-inflammatory cytokine IL-23 (62).

IBD-risk loci also implicate processes of T cell trafficking and chemotaxis to inflamed intestinal mucosa in UC, including chemokine receptor loci (*CCL2, CCL7, CCL8*), *IL8RA/B,* and *ITGAL* (7, 46). T cell regulation is also important, and UC-risk loci point to a role for members of the tumour necrosis factor superfamily (*TNFSR8/9/14*) (7, 73).

The human leucocyte antigen (HLA) complex expressed by innate immune cells in the gut, functions to process and present antigens to T lymphocytes, thereby activating the adaptive immune system. Risk loci located within the *HLA* complex on chromosome 6p21, have long been recognised to impart susceptibility risk for UC (more than CD), as well as associated primary sclerosing cholangitis (PSC) (74-77). There are multiple independent associations in the HLA complex in UC, of both class I and II, including *HLA-DQB1, HLA-DRB1, HLA-DQA1,* and *HLA-DRA*, however defining causal alleles in HLA complex has been difficult due to linkage disequilibrium (13). Recent high-density mapping of the HLA complex in patients with IBD, has revealed that HLA class II alleles are three-fold more important than class I alleles in UC, in particular alleles in *HLA-DRB1*01:03* (13).

Regulatory T cells (Treg), and their cytokine mediators IL-10 and transforming growth factor β (TGF- β), are crucial for a balanced tolerant immune response as well as immune tolerance. GWAS have identified multiple members of the IL-10 signalling pathway as risk loci for both UC and CD, including the IL-10 receptor (*IL10*R), *IL10, STAT3*, *TYK2*, and *JAK2* (4, 7). Both rare and common variants involve the IL-10 signalling pathway; loss of function mutations in *IL10, IL10RA,* and *IL10RB* have also been shown to lead to severe early onset IBD (78-81).

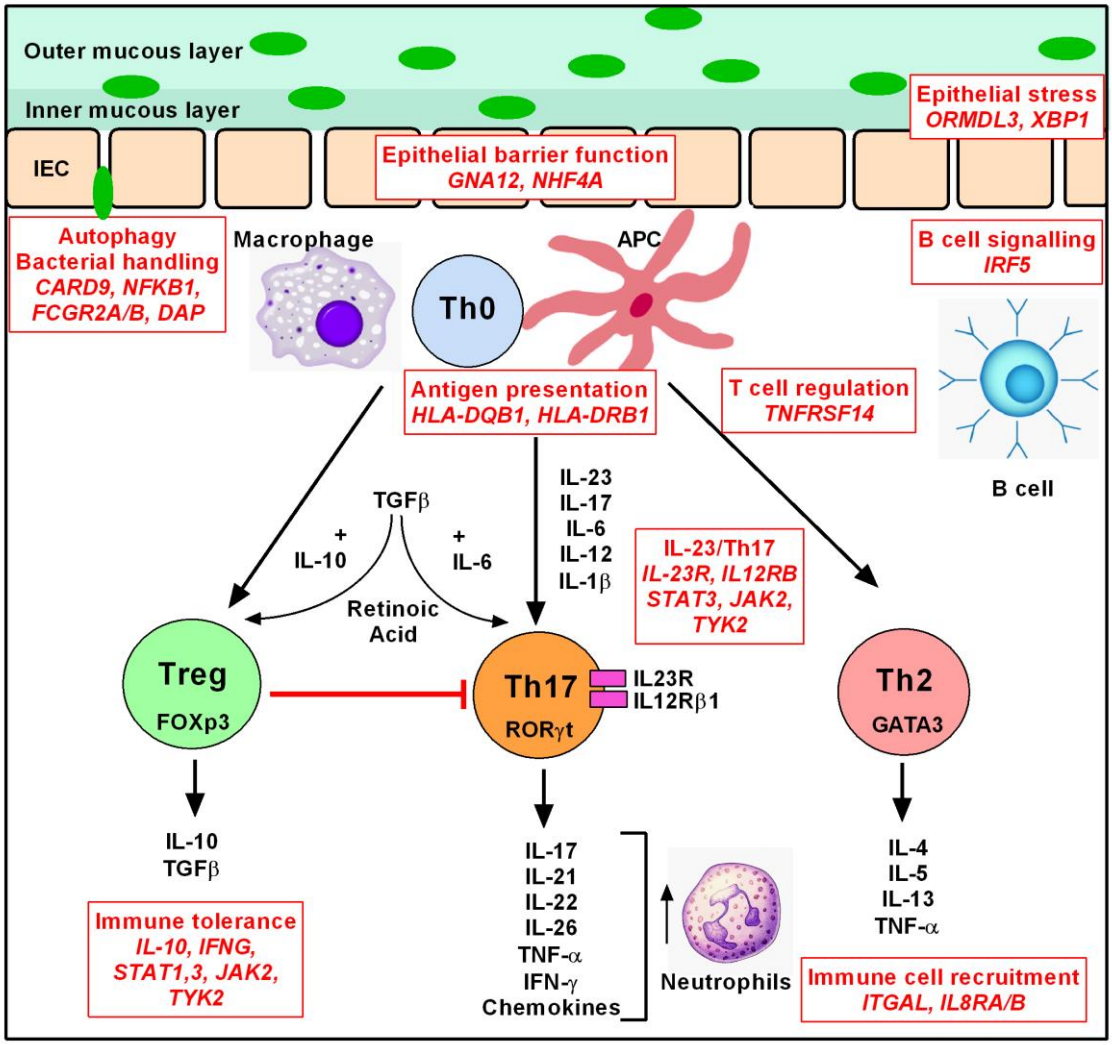

Figure 1.1. Immunological pathways and associated genetic loci in UC. *The diagram depicts the putative immunological pathways involved in the UC pathogenesis described in Table 1.3. Adapted from (60, 71).*

1.5 Missing heritability in UC

The vast majority of the GWAS and ICHIP IBD-risk loci are associated with a very small effect size, and account for a small proportion of heritability in UC (7). Current GWAS and ICHIP studies are mostly powered to characterise variants of >1% frequency, however detection of rare variants (<1%) is limited (8). The explanation for 'missing heritability' in UC, is hypothesised to relate to rare and private genetic variants, structural variants, the influence of gene-gene interactions, environmental

factors, and gene-environment interactions, each of which are not accounted for by conventional GWAS (7, 9-12, 46) (*Table 1.4*).

1.5.1 Rare and private genetic variants.

The identification and functional characterisation of rare and private variants associated with intestinal inflammation is an expanding research niche (9, 10). 'Sequencing of the extremes' of IBD phenotype, in particular patients with very early onset IBD (VEOIBD), has led to the discovery of multiple novel genes, as there is enrichment for monogenic diseases amongst such groups (10, 28, 82). The discovery of monogenic disorders associated with intestinal inflammation has facilitated deeper insights into the pathogenesis of IBD, including disorders relating to neutrophil phagocytic defects (*NCF2* variants) (83, 84), epithelial barrier dysfunction (ADAM17 deficiency) (85), immune regulation and IL-10 signalling (78, 79, 86), hyper-inflammatory disorders (XIAP deficiency) (87), and T and B-cell defects (combined variable immunodeficiency) (9, 10).

1.5.2 Structural variants.

Structural variants, including rare copy number variants (CNVs), have been implicated in the causality of rare diseases, such as spinal muscular atrophy and neonatal onset diabetes mellitus (88). However, direct association analysis of the CNVs in more common diseases (including IBD), did not discover CNV associations beyond those already recognised by SNP variants, implying that CNVs are a less likely cause of missing heritability in IBD (89, 90).

1.5.3 Gene-gene interactions.

Many of the GWAS and ICHIP identified IBD-risk loci are non-coding variants (7). Non-coding variants can communicate with exonic variants via gene-gene interactions,

thereby regulating transcription through processes such as gene splicing, and regulation of transcription factors and microRNA binding sites (4, 8, 46, 91). Conserved non-coding DNA sequences have been shown to regulate Foxp3 induction and influence Treg differentiation (92). A noncoding polymorphism (rs12212067), has been shown to regulate FOX03A transcription in CD, limiting inflammatory responses in activated monocytes via a paracrine TGF-β1 mechanism, and thereby conferring a milder CD disease course (93).

1.5.4 Epigenetics and gene-environment interactions.

Epigenetics has been defined as 'mitotically heritable changes in gene function that are not accounted for by changes in the DNA sequence' (94). Epigenetic changes have emerged as a possible link between the environment and genetic architecture in IBD, via processes of DNA methylation, histone modification, and RNA interference (94). As such, GWAS risk loci include several epigenetic regulatory loci, including the region encoding DNA methyltransferase 3a (7).

Cigarette smoking is an illustrative example of a gene-environment interaction in UC (45). A strong overall inverse correlation has been demonstrated between smoking and UC (95), with the likelihood of a disease-flare increased in patients with UC who stop smoking (96). Genetic interaction with cigarette smoking in UC has been demonstrated using logistic regression techniques, showing that gene-gene and gene-environment interactions can improve determination of disease variance in UC (97). Genetic polymorphisms in metabolising enzymes (such as CYP2A6) have also been shown to influence the susceptibility to IBD in the context of smoking status (98).

1.5.5 Intestinal microbiota.

As implicated by genetic risk loci, intestinal mucosal interaction with the luminal microbiota is the major feature of the pathogenesis of IBD. Studies have consistently characterised the luminal microbiota in IBD to show a reduction in the diversity of microbial communities compared with healthy individuals (99). This 'dysbiosis', is thought to have a bidirectional relationship with host genetics in IBD, as genetic predisposition can induce 'dysbiosis', yet transfer of 'dysbiotic' microbiota into a non-susceptible host can also induce disease (5, 100). Environmental factors are also a major influence on the intestinal microbiota, and differences can be detected between those consuming a 'Western diet', high in animal and saturated fats, compared with those consuming a vegetable and fibre-rich diet (101).

1.5.6 Environmental factors.

Multiple putative environmental factors (the 'exposome') influence risk in UC, including medications (in particular antibiotics and non-steroidal anti-inflammatory drugs (NSAIDs)), diet (dietary fibre, fat, and vitamin D), enteric infection, and lifestyle factors (sleep deprivation and stress) (45).

Missing heritability	Key examples
Rare and private genetic variants	IL-10 cytokine signalling pathway, neutrophil phagocytic defects, hyper-inflammatory and auto-inflammatory pathways, epithelial barrier function defects.
Gene-gene interactions	Many GWAS IBD-risk loci are non-coding, and may play a role in regulating transcription through gene splicing, regulation of transcription factors and microRNA binding sites.
Epigenetics and gene-environment interactions	Cigarette smoking Luminal microbiota
Intestinal microbiota	Reduced diversity of luminal microbial communities ('dysbiosis'), consistently demonstrated in UC.
Environmental factors ('exposome')	Medications (antibiotics, NSAIDs) Diet (Western diet vs. high fibre diet) Enteric infections Lifestyle factors (stress and sleep deprivation) Vitamin D Appendicectomy

Table 1.4. 'Missing heritability' in UC. *The table summarises the potential sources of susceptibility for UC, which may not be accounted for by GWAS in IBD. The table is drawn from multiple sources, cited within the text. Key references include (4, 5, 10, 45, 46, 94).*

1.4 Genotype- phenotype correlation in UC

Beyond genetic risk loci as markers of susceptibility for UC, there is impetus for investigating associations between genotype and disease phenotype (102). Given the marked heterogeneity in the natural history of UC, genetic markers have been proposed as a possible means of predicting the likelihood of an aggressive or mild disease course (46, 102). This would allow identification of patients who would be more likely to benefit from early intensive therapy, thus moving toward personalised treatment of IBD.

1.5 Aims of this thesis

The objectives of this thesis were to investigate two distinct aspects of the genetics of UC:

1. To investigate the influence of polygenic burden on disease phenotype in UC. In particular, it was aimed to investigate whether genetic risk scores or candidate polymorphisms, derived from GWAS and ICHIP risk loci, may be able to predict disease severity in UC.
2. To investigate a rare mutation in the *NOX1* gene, encoding nicotinamide adenine dinucleotide phosphate (NADPH) oxidase 1 (NOX1), in a single patient with very early onset colitis, so as to explore the possibility of a causal link between the genotype and the clinical phenotype.

CHAPTER 2: QUANTIFYING GENETIC RISK IN ULCERATIVE COLITIS PHENOTYPES

2.1 INTRODUCTION

The propensity for genetic polymorphisms to predict disease phenotype is well demonstrated in CD. Mutations in *NOD2* have been associated with ileal CD location, fibrostenosing and complicated CD, and requirement for surgery (67, 68, 103-105). *ATG16L1* variants have also been associated with ileal disease location in CD (106). A non-coding polymorphism in *FOX03A*, although not associated with susceptibility to CD, has been shown to be associated with a milder disease course (93). The integration of genetic factors into clinical algorithms in CD, has been shown to better predict clinical outcomes (107-109). Furthermore, in other chronic inflammatory conditions, such as rheumatoid arthritis, genetic burden has been shown to be useful in predicting disease phenotype (110, 111).

Yet, there are few studies, with contrasting findings, exploring genetic predictors of phenotype in UC (14, 15). The lesser enthusiasm for exploring genetic risk in UC, is likely related to the smaller fraction of heritability accounted for by known risk alleles (7).

2.1.1 Predicting the natural history of UC

Any prediction of the future risk for a complicated or severe disease course in UC is largely reliant upon clinical factors in current practice (112). Clinical factors that have been shown to increase the risk of severe outcomes of colectomy and hospitalisation in UC, include a younger age at diagnosis (113), extensive disease distribution (113, 114), and elevated biomarkers of inflammation (CRP and faecal calprotectin), both early in disease course and during a flare (114-118). Endoscopic features such as deep

ulceration or a high UCEIS, correlate with risk of colectomy in UC (22, 23, 37). Non-smoker or ex-smoker status confers a higher risk of ASUC and colectomy than does current smoker status in UC (95, 112, 119). In addition, the effect of treatment in UC, in particular, whether or not mucosal healing is achieved, needs to be taken into account (40, 120). A scoring system has been proposed for use at diagnosis of UC, incorporating haemoglobin, CRP, and disease extent, which has been validated in discriminating the likelihood of ASUC within 3 years (117).

There is currently no complex risk model incorporating clinical and genetic factors to predict outcomes in UC. In CD however, a risk model including disease phenotype, serological markers (anti-*Sachharomyces*), psychological factors, and polymorphisms in candidate genes (*IL23, NOD2, ATG16L1, IL12B*), has been variably shown to predict complicated disease and surgery in CD (108, 109, 121).

2.1.2 Genotype-phenotype correlations in UC

2.1.2.1 Candidate risk loci

There are several studies in UC which implicate particular genetic loci with risk of an extensive or severe phenotype (*Table 2.1*). HLA risk alleles, in particular *HLA-DRB1* (*DR13*) have been shown to predict risk of extensive disease distribution in UC as well as higher rates of colectomy (74, 122, 123). In addition, the multidrug resistance (*MDR1*) locus, as well as *IL1RA*, have been implicated in extensive and severe disease (123-125). A polymorphism in the *CLEC7A* gene, which encodes the fungal innate immune receptor Dectin-1 in the gastrointestinal tract, has been associated with medically-refractory colitis (15, 126).

An unbiased GWAS by Haritunians *et al*, compared patients with UC who had undergone colectomy for medically-refractory disease (n=324), to patients with

treatment responsive disease (n=537), and healthy controls (n=2,601) (15). The median disease duration was shorter amongst those with refractory disease, and a significantly higher proportion of medically-refractory patients had extensive disease and a family history of IBD (15). Analyses revealed 10 SNPs in the major histocompatibility complex (MHC) on chromosome 6p which reached genome-wide significance, in addition to the *TNFSF15, IL-10, ORMDL3, IL12B, and IFNG* loci (15).A subsequent study, analysed 45 candidate SNPs (identified by Haritunians *et al*), amongst 111 patients with ASUC, and replicated a positive association with the SNP rs2403456 (127).

2.1.2.2 Genetic risk scores (GRS)

The rationale behind a GRS approach, is that most of the IBD-risk loci identified by meta-GWAS and ICHIP studies, are associated with a small effect size for disease (7). Thus, examining the cumulative genetic burden of risk may yield more meaningful results than the examination of individual polymorphisms (14). The burden of genetic risk alleles, computed as a GRS, has been assessed as a model for predicting UC phenotype in two studies with contrasting findings (*Section 2.4.2*) (14, 15).

UC disease factor	Candidate genetic loci
Extensive UC	*MHC, HLA-DRB1 (DR13)* (74, 122, 123) *MDR1* (124, 128) *IL1RA* (123, 125)
Medically-refractory UC or colectomy	*MHC, HLA-DRB1* (15, 74, 122, 123) *TNFSFR15* (15) *IL10* (15) *IL12B* (15) *IFNG* (15) *KIF1A* (15) *ORMDL3* (15) *BICD1* (15) *CLEC7A (15, 126)*

Table 2.1 Candidate genetic loci conferring risk of UC disease phenotype. *The table depicts candidate genetic loci that confer risk for either extensive or medically refractory UC. The references are cited within the table.*

2.1.3 ICHIP: design and limitations

The ICHIP is an Illumina® Infinium SNP microarray platform, which was first designed in 2009 by a collaboration of investigators of autoimmune diseases (129, 130). The probes on the ICHIP array report on 195,806 SNPs and 718 small insertion-deletions from 187 distinct loci, each of which has evidence of association with at least one immune-mediated trait of genome wide significance (129). The ICHIP was designed for two primary purposes; deep replication and fine-mapping of GWAS identified IBD-risk loci (8). The ICHIP includes all SNPs identified in the 1000 Genomes project, and there is dense MHC coverage (131). The breadth of cover of the ICHIP comes at a fraction of the cost of whole genome sequencing, making it a viable proposition for the study of large patient cohorts.

The limitations of ICHIP genotyping must be acknowledged. The ICHIP has incomplete coverage of lower frequency variants, because its design was solely dependent on GWAS-identified risk alleles. Newly identified variants are not reported, and imputation

is used, which can lead to stronger associations for imputed SNPs (8, 129). ICHIP probe quality is highly variable, and there is inconsistency amongst the available genotype-calling algorithms (132). The ICHIP is designed for use in white European populations, and non-European populations are under-represented in its development (129).

2.2 METHODS

2.2.1 Oxford IBD Cohort

2.2.1.1 Ethics and patient recruitment

The Oxford IBD Cohort was established in 2010 at the John Radcliffe Hospital, Oxford University Hospitals (OUH) Trust, as a means of generating a prospective cohort for evaluation of outcomes, treatments, and predictors in IBD. The population of patients with IBD in Oxford is representative of a spectrum of referral sources, and draws from a catchment of 620,000 people within Oxfordshire.

Data collected and stored include basic demographics, IBD phenotype (including disease distribution, severity, treatment, and results of diagnostic tests), and non-IBD clinical data (co-existing medical and surgical conditions).

The necessary ethical approval for the collection and storage of patient information in a database, as well as for the use of samples for research has been granted: Inflammatory Bowel Disease in Oxford: prospective cohort for outcomes, treatment, and predictors. Research Ethics Committee Reference: 09/H1204/30 (Granted June 2009).

2.2.1.2 Phenotyping of patients with IBD

Clinical data were compiled and entered into an encrypted database held within the hospital IT network with the assistance of data-clerks. Data sources included patient case-notes, outpatient clinic letters, and results of diagnostic and endoscopic investigations. In addition, access was granted to surgical and pharmaceutical databases within the OUH Trust, facilitating extraction of all surgical encounters of patients within the IBD Cohort since 2007, as well as centralised prescriptions dispensed for biological agents (infliximab and adalimumab).

In order to ensure that the compiled clinical data was accurate, at least 10% of patient data entry was duplicated by clerks to ensure consistency of findings. In addition, at least 10% of datasets were personally reviewed by a dedicated IBD clinician (RVB). During the course of this thesis, both retrospective and prospective identification of UC sub-phenotypes within the Oxford IBD Cohort was undertaken. Phenotypic classification of UC was undertaken according to multiple criteria, including the age of diagnosis, distribution and behaviour of disease (Montreal classification), and disease severity (20). Particular focus was directed toward the identification of patients who have suffered from ASUC, as defined using the Truelove and Witts' clinical criteria (*Table 2.2*) (35). Rigorous retrospective searching through patient case-notes and electronic clinic letters of patients within the Cohort was performed to identify those patients with a history of ASUC. In addition, prospective recruitment of hospitalised patients with ASUC to the Cohort was undertaken at the John Radcliffe Hospital.

Activity	**Truelove and Witts' Severity Criteria**
Stool frequency	≥6 bloody stools per day *AND one or more of the following*
Heart rate	Tachycardia >90 bpm
Temperature	Fever >37.8°C
Haemoglobin (Hb)	Hb <10.5 g/l
Inflammatory markers	Erythrocyte sedimentation rate (ESR) >30 mm/hr, or CRP >30 mg/l

Table 2.2. Truelove and Witts' criteria for ASUC (35). *A diagnosis of ASUC is defined by ≥6 bloody stools per day and one or more of tachycardia, fever, anaemia, or raised inflammatory markers.*

2.2.1.3 Description of the Oxford IBD Cohort

A description of the overall Oxford IBD Cohort is provided so as to interpret selection bias amongst the subgroup of patients who were genotyped by ICHIP, as well as the generalisability of the study findings (*Table 2.3*).

At the time of data analysis (January 2015), there were 2290 patients with IBD consented to the cohort for whom basic phenotypic information was available. Overall,

there were 1096 patients with CD, 1052 patients with UC, and 142 patients with IBD yet to be classified (IBDu). Aside from primary diagnosis, approximately 10% of data was unavailable for each of the variables analysed. Given that the data is missing completely at random, the available case analysis is presented and imputation of data was not performed.

2.2.2 ICHIP genotyping of Oxford IBD Cohort

ICHIP genotyping of 911 patients from within the Cohort was performed using methodology described by Jostins *et al* (7). Briefly, approximately 10ml of peripheral blood was drawn from all patients and 3-5µg of DNA was isolated and applied to an Illumina® Infinium ICHIP gene custom microarray platform at the Sanger Institute (Cambridge, UK). A gene-calling algorithm was used to interpret the binding of normalised measures of DNA to allele specific probes to ascertain the genotype of an individual at a given SNP (132). The optiCall® algorithm was used to sequence the first 231 patients with IBD (132). Due to a change in availability, an alternative gene-calling algorithm, Illuminus®, was used for genotyping the remaining 680 patients (133).

	Overall	CD	UC	IBDu
Patient number (% cohort)	2290 (100%)	1096 (48%)	1052 (46%)	142 (6%)
Gender (male, %)	1117 (49%)	515 (47%)	535 (51%)	67 (47%)
Family history of IBD (1° relative)	157 (7%)	78 (7%)	65 (6%)	14 (10%)
Age at diagnosis (median, IQR)	30 19-39	23 17-35	31 22-44	25 13-41
Montreal criteria	-	A1 24% L1 21% A2 60% L2 29% A3 16% L3 50% B1 65% +p 19% B2 20% +L410% B3 15%	E1 18% E2 40% E3 42%	A1 34% L1 1% A2 39% L2 86% A3 26% L3 13% +P 4% +L4 5%
EIM's				
Overall	477 (21%)	263 (24%)	194 (18%)	20 (14%)
PSC	75 (3%)	16 (1%)	54 (5%)	5 (4%)
Arthropathy	220 (10%)	136 (12%)	77 (7%)	7 (5%)
Eye disease	69 (3%)	35 (3%)	32 (3%)	2 (1%)
Cutaneous disease	113 (5%)	76 (7%)	31 (3%)	6 (4%)
Surgical history				
Any surgery	730 (32%)	541 (49%)	176 (17%)	13 (10%)
>3 operations	226 (10%)	179 (16%)	45 (4%)	2 (1%)
Colectomy/ileo-caecal resection	628 (27%)	460 (42%)	160 (15%)	8 (6%)
Stoma	333 (15%)	204 (18%)	122 (12%)	7 (5%)
Fistula/abscess	206 (9%)	169 (15%)	33 (3%)	4 (3%)
Stricture surgery	89 (4%)	83 (8%)	6 (0.6%)	0
IPAA	41 (2%)	5 (0.5%)	35 (3%)	1 (0.7%)
Medications (current)				
5-ASA	719 (31%)	94 (9%)	544 (52%)	81 (57%)
Thiopurine	588 (26%)	358 (33%)	192 (18%)	38 (27%)
Other IM	112 (5%)	57 (5%)	53 (5%)	2 (1%)
Infliximab	169 (7%)	102 (9%)	55 (5%)	12 (8%)
Adalimumab	219 (10%)	199 (18%)	18 (2%)	2 (1%)
Corticosteroid	98 (4%)	37 (3%)	52 (5%)	9 (6%)
Colorectal cancer	31 (1%)	13 (1%)	16 (2%)	2 (1%)
ASUC	-	-	119 (11%)	-

Table 2.3. Phenotypic description of the Oxford IBD Cohort. *The table provides a detailed phenotypic description of the IBD cohort at the time of analysis (January 2015). Colectomy and ileocaecal resection combined; colectomy includes total, subtotal and partial colectomy. Stoma includes prolonged or permanent stoma, including diversion stoma (even if reversed). >3 operations does not include re-anastomosis operations. Stricture surgery refers to stricture resection and strictureplasty. Medication lists represent current use (not past use). Key: EIM, extra-intestinal manifestations; PSC, primary sclerosing cholangitis; IM, immunomodulator; IPAA, ileal pouch-anal anastomosis; IQR, interquartile range; 5-ASA, 5-aminosalicylic acid.*

2.2.2.1 Selection of IBD risk loci

The ICHIP IBD-associated loci examined in this chapter, were those identified in GWAS and ICHIP meta-analysis by Jostins *et al*, described in *Section 1.3.2*, the most comprehensive genetic study in IBD to date (7). This study identified 193 statistically significant independent signals of genome wide significance ($p<5 \times 10^{-8}$) for IBD, which were merged into 163 regions due to similarity of underlying functional subunits (7). Through direct correspondence with the authors (LJ), a file (labelled the 'Mangrove file') was obtained, providing data on each of 193 significant loci. Of the 193 IBD risk alleles, 137 are shared between CD and UC, 27 are UC-specific, and 29 are CD-specific. For each risk alleles, both the risk allele frequency (RAF) and effect size is provided for both CD and UC.

2.2.2.2 ICHIP data integration and normalisation

The following steps were taken to generate an integrated dataset to ensure consistent and correct interpretation of the ICHIP data from the Oxford Cohort (*Figure 2.1*):

1. *Identification of the IBD-associated risk allele.* The correct ICHIP IBD-associated susceptibility allele at each locus was identified. The ICHIP gene-calling algorithms report the minor allele frequency, which does not always correspond with the disease susceptibility allele.
2. *Normalisation of the ICHIP gene-calling algorithms.* The Oxford IBD Cohort ICHIP genotype dataset was generated using two different gene-calling algorithms; optiCall® and Illuminus®. There were differences between the alleles reported by these algorithms, which required normalisation to allow consistent interpretation of the entire dataset.

3. *Identification of UC- and CD-specific RAF and effect sizes at each loci.* This was achieved using the 'Mangrove' file data.

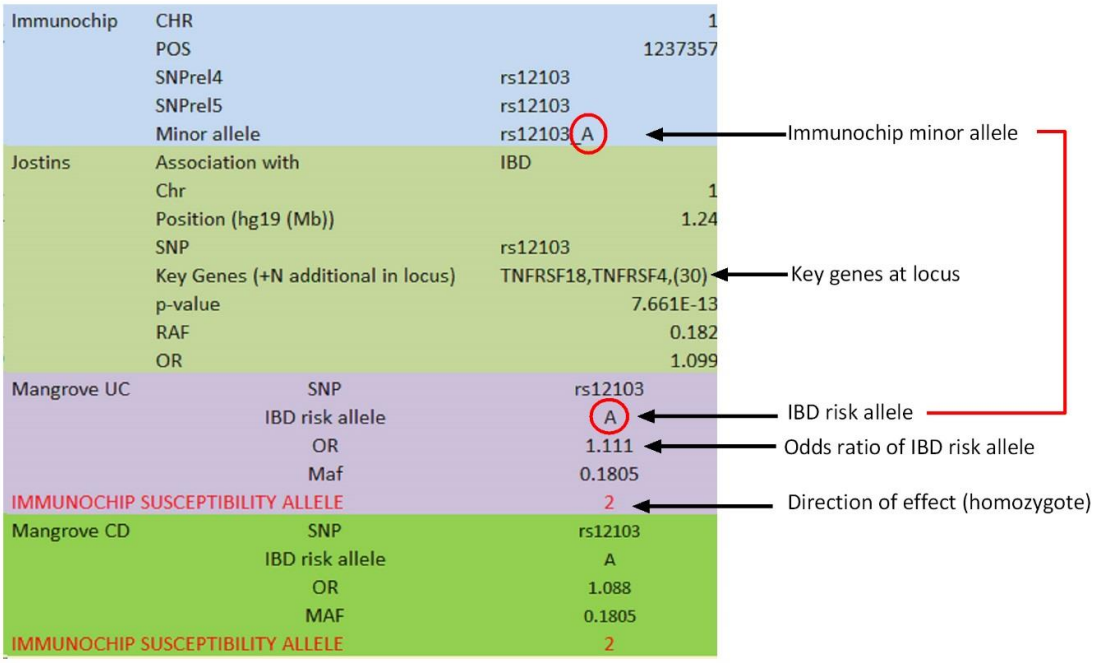

Figure 2.1. ICHIP data integration and normalisation. *Integration between the Oxford IBD ICHIP dataset, Jostins et al 'Mangrove' files IBD-associated risk alleles, ICHIP calling algorithms, and the key genes at the locus.*

2.2.2.3 ICHIP quality control

In order to assess the quality of the ICHIP data from both the optiCall and Illuminus algorithms, the observed RAF within the Oxford IBD cohort, was compared to the expected RAF derived from the Jostins *et al* dataset using a linear regression analysis (7). RAF is derived via the following calculation, where A is the risk allele and B is the non-risk allele at the locus:

Risk allele frequency (allele A) = Heterozygous (A) allele + 2(Homozygous (A))/ Total (A) + (B) alleles*

This analysis, revealed a close linear correlation between the observed and expected RAF, providing a reassuring quality control between the ICHIP calling algorithms and overall for the Oxford IBD Cohort ICHIP dataset (*Figure 2.2*).

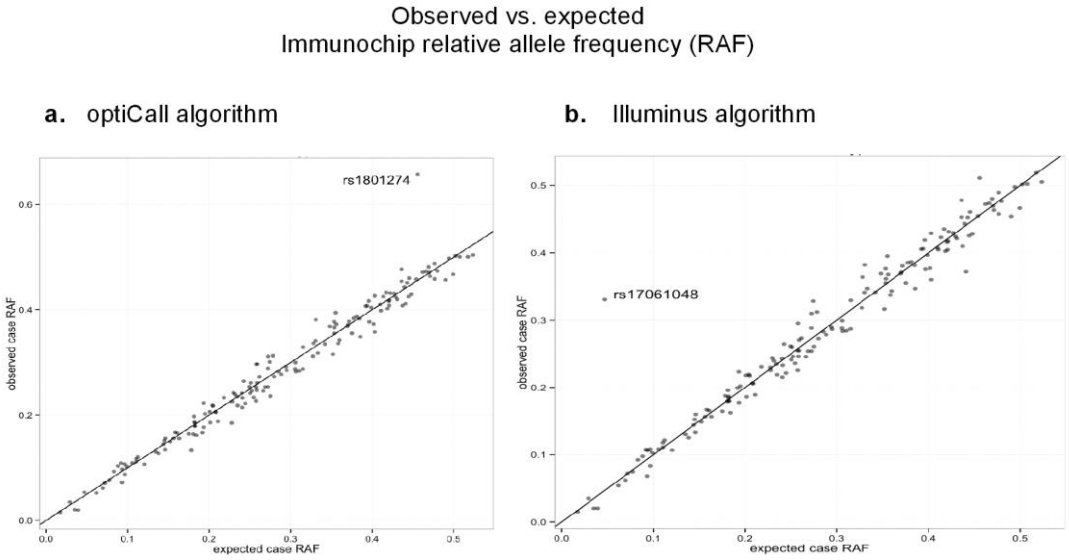

Figure 2.2. Quality control of the Oxford IBD ICHIP Cohort. *The observed RAF in the Oxford IBD ICHIP Cohort (n=911) is compared to the expected RAF derived from the Jostins et al cohort (n=25,683) of 166 CD risk loci. Two outlying SNPs are marked (rs1801274 and rs17061048) which were excluded from subsequent analysis.* ***a).*** *Observed vs. expected RAF in the dataset called using the optiCall algorithm (n=231).* ***b).*** *Observed vs. expected RAF in the dataset called using the Illuminus algorithm (n=680). Performed in collaboration with MQ.*

2.2.3 IBD genetic risk scores (GRS)

2.2.3.1 Computation of GRS

In order to assess whether overall genetic burden determines phenotypic expression in UC, weighted GRS were calculated using the 193 GWAS and ICHIP IBD-associated risk alleles defined by Jostins *et al* (7).

GRS calculation, similar to previously described GRS methodology, was performed in collaboration with statistical geneticists at the Wellcome Trust Centre for Human Genetic Studies (DM) (*Box 2.1*) (14).

For UC, the computation of three distinct GRS was performed:

1. ***Overall GRS for UC.*** This was performed using 164 risk loci (137 shared with CD, and 27 UC-specific loci).
2. ***GRS using UC-specific risk loci.*** This was performed using 27 UC-specific loci.
3. ***Comparative CD vs. UC GRS.*** The 'Mangrove' files provided a CD vs. UC OR for 120 risk loci, providing a summation of the heterogeneous effect sizes between CD and UC at each of these loci. The CD vs. UC OR was used to generate GRS, which allowed for comparison to be made between patients with CD or UC phenotypes.

Genetic risk score methodology
Contributed by statistical geneticists (DM)
Wellcome Trust Centre for Human Genetics

R defined as the total risk for conferred from IBD risk loci, and *Rj* to be the contribution to the risk score from the locus j. The observed odds ratio (OR) for an individual at locus *j* is denoted *iORj*, and is calculated using the log of the number of IBD-associated risk alleles present at the locus. If the individual is heterozygous for the risk allele at the locus, then the observed OR is *iORj1 (iORj^{1}HET)*. In the case of homozygosity for the risk allele at the locus, the *iORj* is squared *(iOR^{2}HOM*).

1. *The population-wide expected OR at the locus j is denoted pORj. This is calculated using the following equation, where fj is the frequency of the risk allele at locus j.*
   pORj = 1(1 – fj)2 + ORj1HET*2fj(1-fj) + OR2HOM*fj2*
2. *The risk score for the individual at locus j, denoted Rj, is then calculated using the following equation:*
   Rj = iORj / pORj
3. *In order to determine a total genetic risk score for all IBD risk loci in an individual, denoted R, the risk across all loci (j) is multiplied by the total number of risk loci, denoted n.*
   *R = n*Rj*

***Box 2.1. GRS computation methodology**. The GRS calculation was derived from the RAF and OR for IBD-risk loci derived from GWAS meta-analysis and ICHIP studies by Jostins et al (7). The GRS were performed in collaboration with statistical geneticists at the Wellcome Trust Centre for Human Genetics (DM).*

2.2.3.2 Normality of distribution of GRS

The normality of distribution of the GRS data was analysed, so as to interpret the appropriate approach to statistical analysis of the dataset. The D'Agostino and Pearson omnibus normality test was undertaken for the UC GRS dataset, revealing an alpha value of $p < 0.0001$. Thus, the chance that a random sample of data would deviate from the Gaussian ideal was significant.

The Gaussian curve fitted to the UC GRS dataset showed a skewed distribution (*Figure 2.3*). Thus, the appropriate summary statistic for the dataset is median and interquartile range (IQR) and nonparametric statistical analysis was performed.

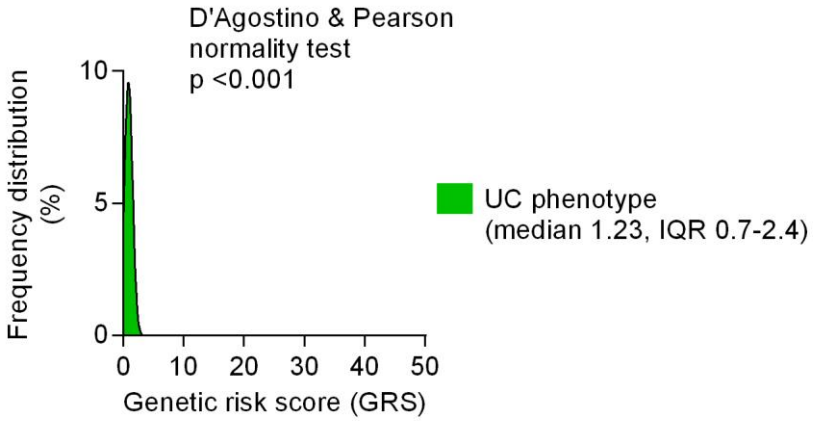

Figure 2.3. Distribution of the GRS in UC. *The GRS for UC range from 0.07 to 12.46. D'Agostino and Pearson normality tests show an alpha value of p<0.0001, meaning that the chance of a random sample of data lying outside of the Gaussian ideal is significant. The Gaussian curves plotted for UC GRS are skewed to the left.*

2.2.4 Variance analysis of candidate risk loci

A variance analysis of candidate risk loci was performed between UC severity phenotypes. For each of the 164 UC-risk loci, the observed RAF was compared between ASUC, severe and non-severe UC phenotypes, as well as with the expected RAF derived from the Jostins *et al* dataset (7). On identification of a enrichment or reduction of expression of a candidate SNP between the groups, the relative proportions of homozygotes and heterozygotes determined. Chi-squared analysis was used to compare the proportions of risk to non-risk alleles at the loci in the groups, from which p values were derived.

2.2.5 Statistical analysis

All statistical analyses were performed using GraphPad Prism software (version 5.0a). Continuous variables of non-normally distributed data are summarised as medians and IQR. Categorical variables are expressed are proportions.

Comparison between non-normally distributed data was performed using an unpaired nonparametric Mann Whitney test. Correlation coefficients were calculated using a nonparametric Spearman's rank test. Comparison between categorical variables was performed using a chai-square test. Receiver operating characteristic (ROC) curves were used to determine the capacity of GRS to discriminate between phenotypes, from which area under the curve (AUC), sensitivity, and specificity was able to be derived. P values of <0.05 were considered statistically significant.

2.3 RESULTS

2.3.1 Phenotypic analysis of the Oxford ICHIP cohort

Detailed phenotypic analysis of the patients with IBD who underwent genotyping using ICHIP was performed. Overall, a sample of 911 patients with IBD underwent genotyping via ICHIP; 478 (52%) with CD, 373 (41%) with UC, and 60 (7%) with IBDu (*Figure 2.4*, *Table 2.4*).

The population selected for ICHIP genotyping was enriched for severe disease as compared to the overall Oxford IBD Cohort. The median age of IBD diagnosis amongst the ICHIP Cohort was younger than that of the overall cohort (25 *vs*. 30 years old respectively, p< 0.001). Rates of surgery were higher in the ICHIP cohort compared to the overall cohort (37% *vs*. 32% respectively, p=0.01), as were rates of biologic use (22% *vs.* 17%, p< 0.001). Recognition of this selection bias is important, as it is informative for the generalisability of the genotyping analysis.

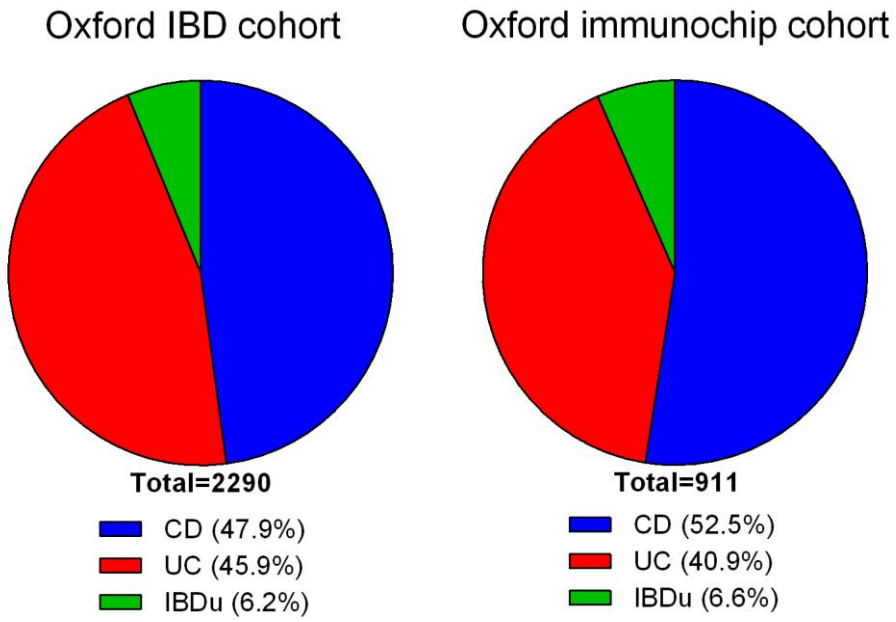

Figure 2.4. Phenotypic characteristics of the Oxford ICHIP cohort. *The figure depicts the cohort selected for ICHIP genotyping (n=911), as compared to the overall Oxford IBD Cohort (n= 2290).*

	Overall	CD	UC	IBDu
Patient number (% cohort)	911 (100%)	478 (52%)	373 (41%)	60 (7%)
Gender (male, %)	437 (48%)	221 (46%)	190 (51%)	26 (43%)
Family history of IBD (1° relative)	7%	33 (7%)	19 (5%)	9 (15%)
Age at IBD diagnosis (median, IQR)	25 (16-37)	21 (15-31)	30 (21-43)	14 (10-35)
Montreal criteria (% of patients)	-	A1 31% L1 21% A2 58% L2 32% A3 11% L3 47% B1 64% +p 22% B2 20% +L4 14% B3 16%	E1 21% E2 43% E3 36%	A1 50% L1 0% A2 25% L2 94% A3 25% L3 6% +p 4%
EIM's				
Overall	180 (20%)	116 (24%)	55 (15%)	9 (15%)
PSC	17 (2%)	5 (1%)	10 (3%)	2 (3%)
Arthropathy	111 (12%)	74 (15%)	34 (9%)	3 (5%)
Eye disease	30 (3%)	19 (4%)	10 (3%)	1 (2%)
Skin disease	57 (6%)	41 (8%)	13 (3%)	3 (5%)
Surgical history				
Any surgery	333 (37%)	254 (53%)	73 (19%)	6 (10%)
>3 operations	122 (13%)	98 (20%)	22 (6%)	2 (3%)
Colectomy/ileocaecal resection	285 (31%)	214 (45%)	67 (18%)	4 (7%)
Stoma	164 (18%)	107 (22%)	54 (14%)	3 (5%)
Fistula/abscess	107 (12%)	88 (18%)	16 (4%)	3 (5%)
Stricture surgery	114 (13%)	111 (23%)	3 (0.08%)	0
IPAA	33 (4%)	1 (0.02%)	31 (8%)	0
Medications (current)				
5-ASA	307 (34%)	47 (10%)	218 (58%)	42 (70%)
Thiopurine	292 (32%)	188 (39%)	85 (23%)	17 (32%)
Other IM	51 (6%)	28 (6%)	25 (7%)	1 (2%)
Infliximab	84 (9%)	55 (12%)	24 (6%)	5 (8%)
Adalimumab	118 (13%)	107 (22%)	10 (3%)	1 (2%)
Corticosteroid	44 (5%)	18 (4%)	24 (6%)	2 (3%)
Colorectal cancer	10 (1.1%)	3 (0.6%)	7 (2%)	0
ASUC	-	-	47 (13%)	-
Follow-up period (months, median,IQR)	90 (44-172)	97 (54-174)	90 (40-175)	42 (18-101)

Table 2.4. Phenotypic characteristics of the Oxford ICHIP cohort. *The table depicts the cohort selected for ICHIP genotyping (n=911). Colectomy and ileocaecal resection combined; colectomy includes total, subtotal and partial colectomy. Stoma includes prolonged or permanent stoma, including diversion stoma (even if reversed). >3 operations does not include re-anastomosis operations. Stricture surgery refers to stricture resection and strictureplasty. Medication refers to current use (not past use). Key: EIM, extra-intestinal manifestation; PSC, primary sclerosing cholangitis; IM, immunomodulator; IPAA, ileal pouch-anal anastomosis; IQR, interquartile range.*

2.3.2 Differentiating CD from UC using GRS

A comparative CD vs. UC OR, available for 120 IBD-risk loci at which there is heterogeneity of effect sizes between CD and UC, was to used validate the capacity of GRS to differentiate between IBD phenotypes in the Oxford ICHIP cohort (7).

The frequency of distribution of CD vs. UC GRS was calculated for patients with CD (n = 478) and UC (n = 373) phenotypes, and a Gaussian curve fitted to the results (*Figure 2.5*). The median CD vs. UC GRS was significantly higher amongst patients with CD than with UC (1.14 (IQR 0.6-2.3) vs. 0.54 (IQR 0.3-1.0), p <0.001, CD vs. UC phenotype respectively).

Thus, using the comparative OR's at shared IBD-risk loci, GRS were able to differentiate between CD and UC phenotypes on a population level. However, there is significant overlap of GRS between the groups, such that the GRS cannot be used as a discriminatory tool for phenotypic differentiation for individual patients.

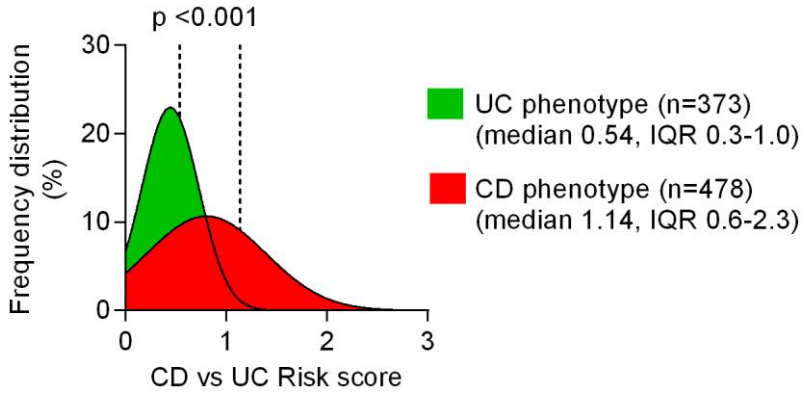

Figure 2.5. Differentiating CD from UC using GRS. *The comparative CD vs. UC OR of 120 IBD-risk loci of heterogeneous effect size was compared between patients with CD and UC phenotypes. The frequency of distribution of GRS was calculated and a Gaussian curve fitted. The median GRS and IQR is presented for each group. Statistical analysis performed using the Mann Whitney nonparametric test.*

2.3.3 GRS in UC phenotypes

GRS derived from 164 UC-risk loci (137 shared with CD, and 27 UC-specific loci) were calculated, and comparisons were made between UC phenotypes. This analysis was performed in order to investigate whether genetic risk burden is a determinant of the phenotypic expression of UC.

2.3.3.1 GRS according to age of UC diagnosis

Patients were stratified according to age of diagnosis of UC, and GRS were calculated for the particular groups. The Montreal age classification was used (age at diagnosis <17 years, 17-40 years, or >40 years), as well as analysis of patients with early onset IBD (EOIBD, <10 years) as a separate group (10, 20, 28).

Analysis revealed a significant enrichment of genetic risk burden amongst those with EOIBD (n=13), compared to those diagnosed with UC between the ages of 17-40 years (n=201) as well as those diagnosed after 40 years of age (n=128) (median GRS 2.9 (IQR 1.3-6.3) vs. 1.3 (0.7-2.4), p=0.02, vs. 1.1 (IQR 0.6-2.0), p=0.005; EOIBD vs. 17-40 years vs. >40 years respectively) (*Figure 2.6*). There was a trend toward higher GRS amongst patients diagnosed with UC before the age of 17 years (n=44) (median GRS 1.7 (IQR 0.6-3.4)), however this did not reach statistical significance. Linear regression analysis was performed for age of UC diagnosis and GRS, revealing a trend toward to diminishing genetic burden with advancing age of diagnosis, though not to significance (r = -0.07, p=0.18) (*Figure 2.6*).

Thus, genetic risk burden amongst patients with EOIBD is significantly higher than amongst patients diagnosed with UC in adulthood. There is a trend, though not to significance, of lower GRS with advancing age at UC diagnosis.

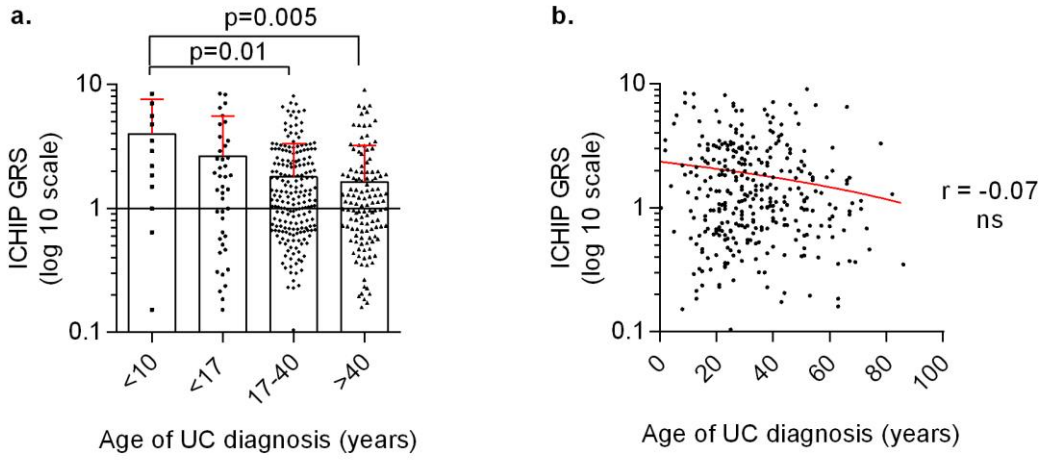

Figure 2.6. GRS according to age of diagnosis of UC. a). *Patients with UC were classified according to the age of diagnosis of UC: early onset IBD (EOIBD, <10 years, n=13), <17 years (n=44), 17-40 years (n= 201), >40 years (n= 128). Data presented as median and IQR. Statistical analysis performed using the nonparametric Mann Whitney test.* ***b).*** *Linear regression analysis of age of diagnosis and genetic risk score. Statistical analysis performed using Spearman nonparametric correlation (ns= non-significant).*

2.3.3.2 GRS according to UC disease extent

Patients were stratified according to disease extent of UC, and GRS were calculated and compared between the groups. The Montreal classification was used to divide patients into E1 (proctitis, n=58), E2 (left-sided disease not extending beyond the splenic flexure, n=121), and E3 (extensive disease beyond the splenic flexure, n= 102) categories (20).

The analysis did not reveal a significant difference in genetic risk burden between groups stratified according to the distribution of UC. However, there was a non-significant trend toward lower GRS amongst patients with limited disease (E1), as compared to those with more extensive disease (E2 and E3) (median GRS 0.88 (IQR 0.5-2.3) vs. 1.36 (IQR 0.7-2.4), p=0.06, E1 vs. E2/3 respectively) (*Figure 2.7*).

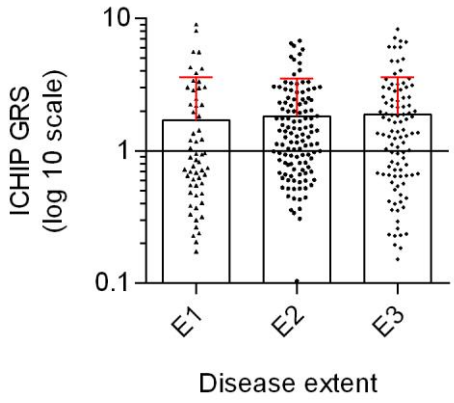

Figure 2.7. GRS according to extent of disease distribution in UC. *Patients with UC were classified according to the extent of disease distribution as per the Montreal criteria: E1 (proctitis, n=58), E2 (left-sided disease not extending beyond the splenic flexure, n=121), and E3 (extensive disease beyond the splenic flexure, n=102). Data presented as median and IQR.*

2.3.3.3 GRS according to family history of IBD

Patients with UC were stratified according to family history of IBD in a 1st degree relative (1^{O}FHx). Overall, 19 (5%) of patients with UC reported a 1^{O}FHx of IBD. GRS were calculated and compared between UC patients with and without a 1^{O}FHx of IBD (*Figure 2.8*).

This analysis did not reveal a significant difference in GRS between the groups stratified by 1^{O}FHx of IBD, although there was a trend evident toward higher GRS amongst those with a 1^{O}FHx of IBD, as compared to those without (median 2.29 (IQR 1.1- 3.1) vs. 1.17 (0.7- 2.3), p=0.09).

The ability to draw a meaningful conclusion from this analysis is limited by Type 2 error, as well as by the quality of family history data available.

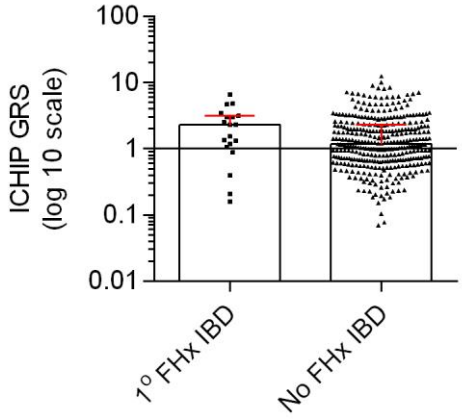

Figure 2.8. GRS in UC patients stratified by family history of IBD. *Patients with a 1st degree family history of IBD (n=19) were compared to those without (n=354). Data presented as median and IQR.*

2.3.4. Categorisation of UC severity

The UC Cohort was stratified in three groups according to severity of disease (*Figure 2.9, Table 2.5*):

1. ***ASUC*** (n=47). UC patients with a history of a defined episode of ASUC according to Truelove and Witts' clinical criteria, for which they required hospitalisation and intravenous corticosteroid therapy (35). For each of these patients, infection was excluded, and their disease was objectively assessed with endoscopy to confirm severity. Patients were classified as ASUC as such, regardless of concurrent need for biologic therapy or colectomy.
2. ***Severe UC*** (n=82). UC patients with a history of colectomy or a requirement for biologic therapy. These patients did not have a documented prior episode of ASUC, but rather had refractory disease.
3. ***Non-severe UC*** (n=244). The remainder of the UC cohort was classified as having non-severe disease.

Patients with ASUC and severe UC were more likely to have an extensive UC disease distribution than those with non-severe disease (49% vs. 51% vs. 32%; p=0.03, p=0.01; ASUC, severe UC and non-severe UC, respectively). There was no significant difference in the age of UC diagnosis between the severity groups. Around one third of patients presented with ASUC at diagnosis, and one quarter had multiple admissions with ASUC over their disease course. Rescue therapy with either infliximab or ciclosporin was required for 40% of patients with ASUC, and 30% of patients underwent colectomy, a significantly higher proportion than in the overall ICHIP UC cohort (30% vs. 15%, p<0.001). There was no mortality within the ASUC cohort.

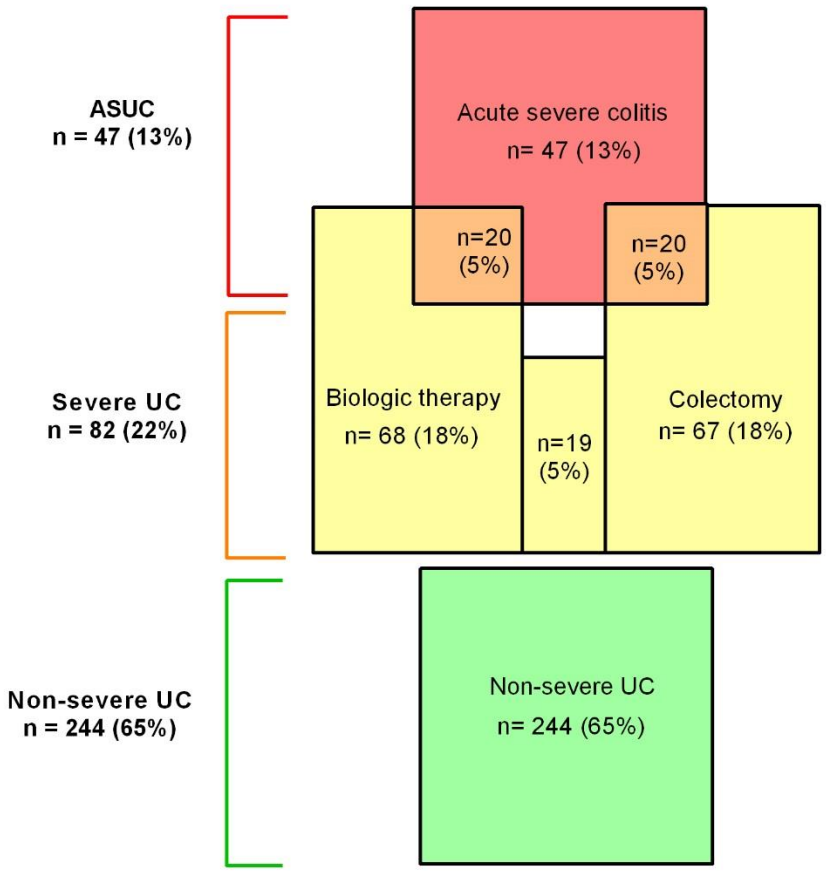

Figure 2.9. Categorisation of UC severity in Oxford ICHIP cohort. *Patients with UC were categorised according to a history of ASUC, severe UC (defined as colectomy or prior requirement for biological therapy), or non-severe UC (not meeting the prior criteria). The percentages provided are of the ICHIP UC cohort.*

	ASUC	Severe UC	Non-severe UC
Patient number Proportion of ICHIP UC cohort	47 13%	82 22%	244 65%
Gender (n, % male)	26 (55%)	45 (55%)	119 (49%)
Family history of IBD (1° relative)	8 (17%)	10 (12%)	8 (3%)
Age at UC diagnosis (median, IQR)	29 (22-42)	28 (17-38)	31 (22-44)
Duration of follow-up (months)	58 (29-125)	98 (55-185)	88 (41-200)
Montreal criteria	E1 2% E2 49% E3 49%	E1 17% E2 32% E3 51%	E1 24% E2 44% E3 32%
Extra-intestinal disease			
Overall	9 (19%)	17 (20%)	29 (12%)
PSC	1 (2%)	3 (4%)	6 (2%)
Arthropathy	6 (13%)	10 (12%)	18 (7%)
Eye disease	1 (2%)	5 (6%)	4 (2%)
IBD-associated skin disease	2 (4%)	6 (7%)	5 (2%)
Medications (past or current)			
5-ASA	35 (75%)	50 (61%)	195 (80%)
Immunomodulator	28 (60%)	53 (64%)	77 (32%)
Biological therapy	23 (50%)	45 (55%)	0
Surgical history			
Colectomy	14 (30%)	53 (65%)	0
IPAA (pouch surgery)	6 (13%)	25 (31%)	0
Timing of ASUC			
Age at ASUC (median, IQR)	35 (28-44)		
Disease duration at ASUC (months, median, IQR)	14 (0-116)		
ASUC at UC diagnosis (n, %)	14 (30%)		
Multiple admissions ASUC (n, %)	15 (32%)		
Rescue therapy			
Overall	20 (43%)		
Infliximab	14 (30%)		
Ciclosporin	6 (13%)		
Multiple admissions for ASUC	15 (32%)		

Table 2.5. Categorisation of UC severity in Oxford ICHIP cohort. *UC disease severity was categorised for the purposes of genetic analysis into 3 groups: ASUC (n=47), severe UC (n=82), and non-severe UC (n=244). A detailed description of the UC severity groups is provided. Immunomodulator therapy includes thiopurines and methotrexate. 5-ASA, 5-aminosalicylic acid.*

2.3.5 GRS according to UC severity

Analysis according to disease severity of UC revealed a significant enrichment of genetic burden amongst patients with ASUC, as compared to patients with non-severe UC (median GRS 1.83 (IQR 1.0-3.0) *vs.* 1.12 (0.6-2.2), p=0.001, ASUC *vs.* non-severe UC respectively) (*Figure 2.10*). There was a trend toward increasing GRS amongst patients with severe UC as compared to those with non-severe UC, although not to significance (median GRS 1.33 (IQR 0.6-2.6), p=0.39). However, when ASUC and severe UC patients were analysed as a combined group, there was significant enrichment of genetic risk burden compared with non-severe patients (median GRS 1.41 (IQR 0.8-2.7) vs. 1.12 (IQR 0.6-2.2), p=0.018, severe combined group *vs*. non-severe UC respectively).

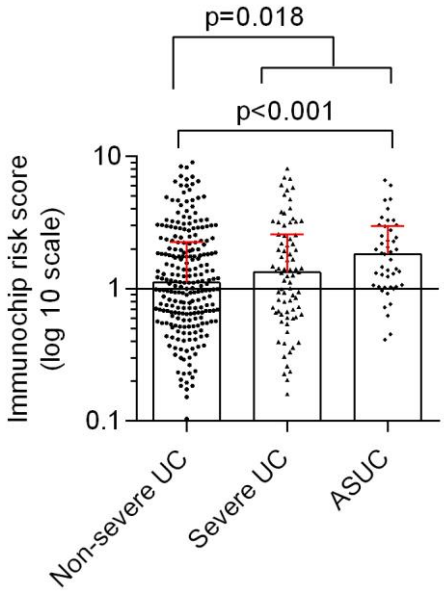

Figure 2.10. GRS according to severity of UC*. Patients with UC were classified according to severity of disease: ASUC (n=47), severe UC (n=82), and non-severe UC (n=244). GRS calculated and statistical analysis performed using the nonparametric Mann Whitney test. Data presented as median and IQR.*

The frequency of distribution of GRS was calculated for patients with ASUC, severe UC, and non-severe UC phenotypes, and a Gaussian curve fitted to the results. The analysis provides a graphical depiction of increased GRS amongst patients with ASUC and severe UC phenotypes (*Figure 2.11*).

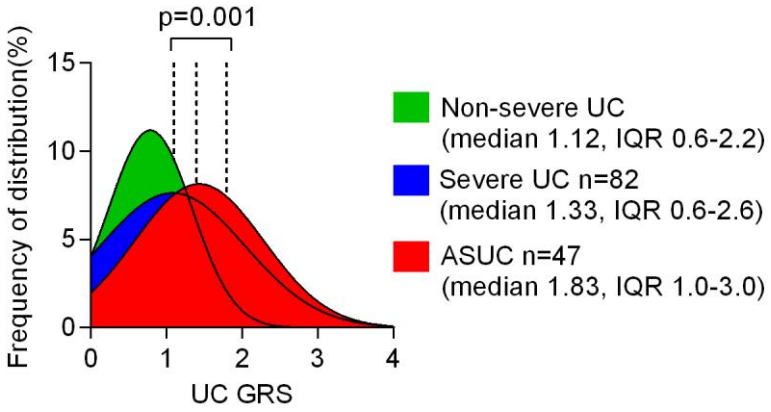

Figure 2.11. Differentiating severity of UC using GRS. *GRS were calculated for patients with UC according to the severity of their disease; ASUC (n-=47), severe UC (n=82), and non-severe UC (n=244). The frequency of distribution of GRS was calculated and a Gaussian curve fitted. The median GRS and IQR is presented for each group. Statistical analysis performed using nonparametric Mann Whitney test.*

Thus, there was a significant enrichment of GRS amongst patients with ASUC. However, there is a significant overlap of GRS between the severe and non-severe UC groups, and further analysis is required to determine the discriminatory function of GRS in UC severity.

2.3.5.1 GRS ROC curves for UC severity

In order to assess the discriminatory capacity of GRS in predicting UC severity, ROC curve analysis was performed (*Figure 2.12*).

ROC curve analysis comparing the GRS of patients with ASUC and those with non-severe UC, revealed an AUC of 0.65 ($p<0.001$). This confirms a modest but significant discriminatory value of GRS in differentiating between ASUC and non-severe

phenotypes. There was no discriminatory value of GRS in differentiating between patients with severe and non-severe phenotypes (AUC 0.53, p=0.39).

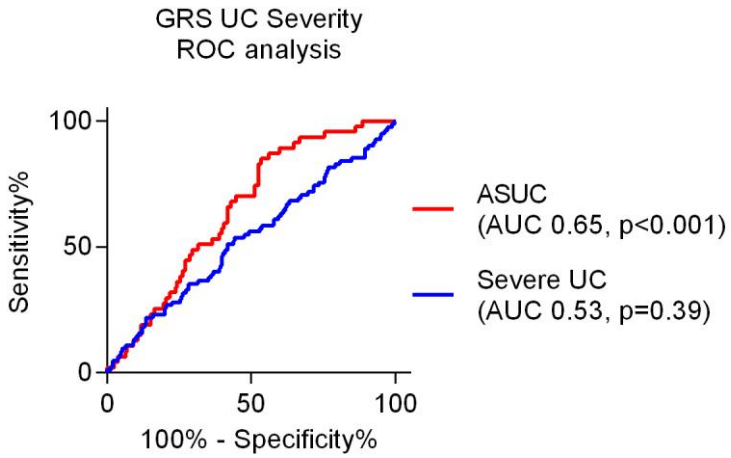

Figure 2.12. GRS ROC curve for UC severity. *In order to determine the capacity for GRS to discriminate between non-severe UC and either ASUC or severe UC, a ROC curve analysis was performed. The AUC and p value were calculated.*

2.3.5.2 GRS quartiles in UC severity

Given that ROC curve analysis revealed a modest but significant capacity for GRS to discriminate between ASUC and non-severe UC, GRS were stratified into quartiles (derived from median and IQR) (*Figure 2.13*) . The observed range of GRS amongst UC patients was 0.069- 12.45.

There was significantly higher proportion of ASUC patients with GRS in the 3rd and 4th quartiles, as compared to non-severe UC patients (p=0.002). However, sensitivity and specificity analysis of the GRS quartiles in discriminating between ASUC and non-severe UC, derived from the ROC curve analysis, revealed a poor combination of sensitivity and specificity for each of the GRS quartiles (*Figure 2.13 and Table 2.6*).

Thus, although GRS are enriched amongst patients with ASUC compared with non-severe UC overall, the capacity to use GRS to discriminate between UC severity phenotype for individual patients is limited.

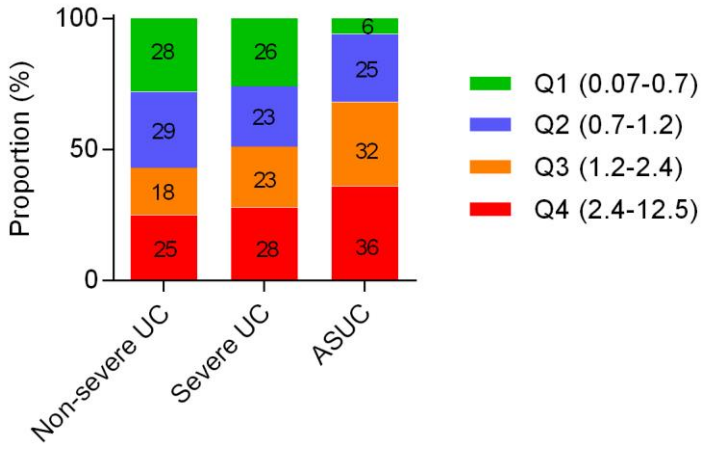

Figure 2.13. GRS quartile analysis in UC severity. *The UC GRS (range 0.069 - 12.46) were stratified into quartiles according to median and IQR as presented. The GRS quartiles for each of the UC severity groups is presented.*

GRS Quartiles (median, IQR)	**ASUC**		
	Proportion	Sensitivity (%)	Specificity (%)
Q1 (n=93) (0.069 - 0.67)	3 (3%)	100	<20
Q2 (n=101) (0.67-1.23)	12 (12%)	93.6	27.9
Q3 (n=78) (1.23-2.37)	15 (19%)	70.2	55.3
Q4 (n=101) (2.37-12.46)	17 (17%)	31.9	77.1

Table 2.6. GRS quartile analysis in UC severity. *Sensitivity and specificity combination for each of the GRS quartiles, for discriminating between non-severe UC and ASUC, as calculated using ROC curve analysis. The lowest GRS of the quartile was used for the sensitivity and specificity analysis.*

2.3.5.3 GRS according to duration of follow-up

Further analysis was performed to interpret whether the duration of patient follow-up influenced the frequency of severity outcomes (ASUC, biologic therapy, or colectomy).

In particular, further analysis of the group of patients with non-severe UC, but higher GRS was undertaken, so as to exclude a follow-up time bias as a factor limiting recognition of severe outcomes.

The duration of follow-up for each of the UC severity groups is shown in *Table 2.7* and depicted in *Figure 2.14*. There was a significantly shorter duration of follow-up observed for patients with ASUC as compared to those with severe UC (median 58.0 vs. 98.0, p=0.008), and a trend toward shorter follow-up as compared to those with non-severe UC (median 58.0 vs. 87.5, p=0.075). The outcome of ASUC was observed to occur at a median of 14 months after UC diagnosis (IQR 0 - 116), and 30% of patients were hospitalised with ASUC at the time of diagnosis of UC. The occurrence of ASUC early in the course of disease is well-documented (127).

UC disease severity category	**Duration of follow-up (median, IQR)**
ASUC (n=47) Median duration to diagnosis ASUC Patients with ASUC at diagnosis of UC	58.0 (28-125) 14 (0-116) 30%
Severe UC (n=82)	98.0 (54-185)
Non-severe UC (n=244)	87.5 (41-200)
Non-severe UC (n=79) GRS >1.8	91.0 (48-251)
Non-severe UC (n= 165) GRS <1.8	82.5 (33-183)

Table 2.7. Duration of follow-up of UC patients according to disease severity. *The median duration of follow-up (IQR) was calculated for patients with UC in each of the severity categories. Those patients with non-severe UC were divided according to their GRS. A cut-off GRS of 1.8 was chosen as this was the median score amongst patients with ASUC.*

Patients with non-severe UC were divided into two groups according to a GRS of >1.8 or ≤1.8. A GRS cut-off of 1.8 was chosen, as this is the median score for patients with ASUC. There was no significant difference in the duration of follow-up between the

two groups. Thus, a follow-up time bias is not an explanation for the lack of severe outcomes amongst patients who have a high GRS.

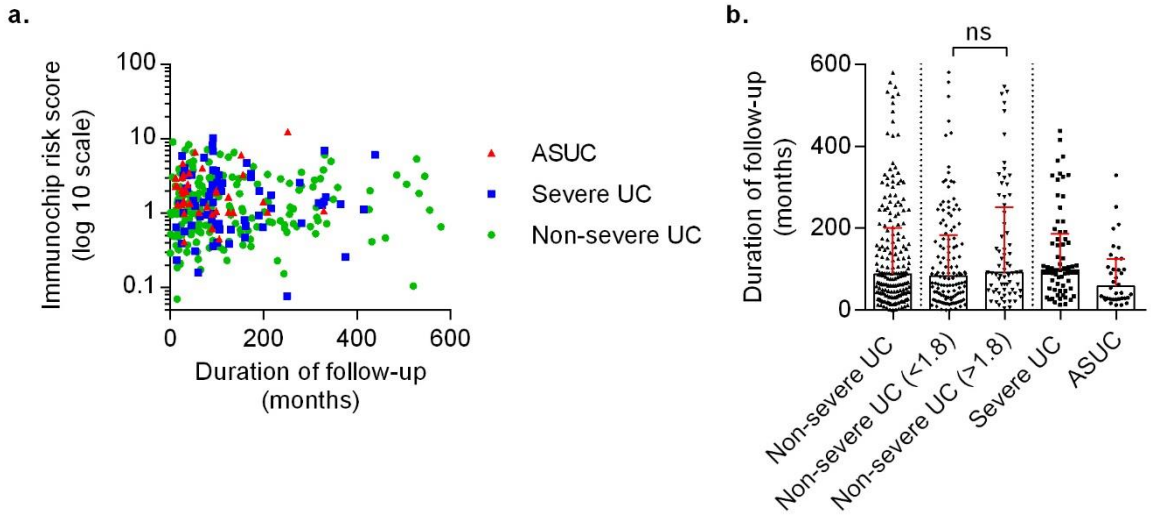

Figure 2.14. Duration of follow-up of UC patients according to disease severity. a). *The graph depicts the correlation between the UC severity categories (ASUC, severe UC, non-severe UC), the duration of follow-up, and the GRS.* ***b).****The median duration of follow-up (IQR) was calculated for patients with UC in each of the severity categories. Those patients with non-severe UC were divided according to their GRS. A cut-off GRS of 1.8 was chosen as this is the median score amongst patients with ASUC. Statistical analysis performed using nonparametric Mann Whitney test (ns, non-significant).*

2.3.5.4 UC-specific loci GRS according to disease severity

In order to investigate whether UC-specific risk loci confer risk for severe disease, GRS were calculated using only the 27 UC-specific loci (*Figure 2.15*).

Analysis of the UC-specific risk loci did not reveal a differential burden of genetic risk between the severity categories. Thus, it is less likely that UC-specific risk loci confer the additional genetic risk burden observed in patients with ASUC. However, the result is influenced by Type 2 error, as the power to detect a difference between the severity groups was reduced by the calculation of GRS from a small number of risk loci.

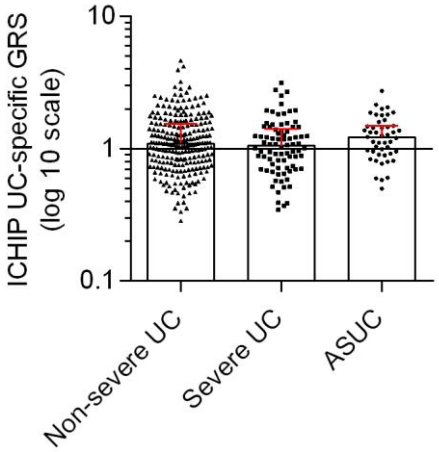

Figure 2.15. GRS derived from UC-specific loci according to severity of UC. *GRS were calculated using the 27 UC-specific risk loci for comparison between the UC severity categories. Data presented as median and IQR.*

2.3.6 RAF analysis in UC severity

Given that the burden of genetic risk was observed to be higher amongst patients with ASUC as compared to non-severe UC, analysis was performed to identify differences in RAF between the groups, both overall and for candidate SNPs.

2.3.6.1 Observed vs. expected RAF in UC severity groups

An initial correlation analysis was performed, in order to compare the observed RAF amongst the UC severity groups, to the expected RAF derived from the Jostins *et al* dataset (7). The observed RAF for the UC severity groups was calculated for each of the 164 SNPs used to calculate the GRS (137 SNPs shared with CD, and 27 UC-specific SNPs) (*Figure 2.16*).

This analysis revealed minimal difference in the overall RAF between the UC severity groups; each group correlated well with the expected RAF (ASUC, r 0.89, $p<0.001$;

Severe UC, r 0.94, p <0.001; non-severe UC, r 0.95, p <0.001).

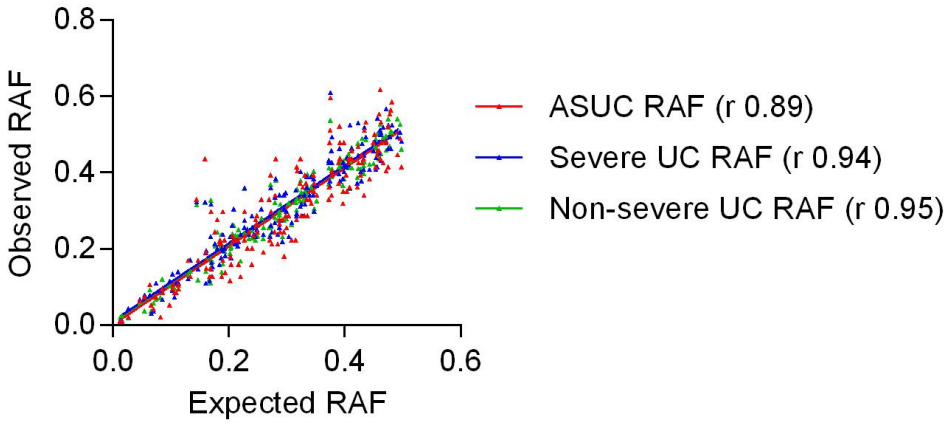

Figure 2.16. Observed vs. expected RAF in UC severity groups. *A correlation analysis was performed to compare the observed RAF amongst the UC severity groups, to the expected RAF derived from the Jostins et al dataset, amongst the 164 UC risk SNPs. Correlation coefficient statistical analysis performed using a nonparametric Spearmans' rank test.*

A further correlation analysis was performed to analyse the observed RAF in patients with ASUC and severe UC, as compared patients with non-severe UC as the 'expected RAF' cohort (*Figure 2.17*). This analysis also revealed a close correlation between the RAF of the ASUC and severe UC severity groups, as compared to the non-severe UC group (ASUC, r 0.93, p<0.001; Severe UC, r 0.97, p <0.001).

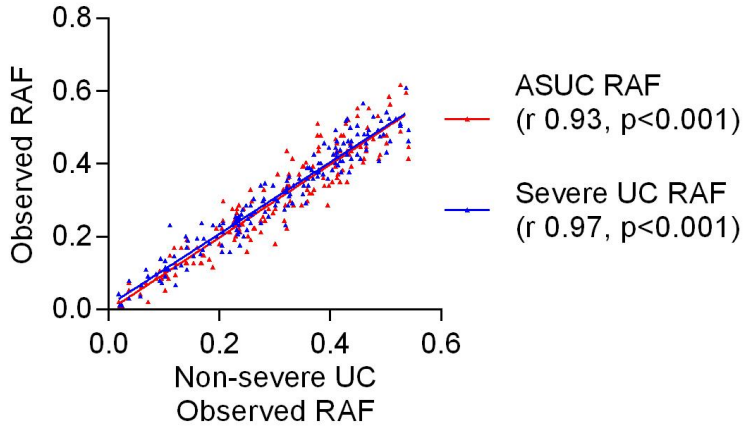

Figure 2.17. ASUC and severe UC RAF compared to non-severe UC 'expected' RAF. *A correlation analysis was performed to compare the observed RAF amongst the ASUC and severe UC group, to the 'expected' RAF derived from the non-severe UC group, amongst the 164 UC risk SNPs. Statistical analysis performed using a nonparametric Spearmans' rank test.*

This analysis implies that the difference in GRS between the UC severity groups may be mediated by differential expression of candidate SNPs, particularly those with a larger OR. It is also possible that multiple small differences in RAF between the groups are amplified by variable effect sizes, thereby generating a slight shift and separation of the GRS.

2.3.6.2 Variance analysis of candidate risk loci in UC severity groups

A detailed variance analysis of differential RAF expression at each of the 164 SNPs was performed, to determine whether any enrichment or reduction of expression of candidate SNPs may have mediated the difference in GRS observed between the UC severity groups.

Initially, variance analysis of the observed RAF of candidate loci amongst patients with ASUC, as compared to the expected RAF derived from the Jostins *et al* dataset, was performed (7). This analysis revealed a >10% differential RAF in multiple SNPs in the

ASUC group, as compared to the expected RAF. The differences were both protective and pathogenic as depicted in *Figure 2.18*. The loci at which the RAF variance conferred risk for UC, either by enrichment of risk alleles, or by reduction in protective alleles, are listed in *Table 2.8*.

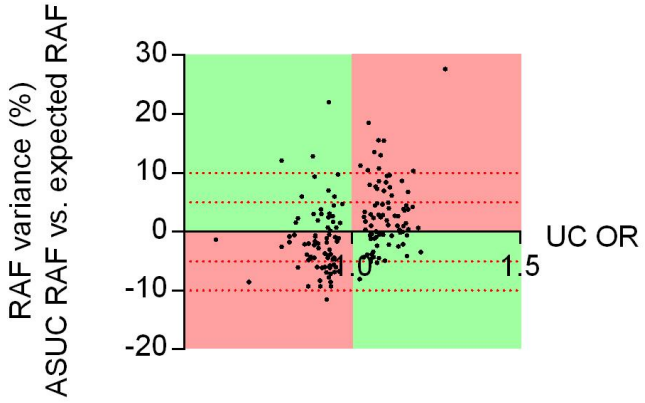

Figure 2.18. Variance analysis of differential RAF in ASUC as compared to expected RAF. *The observed RAF amongst ASUC patients was compared to the expected RAF for 164 UC-risk alleles derived from Jostins et al. The variance (%) is plotted as the difference between the ASUC RAF and the expected RAF. The UC OR is derived from Jostins et al. The red shading illustrates enrichment or reduction in expression of loci denoting 'risk' for UC (higher GRS). Green shading illustrates enrichment of reduction of loci denoting 'protection' for UC (lower GRS).*

SNP	Gene	RA	OR (UC)	Expect RAF	ASUC RAF	Variance
rs3024505	*IL10^*	A	1.277	0.159	0.436	27.7%
rs4256159		A	1.049	0.145	0.329	18.1%
rs11168249	*VDR*	G	1.079	0.461	0.617	15.6%
rs2226628		A	1.095	0.281	0.436	15.5%
rs9358372	*CDKAL1**	G	1.066	0.374	0.510	13.6%
rs2111485	*IFIH1*	A	1.085	0.391	0.521	13.0%
rs670523	*UBQLN4"*	A	1.025	0.323	0.436	11.2%
rs2266959	*MAPK1+*	A	1.08	0.189	0.297	10.8%
rs2930047	*DAP*	G	1.047	0.374	0.478	10.5%
rs4409764	*NKX2-3*	A	1.182	0.4817	0.585	10.3%
rs4743820	*NFIL3*	G	0.924	0.296	0.180	-11.5%

Table 2.8. Variance analysis of differential RAF in ASUC as compared to expected RAF. *The observed RAF amongst patients with ASUC at each of the 164 UC loci was compared to the expected RAF at each loci derived from Jostins et al. The SNPs depicted are those for which there was a 10% variance observed between the RAF in the ASUC group as compared to the expected RAF. *Additional genes associated with locus include E2F3. ^Additional genes associated with locus include IL20, IL19, IL24, PIGR, and MAPKAPK2. +Additional genes at the locus include YDJC, UBE2L3, RIMBP3, CCDC116. "Additional genes at the locus include RIT1, MSTO1. RA, risk allele for UC.*

In a subsequent variance analysis, the observed RAF of candidate loci amongst patients with ASUC, was compared to the RAF amongst patients with non-severe UC, in order to identify candidate SNPs that may have mediated the difference in GRS between the groups (*Figure 2.19 and 2.20, Table 2.9*).

This analysis also revealed >10% differential RAF in multiple SNPs in the ASUC group, as compared to the non-severe UC group. All of these SNPs, aside from one (rs1801274), overlap with those identified in the prior analysis using the expected RAF from the Jostins *et al* dataset (7).

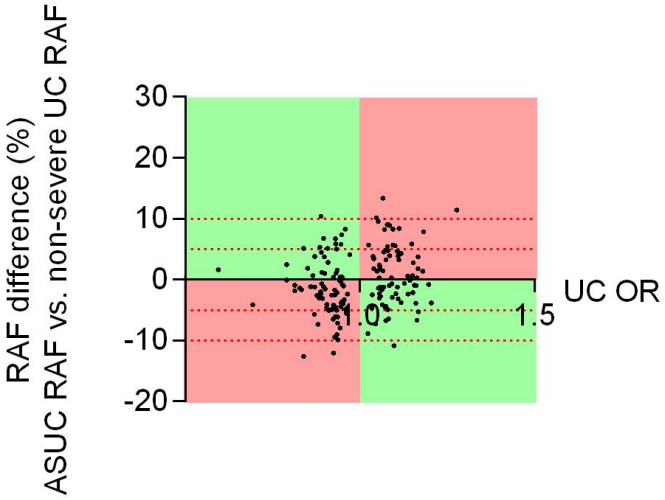

Figure 2.19. Variance analysis of differential RAF in ASUC as compared to non-severe UC. *The observed RAF amongst ASUC patients was compared to the RAF amongst patients with non-severe UC for 164 UC-risk alleles. The variance (%) is plotted as the difference between the ASUC RAF and the non-severe RAF at each loci. The UC OR derived from Jostins et al. The red shading illustrates enrichment or reduction in expression of loci denoting 'risk' (higher GRS). Green shading illustrates enrichment of reduction of loci denoting 'non-risk' (lower GRS).*

SNP	Gene	OR (UC)	Expect RAF	ASUC RAF	Severe RAF	N-S RAF	Var-iance	P value
rs9358372	*CDKAL1**	1.07	0.375	0.510	0.378	0.377	13.5%	0.015
rs3024505	*IL10*^	1.28	0.159	0.436	0.323	0.321	11.4%	0.032
rs2930047	*DAP*	1.05	0.374	0.478	0.365	0.377	10.2%	0.065
rs1801274	FCGR2A~	0.84	0.475	0.414	0.463	0.541	-12.6%	0.025
rs4743820	*NFIL3*	0.92	0.296	0.180	0.305	0.301	-12.0%	0.018

Table 2.9. Variance analysis of differential RAF in ASUC as compared to non-severe UC. *The RAF amongst patients with ASUC at each of the 164 UC loci was compared to the RAF amongst patients with non-severe UC. The SNPs depicted are those for which there was a 10% variance observed between the RAF in the ASUC group as compared to the expected RAF. *Additional genes associated with locus include E2F3. ^Additional genes associated with locus include IL20, IL19, IL24, PIGR, and MAPKAPK2. ~Additional genes associated with locus include* FCGR2B, FCGR3A, HSPA6, FCGR3B, FCRLA. *RA, risk allele for UC, N-S, non-severe. Statistical analysis performed using Chi-square test (comparing ASUC to non-severe UC).*

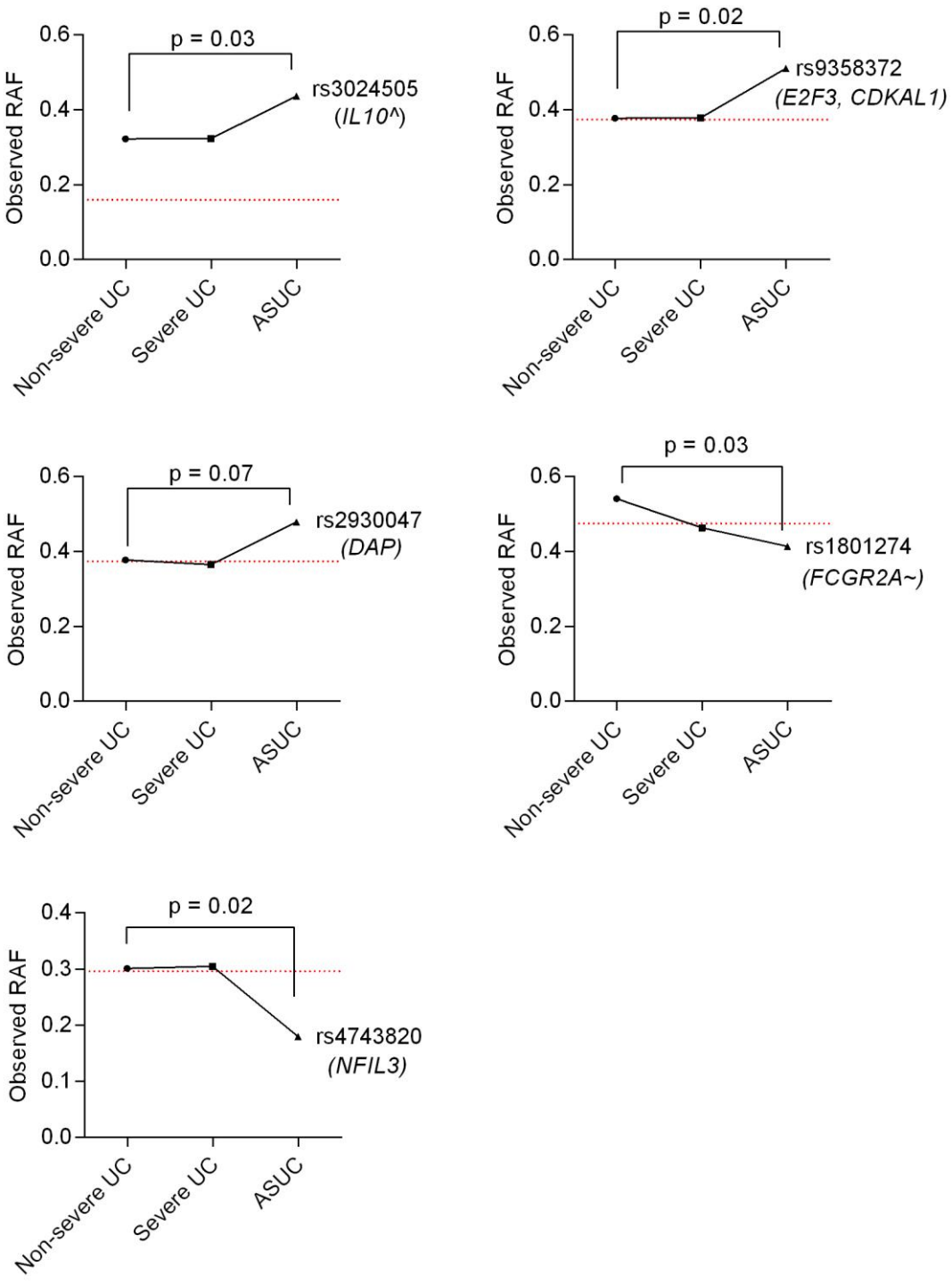

Figure 2.20. SNPs showing differential RAF in ASUC as compared to non-severe UC. *The 5 SNPs for which there was a 10% variance in RAF observed between patients with ASUC as compared to patients with non-severe UC. ^Additional genes associated with locus include IL20, IL19, IL24, PIGR, and MAPKAPK2. ~Additional genes associated with locus include* FCGR2B, FCGR3A, HSPA6, FCGR3B, FCRLA. *Statistical analysis performed using Chi-square test (comparing ASUC to non-severe UC).*

2.3.6.3 Heterozygous and homozygous status of candidate risk loci in ASUC

In order to interpret the significance of the candidate loci variance between patients with ASUC and non-severe UC, the rates of heterozygosity and homozygosity were analysed between the groups (*Table 2.10*).

The analysis did not reveal a significant difference between the non-severe UC and ASUC groups in the relative proportions of patients homozygous for the risk or protective alleles at the candidate SNPs.

SNP	**Gene**	**ASUC**		**Severe UC**		**Non-severe UC**		**p value**
		Het	**Homo**	**Het**	**Homo**	**Het**	**Homo**	
rs9358372	E2F3, CDKAL1	26 0.55	11 0.23	38 0.46	12 0.14	104 0.42	40 0.16	0.25
rs3024505	*IL10*^	17 0.36	12 0.26	27 0.33	13 0.16	77 0.32	40 0.16	0.13
rs2930047	*DAP*	23 0.49	11 0.23	30 0.37	15 0.18	110 0.45	37 0.15	0.16
rs1801274	FCGR2A~	23 0.49	16 0.17	44 0.54	22 0.20	114 0.47	55 0.31	0.09
rs4743820	*NFIL3*	13 0.28	2 0.04	36 0.44	7 0.09	99 0.41	24 0.10	0.22

Table 2.10. Heterozygous and homozygous analysis of candidate risk loci in ASUC. *The absolute and relative frequency heterozygotes and homozygotes for the 5 SNPs for which there was a 10% variance in RAF observed between patients with ASUC as compared to the RAF for patients with non-severe UC. ^Additional genes associated with locus include IL20, IL19, IL24, PIGR, and MAPKAPK2. ~Additional genes associated with locus include* FCGR2B, FCGR3A, HSPA6, FCGR3B, FCRLA. *Het, heterozygous; homo, homozygous. Statistical analysis performed using Chi-square test (comparing ASUC to non-severe UC).*

2.3.7 Interrogation of IL-10 signalling pathway in ASUC

Enrichment of the risk allele at the SNP rs3024505, associated with the *IL10* gene, is a plausible contributor to the risk of ASUC in the examined cohort. Further implicating the IL-10 signalling pathway in ASUC, is the significant reduction in expression of the protective allele at the SNP rs4743820, associated with the *NFIL3* gene. NFIL3 is a

transcription factor, which has been identified as a key component of the IL-10 immune-regulatory pathway (134).

In order to further investigate the possibility of cumulative genetic defects within the IL-10 signalling pathway contributing to risk of ASUC, candidate SNPs associated within known gene loci within the pathway were examined (*Table 2.11, Figure 2.21*).

The IL-10 signalling pathway analysis, incorporating 7 SNPs, suggested a cumulative burden of polymorphisms conferring 'risk' for UC. The majority of the alleles within the IL-10 signalling pathway confer a 'protective' effect (OR <1), which is consistent with the regulatory and homeostatic function of the pathway. Thus, cumulative defects signal a loss of immune regulation in UC.

The analysis is grossly underpowered for any conclusive findings, however the signal yielded is valuable, as it implicates a plausible biological pathway in ASUC, and sets the scene for analysis in a replication cohort.

SNP	**Gene**	**OR**	**Expect RAF**	**ASUC RAF**	**Severe RAF**	**Non-severe RAF**	**Var-iance**	**P value**
rs3024505	*IL10^*	1.28	0.159	0.436	0.323	0.321	11.4%	0.032
rs4743820	*NFIL3*	0.92	0.296	0.180	0.305	0.301	-12.0%	0.018
rs2284553	*IL10RB~*	0.89	0.399	0.352	0.379	0.398	-4.6%	0.397
rs12942547	*STAT3"*	0.92	0.422	0.362	0.372	0.387	-2.6%	0.448
rs1517352	*STAT1 STAT4*	0.94	0.392	0.436	0.463	0.439	-0.2%	0.929
rs11879191	*TYK2+*	0.89	0.203	0.180	0.232	0.201	-2.0%	0.608
rs10758669	*JAK2*	1.17	0.3466	0.351	0.384	0.403	-5.26%	0.105

Table 2.11. Candidate loci in the IL-10 signalling pathway in ASUC. *The RAF at SNPs implicated in IL-10 signalling pathways, was compared between ASUC and non-severe UC patients. ^Additional genes associated with locus include IL20, IL19, IL24, PIGR, and MAPKAPK2. ~Additional genes at the locus IFNGR2, IFNAR2, IFNAR1."Additional genes associated with locus include STAT5B, STAT5A. + Additional genes at the locus PPAN-P2RY11, ICAM1. All odds ratios (OR) are provided for UC, aside for IL10RB which has only a CD-specific OR.*

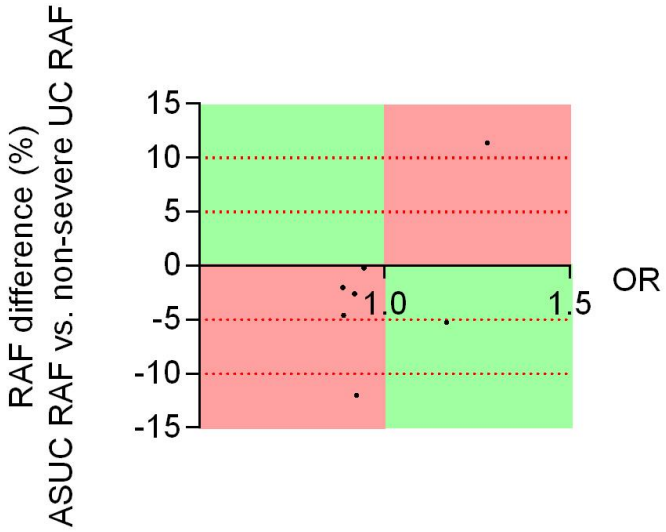

Figure 2.21. Candidate loci in the IL-10 signalling pathway in ASUC. *The observed RAF amongst ASUC patients was compared to the RAF amongst patients with non-severe UC at loci associated with the IL-10 signalling pathway. The variance (%) is plotted as the difference between the ASUC RAF and the non-severe RAF as each loci. The UC OR is derived from Jostins et al. The red shading illustrates enrichment or reduction in expression of loci denoting 'risk' (higher GRS). Green shading illustrates enrichment of reduction of loci denoting 'non-risk' (lower GRS).*

2.4 DISCUSSION

In this thesis chapter, it was investigated whether the burden of genetic risk in patients with UC, as reflected by a GRS, is associated with clinical disease phenotype. Furthermore, a detailed examination of candidate risk loci was performed upon identification of enriched GRS amongst patients with ASUC.

2.4.1 GRS and age of diagnosis of UC

It is demonstrated in this chapter, that patients who are diagnosed with UC before the age of 10 (EOIBD), have a higher burden of genetic risk than those who are diagnosed with UC in adulthood. This finding is consistent with established literature on heritability in the EOIBD cohort, as there is a higher prevalence of first degree family members affected by IBD among this group (9, 10, 27).

2.4.2 GRS and UC disease severity

In this thesis chapter, it is demonstrated that patients who have a history of ASUC, have a significantly higher genetic risk burden than those patients who have had a non-severe UC disease course. The association between GRS and clinical outcome in this cohort was not accounted for by the duration of follow-up. In fact, patients with a diagnosis of ASUC had a shorter median duration of follow-up overall. Patients with a history of severe UC, defined by a requirement for surgery or biologic therapy, but without a discrete episode of ASUC, had a higher median GRS than patients with non-severe UC, although not significantly so.

Prior studies analysing the use of GRS in predicting the course of UC have revealed conflicting findings (14, 15). In a cohort of 861 patients with UC, Haritunians *et al*, showed that a GRS, comprising 46 SNPs identified during unbiased GWAS, was able to explain 48% of variance in colectomy risk, with a sensitivity of 79% and specificity of

86% (15). Amongst patients in the highest GRS quartile, the colectomy rate was 100% (15). In contrast, amongst a cohort of 408 patients with UC, GRS incorporating 133 UC-risk loci (7), did not show any association with disease phenotype (14). The definition of 'severe UC' in this latter study was broad, and included patients requiring immunomodulatory therapy, as well as those requiring biologics or colectomy. There was however, an association observed between a family history of UC and GRS.

The categorisation of patients with ASUC as a distinct group is important, as it represents the most severe manifestation and extreme phenotype of UC (30, 35). Patients with ASUC require hospitalisation, and depending on the biologic severity of disease on admission, rates of colectomy range from 8.5% to 48% per episode (41, 118, 135). Furthermore, ASUC carries a small but real risk of mortality (around 1%), which is particularly confronting given the young demographic afflicted (32). Recognition of ASUC as distinct from 'refractory' UC, is in keeping with a 'sequencing of the extremes' approach, akin to prior studies of genetic prognostication in CD (11, 93).

ASUC is not described as a distinct phenotype in prior genotype-phenotype studies using GRS (14, 15). There is only a single prior study reporting on ICHIP analysis of 111 patients meeting clinical criteria for ASUC (127). Analysis of 45 SNPs (derived from the 46 SNPs identified by Haritunians *et al* (15)), revealed a significant association for only one SNP (rs2403456) with ASUC.

2.4.3 Discriminatory capacity of GRS in UC severity

The clinical applicability of any risk prediction tool is dependent upon its capacity to discriminate between individual patients. In this thesis chapter, it is shown that the application of GRS alone, has only a very modest capacity to discriminate between individual patients with ASUC and non-severe UC. ROC curve analysis revealed an

AUC of 0.65 ($p<0.001$), which means that only 65% of patients with ASUC will have a higher GRS than patients with non-severe UC. Although a larger proportion of patients with ASUC were represented in the higher GRS quartiles, the concordant sensitivity and specificity was poor. Further analysis of patients with non-severe UC but a high GRS, did not reveal a follow-up time bias to account for the limited detection of severity outcomes in this group. Thus, GRS alone, do not offer sufficient discriminatory capacity to prognosticate the risk of ASUC in patients with UC. However, it should be acknowledged that the failure to generate a more comprehensive predictive model of UC severity, incorporating known clinical predictive factors of UC severity (described in *Section 2.1.1*), is a primary limitation of experimental strategy in this chapter (further discussed in *Section 2.4.5*).

2.4.4 Variance of candidate loci in ASUC

In order to further investigate the finding of higher GRS amongst patients with ASUC, variance analysis of risk allele expression between the UC severity groups was performed.

Given the close overall correlation between the observed RAF for each of the UC severity groups, it was hypothesised that the difference in GRS between the UC severity groups was mediated by differential expression of candidate risk loci, particularly those carrying a higher OR. Another possibility was that multiple small differences in RAF between the groups, may be amplified by the effect size (OR) imparted by differentially expressed SNPs, thereby separating the risk scores.

The candidate SNP variance analysis revealed both significant enrichment and reduction of candidate loci in patients with ASUC. Accordingly, the biological roles of the implicated genes were further explored (*Table 2.12*).

Risk loci	Gene	Cellular expression and function	Putative role in intestinal inflammation
rs9358372	*CDKAL1**	-Expressed in CD4+ and CD19+ lymphocytes. -Regulatory subunit protein. -Strong association with diabetes mellitus (136).	-Regulatory subunit protein -Down-regulated in the context activation (137). -Likely related to T cell signalling though no clear experimental evidence in IBD.
rs3024505	*IL10*^	-Expressed in Treg cells and APC's -Regulatory cytokine, important in intestinal homeostasis.	-IL-10 and IL-10R deficient mice develop spontaneous enterocolitis (138, 139). -*IL10* and *IL10R* mutations cause VEOIBD (10, 78, 80).
rs1801274	FCGR2A~	-Expressed in many immune cells. -Encodes Fc receptor of gamma immunoglobulins.	-Polymorphisms confer protection in UC (7, 55). -Variants in *FCGR2A* associated with risk of relapse in UC (140).
rs4743820	*NFIL3*	- Expressed in NK cells, myeloid cells, innate lymphoid cells. -Transcription factor. -Role in IL-10 regulation pathway.	-Mouse models show that NFIL3 is critical in gut innate lymphoid cell development (141). -NFIL3 deficient mice show increased susceptibility to bacterial infection *Citrobacter rodentium* and *Clostridium difficile* (142, 143).

Table 2.12. The cellular expression and biological function of differentially expressed risk alleles in ASUC. *^Additional genes associated with locus include IL20, IL19, IL24, PIGR, and MAPKAPK2. *Additional genes associated with locus include E2F3. ~Additional genes associated with locus include* FCGR2B, FCGR3A, HSPA6, FCGR3B, FCRLA.

2.4.4.1 IL-10 signalling pathway in ASUC

IL-10 is a key regulatory cytokine, which plays an important role in intestinal homeostasis, maintaining the delicate balance between pro-inflammatory and anti-inflammatory cytokines in the setting of commensal microbiota (*Figure 2.1, Figure 2.22*) (144). IL-10 is primarily derived from Treg cells, as well as via autocrine-paracrine signalling from activated myeloid cells (138, 145). IL-10 drives the generation of Treg cells, and acts to antagonise the expression of MHC class II molecules, as well

as pro-inflammatory cytokines IL-1β, IL-6, IL-8, TNF-α, and IL-12/IL-23 (138, 146-149).

The crucial role of IL-10 in preventing deleterious intestinal inflammation has long been demonstrated by the development of spontaneous enterocolitis in IL-10 knock-out mice (139, 150). Loss of function mutations in the *IL10* and *IL10R* genes have been identified in patients with VEOIBD, with associated defects in functional IL-10 signalling pathways (9, 10, 78, 80, 81, 86). Immunosuppression of affected patients is ineffective, but rather therapy with allogeneic stem cell transplantation has some efficacy in remission induction (78, 81, 151).

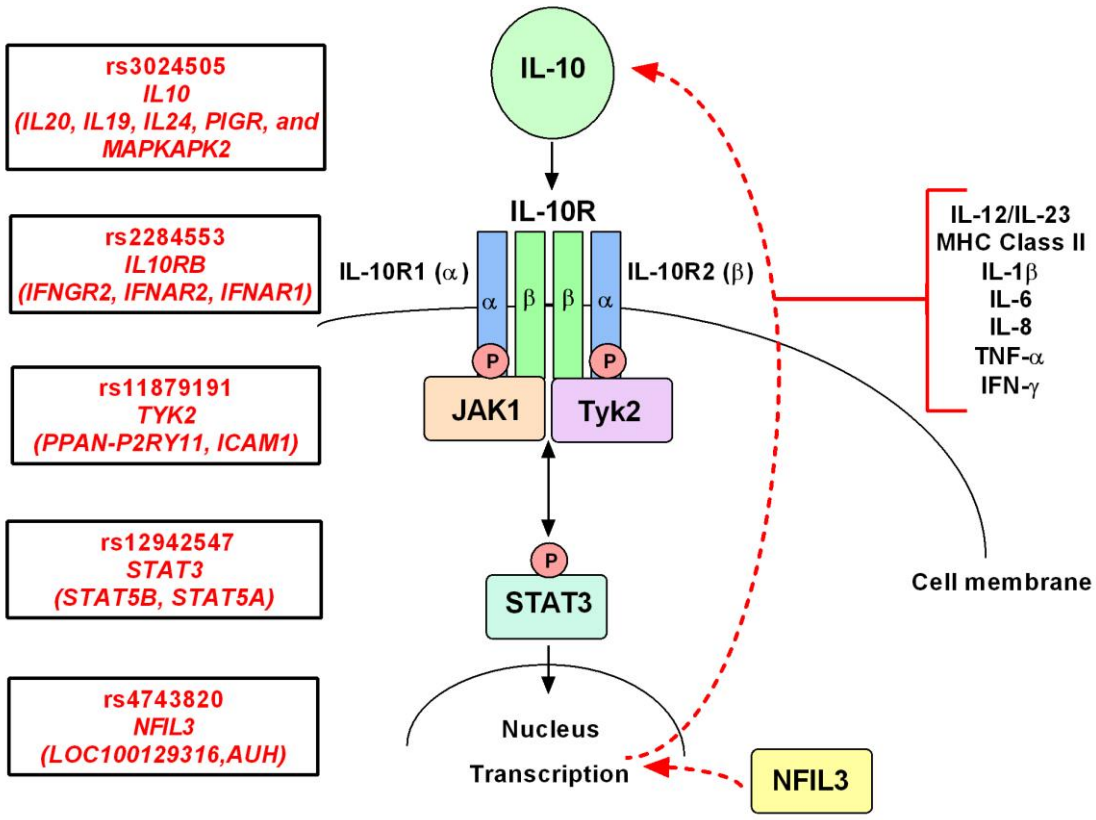

Figure 2.22. IL-10 signalling pathway and associated genetic loci. *Interaction of IL-10 cytokine with the IL-10 receptor (consisting of a tetramer: IL-10R1 and IL-10R2), leads to activation of JAK1 and Tyk2, with subsequent phosphorylation of STAT3. STAT3 then translocates to the cell nucleus where it regulates transcription of target genes. Further regulation of transcription is mediated NFIL3, which is under the influence of the IL-10 signalling pathway. The SNPs corresponding with the genetic loci within the IL-10 pathway are listed. Adapted from (7, 86).*

Significant enrichment of the risk allele at the SNP rs3024505 was demonstrated in patients with ASUC (*Figure 2.23*). The effect size reported for this SNP is amongst the largest for any UC polymorphism (OR 1.277), behind only *IL23R* and *HLA-DQB1/HLA-DRB1* polymorphisms (7). When the effect size is coupled with the significant variance of expression between ASUC and non-severe patients, it seems likely that rs3024505 wielded a significance influence on the enrichment of GRS observed amongst patients with ASUC.

The rs3024505 SNP is reported to flank the *IL10* gene (59). The SNP is in close linkage with other polymorphisms within the *IL10* gene, and is thus considered a likely regulator of *IL10* gene expression (59). Jostins *et al* report the SNP to be also associated with *IL20, IL19, IL24, PIGR, and MAPKAPK2 (7).* The rs3024505 polymorphism has been associated with UC susceptibility in three European GWAS meta-analyses (7, 55, 59), as well as an association study in a North Indian UC cohort (152). In addition, the rs3024505 polymorphism is strongly associated with other autoimmune diseases, in particular SLE (153). The rs3024505 polymorphism has been associated a younger age of diagnosis of UC (<40 years) in a Danish cohort study (154). Furthermore, the rs3024505 polymorphism has previously been identified to be associated with medically-refractory UC in the study by Haritunians *et al* (15). In CD, the rs3024505 polymorphism has been associated with an early age of CD diagnosis, stricturing disease, and requirement for surgery, however no difference in serum IL-10 levels were demonstrated (155).

Detailed analysis of genes within the IL-10 signalling pathway, revealed that for the majority of loci, there was differential expression between patients with ASUC and non-severe UC, which conferred a loss of the immunoregulatory 'protective' effect of the IL-10 signalling pathway (*Table 2.11, Figure 2.22*). In particular, a significant reduction

in expression of the protective allele at the SNP rs4743820, associated with the *NFIL3* (nuclear factor, IL3 regulated) gene, was demonstrated in ASUC patients. IL-10 has been shown to regulate NFIL3 expression in activated macrophages, implicating NFIL3 as a component of the IL-10 signalling pathway (134). Although it is acknowledged that this study was grossly underpowered for conclusive findings, this analysis suggests a cumulative defect in the IL-10 signalling pathway in patients with ASUC.

2.4.5 Limitations of experimental strategy

There are important weaknesses of the experimental strategy employed in this chapter which warrant discussion.

ICHIP limitations

The limitations of the ICHIP are discussed in detail in *Section 2.1.3*, one of which is the under-representation of non-European populations in ICHIP development (8, 129). Although the Oxford cohort genotyped by ICHIP is predominantly of white European descent derived from the Oxfordshire population, stringent analysis of racial background was not performed. Thus, there was failure to control for non-European patient sampling within the Cohort, which may have a bearing on results.

Small sample size and lack of replication cohort

Despite the thorough phenotypic dataset, the conclusions that may be drawn from the ICHIP genotyping of UC patients in this chapter are limited due to the small sample size studied. The limited dataset, particularly for patients with ASUC, meant that there was insufficient power for analyses, particularly in the identification of candidate risk loci. The small patient numbers also precluded meaningful GRS in immunological pathways, as analysis of a smaller number of risk loci, further diminished power for significant observations to be made.

Any novel genetic observations within a small cohort of patients, requires a replication dataset to confirm the findings, which was not performed as a part of the work for this thesis chapter (102).

Lack of control for clinical and environmental factors

The lack of incorporation and control of clinical variables, alongside genetic factors in predicting UC phenotype is a primary limitation of this thesis chapter. The inclusion of clinical variables may add strength to the GRS data, yielding greater predictive power than either factor alone. The alternative is also possible, that the inclusion of clinical factors may null any predictive value of GRS.

The lack of control for environmental factors, in particular, factors such as smoking and the intestinal microbiota 'enterotype', also limits interpretation of GRS in predicting UC phenotype.

Family history data

A primary strength of the analysis in this thesis chapter is the quality of the phenotypic dataset, however, the data on family history of IBD is lacking. The overall first degree family history amongst UC patients genotyped by ICHIP was 5%, which is lower than expected given the cohort is enriched for severe disease (14). This may have limited the ability to detect an increased genetic risk burden amongst those with a family history of IBD, which has been shown by other groups (14). The likely explanation is that family history was gleaned in retrospect from the patient case-notes by data-clerks, rather than via a dedicated history or questionnaire.

2.4.6 Conclusions and future directions

The findings of this thesis chapter provide the basis for further research into genotype-phenotype relationships in UC. It is demonstrated that GRS are higher amongst patients with early onset UC, as well as amongst those with a history of ASUC. Genetic variance is demonstrated in the IL-10 cytokine signalling pathway in patients with ASUC, particularly at the SNP rs3024505, which is hypothesised as the likely explanation for the enrichment of GRS in the ASUC group. Despite the small sample size being underpowered for definitive analysis, the signal for a cumulative defect in IL-10 signalling in patients with ASUC, provides the basis for further analysis in a larger replication cohort.

Further experimental work planned by our group includes:

- Further detailed interrogation of genetic loci within immunological pathways, in particular, the IL-10 signalling pathway.
- Recruitment of a replication cohort for GRS and candidate risk loci (IL-10 signalling) analysis from a collaborative Centre.
- Multivariate analysis including clinical, environmental, and genetic factors to establish a more comprehensive risk predictive model in UC.

CHAPTER 3: *NOX1* VARIANT IN VERY EARLY ONSET COLITIS

3.1 INTRODUCTION

The GWAS and ICHIP risk loci explain only a small proportion of total disease variance in UC (7). At least some of the 'missing heritability' in IBD is hypothesised to relate to rare variants (9, 10, 129). Rare variants may have larger functional effects than common variants, and thus may be enriched in the population of patients with onset of IBD at a very young age and amongst those with a severe disease phenotype. There is an increasingly recognised spectrum of monogenic diseases that lead to IBD-like intestinal inflammation, via mechanistic pathways such as epithelial barrier function disruption, impaired phagocytosis, T and B cell defects, hyper- and auto-inflammatory disorders, and deranged immune-regulation (9, 10).

In this thesis chapter, investigation of a novel rare *NOX1* variant in a single patient with VEOIBD is performed.

3.1.1 Reactive oxygen species

Oxygen is a reactive molecule that can react with a wide range of organic elements and compounds (156). Reactive oxygen species, metabolites, or intermediates (ROS), are a group of oxygen-derived chemically reactive ions, radicals, and molecules (*Figure 3.1*) (156, 157). Oxygen radicals include superoxide, hydroxyl, peroxyl, and non-radicals include hydrogen peroxide, ozone, singlet oxygen, and hypochlorous acid. ROS generation involves a sequence of reactions that begin with the generation of superoxide from oxygen (156, 157).

The reactivity of individual ROS varies greatly. Superoxide can function as either a reductant or as an oxidant, depending on the oxidation-reduction potential of the reacting molecule (158). Superoxide is considered only weakly toxic, as it does not

disseminate far from the site of production, is largely membrane-impermeable, and reacts with only a limited number of molecules (156, 158). However, superoxide is the precursor to more reactive ROS, as it rapidly and spontaneously dismutates to hydrogen peroxide, particularly in the setting of a low pH, or upon enzymatic conversion via superoxide dismutase (SOD).

Hydrogen peroxide is a more potent oxidant than superoxide and reacts with a wider range of biological molecules and compounds. The wider reactivity of hydrogen peroxide is aided by features of membrane permeability and relatively stability, enabling wider diffusion from the site of production (156). The toxicity of hydrogen peroxide is increased by its conversion to highly reactive ROS. Peroxidases, such as myeloperoxidase (MPO) produced by phagocytes, act to convert hydrogen peroxide to the highly toxic hypochlorous acid, which is the primary MPO product in neutrophil phagosomes. Hypochlorous acid is highly reactive, and reacts to form hydroxyl radicals, chloramines, and singlet oxygen, all of which are toxic and produce marked oxidative damage in cells. Conversion of hydrogen peroxide to the hydroxyl radical, may also occur via reaction with ferric (Fe^{3+}) or ferrous (Fe^{2+}) iron (156).

The more toxic ROS species described, are usually only generated in the context of inflammation in the presence of MPO, in which setting they are normally contained within intracellular compartments such as the phagosome (156, 158). The ROS produced by non-phagocytic cells is more limited and less reactive, and is thus likely to oxidise only a narrow range of target molecules for specific biological functions, rather than inducing wide-spread tissue damage (158).

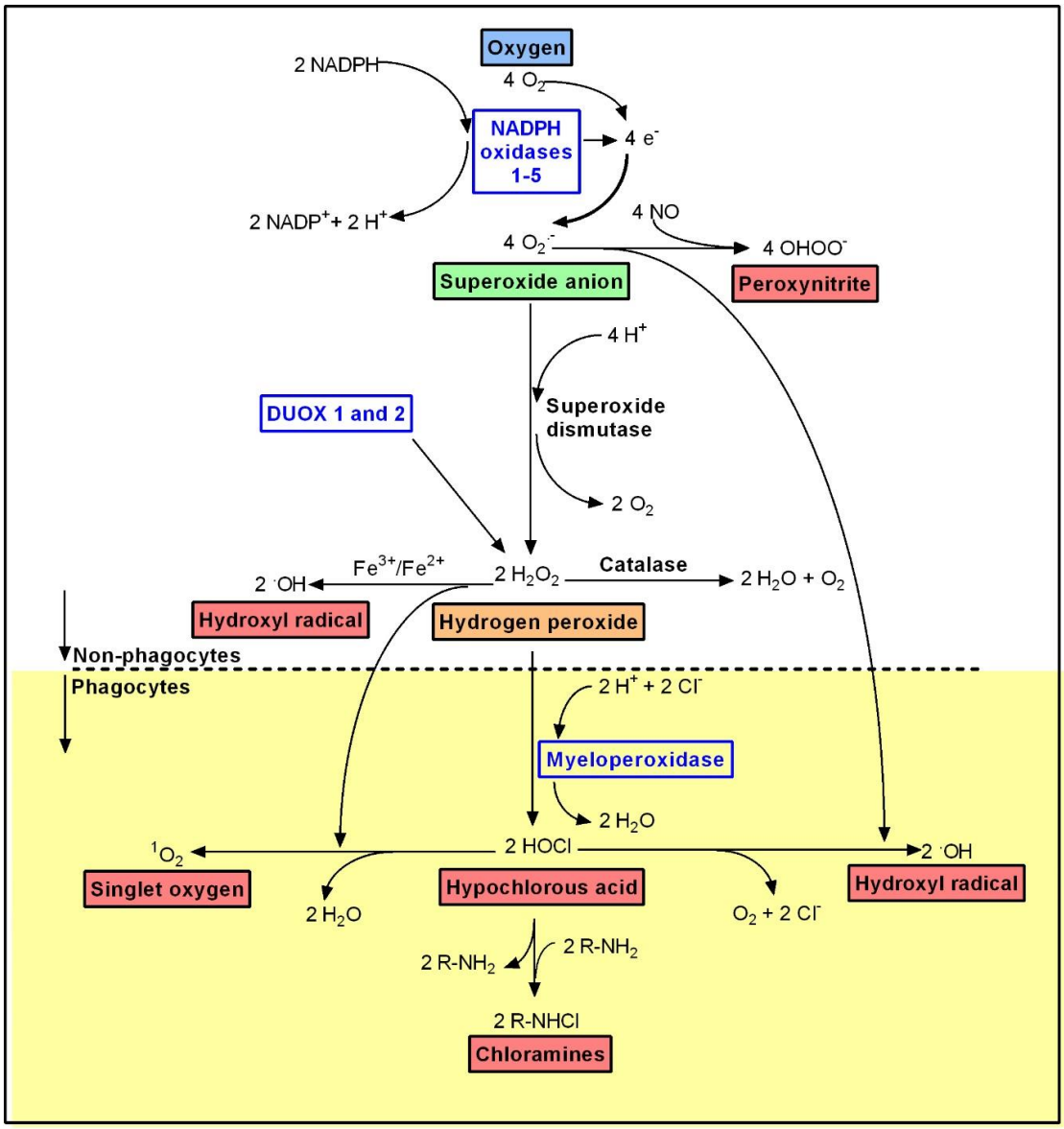

Figure 3.1. ROS derived from the NOX and DUOX enzymes. *Superoxide is the primary ROS generated by NOX1-5 and leads to a cascade of reactions which generate ROS including hydrogen peroxide and the hydroxyl radical. DUOX1 and 2 directly generate hydrogen peroxide. The lower portion of the diagram depicts the highly toxic ROS generated within phagosomes of phagocytes in the presence of MPO. Key to reactivity of oxygen species: blue, relatively unreactive; green, limited reactivity; orange, moderate reactivity; red, high reactivity and non-specificity. (Diagram adapted from (156, 158)).*

3.1.2 Sources of ROS and cellular antioxidants

There are both exogenous and endogenous sources of ROS (*Figure 3.2*). Environmental exposures including tobacco smoke, air pollutants, and ionising radiation are well-described exogenous sources of ROS (159-162). Endogenous sources of ROS include the NOX and dual oxidase (DUOX) enzymes, mitochondria, ER, xanthine oxidase, and cyclooxygenases. In order to maintain ROS homeostasis, there are cellular mechanisms for catabolism of ROS by antioxidant systems, as well as non-enzymatic reaction with small molecules (162). SOD catalyses the conversion of superoxide into hydrogen peroxide and oxygen. Catalase then catalyses the decomposition of hydrogen peroxide to water and oxygen. Glutathione is an antioxidant with conserved function across many species of plants and animals, which in its reduced form, is able to donate a reducing equivalent (hydrogen ion or an electron) to ROS.

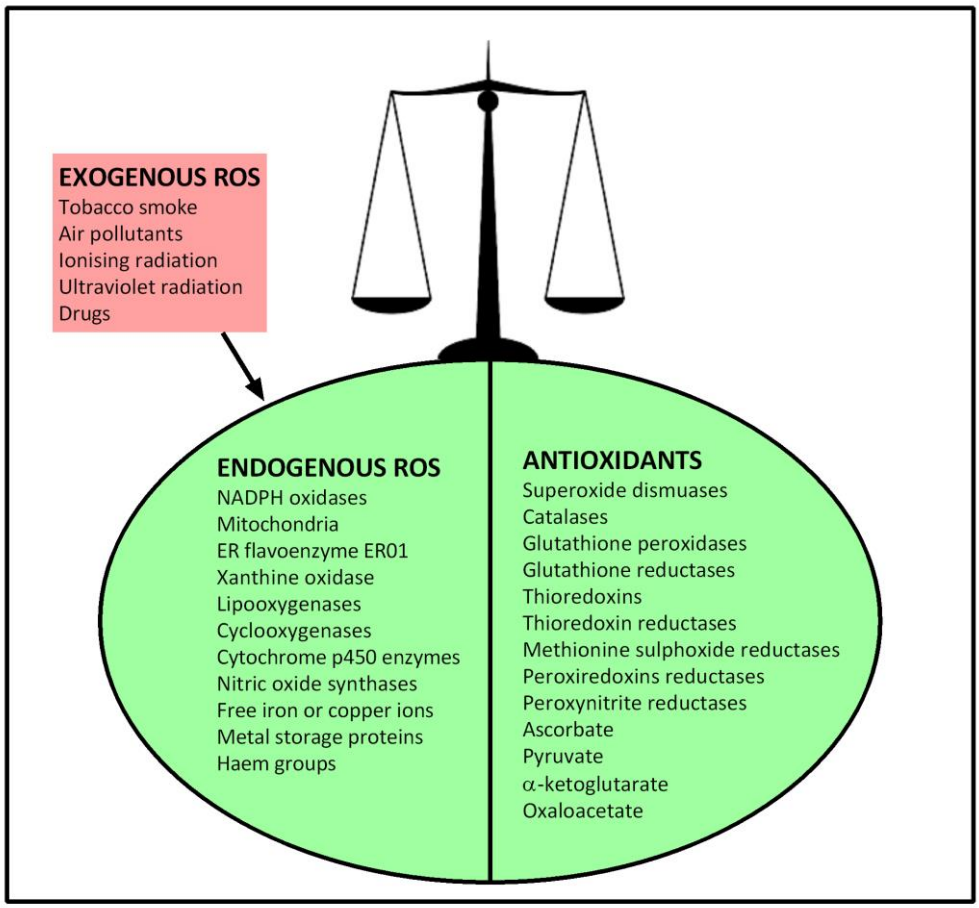

Figure 3.2: Sources of ROS and cellular antioxidants. *Exogenous and endogenous sources of ROS along with antioxidant systems. Figure adapted from (162).*

3.1.3 The structure of the NOX and DUOX enzymes

The NOX family consists of 7 members; NOX1-5 and DUOX1-2, each of which demonstrates conserved common catalytic components to facilitate transmembrane electron transfer to molecular oxygen, in order to generate ROS (156, 157, 163).

Each of the NOX family has a C-terminus intracellular domain containing NADPH and flavin adenine dinucleotide (FAD) binding sites, 6 conserved transmembrane domains adjoining an N-terminus, and 2-4 conserved haem-binding histadines within the transmembrane domain (*Figure 3.3*) (164, 165). This structure allows cytoplasmic NADPH to be converted into NADP+ at the NADPH binding site, thereby liberating

two electrons, which are passed to FAD. The electrons are then passed via the haem groups onto molecular oxygen in the extracellular or intra-phagosomal space, resulting in the formation of superoxide anion (156).

The NOX and DUOX family may be subdivided into three groups based on the presence of structural components in addition to the basic $gp91^{phox}$ heterodimer, which was first identified to be the fundamental catalytic unit of the NOX2 enzyme (158).

1. NOX1, NOX3, and NOX4 are structurally very similar to NOX2, and each produces superoxide (164).
2. NOX5 is unique in that it demonstrates an additional cytoplasmic domain at the N-terminus that contains 4 EF- hands that act as binding sites for calcium (157, 164). Accordingly, NOX5 is able to be activated in response to elevated cytoplasmic calcium concentrations, and is also a superoxide producing enzyme (166).
3. DUOX 1 and 2 enzymes each have an additional extracellular peroxidase domain as well as intracellular EF hands on the N-terminus to bind calcium (156, 157). DUOX1 and 2 directly generate hydrogen peroxide, although it has been proposed that superoxide is primarily generated but is unable to be detected due to rapid intramolecular dismutation (157). The function of the extracellular DUOX peroxidase domain remains a contentious subject, as the DUOX peroxidase lacks essential amino acids for function, and DUOX is often co-expressed with other peroxidases (lactoperoxidase and thyroid peroxidase) (157).

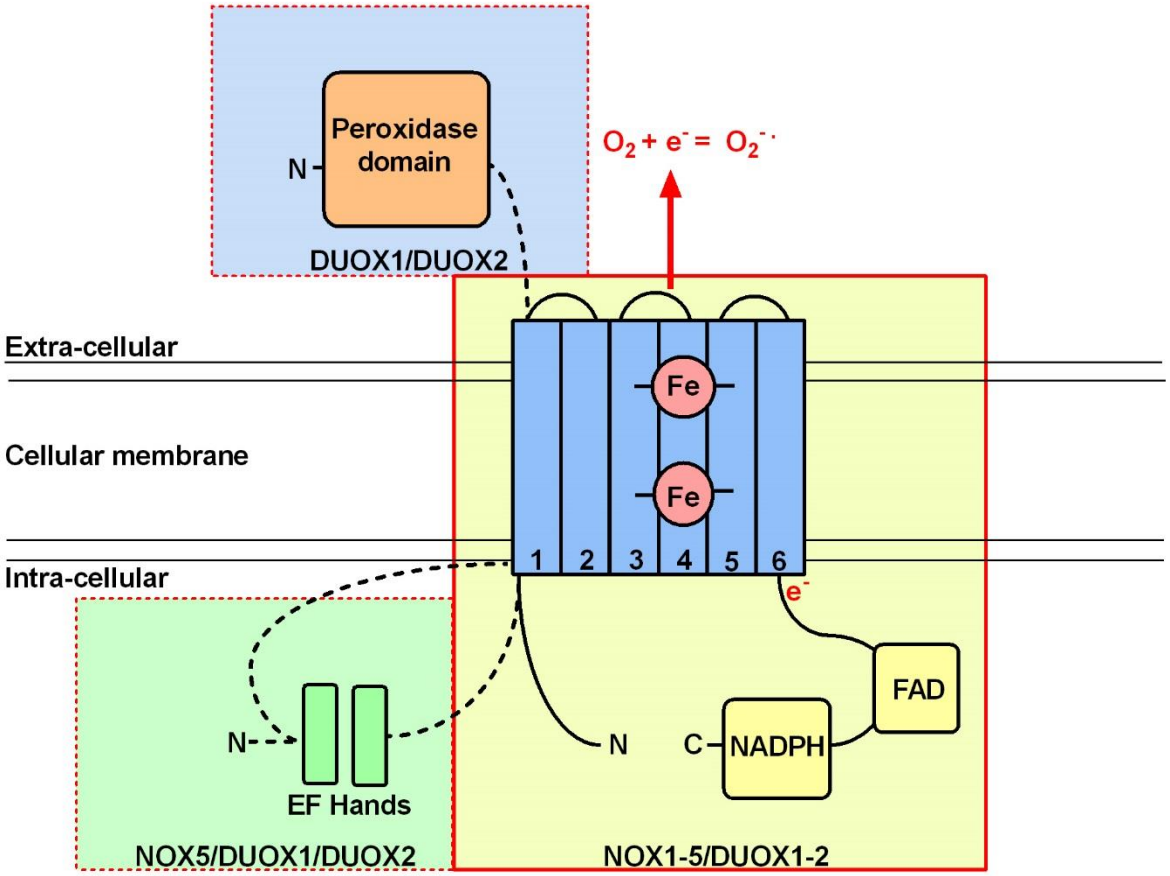

Figure 3.3. Structure of the NOX and DUOX enzymes. *All of NOX and DUOX enzymes have the basic components necessary from superoxide production. The cytosolic C-terminus containing NADPH and FAD act to generate and transfer electrons across the transmembrane heterodimer consisting of 6 transmembrane domains bound by 2 haem groups (spanning across transmembrane domains 3-5). The electrons are passed to across the membrane to molecular oxygen for generation of superoxide. NOX5 and DUOX1/2 have an N-terminus extension containing EF hands (NOX5 has 4 EF-hands and DUOX1/2 have 2 EF hands), which are able to bind calcium for activation. DUOX1/2 also have an extracellular peroxidase domain attached to an extracellular N-terminus domain. Adapted from (156, 157).*

The function of many members of the NOX and DUOX family requires interaction and activation by regulatory subunits (*Table 3.1*). The first regulatory subunits were characterised for the NOX2 enzyme, which requires assembly of cytosolic components for activation in the context of phagocytosis (described in detail in *Section 3.1.5.1*). The multi-step activation pathway for NOX2 provides an explanation for the regulation and tight control of the potentially harmful levels of

ROS generated by phagocytic cells (158). In contrast, other NOX enzymes, such as NOX1, are collocated with their cytosolic subunits in the plasma membrane, allowing constitutive generation of lower levels of superoxide (156).

Gene	Other names	Functional subunits	Chromosome loc. Gene length Amino acids	Protein weight (kDa)	Protein similarity to NOX2
NOX1	*MOX-1, GP91-2*	NOXO1 NOXA1	Xq22 30374bp 564	65	56%
NOX2	*CYBB, gp91^{phox}*	p22^{phox} p47^{phox} (organiser) p67^{phox} (activator)	Xp21.1 33451 570	65	100%
NOX3	*GP91-3*	NOXO1 (p67^{phox})	6q25.1-26 60534 568	65	58%
NOX4	*KOX*	Nil	11q14.2-q21 165139 578	67	39%
NOX5	-	Nil	15q22.31 42392 747	85	27%
DUOX1	*Thox1*	DUOXA1	15q21 35583 1551	180	50%
DUOX2	*Thox2*	DUOXA2	15q15.3-q21 20757 1548	180	50%

Table 3.1. NOX and DUOX enzymes genetics and functional subunits. *NOX2 is the best characterised of the NOX family of enzymes, and is the common comparator for the other NOX and DUOX isoforms. Many of the NOX and DUOX enzymes require interaction with regulatory subunits for activation. The chromosomal location, gene length, and number of amino acids for each of the NOX enzymes has been defined, along with the protein size (kilo-Daltons, kDa). Adapted from (157, 164, 167).*

3.1.4 Tissue expression and function of the NOX and DUOX enzymes

The NOX and DUOX enzymes are widely expressed throughout human tissues. Each of the NOX/DUOX family has distinct functions, which are highly variable and dependent on the tissue in which it is expressed. The tissue expression, cellular location, and proposed function of each of the NOX and DUOX enzymes is summarised in *Table 3.2*.

Beyond 'oxidative stress', there has been an increasing recognition of the importance of ROS homeostasis in cellular systems. The generation of ROS by NOX and DUOX enzymes plays an important role in innate immune defence, as well as many other cellular processes, including proliferation, differentiation, and regulation of gene expression (156-158). It is now established that a basal level of ROS is essential for cell survival. The opposing functions, both protective and pathogenic, of NOX- and DUOX-derived ROS, is likely to relate to the type and amount of ROS produced, the tissue type and target intracellular molecules, as well as the sub-cellular location of the NOX enzyme (156-158, 162). The putative functional roles of ROS derived from NOX and DUOX, both protective and pathogenic, are summarised in *Table 3.3.*

Enzyme	Tissue expression		Cellular Location Function
	Primary	Other	
NOX1 (167, 168)	**Colon**	Vascular endothelium and smooth muscle, perivascular adipocytes, uterus, placenta, prostate, osteoclasts, retinal pericytes, neurons.	-Plasma membrane -Constitutive ROS production -Role in innate immunity, cell signalling, proliferation, and migration
NOX2 (164, 165)	**Phagocytes** (neutrophils, macrophages, eosinophils)	Fibroblasts, neurons, cardiomyocytes, skeletal muscle, hepatocytes, B lymphocytes, endothelium, smooth muscle	-Intracellular vesicle membranes -NOX2 complex assembly upon activation -Role in innate immunity
NOX3 (169, 170)	**Inner ear**	Foetal kidney, foetal spleen, brain	-Plasma membrane -High constitutive activity -Role in balance perception
NOX4 (171, 172)	**Kidney** **Brain**	Vascular endothelium , osteoclasts, smooth muscle, haematopoietic stem cells, fibroblasts, keratinocytes, hepatocytes, neurons	-Plasma membrane and endoplasmic reticulum -High constitutive activity -Role in oxygen sensing, neuronal signalling and inflammatory pathways
NOX5 (164, 173)	**Lymphoid tissue** **Testis**	Smooth muscle, pancreas, placenta, ovary, uterus, stomach, foetal tissues	-Activated by intracellular calcium -Signalling role in lymphocytes and spermatozoa
DUOX1 (174)	**Thyroid**	Airway epithelia, cerebellum, prostate	-Activated by intracellular calcium -Role in thyroid hormone synthesis
DUOX2 (174-176)	**Thyroid**	Gastrointestinal epithelia, salivary and rectal glands, airway epithelia, uterus, gallbladder	-Activated by intracellular calcium -Role in thyroid hormone synthesis -Role in airway and gastrointestinal barrier function

Table 3.2. NOX and DUOX enzymes tissue expression and function in humans. *The NOX and DUOX family are expressed in a diverse range of human tissues. The function of each of the NOX enzymes is highly dependent on the tissue in which it is expressed. The table is derived from multiple sources, though basic data derived from (156-158, 162). Other key references are cited within table and text.*

Functional Role	Mechanisms
Protective and physiological roles	
Innate immunity and inflammation	Phagocytosis: ROS-dependent and independent (pH and potassium channel) roles in microbial killing during phagocytosis (156, 177)
	ROS-dependent bacterial killing at epithelial surfaces (175, 176)
	Anti-inflammatory role: ROS inhibition of inflammatory pathways (IL-8 (178), NF-κB (179))
Cellular signalling	Phosphatase inhibition via redox sensitive cysteine residues (e.g. PTEN) which play a role in cell migration and adhesion (180-182)
	Calcium signalling. Calcium regulates ROS production by NOX5 and DUOX1/2. ROS also controls intracellular calcium concentrations through plasma membrane calcium channels and release from intracellular stores (157)
	Kinase activation. Redox sensitive kinases such as p38 mitogen activated (MAPK) and extracellular signal related (ERK) kinases activated via ROS, playing a role in cell adhesion and migration (183, 184)
Gene expression	NOX generated ROS has been shown to modulate the expression of multiple genes, including NF-κB and TNF-α, through transcriptional up-regulation (179) (157).
Cellular proliferation, adhesion and migration	ROS plays an important role in control of cell growth through cellular senescence and apoptosis (158). ROS also mediates cellular adhesion and migration, which are functionally important in tissue repair (181)
Intracellular redox pathways	ROS is important in reduction of intracellular ions, including ferric iron. ROS also regulates cellular redox potential and interacts with nitric oxide, through which a wide range of effects are mediated (157)
Extracellular matrix	NOX are implicated in biosynthesis of extracellular matrix proteins; well-demonstrated by the role of the dual oxidases in thyroid hormone production (158)
Pathogenic roles	
Carcinogenesis	Tumour cells have been shown to release large amounts of ROS and up-regulation of NOX enzymes has been demonstrated in tumour cells and cell–lines (167, 168, 185-187)
Cellular aging	'Oxidative stress' has been described as a key mechanism in the biology of aging, through accelerated cellular senescence and DNA damage and instability (188, 189)

Table 3.3. The physiological and pathogenic roles of ROS in human cellular processes. *The table outlines the putative protective and physiological functions of ROS derived from NOX and DUOX, as well as the potentially harmful consequences of 'oxidative stress'.*

3.1.5 NOX and DUOX relevant to gastrointestinal tract immunology

3.1.5.1 NOX2

NOX2 is the prototypical phagocytic NOX enzyme, highly expressed in granulocytes and monocytes/macrophages, and responsible for the respiratory burst which kills microbes. The central component of the NOX2 protein complex is the large membrane-embedded flavocytochrome $gp91^{phox}$, which is constitutively located with the $p22^{phox}$ protein in the membrane of intracellular vesicles (*Figure 3.4*) (157). In the inactive state in neutrophils, the $gp91^{phox}$/p22phox complex localises to intracellular vesicles. $p22^{phox}$ is necessary for the stability and function of NOX2. Activation of the NOX2 complex requires translocation of cytosolic proteins to the $gp91^{phox}$/$p22^{phox}$complex. $p47^{phox}$ is phosphorylated upon activation, resulting in a conformational change in the protein which allows it to bind to $p22^{phox}$, thereby 'organising' the binding of the 'activator' subunit $p67^{phox}$, as well as $p40^{phox}$ (190, 191). Guanosine diphosphate (GDP) is converted to guanosine triphosphate (GTP) on ras-related C3 botulinum toxin substrate (RAC), which then binds to both $p67^{phox}$ and directly to $gp91^{phox}$, completing the formation of the active NOX2 complex (192). The active NOX2 complex then translocates to the surface of the granules which fuse with the phagosomal or the plasma membrane (193).

During phagocytosis, intra-phagosomal superoxide released by NOX2, is rapidly dismutated to hydrogen peroxide, which undergoes peroxidation to other highly toxic oxygen radicals by MPO. At high concentrations within the phagosome, radicals such as hypochlorous acid have the capacity to directly kill bacteria (194). NOX2 activation also plays a role in maintenance of neutral phagosomal pH, purported to enhance bacterial killing (177). Furthermore, NOX2 activation creates a large depolarisation

across the phagosomal membrane, which may be compensated for by potassium flux into the phagosome, creating an ionic gradient proposed to enhance bacterial killing by changes in osmolarity within the phagosome, as well as activation of proteases (177, 195). NOX2-mediated oxidative killing is only effective against certain bacteria and fungi, including *Staphylococcus aureus, Burkholderia cepacia*, and *Aspergillus fumigatus* (156).

Chronic granulomatous disease (CGD) is a rare genetic disorder with a prevalence of around 1:250,000 people that is caused by X-linked and autosomal recessive mutations of genes encoding components of NOX2, leading to attenuation of the 'respiratory burst' (196). Mutations have been described in four genes; *CYBB* (encoding $gp91^{phox}$, located on the X-chromosome), *NCF1* ($p47^{phox}$), *NCF2* ($p67^{phox}$)) and *CYBA* ($p22^{phox}$) (197-199). CGD was initially coined 'fatal granulomatosus', and is characterised by a propensity to recurrent pyogenic infection, lymphadenopathy, and granulomatous inflammation in children (197, 200). It has also been reported that up to 40% of patients with CGD develop gastrointestinal granulomatous inflammation akin to a CD phenotype (197). This non-infectious inflammation has been linked to defects in autophagy and inflammasome regulation amongst patients with CGD (201, 202).

Recent studies demonstrate that a missense variant of the *NCF2* gene, that does not cause CGD, leads to neutrophil dysfunction and the development of VEOIBD, supporting the role of defective ROS production by phagocytes in the pathogenesis of IBD (83, 84).

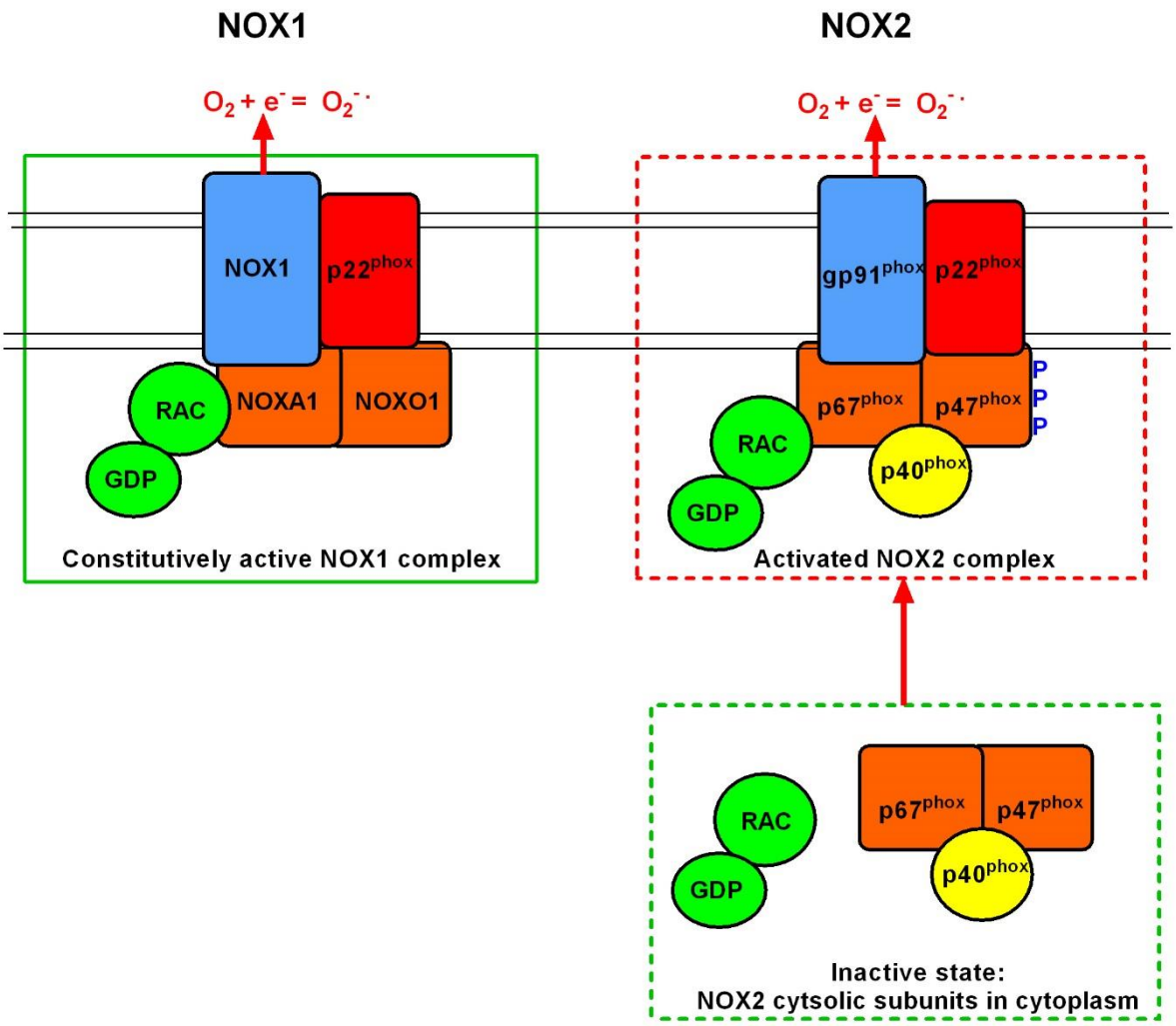

Figure 3.4. Regulatory subunits of NOX1 and NOX2 enzymes. *NOX1 is constitutively expressed in the plasma membrane along with the necessary subunits for generation of superoxide ($p22^{phox}$, NOXO1, NOXA1). Exchange of GDP for GTP on RAC1 is involved in activation of NOX1. NOX2 ($gp91^{phox}$) is co-located with $p22^{phox}$ in resting phagocytic cells, primarily in intracellular membranes. The subunits only assembly upon activation. In the setting of activation, RAC is activated, which along with phosphorylation of $p47^{phox}$, allows interaction between $p47^{phox}$with $p22^{phox}$and subsequently $p67^{phox}$ and $p40^{phox}$, leading to the assembly of the active NOX2 complex. Adapted from (156-158).*

3.1.5.2 NOX1

NOX1 was the first homolog of $gp91^{phox}$ (NOX2) to be identified and cloned in non-phagocytic tissues in 1999 by Suh *et al* (167). The NOX1 gene is located on the X-chromosome, and encodes a protein of around 65kDa that is 56% identical to NOX2

(*Table 3.1*) (164, 167, 203). The generation of superoxide by NOX1 is dependent on two cytosolic subunits: NOXO1 (organiser) and NOXA1 (activator) (204, 205). Unlike NOX2 and its homologs $p47^{phox}$ and $p67^{phox}$, NOX1 is constitutively co-expressed with NOXO1 and NOXA1 in the cell membrane, and therefore does not require activation prior to full membrane assembly (206). Accordingly, NOX1 exhibits significant constitutive activity, although produces only a fraction of the ROS generated by activated NOX2 in phagocytic cells (156). In addition to its cytosolic subunits, NOX1 requires the membrane subunit $p22^{phox}$ for functional activity (207). The GTPase RAC1 has been shown to regulate the activity of NOX1, both through binding to NOXA1 as well as direct binding to NOX1 (206). The subcellular localisation of NOX1 remains vague and is likely to vary between cell types; keratinocytes have been shown to demonstrate strong nuclear and weak cytoplasmic NOX1 protein expression, whereas vascular smooth muscle cells show an ER pattern of expression (208, 209). NOX1 generates both intra- and extracellular superoxide (167, 210).

NOX1 mRNA is mostly highly expressed in the colonic epithelium, where there exists a gradient of expression from the proximal colon (intermediate) to the distal colon (high) (167, 168, 204, 211). NOX1 protein expression is highest in the apical (luminal) pole of terminally differentiated colonic epithelial cells within the upper portion of the crypts (156, 212). Lower levels of NOX1 expression are also evident in a number of other tissues and cell types listed in *Table 3.2* (213-217).

NOX1 has been proposed to play both physiological and pathogenic roles in the gastrointestinal tract, although such data has largely been derived from animal and cell-line constructs and human data is scarce (*Table 3.4*). NOX1 plays an important role in bacterial handling and barrier function, mediating anti-inflammatory cell signalling upon interaction between commensal bowel flora, such as *Lactobacillus* species, with

formyl peptide receptors (FPRs) (179, 182, 184, 218). Commensal bacteria-induced ROS generation has been shown to attenuate the NF-κB pro-inflammatory signalling pathway, as well as stimulate the ERK pathway (179, 184). Furthermore, interaction with commensal bowel flora leads to colonic epithelial cell migration and proliferation, which has an important role in intestinal restitution following epithelial disruption (182, 218-220). NOX1 derived ROS may also play a role in autophagy within gastrointestinal epithelial cells, via facilitation of LC3 co-localisation and fusion between autophagosomes and endosomes (201, 221). NOX1 also may influence goblet cell development and function; NOX1 knock-out models show reduced numbers of goblet cells, increased intracellular mucin accumulation, and increased goblet cell apoptosis (221-223). The role of NOX1 in barrier function and bacterial handling is also supported by the colonic NOX1 mRNA expression gradient paralleling density of bacterial colonisation (168).

The role of NOX1 in IBD is uncertain; NOX1 mRNA expression of the colonic epithelium has been shown to be both upregulated and down-regulated in the setting of IBD (168, 223). Mouse models also demonstrate contradictory roles of NOX1 in IBD; NOX1 may be upregulated in the context of intestinal inflammation upon stimulus with TNF-α or IFN-γ, however a NOX1 and IL-10 double knock-out (IL10/NOX1^{dKO}) mouse model develops severe and early onset colitis (223-226). IL-10/NOX1^{dKO} mice have been shown to develop spontaneous early-onset colitis, histologically similar to UC (crypt abscesses and erosions without granuloma formation), which is more severe than that occurring in IL-10^{KO} mice (223). The IL-10/NOX1^{dKO} mice demonstrated early aberration of goblet cells prior to the onset of colitis, along with alterations of chronic ER stress (223).

Initially coined, 'mitogenic oxidase', NOX1 over-expression has been reported to potentiate carcinogenesis (167, 168, 185, 208, 212, 227). Although conflicting data exist (168), NOX1 has been shown to be over-expressed in colonic adenocarcinoma, with the highest NOX1 levels observed in well-differentiated tumours (208, 212, 227). The increased expression of NOX1 is strongly correlated with activating mutations in k-RAS (212). NOX1-derived ROS may exert a cancer-promoting effect by increasing resistance to programmed cell death of malignant cells, as well as through mediation of the Wnt signalling pathway (228, 229).

NOX1 Role	**Experimental model**	**Critical findings**
Bacterial handling	Human colonic epithelium	-Increasing gradient of NOX1 expression from the proximal to the distal colon, parallels bacterial load (168, 204, 211).
	Colon cancer cell-lines (T84, Caco2, HeLa, T-84, SK-CO15)	-TLR5 mediated induction of NOX1 superoxide by recombinant- flagellin from *S. enteridis (230).* -L. *rhamnosus* induced ROS production via FPR (182, 183, 219, 220, 230-232). -Modulation of NF-κB inflammatory pathways via inhibition of E3-$SCF^{\beta TrCP}$ neddylation as well as via ERK anti-inflammatory pathway (179, 184).
	$NOX1^{KO}$ mice	- L. *rhamnosus* (but not E. *coli)* ingestion resulted in NOX1-dependent colonic ROS generation and increased proliferation of epithelial cells (218).
	Drosophila species	-L. *plantarum* leads to NOX1-dependent ROS and increased proliferation of mid-gut cells (218).
Epithelial barrier function	$NOX1^{KO}$ mice	-Increased differentiation of progenitor cells into goblet cells (without the development of colitis) via modulation of the Wnt, beta-catenin and Notch1 signalling pathways (222). -Increased goblet cell mucin accumulation due to defective autophagy (221)
	$IL10/NOX1^{dKO}$ mice	-Decreased mature goblet cell size and number prior to the onset of colitis. Associated ER stress and apoptosis of goblet cells (223).
Intestinal epithelial migration, proliferation and repair	Colon cancer cell-lines (HT-29, SK-CO15)	-NOX1 superoxide production regulates cell migration via α2β1 integrin and p38 MAPK phosphorylation (233). -ANXA1 ligand binds to FPR, inducing NOX1-mediated ROS and intestinal epithelial migration (182, 218-220, 231, 232)

Autophagy	Mouse models	- Goblet cells from colonic epithelial spheroids from $p22^{phox}$ knock-out mice shown defective autophagy due to lack of LC3 co-localisation and increased intracellular calcium leading to mucin granule accumulation in goblet cells (201, 221).
Inflammation	Colon cancer cell-lines (T84)	-NOX1 expression is inducible via IFN-γ, TNF-α, IL-1β, IL-18, TLR5 ligand (flagellin), and 1α,25-dihydroxyvitamin D_3 (225-227, 230). -IL-10 and TGF-β block TNF-α stimulated NOX1 expression (228).
	Mouse models	- $IL10/NOX1^{dKO}$ mice develop spontaneous colitis at 6-7 weeks of age (223).
		-Intraperitoneal TNFα causes colonic inflammation, up-regulation of NOX1 (224).
Cancer	-Colon-cancer cell-lines (HT-29, Caco-2, DLD-1) -Human colonic epithelium	Sub-confluent cells produce higher levels of ROS concordant with higher mitotic rates (234)
		-NOX1 is over-expressed in colonic adenocarcinoma (well-differentiated tumours) (186, 208, 212, 227). -Increased expression of NOX1 is strongly correlated with activating mutations in k-RAS (212). -NOX1-derived ROS may increase resistance to programmed cell death of malignant cells, through mediation of the Wnt signalling pathway (228, 229).

Table 3.4. The protective and pathogenic roles of NOX1 in the gastrointestinal tract. *NOX1 has been reported to play roles in bacterial handling, epithelial barrier function, intestinal epithelial restitution and repair, autophagy, inflammation, and carcinogenesis.*

3.1.5.3 DUOX2

DUOX2 is expressed in the epithelia of the gastrointestinal tract, salivary ducts, and airways, where it is purported to play an important role in barrier function and innate defence (156). DUOX2 is most highly expressed in differentiated enterocytes within the apical membrane of the brush border of the lower gastrointestinal tract (235).

The importance of the role of DUOX2-derived hydrogen peroxide in gastrointestinal barrier function was demonstrated by the impaired resistance to pathogenic *Helicobacter pylori* colonisation in DUOX knock-out mice (176). In Drosophila

species, knock-down of ‘dDUOX’ led to increased mortality rates after ingestion of microbe-contaminated food (236). Reintroduction of DUOX led to restoration of ROS generation and anti-microbial function which reversed this increased mortality rate. In the airways, the generation of hydrogen peroxide by DUOX has been shown to act as a substrate for lactoperoxidase in airways, producing the biocidal compound hypothiocyanite (OSCN-), thereby playing a role in innate immune defence against bacterial pathogens, especially *Staphylococcus aureus* and *Pseudomonas aeruginosa* (175, 237).

DUOX2 has been shown to be an important protagonist in the pro-inflammatory milieu of IBD (238). Ileal RNA expression was analysed in a large paediatric IBD inception cohort, and the core gene expression signature was compared to healthy controls (238). DUOX2 expression was found to be upregulated, which was associated with NF-κB inflammatory pathway signalling, as well as a shift in the microbial community profiles toward ‘dysbiosis’. In another study, DUOX2 has been shown to interact with NOD2 to generate epithelial cell responses to bacterial ligands (239).

3.1.6 The ROS ‘toolbox’

The detection and measurement of ROS can be difficult, particularly in non-phagocytic cells, due to low levels of ROS produced, the presence of multiple NOX isoforms in different cellular locations, and differences in subcellular ROS levels (240). Furthermore, there are multiple cellular sources of ROS other than NOX, including mitochondria, xanthine oxidase, and cyclooxygenase. Endogenous antioxidants also quench NOX-generated ROS, meaning that superoxide and hydrogen peroxide are only transiently present before they are scavenged (240).

The difficulty of measuring ROS in cells is further compounded by the lack of specificity and cross-reactivity of many of the currently available ROS probes, stimuli, and inhibitors. Therefore, the term 'ROS toolbox' has been coined, given that multiple techniques must be employed to determine the nature and origin of cellular ROS (*Table 3.5*) (241).

Factor	Feature	Consideration
Probe	Probe chemistry	*How does the probe interact with the ROS?*
	Probe sensitivity and specificity	*What is the sensitivity of the probe for its target ROS?* *What is the cross-reactivity?*
	Cellular uptake of the probe	*Is the probe membrane permeable?* *Does the probe reaction product diffuse out of the cell?*
	Multiple methods of ROS detection	*Have at least two probes been used as is recommended for detection of ROS species?*
Cell type	Origins and location of ROS generation within the cell/tissue	*What are the origins and cellular locations of ROS generation within the cellular phenotype?*

Table 3.5. The ROS 'toolbox': key considerations for the detection of ROS*. The table details the working knowledge necessary for the ROS probe in use as well as the cell/tissue being analysed. Adapted from (240).*

3.1.6.1 ROS probes

There have been multiple probes developed for the purpose of detecting ROS. Each of the available ROS probes has a caveat, and many probes have broad cross-reactivity and kinetic profiles that may limit interpretation of the ROS species detected (240). A specific knowledge of the capabilities and limitations of the ROS probe in use is required for interpretation of experimental data. In this thesis chapter, two ROS probes are successfully used (*Table 3.6*).

Chemiluminescence probes. There are multiple chemiluminescence probes available for measuring ROS, the most advanced of which is the L-012 enhanced luminol probe

used in this thesis (*Table 3.6*). L-012 was first synthesised in 1993 and is specific for the detection of superoxide. L-012 has been shown to be more sensitive and to generate greater light intensity than other chemiluminescence probes such as luminol and MCLA (242). L-012 needs to undergo a one-electron oxidation to form an L-012- derived radical ($LumH^{\cdot -}$), which then reacts with superoxide to emit luminescence, however during this reaction there is the potential to self-generate superoxide (243).

Precipitate probes. Nitroblue tetrazolium (NBT) is a cell-permeable compound that can be reduced by superoxide to form a stable blue formazan precipitate, which can be visualised by light microscopy (*Table 3.6*) (244). NBT has been long-used for detection of phagocyte-derived (NOX2) ROS as a diagnostic test for CGD in clinical practice (240, 245-247).

Probe	Mechanism	ROS detected Method	Location	Key points
L-012 enhanced luminol (242)	-L-012 converted to $LumH^{-\bullet}$, generates luminescence signal	**$O_2^{-\bullet}$** $ONOO^-$ **Luminescence**	- Intra- and extracellular - *In vivo* and *ex vivo*	***Pros:*** -Intra- and extracellular ROS. -High sensitivity. -Specific for $O_2^{-\bullet}$. ***Cons:*** -Cross-reacts with $ONOO^-$. -Auto-oxidation.
Nitroblue tetrazolium (NBT) (244, 247)	-Absorbance precipitation reaction (reduced to blue formazan)	**$O_2^{-\bullet}$** NOS **Microscopy**	-Intra- and extracellular - *Ex vivo*	***Pros:*** -Simple and cheap. ***Cons:*** -Low sensitivity. -Semi-quantitative assay using microscopy. -Broad cross-reactivity within cells (directly reduced by xanthine, mitochondrial dehydrogenases, free metals).

Table 3.6: ROS probes used in this thesis. *The table describes the mechanism of action of the various probes, the ROS species detected, the method of detection, and the relative pros and cons of each probe. Adapted from (240). Key: $O_2^{-\bullet}$, superoxide; $ONOO^-$, peroxynitrite; NOS, nitric oxide species.*

3.1.6.2 Inhibitors and stimuli of ROS

In addition to multiple ROS probes, there are multiple reported inhibitors and stimuli of ROS production.

ROS inhibitors. ROS inhibitors may be non-specific for a cellular source of ROS or oxygen species, or specific for a particular NOX enzyme. The most commonly known non-specific ROS inhibitor is diphenyleneiodonium (DPI), which is a flavin protein inhibitor. DPI inhibits not only ROS generated from NADP, but that from nitric oxide synthase, xanthine oxidase, cytochrome p450 oxidoreductase, bacterial nicotine oxidase,

and mitochondria (248-251). In addition, DPI has also been shown to inhibit cholinesterases and internal calcium pumps (252). Another non-specific ROS inhibitor is the RAC1 small molecule inhibitor, which acts to inhibit the RAC1 GTPase involved in the activation of the NOX complex (182, 253).

The hunt for novel chemotherapeutic agents has identified specific inhibitors of NOX enzymes, via the process of high throughput screening (254). One such inhibitor is ML171, a phenothiazine compound with reported selectivity for NOX1 (254). ML171 has been shown not to inhibit ROS production from either mitochondria or xanthine oxidase (254).

ROS stimuli. There are multiple physiological and pharmacological stimuli of ROS that may be employed in experimental strategy. Phorbol 21-myristate 13-acetate (PMA) is a potent activator of protein C, and is a well-known compound which induces ROS production from a variety of cellular sources including the NOX and DUOX enzymes, in a broad range of cell-types (255). For the NOX1 enzyme, PMA has been shown to induce phosphorylation of NOXO1, which allows NOXO1 to interact with NOXA1, which leads to activation of the NOX1 complex and consequent superoxide generation (256).

Ligands and components of the bacterial cell wall that stimulate an innate immune response, such as MDP, lipopolysaccharide (LPS), and FPR ligand, have been shown to stimulate ROS generation by NOX enzymes in multiple *ex vivo* and cellular constructs (157, 182, 218, 231, 257).

3.1.6.3 NOX1 expressing colonic epithelial cell line

As a part of the ROS 'toolbox', the appropriate cell-culture for experimental work needs to be selected on the basis of NOX expression.

An HT-29 human colonic epithelial cell line, derived from a primary colorectal tumour in 1964 using an explant culture method, was selected for use in this thesis (*Figure 3.5*) (258). The HT-29 cell line was selected on the basis of functional NOX1 expression, along with the necessary subunits NOXO1, NOXA1, and p22phox (233, 234, 259). Alternative colonic epithelial cell-lines (Caco-2, HCT-116, DLD-1, HeLa) were not selected as they have been found to have incomplete assembly of the NOX1 complex and necessary subunits (204, 260).

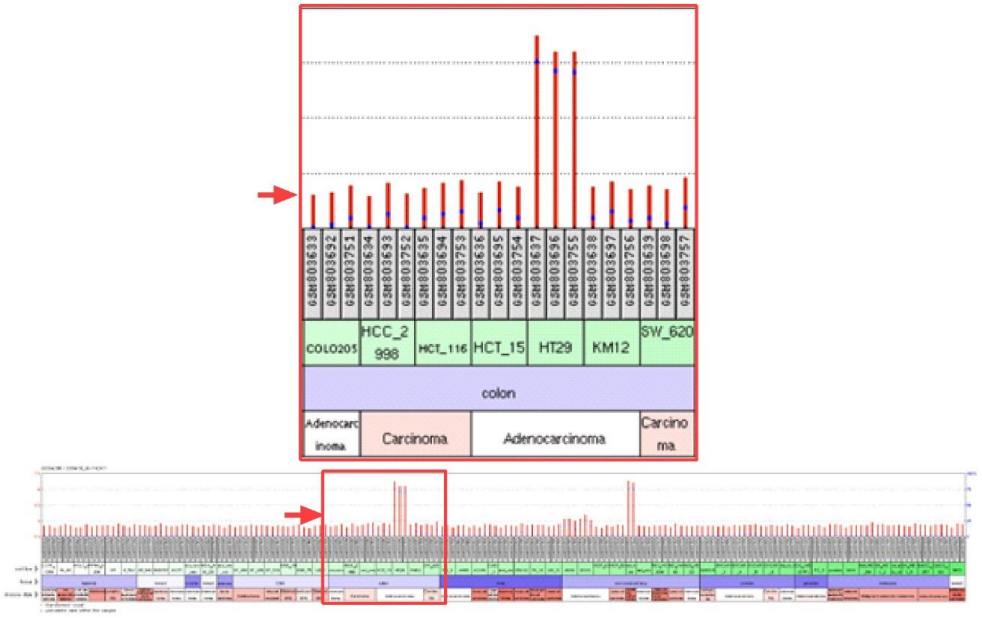

Figure 3.5: NOX1 expression in colorectal cancer cell lines. *The data is derived from the NCI-60 cancer cell line panel. NOX1 expression accessed via gene expression omnibus reporter 206418 ((http://www.ncbi.nlm.nih.gov/geo/). The expression data reveals prominent NOX1 expression in the HT-29 cell line, as compared to other colon cancer lines. Image provided by my supervisor (HU).*

3.1.7 Aims of this chapter

The NOX1 enzyme is predominantly expressed in the human colonic epithelium, where it has been shown to play both a protective and pathogenic role in cellular processes. There is emerging animal and human cell-line data to suggest that NOX1 is an important protagonist in the maintenance of colonic epithelial homeostasis, including intestinal epithelial barrier function, proliferation, and restitution, particularly upon interaction with commensal colonic microflora. However, there is no human data available on the potential pathogenic consequences of a functional defect in NOX1.

The aim of this chapter was to investigate the functional consequences of a missense mutation in the NOX1 gene in a single patient with VEOIBD. It was aimed to establish whether the patient's clinical phenotype was potentially attributable to the *NOX1* p.N122H variant mutation. In particular, it was aimed to:

1. Determine the gastrointestinal expression of NOX1, both in non-inflamed controls, patients with IBD, and the *NOX1* p.N122H variant patient.
2. Evaluate NOX1-derived generation of superoxide in colonic epithelial cells, both in non-inflamed controls, patients with IBD, and the *NOX1* p.N122H variant patient.
3. Explore putative mechanisms by which the *NOX1* p.N122H variant may lead to intestinal inflammation.

3.2 MATERIALS AND METHODS

3.2.1 Basic materials and media

Cell-line and bacteria

The cell-line selected for use on the basis of functional NOX1 expression (with the necessary subunits NOXO1 and NOXA1) was the HT-29 human colonic epithelial cell line, American Type Culture Collection (ATCC®- HTB-38^{TM}) (Middlesex, United Kingdom).

Both invasive and non-invasive bacteria were used in bacterial killing assays, including *Lactobacillus rhamnosus (L. rhamnosus),* Adherent invasive *Escherichia coli reference strain LF82 (*AIEC*), Escherichia coli* Nissle 1917 (EcN), *Salmonella enterica serovar typhimurium NCTC 12023 (S. typhimurium),* and *Staphylococcus aureus (S. aureus).*

Cell culture media

For basic cell-culture, the following solutions were variably used; McCoy's 5A modified medium (1X) (Gibco®, Life Technologies, Paisley, UK), Advanced Dulbecco's modified eagle medium/F12 (AdMEM) (Gibco®, Life Technologies Paisley, UK), Roswell Park Memorial Institute (RPMI) 1640 medium (Sigma-Aldrich, Gillingham, UK), Dulbecco's modified eagle's medium (DMEM) (Sigma-Aldrich, Gillingham, UK).

In cell culture conditions, the media was supplemented with foetal calf serum (FCS) where indicated (Gibco®, Life Technologies, Paisley, UK). For cellular washing, as well as in multiple assays, Dulbecco's phosphate buffered saline (PBS) was used (Sigma-Aldrich, Gillingham, UK).

For bacteria culture, Luria Bertani (LB) broth (Lennox) and De Man, Rogosa, and Sharpe (MRS) broth (69966) were used (Sigma-Aldrich, Gillingham, UK).

Cell culture materials

Cell culture was performed in tissue culture-treated T-75 25cm^2 flasks, 96 well, 48 well, 24 well, 12 well, or 6 well flat-bottom plates (Costar®, Corning Incorporated, Life Sciences, NY, USA). During cell culture and passage, Falcon^{TM} 15mL and 50mL conical tubes were used (Fisher Scientific, Loughborough, UK). For trypsinisation and counting of cells, Trypsin EDTA solution (1X) and Trypan blue solution (0.4%) (Sigma-Aldrich, Gillingham, UK) were used.

3.2.2 Ethics and patient recruitment

Patient samples for analysis were obtained with written and informed consent and approval from a Research Ethics Committee. Samples from patients with IBD were collected under the following ethics: Inflammatory Bowel Disease in Oxford: prospective cohort for outcomes, treatment, and predictors. Research Ethics Committee Reference: 09/H1204/30 (Granted June 2009). Sample from patients without IBD were collected under the following ethics: Oxford Gastrointestinal Illness Biobank. Research Ethics Committee Reference: 11/YH/0020 (Granted June 2011).

3.2.3 Genetic analysis

Genetic analysis and identification of the *NOX1* mutant was performed independently of this thesis according to established methodology (261). In summary, the following steps were taken to identify, confirm, and validate the Oxford *NOX1* p.N122H variant (*NOX1*, c.A364C, p.N122H).

3.2.3.1 Whole genome sequencing (WGS)

WGS was performed using 3-5µg of DNA isolated from blood collected from patients with IBD and controls, as a part of the WGS500 Project (261). Each sample underwent ultrasonification, ligation, and enrichment using polymerase chain reaction, in a step-wise fashion. WGS was then performed on the Illumina® HiSeq2000 system in 100base pair reads.

Variants were screened according to their frequency in the IBD population studied (less than a particular threshold such as <5%), as well as their frequency in non-IBD populations using an Exome Variant Server (http://exac.broadinstitute.org/). Homozygous, hemizygous or potentially compound heterozygous were selected, and subsequent analysis for gene expression in the human intestine or the lymphoid tissue was undertaken through a Human Protein Atlas database (http://www.proteinatlas.org/). Assessment of the evolutionary conservation of the mutation site was performed (predicted by a high conservation score >0.95). Lastly, prior literature was searched for evidence of the gene product relevant to human or mouse intestinal inflammation or bacteria host interaction.

3.2.3.2 *NOX1* Sanger sequencing and family pedigree

Sanger sequencing of the *NOX1* p.N122H variant patient and his mother was performed, in order to generate a family pedigree. In addition, a 'wild-type' IBD-matched control was sequenced. Targeting sequencing was performed around the *NOX1* p.N122H variant mutation site, in collaboration with a laboratory colleague (JJW).

Briefly, 3-5µg of DNA was isolated from blood with PureGene Blood Core Kit C (Qiagen), and amplified using AmpliTaq Gold 360 DNA polymerase (Applied Biosystems, Foster City, CA) and custom *NOX1* p.N122H primers (exon 5).

Bidirectional Sanger sequencing was then performed using BigDye Terminator v3.1 chemistry (Applied Biosystems, Foster City, CA) and an ABI-3730 DNA analyser.

3.2.4 HT-29 cell line culture and passage

HT-29 cells (American Type Culture Collection (ATCC®- HTB-38^{TM})) were cultured in McCoy's 5a Medium Modified, supplemented with 10% FCS (termed McCoys' Complete medium). The cell culture was incubated at 37 degrees Celsius (37°C), 5% carbon dioxide, 95% relative humidity (termed tissue culture conditions) in Corning® T-75 25cm^2 flasks. For experiment work, cell culture was also performed in 96 well, 48 well, 24 well, 12 well, or 6 well flat-bottom tissue culture treated plates (Costar®, Corning Incorporated, Life Sciences, NY, USA).

Cell passage and harvest was performed 2-3 times per week when the HT-29 cell monolayer reached 80% confluence. The cells were washed with 10 mL of PBS prior to trypsinisation (Trypsin (0.5g)-EDTA (0.2g) solution (1X) for 10-15 minutes), until the cell layer was observed under the microscope to have dispersed. McCoys' Complete medium (8mL) was then added to stop the reaction and the cells were aspirated using a glass pipette and transferred to a 15mL Falcon tube. The cells were then centrifuged at 1500 revolutions per minute (rpm) for 6 minutes. Following resuspension of the cell pellet, cell counting was performed using trypan blue and haemocytometer according to standard technique. Cells were then re-inoculated in the flask for ongoing culture at a ratio of 1:4 to 1:8.

3.2.5 Bacterial cultures

Maintenance culture. All bacterial strains were cultured using LB broth autoclaved agar plates, according to standard bacterial culture techniques, except for *Lactobacillus species,* which were cultured in MRS broth (*Table 3.7*).

Overnight incubation. A single bacterial colony was harvested using a pipette tip, and then transferred to 3mL of broth and incubated overnight at 37°C on a rocking plate (200 rpm). BD Falcon™ tubes were sealed with Parafilm® Wrap for anaerobic culture conditions.

Same day incubation for bacterial growth curve. After overnight incubation, approximately 10^7 bacterial cells were re-inoculated in 3mL of broth via serial dilutions. The appropriate volume of overnight culture for re-inoculation was determined by an optical density (OD) reading using a SmartSpec Plus Spectrophotometer (Bio-Rad, UK) at 595 nanometres. Re-inoculated bacteria were returned to incubation on a rocking plate (200 rpm) for 3.5 hours; previously determined to correlate with the mid-log phase of bacterial growth.

Calculation of bacterial number and multiplicity of infection. After 3.5 hours of incubation, the OD was once again determined, allowing calculation of the bacterial number required for cell infection. Calculations were based on an established bacterial growth curve for each organism. The bacterial suspension was centrifuged at 14,000 rpm for 3 minutes, and then re-suspended in PBS glucose media (1 gm/L) (PBS-G) for cell infection. Further dilutions were performed according the desired multiplicity of infection (MOI) for respective experiments.

Bacteria	Culture medium	Condition	Features/ Pathogenicity
L. rhamnosus	MRS broth	Anaerobic; 37^0C	Gram positive Non-invasive Commensal
AIEC	LB broth	Aerobic; 37^0C	Gram negative Invasive
EcN	LB broth	Aerobic; 37^0C	Gram negative Non-invasive Commensal
S. typhimurium	LB broth	Aerobic; 37^0C	Gram negative Invasive
S. aureus	Cooked meat broth	Aerobic; 37^0C	Gram positive Non-invasive^

Table 3.7: Bacterial cultures used in bacterial killing experiments. *Culture conditions and features of bacterial strains used in this thesis. ^S. aureus may be invasive in other tissues but is considered non-invasive in the gut.*

3.2.6 Human gastrointestinal biopsy specimens

3.2.6.1 IBD and non-inflamed control patients

Gastrointestinal epithelial biopsy specimens were collected during endoscopic procedures performed on both patients with IBD and non-inflamed controls, during routine clinical care after the appropriate informed consent was obtained.

The demographics of both IBD and non-inflamed control patients are provided in *Table 3.8*. For patients with IBD, disease distribution was assessed according to the Montreal Criteria (20). Disease activity was dichotomised into active disease and quiescent disease on the basis of a composite clinician's assessment, taking into account endoscopic features, biomarkers (CRP), and histological features of intestinal epithelial biopsies. The use of IBD-related medications was documented at the time of biopsy collection.

	CD	UC	Non-inflamed
Number	19	12	28
Gender (% male)	42%	42%	45%
Age (median, IQR)	22 (29-41)	42 (24-61)	44 (26-64)
Disease distribution (Montreal Criteria) (20)	A1 16% A2 79% A3 5% L1 5% L2 27% L3 68% B1 47% B2 37% B3 16%	E1 17% E2 33% E3 50%	-
Disease activity^ (% active disease)	53%	50%	-
Medications			-
None	42%	0	
5-ASA	0	92%	
Immunosuppressant	21%	0	
Biologic alone	21%	0	
Combination~	16%	17%	
Corticosteroid	0	25%	

Table 3.8: Gastrointestinal biopsies from IBD and non-inflamed control patients. *Gastrointestinal epithelial biopsies were collected from patients undergoing endoscopic procedures during routine clinical care. The table details the demographics of patients from whom biopsies were taken. Disease distribution according to Montreal criteria (20), disease activity, and IBD medications provided for IBD patients. ^Disease activity dichotomised according to composite assessment including endoscopic appearance, biomarkers (CRP), and histology. ~Combination of biologic and immunomodulatory therapy. The median and IQR are provided for continuous variables. Data otherwise provided as percentages of respective cohorts.*

3.2.6.2 Gastrointestinal biopsy collection and handling

A standardised endoscopic biopsy technique was employed using Olympus Endojaw® needle forceps (cup-opening size 7.2mm), performed by experienced endoscopists. Ex-vivo biopsy specimens were immediately transferred to RPMI-1640 medium, kept on ice, and transported to the laboratory within 90 minutes of collection. The biopsy specimens were washed in petri dishes containing PBS under a tissue culture hood prior to experimental work. A pipette technique was used to handle and transfer biopsies to minimise trauma to the tissue.

3.2.7 Colonic epithelial organoid generation and culture

Human colonic crypts were isolated from colonic epithelial biopsies and organoids were cultured in collaboration with colleagues at the National Institute of Medical Research (NIMR), according to a previously described technique (262). Generating colonic epithelial organoids relies on the isolation of self-renewing *Lgr5+* stem cells from within epithelial crypts, which undergo crypt fission events and generate villous-like epithelial domains in which all differentiated cell types are represented (262, 263). Long-term culture in an appropriate medium allows expansion of *Lgr5+* intestinal stem cells to generate organoids, which comprise crypt domains surrounding a central lumen lined by villous epithelium. Thus, organoids represent a continuously expanding, self-renewing epithelial structure that is a similar to normal gut (262).

Crypt isolation. The *ex vivo* colonic biopsy specimens were removed from transport medium and washed in a petri dish of cold PBS. The tissue was then manually chopped into pieces of around 1 millimetre (mm) and then incubated in PBS with 2 mM EDTA for 30 minutes on ice. After removal of the EDTA medium, the tissue fragments were vigorously suspended using a pipette with cold PBS. After centrifugation at 300 G for 5 minutes at 4°C, the supernatant containing the villous fraction was discarded, and the remaining sediment was suspended in PBS. This process was repeated twice, in order to enrich for crypts and to remove the residual villous material. The final fraction used for culture consisted of pure crypts.

Organoid culture. Isolated crypts were embedded in Matrigel™ (BD Biosciences, Oxford, UK) on ice and seeded in 48 well plates. The Matrigel™ was polymerised for 10 minutes at 37°C, and 250 µL/well of organoid culture media was added. The organoid culture media consisted AdMEM, supplemented with penicillin/streptomycin

(10 mM), HEPES (1 M), glutamax (10 mM). The following growth factors were added; Wnt conditioned media (50%) B27 (1X), EGF (50 ng/ml), Noggin (10%), R spondin (20%), gastrin (10 nM), Nicotinamide (10 mM), A83-01 (500 nM) and SB202190 (10 μM) (all provided by NIMR colleagues). Y-27632 (10 μmol/L) was included in the medium for the first 5 days in culture. Once organoid growth was established, the media was changed every 3 days.

Organoid single-cell harvest. Harvest of the organoid culture as a single-cell suspension was achievable after around 8 weeks in culture. The Matrigel™ containing the organoids was disaggregated using vigorous pipetting and then resuspended in AdMEM. The suspension was centrifuged at 300 G for 6 minutes at 4°C. The resulting supernatant was discarded and the remaining cell pellet resuspended in TrypLE™ Select (1X) (BD Biosciences, Oxford, UK) 500 μL per well and incubated in a 37°C water-bath for 15 minutes. AdMEM with 10% FCS was then added in a 1:1 ratio to the TrypLE™ cell suspension, followed by centrifugation at 300 G for 6 minutes at 4°C. The supernatant was discarded and the cell pellet again resuspended in AdMEM. This process was repeated twice to generate a single cell suspension.

3.2.8 ROS assays

Two primary assays were employed to detect and measure ROS in this thesis chapter: chemiluminescence and light microscopy assays. The methodology for each of the assays is detailed in *Table 3.9.*

3.2.8.1 Chemiluminescence assays

L-012 enhanced luminol (8-amino-5-chloro-7-phenylpyrido[3,4-d]pyridazine-1,4(2H,3H)dione) (Wako® Pure Chemicals Industries, Japan) was used for chemiluminescence assays. Cell were seeded in opaque white 96 well flat-bottom tissue

culture-treated plates (Costar®, Corning Incorporated, Life Sciences, NY, USA) for chemiluminescence assays.

Cells or biopsies were washed twice with PBS prior to addition of the L-012 probe. Pre-incubation with the L-012 probe was then performed at an intermediate concentration (200 µM) in 100 µL for 10 minutes in tissue culture conditions. Co-incubation with inhibitors was also performed for selected wells at indicated concentrations. The plate was then removed from the incubator and stimuli (or the appropriate vehicle control) were added to selected wells in 100 µL of media. The final concentration of L-012 was thus 100 µM in 200 µL of media. The probe was protected from light during the experimental work.

The plate was then transferred to a plate-reader (BMG Labtech® Optima microplate reader) and baseline chemiluminescence photoemission (relative light units, RLU) was recorded and thereafter emerging chemiluminescence as a kinetic assay every 1-10 minutes for 60-180 minutes. The gain adjustment (4095), lens setting, and recording temperature (37°C) were standardised for all experiments.

3.2.8.2 Light microscopy assays

Nitroblue tetrazolium chloride (NBT) (2,2′-bis(4-Nitrophenyl)-5,5′-diphenyl-3,3′-(3,3′-dimethoxy-4,4′-diphenylene)ditetrazolium chloride) (Sigma Aldrich, Gillingham, UK)**.** Ex-vivo colonic biopsies (within 90 minutes of collection) were incubated with NBT 100 µg/ml in PBS-G in petri dishes for 60 minutes at room temperature. Co-incubation with stimulatory or inhibitory conditions was performed.

The biopsy specimens were analysed using light microscopy immediately after the 60 minute NBT incubation. Light microscopy (200x magnification) was performed using a Carl Zeiss Axioskop2 microscope. Biopsies were placed on glass slides (Marienfeld

Laboratory glassware, Thermo Scientific, Cramlington, UK) without cover slips for analysis. Images were photographed using Q-Imaging software. Microscopy images were reconstructed and analysed using ImageJ software (Java, National Institute of Health, USA).

Assay	**Probe conc.**	**Analysis Plate**	**Cell/tissue preparation**		
			HT-29 cells	Colonic epithelial biopsies	Colonic epithelial organoids
Chemi-luminescence L-012 probe	100 µm	Plate-reader 96-well white opaque plate (Costar® Corning)	-8 x10^4 –1x10^5 cells per well -Adherent after overnight incubation -200 µl media/well	-Single biopsy per well (washed PBS) -200 µl media/well	Cells in suspension (variable number) -200 µl media/well
Light microscopy Nitroblue tetrazolium	100 µg/ml	Light microscopy Glass slide	-	Single biopsy per slide	-

Table 3.9. Chemiluminescence and light microscopy ROS assay techniques. *The table provides an outline of the final optimised methodology employed for each of the ROS probes, including the concentration of the probe, the method of analysis, the plate used for culture/analysis, the preparation of the cell culture/tissue specimen.*

3.2.8.3 Stimulatory and inhibitory conditions

Experimentation with multiple putative ROS inhibitors and stimuli was undertaken during the course of this thesis, in order to investigate the regulation of superoxide generation by NOX1.

The ROS and NOX inhibitors used in this thesis chapter, including diphenyleneiodonium (DPI) (Sigma-Aldrich, Gillingham, UK), ML171 (2-(trifluoromethyl)- phenothiazine, Tocris® Bio-Techne, UK), RAC1 inhibitor (NSC 23766, Tocris® Bio-Techne, UK), and superoxide dismutase (Sigma-Aldrich, Gillingham, UK), are detailed in *Table 3.10*. Co-incubation with competitive inhibitors was performed over the time-course of experiments. Pre-incubation with irreversible

inhibitors was performed, particularly DPI, which is known to be toxic to cells over a prolonged incubation period (250, 252).

Inhibitor	Pharmacology	Specificity	Cross-reactivity	Dose/ Incubate
DPI	Irreversible non-specific flavin protein inhibitor	Inhibits NOX, ROS, NOS, xanthine oxidase, and mitochondria	Inhibits calcium channel pumps and cholinesterases	1-10 µM 30-60 min Pre-incubation
ML171	Competitive NOX1 specific inhibitor.	NOX1 specific.	Nil reported	1-10 µM 30-60 min Co-incubation
RAC1 inhibitor	Competitive inhibitor of RAC1 (involved in activation of NOX)	RAC1 specific	RAC1 is involved in activation of all NOX and DUOX.	50-100 µM 30-60 min Co-incubation
SOD	Dismutates superoxide to hydrogen peroxide	Specific reaction with superoxide.	Promotes activity of nitric oxide.	5 µM Co-incubation

Table 3.10: Inhibitors of ROS. *The table details the pharmacology, specificity, side-effects, dose, and incubation period of the inhibitors of ROS used during the course of this thesis.*

Given that the baseline superoxide production by colonic biopsies is highly variable and dependent on biopsy size as well as the presence of lamina propria immune cells and blood vessels within the specimen, the reduction of superoxide from baseline (expressed as a percentage) following the addition of inhibitor in individual biopsies was calculated.

Multiple putative NOX and ROS stimuli, as well as stimuli of the innate immune system, were piloted during experimental work in this thesis, including Phorbol 21-myristate 13-acetate (PMA), lipopolysaccharide (Enzo®, Exeter, UK), muramyl dipeptide (InvivoGen®, Toulouse, France), N-formyl-Met-Leu-Phe (fMLP) (unless otherwise stated, all from Sigma-Aldrich, Gillingham, UK). In addition, stimulation of cells with the bacteria listed in *Table 3.7* was piloted (*Table 3.11*).

Stimulus	Mechanism	Dose Incubation
PMA	PKC activator NOXO1 phosphorylation	2.5-5 µg/ml Co-incubation
Various bacteria	Innate immune response	1:100 dilution of overnight culture
LPS	Innate immune response	400 ng/ml
MDP	Innate immune response	10 µg/ml
fMLP	FPR ligand	500 nM

Table 3.11: Stimuli of ROS. *The table details the putative ROS stimuli trialled during the course of this thesis, along with the mechanism of action and the dose used. Key: PKC, protein kinase C. Other abbreviations defined within text.*

3.2.9 Quantitative reverse transcriptase polymerase chain reaction (qRT-PCR)

Tissue collection, storage and handling. In order to minimise degradation of RNA, colonic biopsies were immediately transferred into 500 µl of RNAlater® solution (Qiagen, Crawley, UK) after extraction. Samples were then stored at -80°C and thawed at room temperature prior to experiments. All procedures were performed whilst wearing gloves and using filter tips on a clean working surface.

Total RNA isolation. Unless stated otherwise, total RNA was isolated using an RNAeasy® Mini Kit (Qiagen, Crawley, UK) as per manufacturer's instructions. DNAse digestion was using RNAse-Free DNAse Set (Qiagen, Crawley, UK) as per manufacturer's instruction. For tissue sections, directions for the 'Purification of Total RNA from Animal Tissues' were followed. For cultured cells, directions for the 'Purification of Total RNA from Animal Cells' were followed.

For colonic biopsies, tissues were transferred from RNAlater® solution and placed in RLT Buffer (Qiagen, Crawley, UK) supplemented with β-mercaptoethanol (1:100 dilution). Biopsies were then homogenised using a sterile motorised pestle (Pestle motor

and 1.5 ml microtube: VWR, Lutterworth, UK) to attain an even lysate. Subsequent RNAeasy® Mini Kit steps were followed as instructed.

For RNA extraction from cell cultures, cells were plated in 6- or 12-well tissue culture plates, and then harvested after washing once with PBS. Lysates were attained using RLT Buffer supplemented with β-mercaptoethanol (1:100 dilution). Subsequent RNAeasy® Mini Kit steps were followed as instructed.

RNA quantification. Isolated RNA was quantified by using a NanoDrop Spectrophotometer (NanoDrop ND-1000 Spectrophotometer, Thermo Fisher Scientific, Cramlington, UK). RNA quantification (ng/µl) and purity were measured using 1.2 µl of the sample for analysis. RNA purity was measured using a 260/280 ratio; according to standard practice, values of > 1.95 were considered of satisfactory purity for subsequent qRT-PCR.

Complementary DNA (cDNA) synthesis. Prior to cDNA synthesis, RNA concentrations were normalised to 1µg with DNAse/RNase-free water. Reverse transcription of the RNA into a stable cDNA was then performed using High Capacity cDNA Reverse Transcription Kit (Applied Biosystems®, Life Technologies, Paisley, UK) according to the manufacturer's instructions. All cDNA was stored at -20°C.

qRT-PCR. Gene expression analysis was carried out using manufacturer validated TaqMan® Gene Expression Assay primers with FAM-label (Life-technologies). The following TaqMan Gene Expression Assay primers used were: Hs02758991_g1 (GAPDH), Hs01071088_m1 (NOX1), Hs00166163_m1 (NOX2), Hs01098883_m1 (NOX3), Hs00418356_m1 (NOX4), Hs00225846_m1 (NOX5), Hs00213694_m1 (DUOX1), Hs00204187_m1 (DUOX2), Hs00376045_g1 (NOXO1), Hs00736699_m1 (NOXA1) primers (Taqman®, Life technologies, Paisley, UK).

A master mix to a volume of 8 µl for each primer was used for qRT-PCR; Taqman® MasterMix 5 µl, RNAase-free water 2.8 µl, and Taqman® Gene Expression Assay primer 0.2 µl. 2 µl cDNA was added to each primer master mix in a 96-well plate in duplicates or triplicates. The plate was centrifuged prior to transfer to the BioRAD CFX Real-Time PCR Detection System. PCR protocols and detection parameters were set-up according to TaqMan® Gene Expression Assay kit instructions.

Quantification. Gene expression was quantified relative to the reference gene (GAPDH) for each sample using the threshold cycle value (Ct). Relative expression was calculated based on the 2(-ΔCt) method (264);

Relative gene expression= 2(-ΔCt) = (Power(2, Ct reference gene- Ct gene of interest)).

3.2.10 Bacterial killing assays

HT-29 cells were seeded in 96-well flat bottom plates at 10^5 cells per well and incubated overnight in tissue culture conditions in McCoy's Complete medium. Bacterial culture and inoculation was performed as described in *Section 3.2.5*. One hour prior to bacterial infection, selected wells were co-incubated with ROS inhibitors (DPI 10 µM or ML171 10µM) in McCoy's Complete medium. The cells were then washed twice using PBS prior to bacterial infection.

Gentamicin protection assay. Bacteria suspended in PBS-G were added to HT-29 cell cultures at 100 MOI in 50 µL per well, plates were centrifuged at 3750 rpm for 3 minutes, and subsequently incubated in tissue culture conditions for 2 hours. The HT-29 cells were washed twice with PBS after 2 hours. Thereafter, gentamicin at a concentration of 100 µg/mL, diluted in 200 µL PBS-G, was added to each of the wells and the cells were returned to tissue culture conditions for a further 3 hours. This step kills extracellular bacteria remaining in suspension after the period of infection. The

cells were then washed twice with PBS before 20 µL of trypsin-EDTA solution was added to each well and incubated in tissue culture conditions for 10 minutes. The cells were then lysed using 200 µL of Triton-X 0.1% (in distilled water) per well, which was vigorously pipetted up and down to ensure cell lysis. The plate was incubated for 10 minutes at room temperature on a shaker (850 rpm). The cell- bacterial lysate was then diluted (1:10, 1:100, or 1:1000) in PBS-G. Thereafter, 10 µL of the diluted lysate (in triplicates) was pipetted onto appropriate agar plates by track method, set at an angle of around 45 degrees to allow flow down the agar. The plates were allowed to dry prior to sealing with Parafilm®.

The agar cultures were then incubated overnight in a 37°C bacterial incubator. The following morning, colony-forming units (CFU) were counted for each cell condition (*Figure 3.6*). This was conducted in a blinded manner; the counter was unaware of the conditions. The CFU for each inhibitory condition was then normalised as a percentage of the mean CFU for the untreated condition: *%CFU= (mean of condition/mean of untreated condition)*100*.

Extracellular bacterial killing assay. Bacteria suspended in PBS-G were added to HT-29 cell cultures at 1 MOI in 50 µL per well. The plates were then centrifuged at 3500 rpm for 3 minutes to ensure bacterial contact with the cell layer, prior to incubation in cell culture conditions for 2 to 5 hours. The cells were then washed twice with PBS prior to trypsinisation, cell lysis, and plating on agar plates (as per method described above).

Figure 3.6. Bacterial CFU's on agar plate following bacterial killing assay. *Counting of CFUs was performed by investigator blinded to conditions. The results are expressed as a percentage of the mean CFU for the untreated condition.*

3.2.11 Epithelial cell migration assay

HT-29 cells were seeded in a 24 well collagen I coated plate (Life Technologies, Paisley, UK) at 2 x 10^5 cells per well in 500 µl McCoy's complete medium and incubated in tissue culture conditions until a confluent monolayer (100% confluence) was reached. The monolayer was then washed with PBS to remove cellular debris. A pin was used to make a mark the underside of each well for subsequent orientation during image analysis. A single linear wound was created through the monolayer with a sterile pipette tip.

Images of the linear wound created in each well (10 images per well, 200x magnification) were photographed using Carl Zeiss Axioskop 2 and Q-Imaging software, using the pin marks for orientation. Co-incubation was then performed with competitive inhibitors (RAC1 inhibitor 100 µM, ML171 10 µM) in tissue culture conditions for 24 hours. Pre-incubation with irreversible inhibitor (DPI 10 µM) for 60

minutes was performed before washing with PBS and replenishing well with culture media. The experiment was performed in duplicates.

At 24 hours after cellular injury, images of wound healing were taken using the same camera, microscope, and magnification with orientation as per the pin-mark.

Images taken at 0 hours and 24 hours, were reconstructed and analysed using the ImageJ program (Java, National Institute of Health, USA), allowing calculation of the percentage wound closure over the period.

3.2.12 WST-8 tetrazolium proliferation assay

The WST-8 tetrazolium salt (2-(2-methoxy-4-nitrophenyl)-3-(4-nitrophenyl)-5-(2,4-disulfophenyl)-2H-tetrazolium, monosodium salt) (Sigma Aldrich, Gillingham, UK) is reduced to formazan by a reaction that is catalysed by mitochondrial dehydrogenase, the activity of which is increased during cellular proliferation (265). WST-8 gains a net negative charge after reduction, rendering it largely cell-impermeable.

HT-29 cells were seeded at 5 x 10^4 per well in a 96 well clear tissue culture treated flat-bottom plate (Costar®, Corning Incorporated, Life Sciences, NY, USA). After overnight culture in tissue culture conditions, HT-cells were then removed from the incubator, washed with PBS, and selected wells were treated with inhibitor conditions. Competitive inhibitors (ML171 10 µM) were co-incubated over the 24 time period, whereas pre-incubation with irreversible inhibitors (DPI 10 µM) was performed.

After 24 hours in tissue culture conditions, the plate was removed from the incubator and the wells were treated with the WST-8 compound (WST-8 1:10 per well) for 3 hours in tissue culture conditions. After 3 hours, calorimetric analysis of formazan accumulation was measured by plate-reader absorbance at 460nm. In order to correct

for background absorbance, the absorbance reading from a control well containing culture media but without cells was measured.

Manual counting of cells was performed in parallel at 24 hours. Cell counting was performed using trypan blue and haemocytometer according to standard technique (8 quadrants counted for each well in triplicates).

3.2.13 Ki67 immuno-reactive stain proliferation assay

Ki67 immunohistochemical staining was performed to assess cellular proliferation (266). This staining was performed by the histopathology department at the John Radcliffe Hospital.

In brief, a rabbit monoclonal antibody (SP66, ab16667, AbCam®, Cambridge, USA) to Ki67, an antigen expressed during late G1, S, G2 and M phases of the cell cycle, was used according to manufacturer's instructions. Haematoxylin and eosin (H&E) staining (Mayer's Haematoxylin, Eosin-Y, xylene; Sigma Aldrich, Gillingham, UK) was also performed according to standard technique. Mounting was performed using Vectashield® mounting media (Vector Laboratories, Peterborough, UK) on microscope glass slides and cover slips (Marienfeld Laboratory glassware, Thermo Scientific, Cramlington, UK).

Using a Carl Zeiss Axioskop 2 microscope at 200x magnification, the stained specimens were analysed. Images were photographed using Q-Imaging software and then reconstructed and analysed using ImageJ software (Java, National Institute of Health (USA).

The Ki67 proliferation index was assessed via manual counting of epithelial cells lining 10 longitudinally cut crypts per patient. The proportion of Ki67 immuno-reactive cells to non-immuno-reactive cells was determined (expressed as a percentage) (267).

3.2.14 Alcian blue and PAS staining of colonic epithelial biopsy specimens

Paraffin-embedded colonic epithelial biopsies were retrieved from the John Radcliffe Hospital Histopathology Department. The specimens were deparaffinised using xylene. The specimens were then rehydrated via serial immersion in ethyl alcohol (100%, 90%, 80%, and then 70%) followed by distilled water. Specimens were then stained using an Alcian Blue, and periodic acid/Schiff's reagent (PAS) staining kit (Clin-Tech Limited, UK). In addition, a nuclear fast red stain was used (Sigma Aldrich, Gillingham, UK). The staining was performed in collaboration with colleagues at the Sir William Dunn School of Pathology (RS).

Initially, the specimens were treated with Alcian blue (1% in 3% acetic acid) for 15 minutes. After washing with running tap water for 2 minutes and a subsequent rinse with distilled water, specimens were treated with periodic acid for 5 minutes, and thereafter Schiff's reagent for 10 minutes. Counterstaining was performed with nuclear fast red solution for 5 minutes. The specimens were then again dehydrated, immersed in xylene, and mounted.

The microscopy and software used for analysis are described in *Section 3.2.13*. Goblet cells were counted for a defined distance (300 pixels) from the surface epithelium of 10 longitudinally sectioned crypts for each patient in keeping with described technique (64). The total goblet cell surface area of proximal colonic crypts (defined distance of 300 pixels from the surface epithelium) was calculated from ten longitudinally cut crypts using ImageJ software (colour threshold analysis function) (Java, National Institute of Health, USA). The calculated total goblet cell area of a colonic epithelial crypt was then divided by the number of goblet cells present to obtain the average area

of individual goblet cells. The analysis was performed in a blinded fashion so as to avoid unconscious bias.

3.2.15 Statistical Analysis

All statistical analyses were performed using GraphPad Prism software (version 5.0a). For normally distributed data, the mean and standard error of mean is presented, and statistical comparison between groups assessed using a student's t test (two-tailed). For non-normally distributed data, the median and interquartile range is presented, and statistical comparison between two groups assessed using a non-parametric Mann Whitney test. In the case of paired non-normally distributed data, a Wilcoxon matched-pairs sign rank test was used. A Spearman's rank test was used to calculate correlation coefficients of non-parametric data. P values of <0.05 were considered significant.

3.3 REACTIVE OXYGEN SPECIES PILOT STUDIES

3.3.1 Specificity of L-012 chemiluminescence probe

The L-012 enhanced luminol probe is reported to specifically detect superoxide (243). Given that superoxide is the primary ROS species generated by NOX1, confirmation of L-012 probe specificity for superoxide was important for all subsequent experimental work. SOD, an enzyme that catalyses the formation of hydrogen peroxide from superoxide, was used assess the specificity of the L-012 probe.

Colonic epithelial biopsies were co-incubated with L-012 (100 μM) alone, or with L-012 in addition to SOD 5 μM. The superoxide signal (RLU), was measured via chemiluminescence, and plotted as a kinetic curve over 90 minutes, from which the AUC was calculated. The non-specific ROS inhibitor DPI (10 μM) was used as a comparator.

This experiment demonstrated that SOD significantly attenuates the L-012 chemiluminescence signal ($p=0.02$), confirming specificity of the L-012 probe for superoxide rather than hydrogen peroxide (*Figure 3.7*). DPI however, further abrogated the chemiluminescence signal ($p=0.01$). This suggests that a small proportion of generated superoxide may be detected by L-012 prior to dismutation to hydrogen peroxide by SOD.

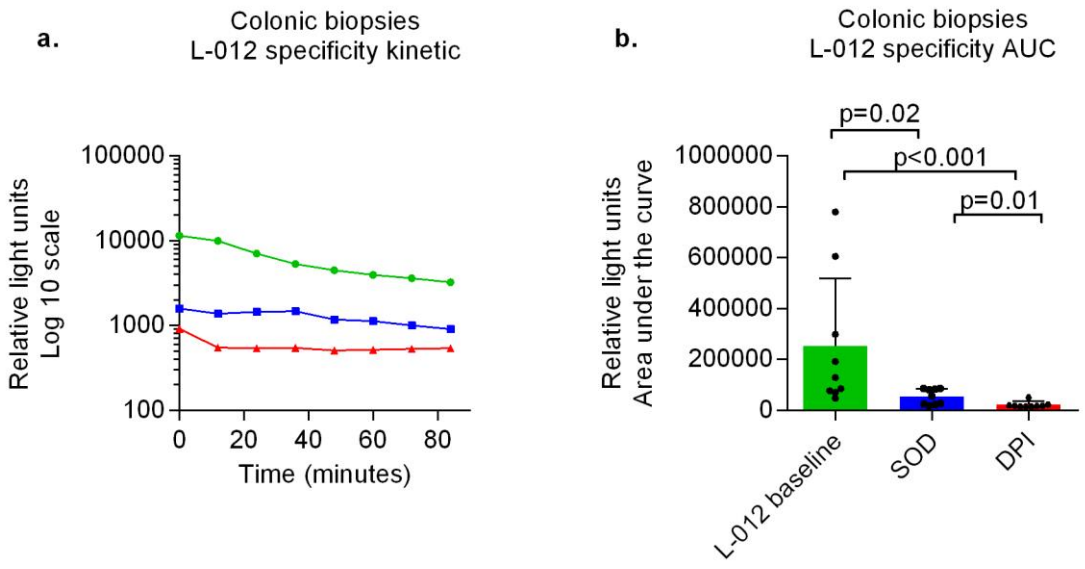

Figure 3.7. L-012 specificity for superoxide using SOD. *Pan-colonic epithelial biopsies from 3 healthy control patients were co-incubated with L-012 100 µM alone, or with SOD 5 µM or DPI 10 µM.* ***a).*** *L-012 chemiluminescence was plotted as a kinetic curve over 90 minutes (RLU).* ***b).*** *AUC of RLU was calculated. Experiment performed in triplicates for each condition (3 biopsies per patient per condition); the kinetic curve plotted as mean of measurements, symbols on AUC graph represent results. Statistical analysis was performed using unpaired nonparametric Mann Whitney test.*

3.3.2 NOX and DUOX mRNA expression in HT-29 cell line

The HT-cell line has been reported to express the functional NOX1 complex including the necessary subunits for superoxide production (233, 234). In order to confirm expression of NOX1 and its subunits NOXO1 and NOXA1 in HT-29 cells, qRT-PCR was performed. Analysis of other NOX and DUOX enzymes was also performed, so as understand other potential sources of ROS within the HT-29 cell line. Analysis of NOX3 was not performed as this NOX is known only to be expressed in the inner ear in humans (157).

qRT-PCR confirmed relatively high levels of expression of NOX1 mRNA in HT-29 cells, along with the NOXO1 and NOXA1 subunits necessary for full NOX1 assembly

and activation (*Figure 3.8*). Thus, HT-29 cell line was considered a suitable cellular phenotype for investigating the functional regulation of NOX1.

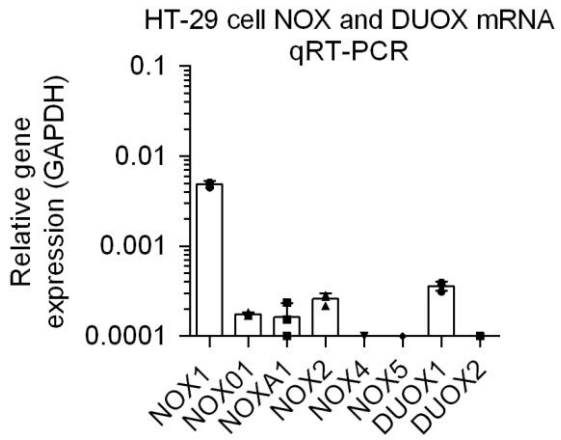

Figure 3.8. NOX and DUOX mRNA qRT-PCR in the HT-29 cell line*. Gene expression was quantified relative to the reference gene (GAPDH) for each sample using the threshold cycle value (Ct). Relative expression was calculated using the 2(-ΔCt) method. Experiment performed in triplicates (each symbol represents a result).*

3.3.3 PMA stimulation of HT-29 cells

PMA has been reported to stimulate NOX1-derived ROS generation, via phosphorylation of NOXO1 at Thr341 residue, allowing NOXO1 to directly interact with NOXA1 and catalyse the generation of superoxide by the complex (255, 256). HT-29 cells were stimulated with PMA so as to confirm the induction of superoxide generated by NOX1. The concentration of PMA was titrated in order to determine the optimal concentration for use as a positive control in future experiments.

PMA was shown to induce superoxide generation by HT-29 cells, measured using the L-012 chemiluminescence assay (*Figure 3.9*). A significant linear correlation with increasing PMA concentration and superoxide generation was demonstrated ($r = 0.96$, $p < 0.001$). During subsequent stimulation assays, a dose of PMA of 5 µg/ml was routinely used.

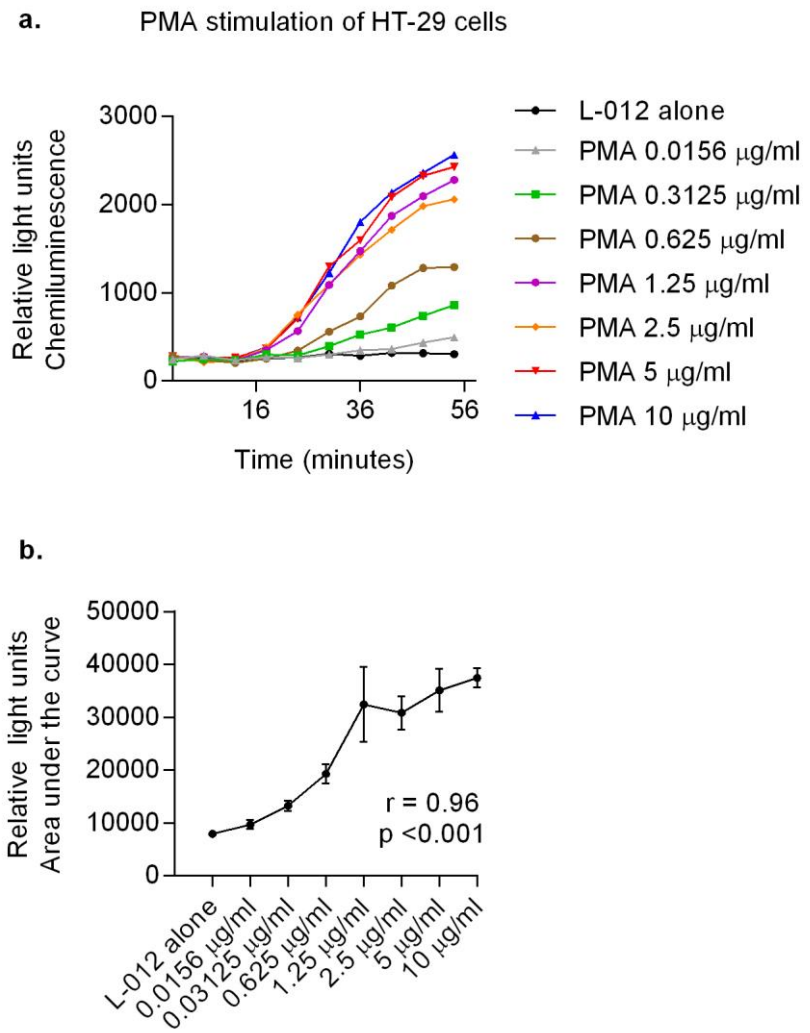

Figure 3.9. PMA stimulation of HT-29 cells. *HT-29 cells were seeded at 8 x 10^4 per well in a 96 well plate and incubated overnight in tissue culture conditions.* ***a).*** *L-012 chemiluminescence was plotted as a kinetic curve (RLU) over 60 minutes during co-incubation with PMA at the various concentrations listed.* ***b).*** *AUC of the L-012 kinetic plot was calculated for each dose of PMA and the correlation coefficient was analysed using linear regression. Experiment performed in triplicates; both the kinetic curve and correlation analysis plotted as mean of measurements (+/- standard deviation (SD) for correlation curve). Statistical analysis performed using non-parametric Spearman correlation coefficient*

3.3.4 NOX and DUOX mRNA expression in HT-29 cells on PMA stimulation

In order to determine whether PMA stimulation of HT-29 cells leads to upregulation of NOX or DUOX mRNA expression, qRT-PCR was performed following stimulation with PMA.

HT-29 cells were co-incubated with PMA 5 μg/ml for 30 minutes. At the time points of 30 minutes, 1 hour, 2 hours, and 6 hours after the PMA stimulation, NOX and DUOX mRNA expression was measured using qRT-PCR. At the same time-points, superoxide generated by HT-29 cells was measured using the L-012 chemiluminescence assay.

The results show minimal upregulation of mRNA expression on PMA stimulation, despite the increase in superoxide generation by HT-29 cells (*Figure 3.10*). This confirms prior data showing that generation of superoxide by NOX1 upon PMA stimulation is due to phosphorylation activation and assembly of the NOX1 apparatus, rather than transcriptional upregulation of the NOX1 mRNA (256).

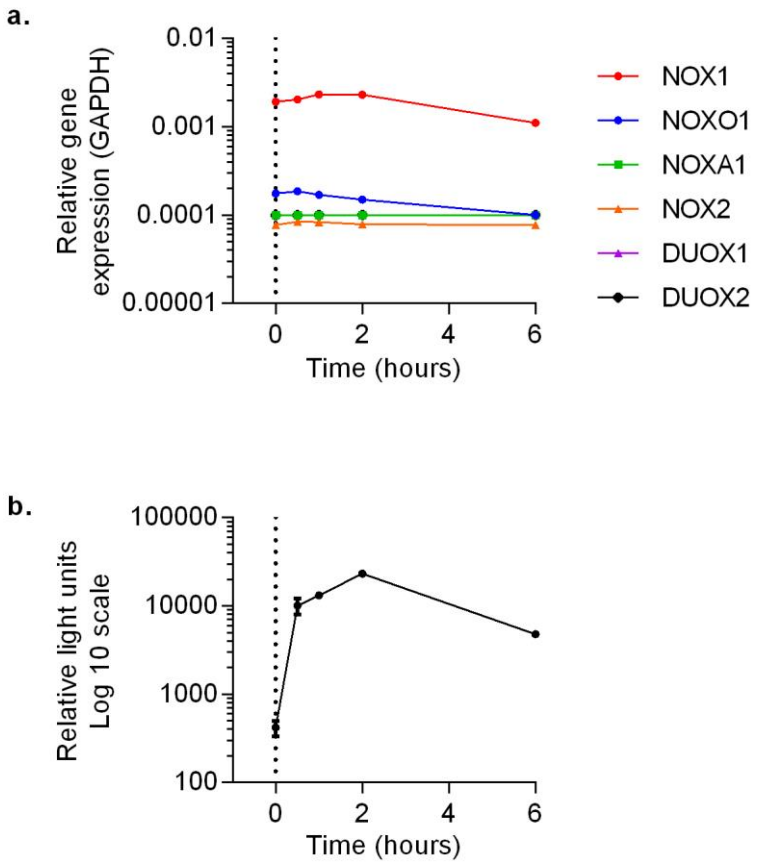

Figure 3.10. NOX and DUOX qRT-PCR and superoxide production in HT-29 cell line upon PMA stimulation. ***a).*** *Baseline unstimulated NOX/DUOX expression measured by qRT-PCR (Time 0, represented by dashed line). HT-29 cells were then co-incubated with PMA 5 µg/ml for 30 minutes, following which they were washed and wells were replenished with McCoy complete media. At the time points of 30 minutes, 1 hour, 2 hours, and 6 hours after PMA stimulation, NOX/DUOX mRNA expression was measured. Gene expression was quantified relative to the reference gene (GAPDH) for each sample using the threshold cycle value (Ct). Relative expression was calculated using the 2(-ΔCt) method. Experiment performed in triplicates, mean values provided.* ***b).*** *At baseline, and at time-points following stimulation (2, 4, 6 hours), superoxide generation was measured using L-012 chemiluminescence assay. Experiment performed in triplicates, mean of baseline RLU value provided at each time-point.*

3.3.5 Influence of media on superoxide detection

To determine the influence of cell culture media on detection of superoxide by the L-012 chemiluminescence assay, PMA stimulation of HT-29 cells was performed in selected cell culture media.

Superoxide generation was abrogated when the L-012 chemiluminescence assay was performed in RPMI (with or without phenol red), McCoy's (with and without FCS), or in PBS supplemented with FCS. The anti-oxidant constituents of cell culture media, as well as the naturally occurring antioxidant compounds in FCS, were the likely factors leading to abrogation of superoxide detected by L-012 chemiluminescence in the various cell culture media.

The cell culture media constituents, derived from the manufacturer's product details, were analysed and multiple putative antioxidant compounds were identified (*Table 3.12*). The supplementation of cell-culture media with antioxidants including pyridoxine, riboflavin, folate, ascorbic acid, vitamin B12, and glutathione, is performed in order to quench the potentially harmful ROS produced by cells in culture conditions (157, 268-270).

In contrast, superoxide generation was enhanced when the L-012 chemiluminescence assay was performed in PBS-G (1g/l), PBS + galactose (PBS-Gal) (1g/l), or PBS + butyrate (PBS-B) (1mM), as compared to PBS alone (*Figure 3.11*). This demonstrates that the provision of energy substrate to the cell culture, potentiates the generation of superoxide following stimulation with PMA. The potentiation of NOX1-generated superoxide is relevant to subsequent functional experiments in both the HT-29 cell-line and primary tissue.

	RPMI 1640	McCoy 5A	PBS
Ph.	7.2	7.0-7.4	7.4
Inorganic salts			
Calcium Nitrate $4H_2O$	0.1	--	--
Calcium chloride	--	0.1	--
Magnesium Sulphate (anhydrous)	0.04884	0.2	--
Potassium Chloride	0.4	0.4	0.2
Potassium phosphate monobasic	--	--	0.2
Sodium Bicarbonate	2.0	2.2	--
Sodium Chloride	6.0	6.464	8.0
Sodium Phosphate Dibasic (anhydrous)	0.8	0.649	1.15
Amino acids			
	Yes	Yes	No
Vitamins			
Ascorbic acid	--	0.0005	--
D-Biotin	0.0002	0.0002	--
D-Calcium pantothenate	--	0.0002	--
Choline Chloride	0.003	0.05	--
Folic Acid	0.001	0.01	--
i-inositol	--	0.36	--
myo-Inositol	0.035	--	--
Niacinamide	0.001	0.5	--
Nicotinic acid	--	0.0005	--
p-Aminobenzoic Acid	0.001	0.001	--
D-Pantothenic Acid (hemicalcium)	0.00025	--	--
Pyridoxine HCl	0.001	0.005	--
Riboflavin	0.0002	0.002	--
Thiamine HCl	0.001	0.002	--
Vitamin B_{12}	0.000005	0.020	--
Other			
D-Glucose	2.0	3.000	--
Glutathione	0.001	0.005	--
Phenol Red	0.0053	0.01	--

Table 3.12. Antioxidant constituents of cell culture media. *Putative antioxidants in cell media are high-lighted in green.*

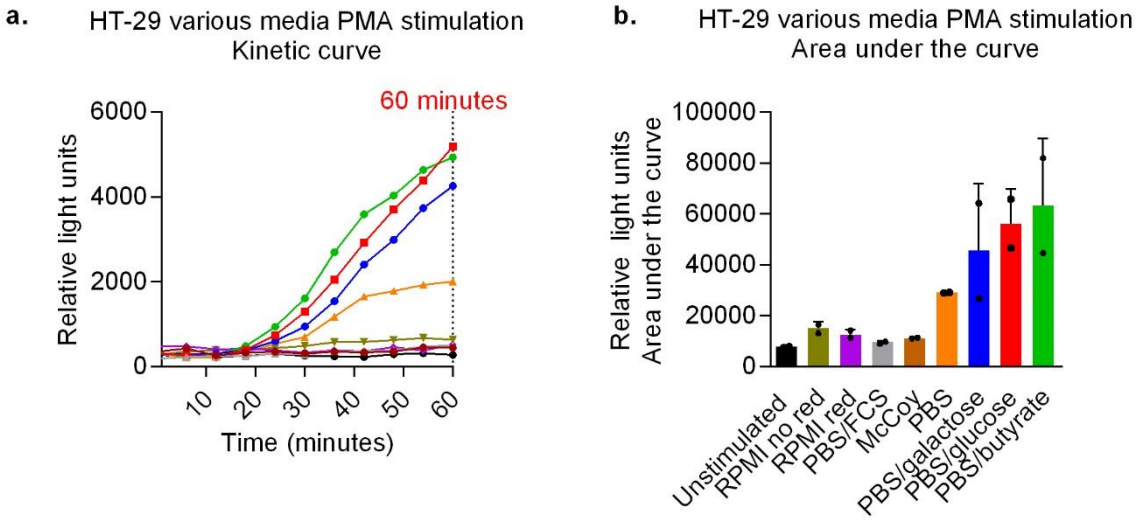

Figure 3.11. Superoxide generated by HT-29 cells on PMA stimulation in various media detected using L-012 chemiluminescence. *HT-29 cells were seeded at 1 x 10^5 per well in a 96 well plate and incubated overnight in tissue culture conditions.* ***a).*** *L-012 chemiluminescence RLU was plotted as a kinetic curve over 60 minutes in the various media conditions. For all conditions aside from that labelled unstimulated, co-incubation with PMA 5 µg/ml was performed over the time course.* ***b).*** *AUC was calculated. Experiment performed in duplicates; the mean value in plotted in the kinetic time course and the mean +/- SD is presented in the AUC graph.*

3.3.6 Potentiation of superoxide generation by HT-29 cells

Supplementation of media, probe, or stimulus. It was observed that the L-012 chemiluminescence kinetic signal (RLU) generated upon co-incubation with PMA stimulation peaks after 60-90 minutes, following which the chemiluminescence signal diminishes. In order to investigate whether reduction in signal over the time-course relates to exhaustion of cellular metabolism or rather consumption of either the stimulus or the chemiluminescence probe, a further experiment was performed.

HT-29 cells were co-incubated with L-012 and PMA in PBS without supplement, or PBS-G 1 g/l. A kinetic plot of L-012 chemiluminescence was recorded over 90 minutes, at which time, selected wells were supplemented with either additional energy substrate (glucose), additional L-012 probe, or additional PMA stimulus (*Figure 3.12*).

Glucose supplementation was shown to potentiate the superoxide generated, whereas no difference was seen with the addition of L-012 probe or PMA. This suggests that the exhaustion of HT-29 cellular metabolism due to lack of energy substrate in the unsupplemented PBS media leads to diminishing superoxide generation after 90 minutes of PMA stimulation.

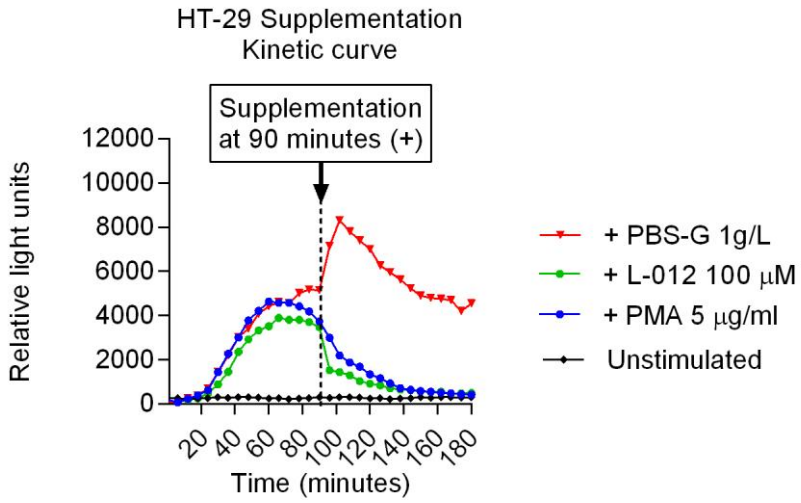

Figure 3.12. Supplementation of media, probe, or stimulus during kinetic superoxide generation. *HT-29 cells seeded at 1 x 10^5 per well in a 96 well plate and incubated overnight in tissue culture conditions. Co-incubation with L-012 (100 µM) and PMA (5 µg/ml) in PBS alone or PBS-G 1g/l was performed and a kinetic plot of L-012 chemiluminescence (RLU) generation was recorded over 90 minutes. At 90 minutes, selected wells were supplemented with either energy substrate (PBS-G 1 g/l), L-012 probe (100 µM), or additional PMA (5 µg/ml). Experiment performed in triplicates; the kinetic curve plotted as mean of measurements.*

Optimal HT-29 cell number for detection of superoxide. In order to determine the optimal HT-29 cell number to assess the influence of a positive control on superoxide generation using the L-012 probe, superoxide generation from decreasing numbers of HT-29 cells was measured upon stimulation with PMA (*Figure 3.13*).

The chemiluminescence signal detected was significantly diminished for 4 x 10^5 cells per well, as compared to 8 x 10^5 cells per well (p=0.01). There was a further significant reduction in signal for 2 x 10^5 cells per well, as compared to 4 x 10^5 per well (p=0.03), below which the sensitivity to detect the PMA stimulus by L-012 chemiluminescence was completely abrogated. On the basis of this experiment, a minimum of 4 x 10^5 cells per well was established as necessary to detect the influence of a positive stimulus using L-012 chemiluminescence.

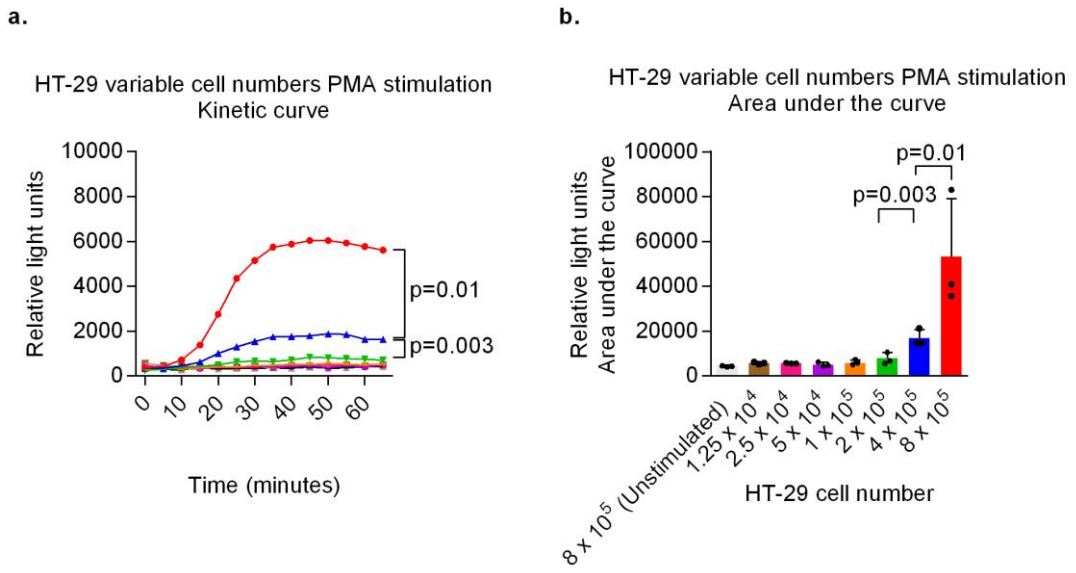

Figure 3.13. Superoxide generation by HT-29 cells of variable numbers detected by L-012 probe chemiluminescence. a). *HT-29 cells were seeded at the prescribed cell numbers in a 96 well plate and incubated overnight in tissue culture conditions. Cells were then co-incubated with PMA (5µg/ml) and L-012 (100 µM) and superoxide generation was plotted over a kinetic time course (RLU)* ***b).*** *AUC of RLU kinetic time course in a). calculated. Experiment performed in triplicates; the kinetic curve plotted as mean of measurements, symbols on AUC graph represent results. Statistical analysis performed using unpaired nonparametric Mann Whitney test.*

Superoxide detection from adherent or suspended HT-29 cells. In order to determine whether superoxide generation differs between HT-29 cells in the adherent state as compared to HT-29 cells in suspension, PMA stimulus was applied to HT-29 cells in adherent or suspended conditions (*Figure 3.14*).

This experiment demonstrated that HT-29 cells generate significantly more superoxide on stimulation with PMA in the adherent state, as compared to cells in suspension (p=0.01). This is likely to reflect that HT-29 cells are a constitutively adherent cell-line. The results of the experiment are relevant to subsequent work with colonic epithelial organoids, for which, chemiluminescence assays are performed on cells in suspension.

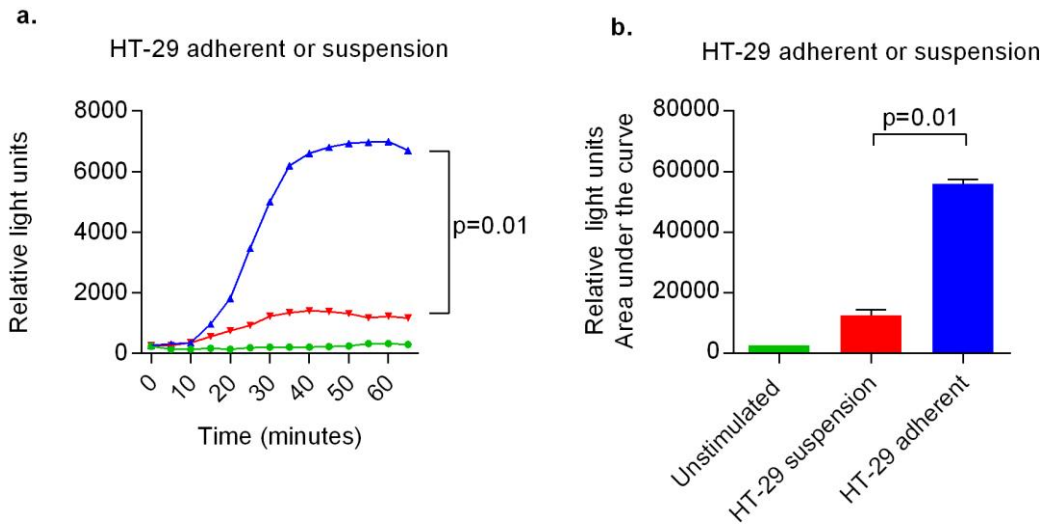

Figure 3.14. Superoxide generation from HT-29 cells either adherent or in suspension. *HT-29 cells seeded at 8 x 10^4 per well in a 96 well plate and incubated overnight in tissue culture conditions.* ***a)****. Cells in the adherent state, or following trypsinisation in suspension, were then co-incubated with PMA (5µg/ml) and L-012 (100 µM) and superoxide generation was plotted over a kinetic time course (RLU).* ***b).*** *AUC of RLU kinetic time course in a). calculated. Experiment performed in triplicates; the kinetic curve plotted as mean of measurements, symbols on AUC graph represent results. Statistical analysis performed using unpaired nonparametric Mann Whitney test.*

3.3.7 Alternative stimuli of superoxide generation by HT-29 cells

Experiments were undertaken to determine whether stimuli of the innate immune system of the intestinal epithelium could induce the generation of superoxide by HT-29 cells. HT-29 cells were co-incubated with either bacteria (EcN, *L. rhamnosus*, *S. aureus*, *S. typhimurium*, AIEC), or bacterial ligands including fMLP, LPS, and MDP, and resultant superoxide generation was measured (*Figure 3.15*).

Multiple strategies were trialled including variable periods of HT-29 cell co-incubation with stimuli of the innate immune system (30 minute, 60 minute, 2 hour, and overnight), as well as multiple ROS-probes and methods of analysis, and optimised cell culture media to potentiate generation of superoxide.

Thus, despite prior literature reporting bacteria species and ligands as potent ROS stimuli in intestinal epithelial cells (179, 182, 218, 219, 231), demonstration of an increase in superoxide production using these stimuli in HT-29 cells was not achieved in this thesis chapter.

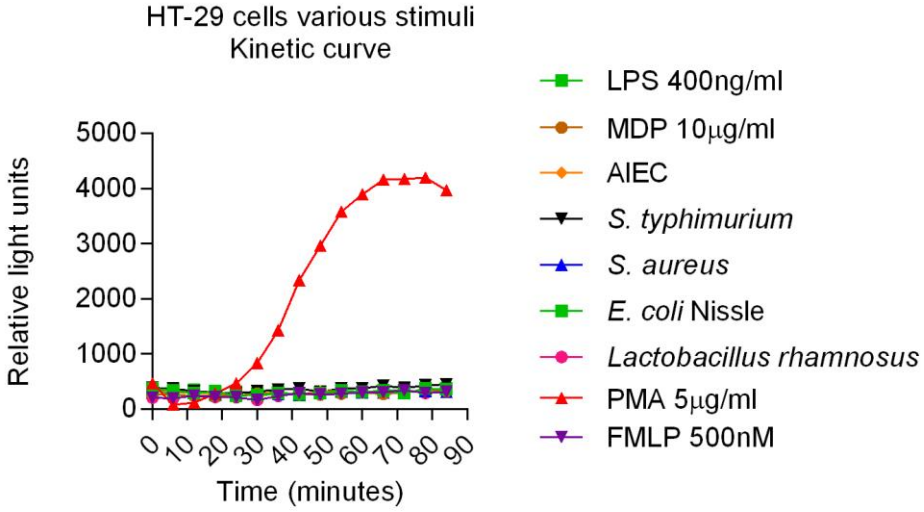

Figure 3.15. Alternative stimuli of superoxide generation by HT-29 cells detected using L-012 chemiluminescence probe. *HT-29 cells seeded at 8 x 10^4 per well in a 96 well plate and incubated overnight in tissue culture conditions. Pre-incubation with stimulus was performed for variable time periods (30 minutes to overnight). Co-incubation with L-012 (100 µM) in PBS-G was then performed and superoxide generated measured over a kinetic time course (RLU). PMA (5 µg/ml) was used as a positive control. The described bacteria were applied to cells at 1:100 dilution of overnight culture, LPS 400 ng/ml, MDP 10 µg/ml, fMLP 500 nM. The experiment was performed in triplicates; the kinetic curve plotted as mean of measurements.*

3.3.8 ROS and NOX inhibitors in HT-29 cells

Experimentation with ROS and NOX inhibitors was undertaken in the HT-29 cell line. In particular, NOX1 inhibitors were used, so as to chemically abrogate superoxide production from NOX1 in HT-29 cells and create a cell-line construct of the *NOX1* p.N122H variant patient for further functional experimental work.

Concentration of ROS and NOX inhibitors. The optimal concentration of a non-specific ROS inhibitor (DPI), as well as NOX1 inhibitors (ML171 and ML090), and a small molecule RAC1 inhibitor was established in HT-29 cells using the L -012 chemiluminescence assay. Pre-incubation with the described inhibitor was performed for 30 minutes prior to co-incubation with L-012 chemiluminescence probe and PMA stimulus (*Figure 3.16*).

Both DPI and ML171 were shown to inhibit generation of superoxide by HT-29 cells on stimulation with PMA, with maximal inhibition achieved using a concentration of 10 µM of DPI and 10 µM of ML171. There was no inhibition of superoxide generation by HT-29 cells demonstrated using ML-090 or RAC1 inhibitors.

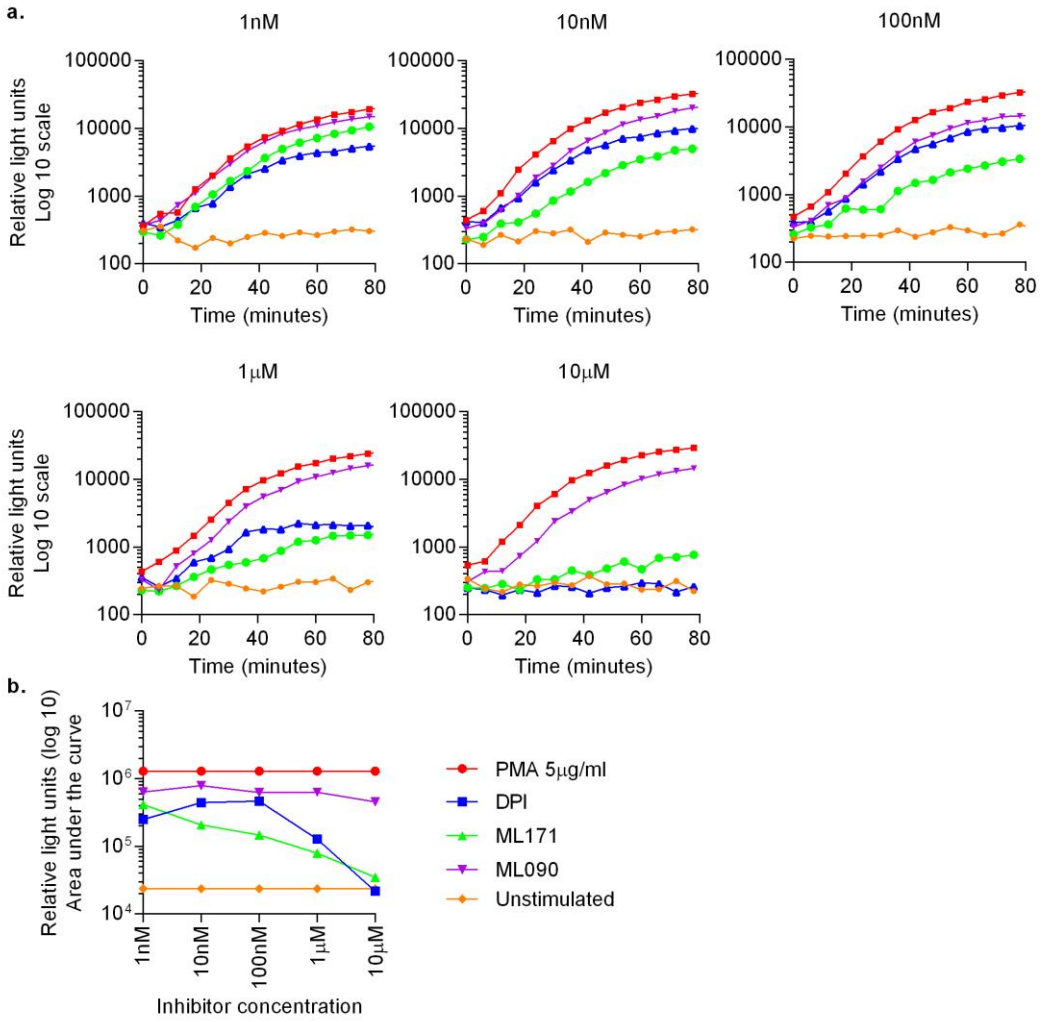

Figure 3.16. Concentration of ROS and NOX inhibitors. *HT-29 cells seeded at 8 x 10^4 per well in a 96 well plate and incubated overnight in tissue culture conditions. Pre-incubation with inhibitor at described concentration for 30 minutes, prior to co-incubation with PMA stimulus (5 µg/mL) and L-012 probe (100 µM).* ***a).*** *Superoxide generation plotted as a kinetic curve (RLU) over 80 minutes.* ***b).*** *AUC of kinetic curve calculated at each inhibitory concentration. The experiment was performed in triplicates; the kinetic curve plotted as mean of measurements. Data for RAC1 not shown in the combined graph.*

Duration of ROS and NOX inhibition. The duration of NOX and ROS inhibition was assessed over a 24 hour time course using selected inhibitors in HT-29 cells.

Co-incubation with competitive inhibitors (ML171 and RAC1) was performed over the 24 hour time-period, whereas pre-incubation with the irreversible DPI inhibitor was performed for 30 minutes prior to washing and replenishing wells with culture media for the time course. Superoxide generation following stimulation with PMA was measured using L-012 chemiluminescence assay at the time points of 2, 6 and 24 hours after initial incubation. The cells were viewed under an inverted light microscope at each of the time points to concurrently assess cell viability and adherence (images not shown) (*Figure 3.17*).

The experiment demonstrated that the NOX1 specific inhibitor, ML171, was effective in abrogating superoxide production by HT-29 cells between the concentrations of 1 µM and 100 µM at the 2 hour and 6 hour time-points. However, after 24 hours, only a concentration of ML171 100 µM was shown to inhibit superoxide production by HT-29 cells. DPI was effective in abrogating superoxide generation by HT-29 cells at each of the time points (2, 6, and 24 hours) at concentrations of 10 µM and 100 µM. Again, there was no inhibition of superoxide generation with the RAC1 inhibitor.

At the 24 hour time point, for each of the inhibitory conditions, the cells were examined under inverted light microscope (200x magnification) and were observed to remain adherent and viable.

These experiments inform future use of the NOX1 and non-specific ROS inhibitors in functional experiments involving the HT-29 cell line.

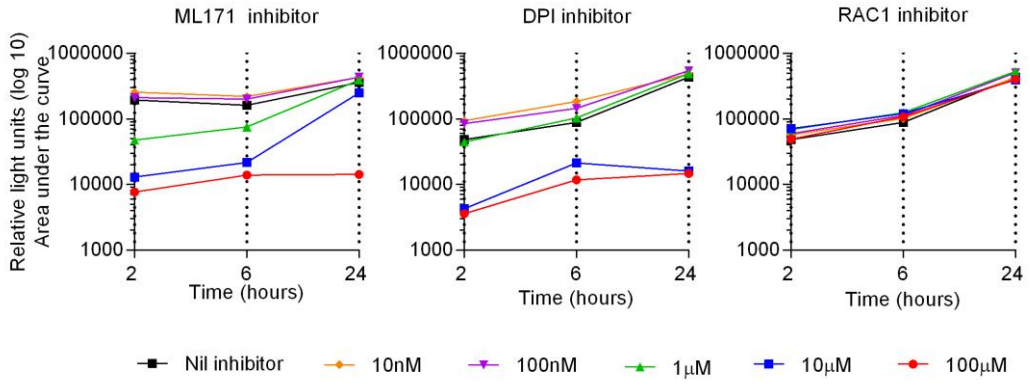

Figure 3.17. Duration of inhibition of ROS and NOX. *HT-29 cells seeded at 8 x 10^4 per well in a 96 well plate and incubated overnight in tissue culture conditions. Co-incubation with ML171 and RAC1 over 24 hours in McCoy's complete medium at variable concentrations. Pre-incubation with DPI at variable concentration for 30 minutes then wash and incubate in McCoy's complete medium over time period. PMA 5 µg/mL stimulation at time points (2, 6, and 24 hours) and L-012 chemiluminescence assay performed. AUC of RLU over 80 minutes presented for each concentration of the inhibitor. Experiment performed in triplicates, the kinetic curve plotted as mean of measurements.*

3.3.9 Summary of ROS pilot studies

The pilot studies evaluating techniques in the use of ROS probes, stimuli, and inhibitors, were informative for the subsequent experimental work in evaluating the functional significance of the *NOX1* p.N122H variant phenotype. In summary, the ROS pilot studies revealed:

- HT-29 cells express functional NOX1 machinery (NOX1, NOXO1, and NOXA1) and are an appropriate cellular phenotype for functional studies of the *NOX1* p.N122H variant mutation.
- The L-012 chemiluminescence probe is specific and sensitive for the detection of superoxide.
- PMA induces superoxide generation by HT-29 cells. Superoxide generation by HT-29 cells was not detected by other stimuli of the innate immune system.

- Superoxide generation may be enhanced by supplementation of media with energy substrates, such as glucose, galactose, or butyrate.
- ML171 inhibits NOX1-derived superoxide generation in HT-29 cells.

3.4 CHARACTERISATION OF THE *NOX1* p.N122H VARIANT

3.4.1 Clinical phenotype of the *NOX1* p.N122H variant patient

The patient carrying the *NOX1* p.N122H variant is a male with VEOIBD, initially diagnosed as inflammatory bowel disease yet to be classified. At the time of investigation he was 19 years old. His disease was of pan-colonic distribution and perianal distribution at diagnosis, however has been more typical of a UC phenotype over the subsequent disease course (*Figure 3.18, 3.19 and Table 3.13*).

He is the second of two siblings (sister), born at normal term delivery, and without a family history of IBD or gastrointestinal illness or malignancy. He does not have significant other medical comorbidities aside from mild eczema, for which he does not require regular medication. He is a non-smoker and works as an apprentice electrician.

His onset of symptoms was at the age of 2 years old with bloody stools and failure to thrive. He was formally diagnosed with IBD at the age of 5 years, at which time endoscopic and histological revealed typical findings of IBD. He required oral corticosteroid therapy at diagnosis. His disease was difficult to treat and after years of inadequate control of disease on 5-ASA therapy, he required immunosuppression with azathioprine and methotrexate therapy, and subsequently antiTNF-α therapy (adalimumab).

His disease was complicated by Epstein Barr virus (EBV)-associated haemophagocytic lymphohistiocytosis (HLH), which occurred whilst on azathioprine therapy at the age of 14 years. At that time, he presented to hospital with high fevers, jaundice, hepatosplenomegaly, and a widespread rash. He was found to be pancytopenic (haemoglobin 10.0 g/L, total white cell count 1.12 $x10^9$/L, neutrophils 0.78 $x10^9$/L, and platelets 59 $x10^9$/L), with deranged liver function tests (bilirubin 127 µmol/L

(conjugated 116 µmol/L), ALT 87 IU/L, ALP 1669 IU/L), and a mild coagulopathy (prothrombin time 14.8 seconds, activated partial thromboplastin time 34.1 seconds). EBV M and G immunoglobulins were found to be positive. Bone marrow trephine revealed a hypocellular marrow, with an excess of macrophages (PGM1 and KP1 positive) showing haemophagocytosis. The features were consistent with HLH and secondary myelodysplasia. His azathioprine therapy was withdrawn and he required intensive care therapy and a protracted hospitalisation.

At the time of investigation his disease was quiescent whilst on adalimumab therapy (40mg every other week). From here on in the thesis, this patient is referred to as the '*NOX1* p.N122H variant patient'.

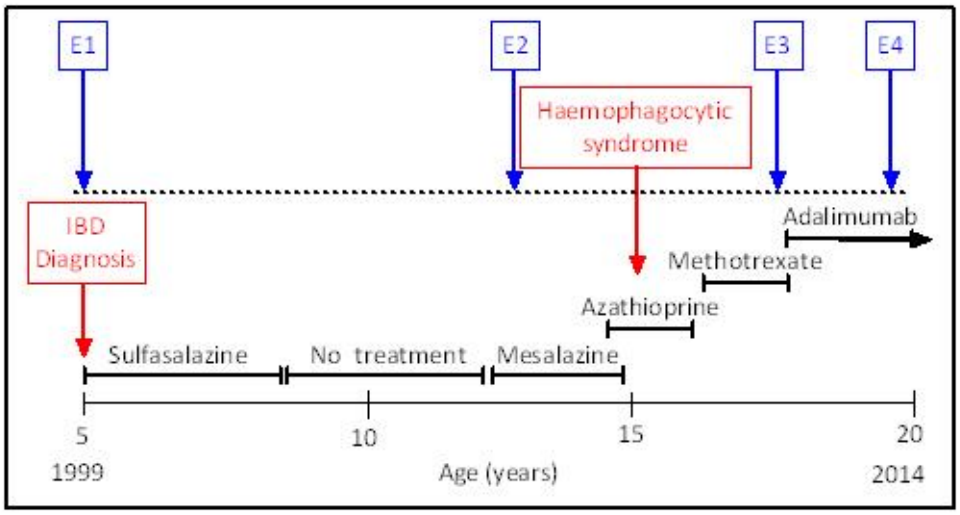

Figure 3.18. NOX1 p.N122H variant patient clinical phenotype. *The figure provides a time-line of diagnosis, medications, investigations, and significant events. The endoscopic investigations are denoted as E1-E4.*

Time-point		Investigation	Report	Histology
E1	Age 5 (1999)	Colonoscopy	-Inflamed perineum, perianal skin tags and chronic fissuring. -Active proctitis.	Severely active chronic inflammation with crypt architectural distortion, focal Paneth cell metaplasia, and a single micro-granuloma.
		Barium follow-through study	Normal small bowel.	
E2	Age 13 (2007)	Colonoscopy	-Perianal skin tags. -Pan-colonic erythema and ulceration. -Normal terminal ileum.	Moderately active chronic inflammation with cryptitis, crypt architectural distortion, and single colonic granuloma.
		Endoscopy	-Normal oesophagus, stomach, and duodenum.	Focal acute and chronic inflammation.
E3	Age 18 (2013)	Colonoscopy	-Perianal skin tags -Pan-colonic erythema, ulceration with shortened and featureless colon. -Normal terminal ileum.	Moderately active chronic inflammation with cryptitis, crypt abscesses, and crypt architectural distortion.
E4	Age 19 (2014)	Colonoscopy	-Quiescent pan-colitis with no active inflammation evident	Quiescent disease without active inflammation.

Table 3.13. NOX1 p.N122H variant patient time-line of clinical investigations. *The table details endoscopic and radiological investigations performed over the clinical history of the NOX1 p.N122H variant patient. The E1-4 coding draws reference from the preceding figure to place the investigations on a time-line.*

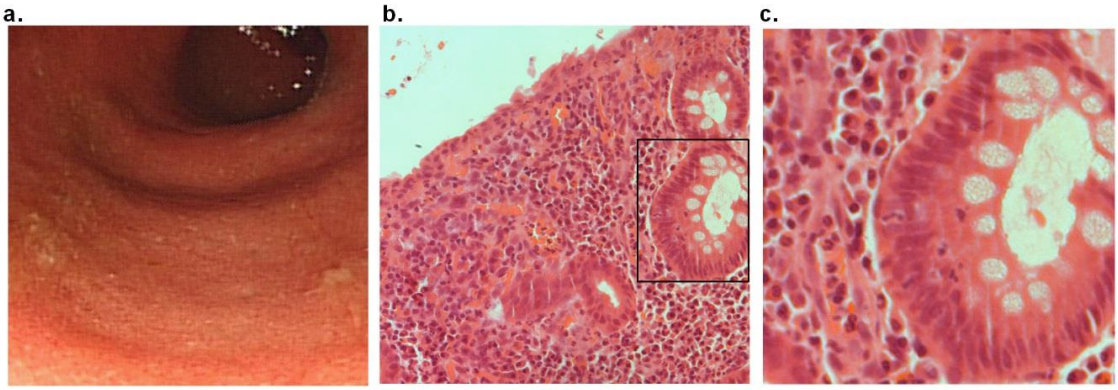

Figure 3.19. NOX1 p.N122H variant patient colonoscopic and histologic findings *(Time point E3, colonoscopy 2013).* ***a).*** *Macroscopic features: pan-colonic erythema and ulceration with a shortened and featureless colon.* ***b).*** *H&E stained histological specimen. Images taken at 200x magnification. Moderately active chronic inflammation with cryptitis, crypt abscesses, and crypt architectural distortion.* ***c).*** *Single crypt at 400x magnification. Crypt abscess demonstrated along with atypical elongated epithelial cell nuclei.*

3.4.2 Genetic analysis of the *NOX1* p.N122H variant

Genetic analysis of the *NOX1* p.N122H variant patient revealed a hemizygous mutation in *NOX1* on the X-chromosome, with an exonic missense substitution of an A for C at position 364 (c.A364C), leading to the substitution of asparagine to histidine (p.N122H). Thus, this is an X-linked protein-encoding missense mutation. The observed mutation has several properties that suggest a functionally relevant variant, as described in my Supervisor's (HU) report in *Box 3.1* and detailed in *Figure 3.20.*

Characteristics of the NOX1 p.N122H variant

- 22 variants of *NOX1* are present in the 12,000 exome dataset but not the *NOX1* p.N122H variant suggesting that this variant is unique (data from 2013).
- Analysis predicts a damaging mutation at an evolutionary conserved site; SIFT 0, polyphen-2 0,999, conservation score 0,999975.
- Since NOX1 is a close homolog of the catalytic subunit of NOX2, similarity analysis between NOX1 and NOX2 allowed prediction that the *NOX1* p.N122H variant is located in the conserved region of the 3rd transmembrane domain, which most likely affects protein function.
- The Oxford variant affects all known isoforms of NOX1.

Box 3.1. Description of the NOX1 p.N122H variant. *The box details the features of the NOX1 p.N122H variant that implicate the mutation to be significant. The initial description as such was made in 2013, by my supervisor (HU).*

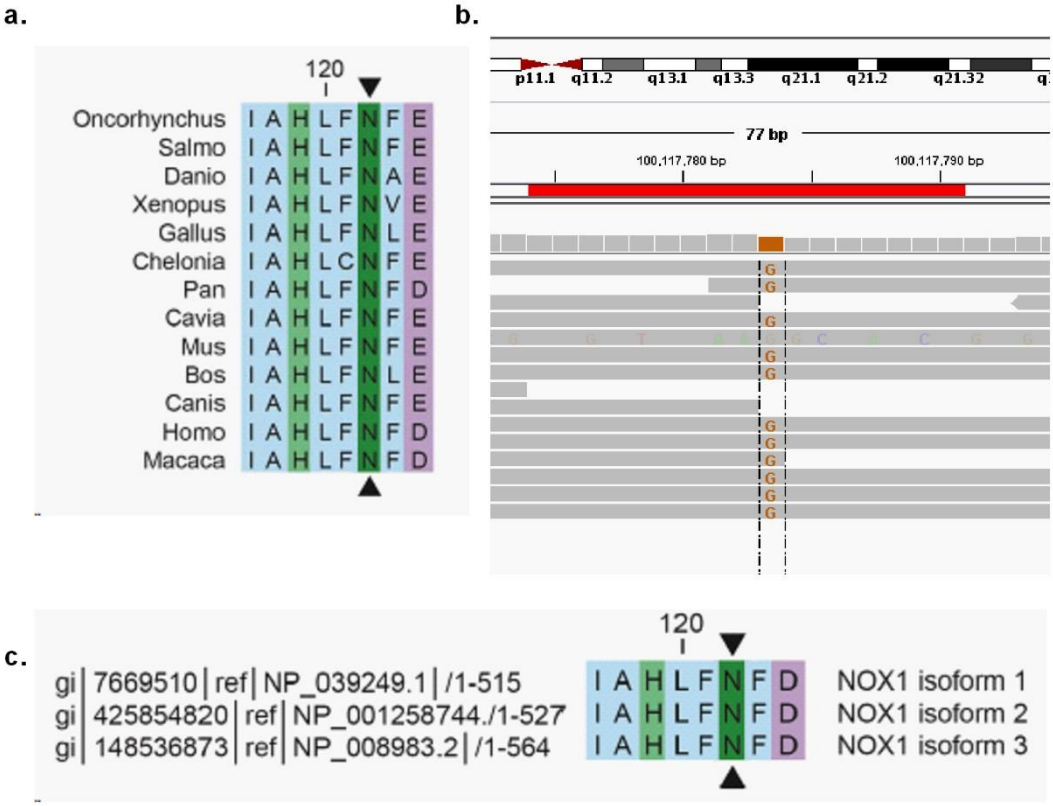

Figure 3.20. Genetic analysis of the NOX1 p.N122H variant. a). *NOX1 protein sequence alignment showing evolutionary conserved asparagine (N) in position 122.* ***b).*** *Coverage of the NOX1 gene by whole genome sequencing.* ***c).*** *The NOX1 p.N122H variant affects all three isoforms of NOX1. Amino acid sequence aligned using ClustaIW software. Data contributed by my supervisor (HU) and figure prepared with colleagues (SP, TS).*

3.4.3 NOX1 family pedigree and genetic validation.

In order to investigate whether the *NOX1* p.N122H variant is of X-linked familial transmission or a spontaneous de novo mutation, targeted sequencing was performed of the mutation site of the patient's mother to construct a pedigree diagram (*Figure 3.21*). A patient with IBD was also sequenced as a wild-type control.

The sequencing confirmed the *NOX1* p.N122H variant patient's mother to be heterozygous for the c.A364C substitution mutation, confirming X-linked transmission of the mutation to the male *NOX1* p.N122H variant patient. The wild-type IBD control

showed the conserved A codon in position 364.

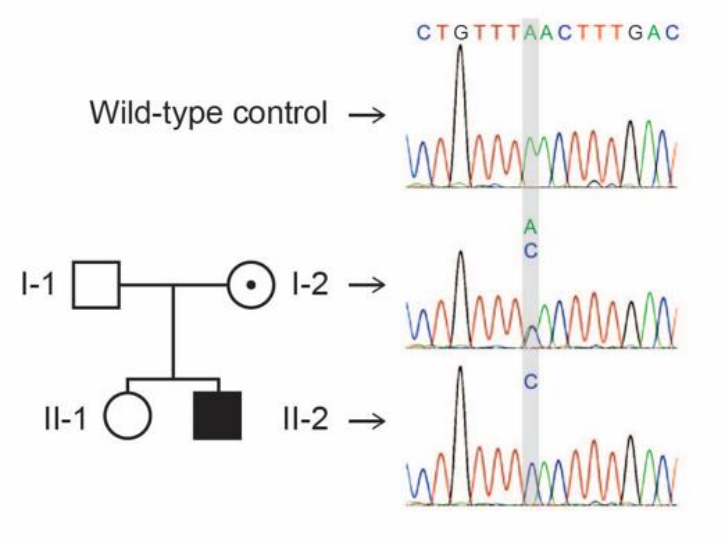

Figure 3.21. Family pedigree and Sanger sequencing of NOX1 gene around the mutation site. *The sequencing revealed the NOX1 p.N122H variant patient's mother to be heterozygous for the c.A364C substitution mutation, confirming X-linked transmission of the mutation to the male NOX1 p.N122H variant patient. Sequencing performed by laboratory colleague (JJW).*

3.4.4 NOX and DUOX mRNA expression in the human gastrointestinal tract

In humans, NOX1 is reported to be predominantly expressed in the colon, where there exists a gradient of expression from the proximal colon (intermediate expression) to the distal colon (high expression) (167, 168). Although NOX1 is reported to be expressed in the stomach of both mice and guinea pigs, this is species dependent as there is no reported expression in the human stomach (230, 271).

In order to explore the gastrointestinal NOX1 mRNA expression profile in humans, pan-enteric biopsies were collected from non-inflamed individuals without endoscopic or histological evidence of gastrointestinal disease and qRT-PCR was performed (*Figure 3.22).*

NOX1 mRNA expression was demonstrated to be highest in the lower gastrointestinal tract (colon), where a gradient of increasing NOX1 expression from the ileum (intermediate) to the left colon (high) was demonstrated. There was co-expression of the NOXA1 and NOXO1 subunits necessary for complete assembly of the NOX1 apparatus in the colon.

NOX2 mRNA was highly expressed throughout the gastrointestinal tract. This expression profile was hypothesised to relate to gastrointestinal biopsy sampling of the lamina propria containing immune cells (phagocytes) expressing NOX2, rather than expression of NOX2 by gastrointestinal epithelial cells. In keeping with prior studies (235), DUOX1 and DUOX2 mRNA was expressed throughout the gastrointestinal tract epithelia, with higher expression in the proximal gastrointestinal tract.

This experiment confirmed the predominant expression of NOX1 in distal gastrointestinal tract, with a gradient of increasing expression from the terminal ileum to the distal colon.

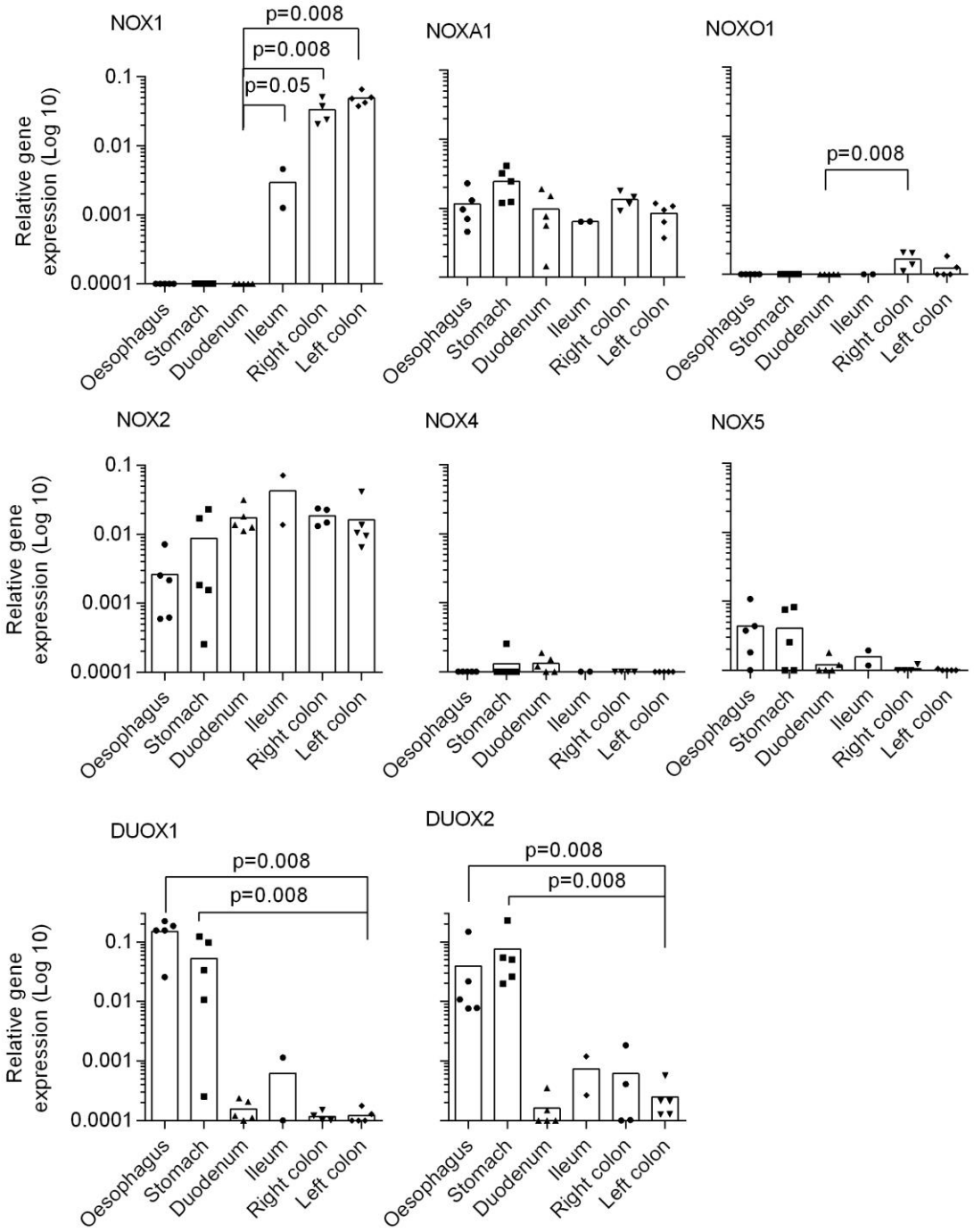

Figure 3.22. NOX and DUOX mRNA expression in the human gastrointestinal tract. *Results representative of biopsy specimens taken from the gastrointestinal tract of 5 healthy, non-inflamed individuals (mRNA from single biopsy per segment from each patient analysed). Experiment performed in duplicates. Gene expression was quantified relative to the reference gene (GAPDH) for each sample using the threshold cycle value (Ct). Relative expression was calculated based on the 2(-ΔCt) method. Statistical analysis performed using unpaired nonparametric Mann Whitney test.*

3.4.5 Superoxide production from pan-enteric human gastrointestinal biopsies

In order to interpret the functional significance of the NOX and DUOX expression profile in the human gastrointestinal tract, superoxide production from pan-enteric biopsy specimens was measured (*Figure 3.23*).

Baseline superoxide production by *ex-vivo* gastrointestinal epithelial biopsy specimens measured by L-012 chemiluminescence, demonstrated an increasing proximal to distal gradient in the gastrointestinal tract, similar to that of NOX1 mRNA expression. This was observed both at baseline and upon stimulation with PMA. This data implicates NOX1 as a primary source of superoxide in the distal gastrointestinal epithelium.

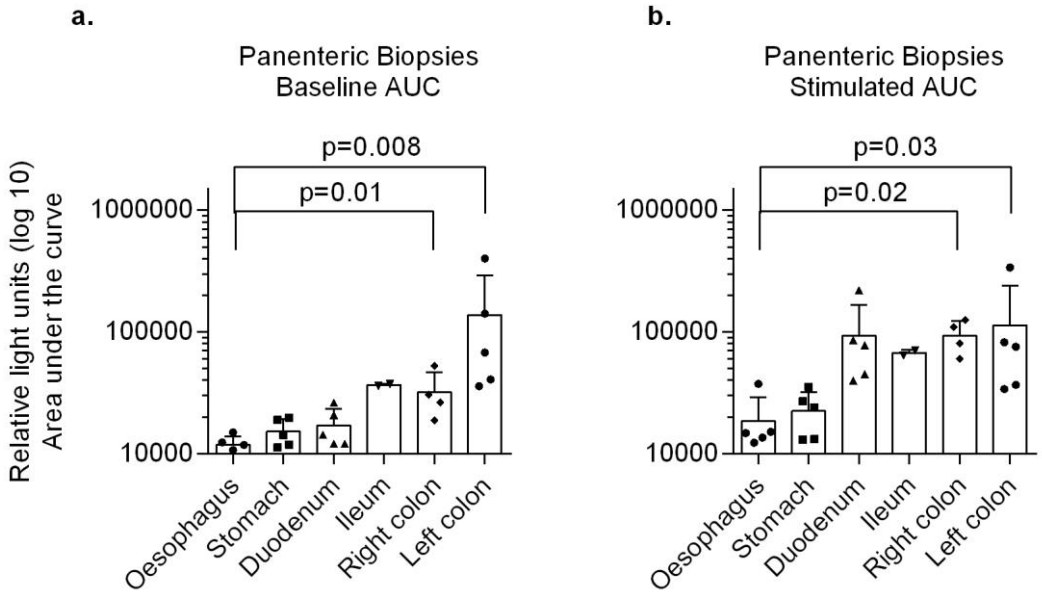

Figure 3.23. Superoxide generation from human pan-enteric biopsies. a). *Superoxide generation from pan-enteric biopsy specimens from 5 healthy control patients. Biopsies co-incubated with L-012 100 µM alone and kinetic curve plotted over 60 minutes (RLU), from which the AUC was calculated. Where more than one biopsy per segment, the mean per segment is presented for each patient.* ***b).*** *Co-incubation with PMA 5µg/mL over time course. Otherwise as per a). Statistical analysis performed using unpaired nonparametric Mann Whitney test.*

3.4.6 ROS inhibitor studies in colonic epithelial biopsies

In order to confirm the role of NOX1 in ROS generation by the human colonic epithelium, superoxide production was measured, in the presence of both a non-specific NOX/ROS inhibitor (DPI) and a NOX1 inhibitor (ML171). The L-012 probe was used to measure superoxide generation by chemiluminescence. In addition, the nitroblue tetrazolium (NBT) probe was used in order to visualise colonic epithelial ROS production via the formation of reduced formazan, which is visible using light microscopy.

The NBT assay demonstrated that baseline ROS production in the colonic epithelium is localised to colonic epithelial crypts. This is demonstrated by 'rings' of reduced formazan deposition at the margin of the colonic crypt epithelial cells (*Figure 3.24*).

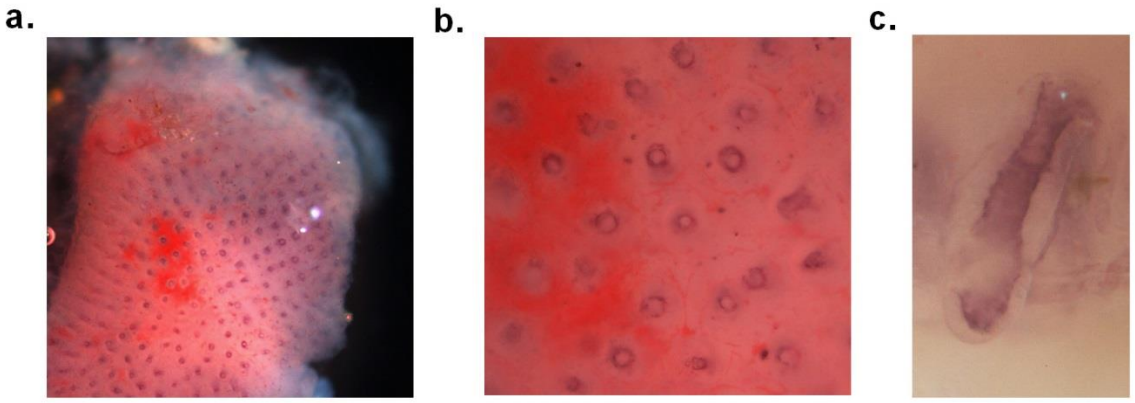

Figure 3.24. NBT assay in colonic biopsy specimens. *Ex-vivo colonic biopsies (within 90 minutes of collection) were incubated with NBT 100 µg/ml in PBS-G (1g/l) in petri dishes for 60 minutes at room temperature. The biopsy specimens were analysed using light microscopy immediately after the 60 minute NBT incubation.* ***a).*** *Colonic epithelial biopsy specimen at magnification of 100x, showing dark crypts containing reduced formazan.* ***b).*** *Colonic epithelial biopsy crypts at 200x magnification. Ring-like deposition of formazan at epithelial margin of crypts clearly evident.* ***c).*** *Single colonic epithelial crypt captured longitudinally at high magnification.*

Baseline ROS production was attenuated by ML171 treatment, demonstrating the role of NOX1 in baseline ROS production by colonic epithelial cells. DPI completely

abrogated the baseline ROS signal from colonic epithelial crypts. This may be hypothesised to relate to complete inhibition of NOX and DUOX2 generated ROS (hydrogen peroxide) (*Figure 3.25*).

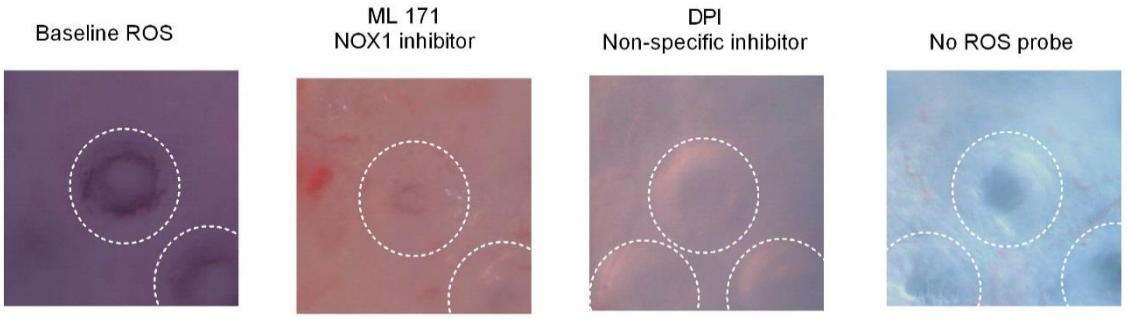

Figure 3.25. NBT assay with inhibitory conditions in colonic epithelial biopsy specimens. *The figure is representative of assay performed in 3 non-inflamed patients showing consistent results. The specimens were co-incubated with NBT 100 µg/ml in PBS-G (1g/l) for 60 minutes prior to analysis by light microscopy (200x magnification). Co-incubation with ML171 10 µM of DPI 10 µM was performed where indicated. The images were taken using Q-imaging software and depict individual colonic epithelial crypts (encircled). The dark blue is formazan which is reduced in the presence of ROS.*

A corresponding L-012 chemiluminescence assay was performed in colonic epithelial biopsies (*Figure 3.26*), which confirmed the findings of the NBT assay. Baseline superoxide production from colonic epithelial biopsy specimens measured using L-012 chemiluminescence was significantly reduced following treatment with ML171 ($p=0.02$). A further reduction in superoxide generation was seen with DPI treatment as compared to ML171 ($p=0.008$), which is in keeping with the broad and non-specific NOX/ROS inhibition from other superoxide sources within biopsy specimens.
These experiments involving the use of two ROS probes, demonstrate that NOX1 is responsible for a significant proportion of the baseline ROS generated by colonic epithelial cells.

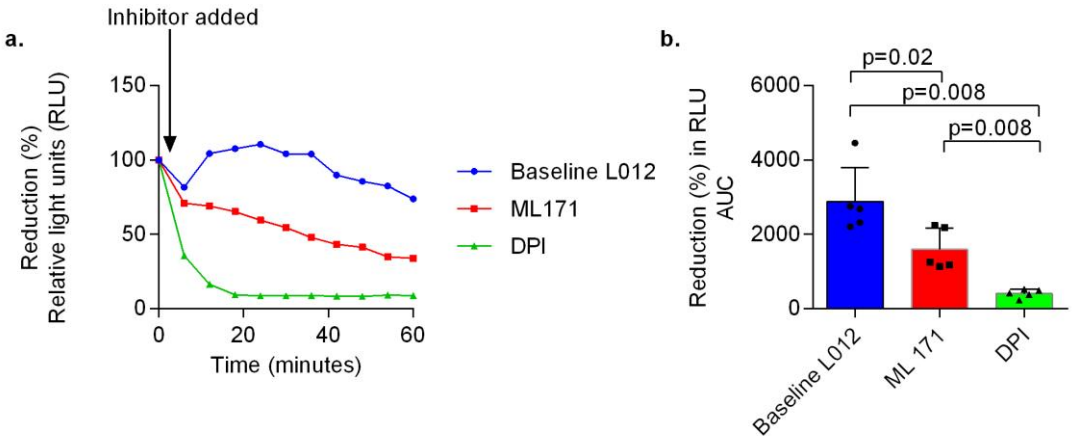

Figure 3.26. L-012 chemiluminescence assay with inhibitory conditions in colonic epithelial biopsy specimens. *The figure is representative of assay performed in 5 non-inflamed patients. The experiment was performed in duplicates for each patient. Biopsy results were excluded where the baseline reading was <1000 RLU.* ***a).*** *After a baseline reading in L-012 alone (100 µM), biopsy specimens were co-incubated with L-012 alone, or with ML171 10 µM, or DPI 10 µM. Superoxide production was plotted as a kinetic curve over 60 minutes (RLU). The reduction (%) in RLU relative to the baseline reading was calculated at each time point.* ***b).*** *AUC of the kinetic plot was calculated. Statistical analysis was performed using unpaired nonparametric Mann Whitney test.*

3.4.7 Colonic epithelial NOX and DUOX mRNA expression in IBD

Given that the *NOX1* p.N122H variant patient has the clinical phenotype of colonic and perianal VEOIBD, the question was posed as to whether NOX1 is differentially expressed in the colonic epithelium of patients with IBD, as compared to non-inflamed controls. Conflicting reports of both upregulated and down-regulated NOX1 expression in the setting of IBD exist in the literature (168, 223).

Colonic epithelial biopsies were collected from IBD patients and non-inflamed controls and NOX and DUOX mRNA expression was analysed using qRT-PCR. Both right and left colon biopsy specimens were collected from each patient so as to normalise the differential NOX1 expression gradient in the colon (*Figure 3.27*).

Significantly decreased NOX1 mRNA expression was demonstrated amongst IBD patients as compared to non-inflamed controls ($p=0.02$). However, this finding must be interpreted with caution, both due to the small numbers of patients, as well the finding that upon exclusion of the single outlying NOX1 mRNA result, the analysis is rendered non-significant. In contrast to NOX1, the expression of NOXO1 and NOXA1 mRNA was significantly increased in patients with IBD compared to non-inflamed controls ($p<0.001$ and $p=0.04$, respectively).

A broad range of expression of DUOX2 mRNA was demonstrated amongst patients with IBD. A significant difference in DUOX mRNA expression was not demonstrated between IBD patients compared to non-inflamed controls overall. However, when stratified by disease activity, patients with active IBD express significantly higher DUOX2 mRNA than those with quiescent IBD and healthy controls ($p=0.03$, $p=0.02$, respectively). This finding is in keeping with recent literature derived from a paediatric IBD cohort (238).

Definitive conclusions from this experiment are limited due to the small patient numbers, however a significant difference in NOX1 expression between patients with IBD and non-inflamed controls seems unlikely. In keeping with prior literature, DUOX2 expression is upregulated in those with active IBD.

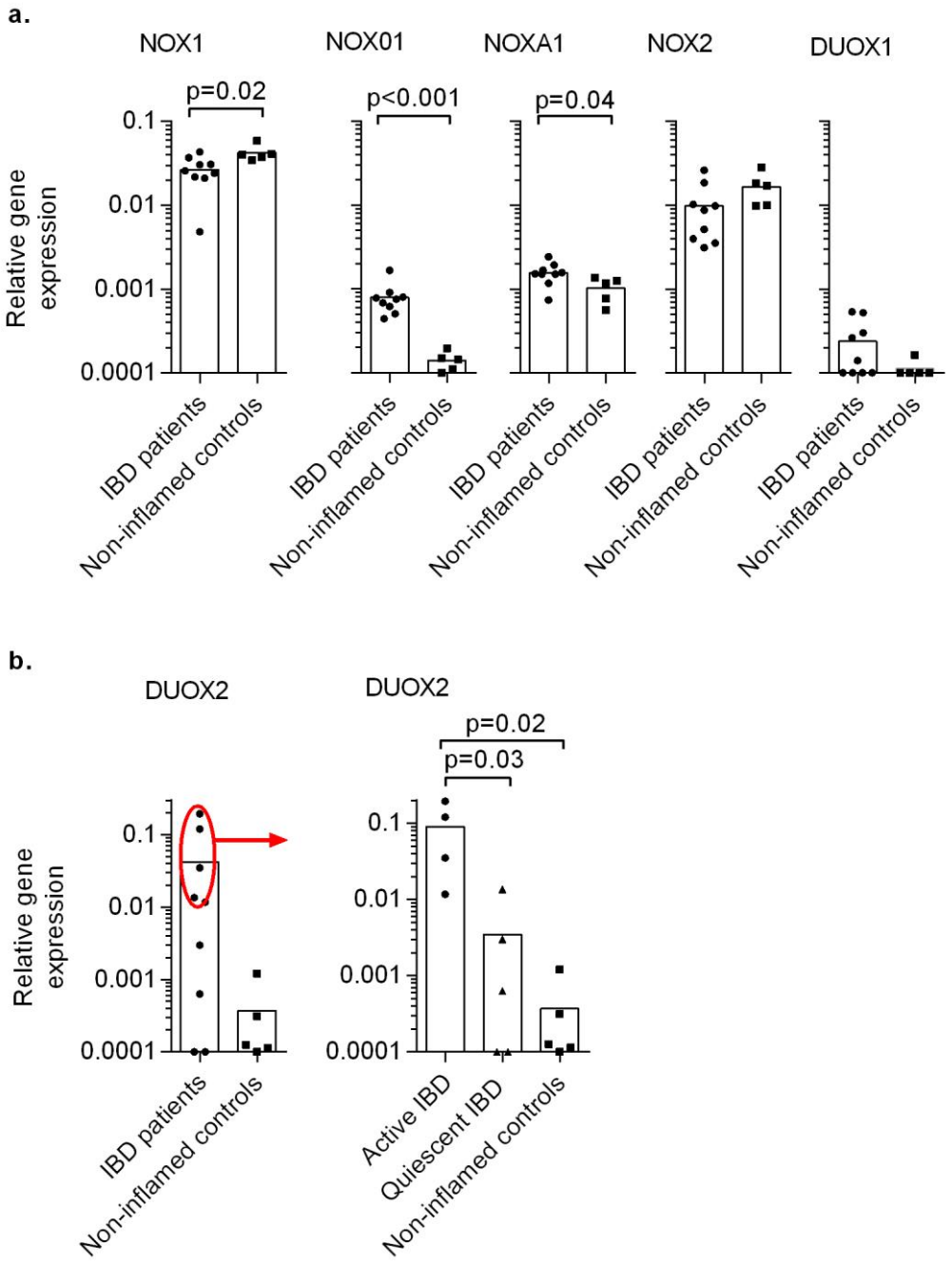

Figure 3.27. NOX and DUOX mRNA colonic epithelial expression in IBD. a). *Colonic epithelial biopsy specimens taken from IBD patients (n=9) and non-inflamed controls (n=5). Two biopsies from each patient analysed; 1 taken from the right colon and 1 from the left colon; the mean is presented for each patient. Gene expression was quantified relative to the reference gene (GAPDH) for each sample using the threshold cycle value (Ct). Relative expression was calculated based on the 2(-ΔCt) method.* ***b).*** *DUOX2 mRNA expression stratified by disease activity. Active vs. quiescent disease dichotomised according to composite assessment including endoscopic appearance, biomarkers (CRP), and histology. Statistical analysis performed using unpaired non-parametric Mann Whitney test.*

3.4.8 Colonic epithelial superoxide generation in the *NOX1* p.N122H variant patient

Superoxide production from *ex vivo* colonic epithelial biopsy samples of the *NOX1* p.N122H variant patient were compared to an individual IBD control patient (IBD Control 1) and a non-inflamed control patients who underwent a colonoscopy on the same day. The clinical features of IBD Control 1 patient and the non-inflamed control are described in *Appendix A1*.

As depicted in *Figure 3.28*, compared to the IBD Control 1 patient and the non-inflamed control patient, the *NOX1* p.N122H variant patient generated less superoxide at baseline. However, upon stimulation with PMA, the *NOX1* p.N122H variant patient generated similar amounts of superoxide to the IBD control and the non-inflamed control patients. Statistical analysis was not possible given that data from the *NOX1* p.N122H variant patient represented a single value.

In order to further examine superoxide generation from *ex-vivo* colonic epithelial biopsy specimens, it was decided that a larger comparative group of IBD patients and non-inflamed controls was required, so as to allow for more meaningful comparisons to be drawn with the *NOX1* p.N122H variant patient.

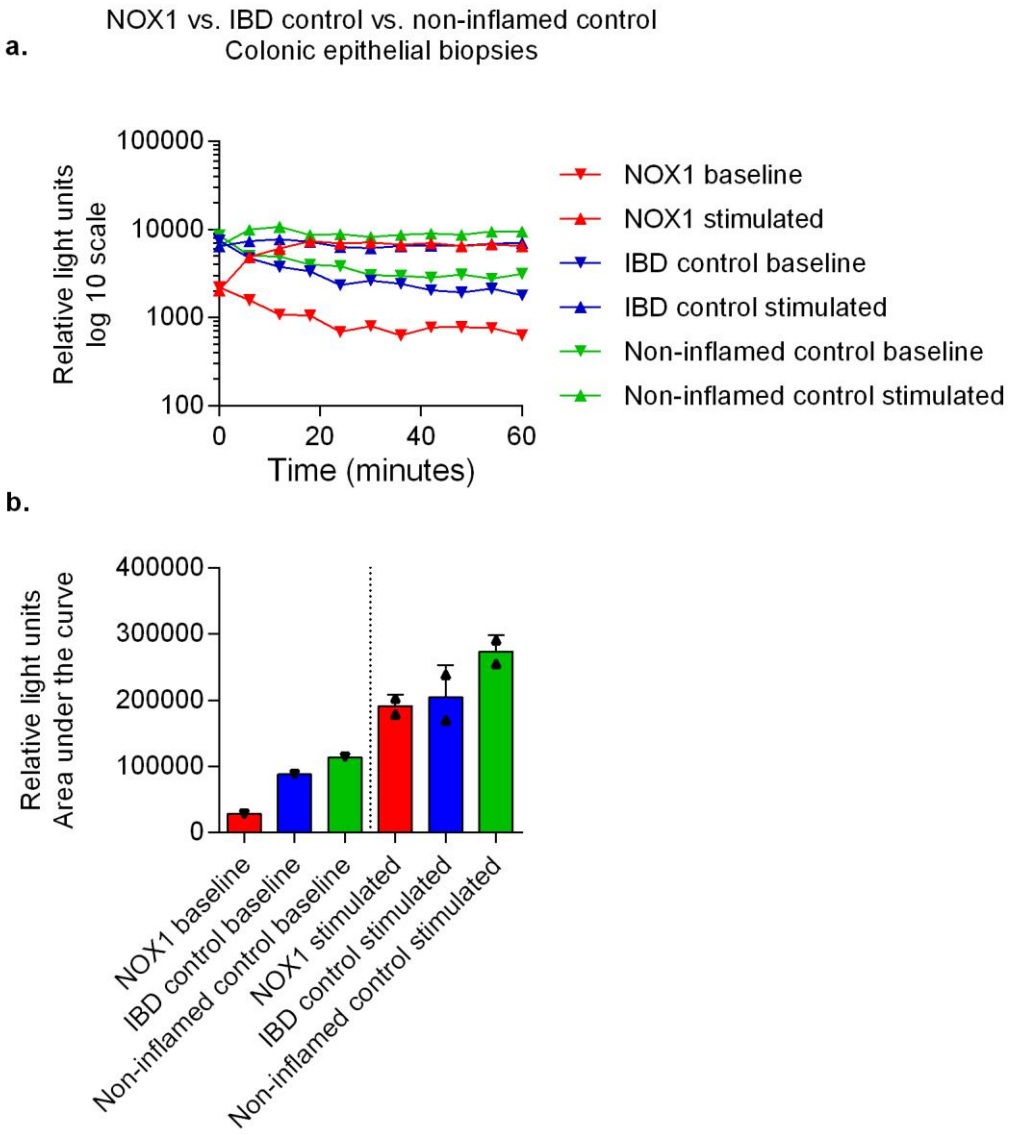

Figure 3.28. Superoxide production by colonic epithelial biopsies from the NOX1 p.N122H variant patient. a). *Superoxide generation by colonic epithelial biopsy specimens from an IBD Control patient, a non-inflamed control, and the NOX1 p.N122H variant patient was compared using L-012 chemiluminescence assay. Specimens were co-incubated with L-012 (100 µM) in PBS, with or without PMA stimulation (5 µg/ml), and the superoxide generated was measured over a kinetic time course (relative light units). An unstimulated kinetic plot is presented (representative of one biopsy per patient), along with a stimulated kinetic plot (representative of two biopsies per patient).* ***b).*** *The AUC of the kinetic plot (RLU) in a). was calculated.*

3.4.9 Colonic epithelial superoxide generation in IBD and non-inflamed control patients

In order to further examine superoxide generation from *ex-vivo* colonic epithelial biopsy specimens from the *NOX1* p.N122H variant patient, a larger comparative group of IBD patients and non-inflamed controls was recruited for analysis.

Colonic epithelial biopsy specimens were collected from patients with CD (n=17) and UC (n=11), as well as non-inflamed controls (n=16). Stratification of IBD patients was performed by disease activity, as well as IBD medication. Statistical analysis for the *NOX1* p.N122H variant patient was not possible given that it is a single value.

Stratification by disease activity revealed that IBD disease activity is the primary determinate of baseline superoxide production. Patients with quiescent CD or UC, produced similar baseline levels of superoxide compared to non-inflamed controls. In contrast, patients with active UC demonstrated significantly higher baseline superoxide production compared to both quiescent UC patients and non-inflamed controls ($p=0.02$ for both) (*Figure 3.29*). Furthermore, upon stimulation with PMA, superoxide production was disproportionately increased in specimens from inflamed UC and CD patients, such that a statistically significant difference emerged between specimens from patients with active UC and CD compared to those with quiescent disease ($p=0.004$, $p=0.04$, respectively) as well as non-inflamed controls ($p<0.001$, $p=0.01$, UC and CD respectively).

The *NOX1* p.N122H variant patient was demonstrated to generate a low level of superoxide, both at baseline and upon stimulation, although this was comparable to other patients with quiescent IBD and non-inflamed controls overall.

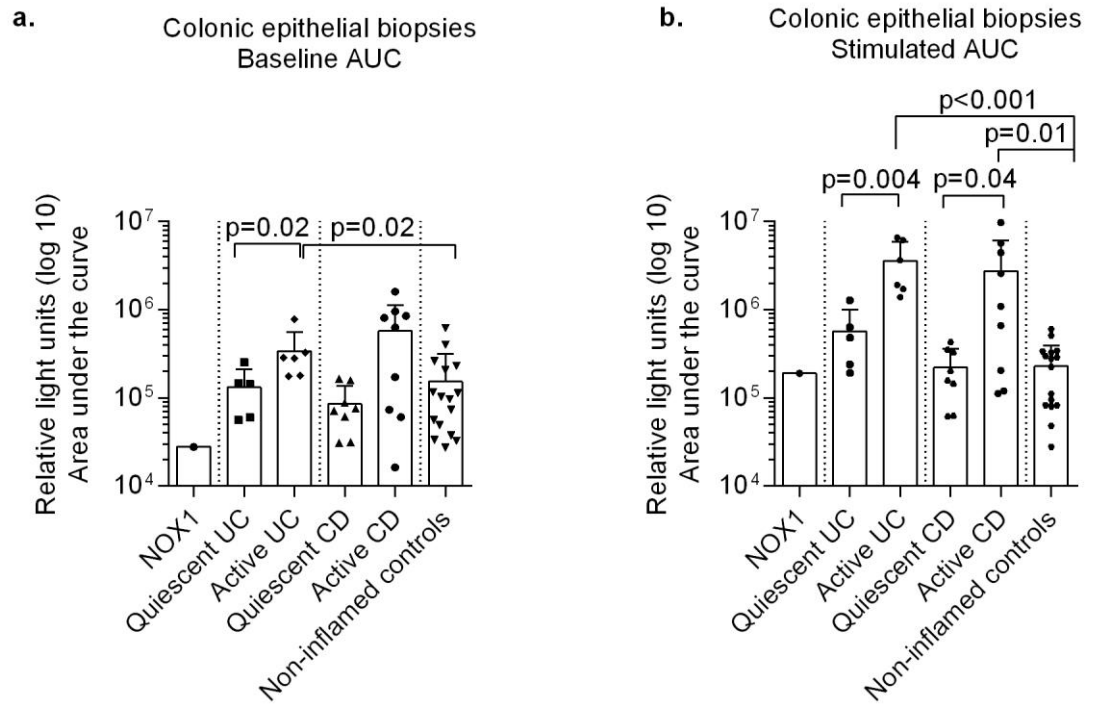

Figure 3.29. Superoxide production by colonic epithelial biopsies stratified by IBD diagnosis and disease activity. ***a).*** *Biopsies co-incubated with L-012 100 µM and kinetic curve plotted over 60 minutes (RLU) and AUC calculated. Results from non-inflamed control patients (n=16), patients with CD (n=17, active disease n=10) and UC (n=11, active disease n=6), and NOX1 variant patient (n=1). The mean of 1-3 pan-colonic biopsy specimens (both right and left sided) per patient is represented in the graphs by a symbol. Active vs. quiescent disease dichotomised as described in Methods. Statistical analysis performed using Mann Whitney unpaired nonparametric tests.* ***b).*** *Stimulated biopsies were co-incubated with PMA 5 µg/ml over the kinetic time-course. Otherwise methodology as per a).*

Stratification by IBD medication did not reveal significant differences in superoxide production between colonic biopsy specimens from patients on either immunomodulatory therapy, biologic therapy, corticosteroids, combination therapy (biologic and immunomodulatory), or no medications (all comparisons non-significant) (*Figure 3.30*). In particular, azathioprine, which has been reported to modulate RAC1 activity (272), did not significantly affect colonic epithelial biopsy superoxide generation.

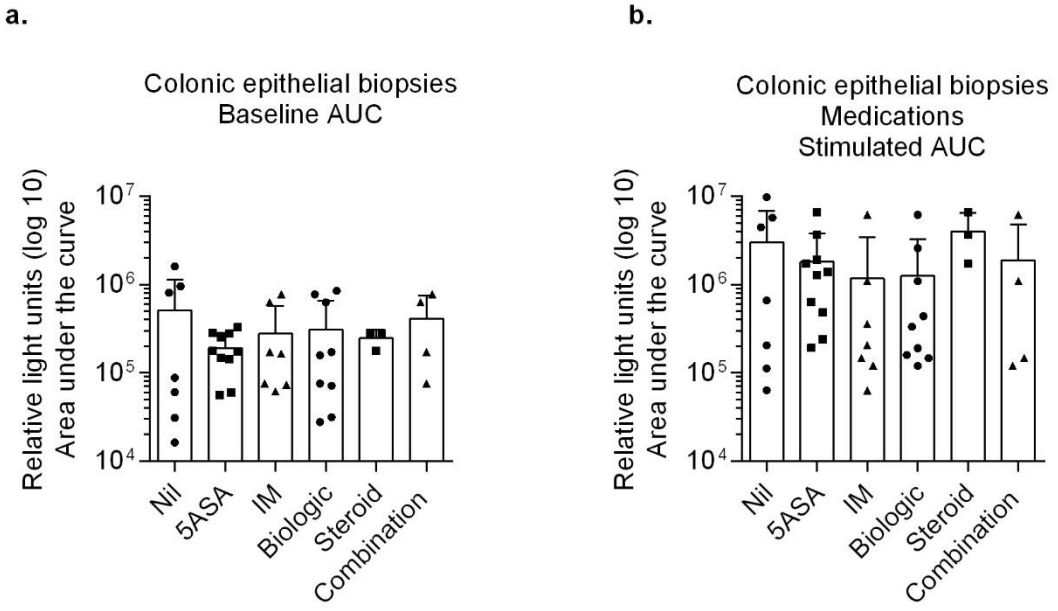

Figure 3.30. Superoxide production by colonic epithelial biopsies stratified by IBD medication. a). *Biopsies co-incubated with L-012 100 µM and kinetic curve plotted over 60 minutes (RLU) and AUC calculated. Results from non-inflamed control patients (n=16), patients with CD (n=17) and UC (n=12 (NOX1 p.N122H variant patient included). Patients stratified by medication regimen; nil, 5-ASA, immunomodulators (IM) (azathioprine or methotrexate), biologic therapy (infliximab or adalimumab), corticosteroid therapy, or combination therapy (biologic and immunosuppressant). The mean of 1-3 pan-colonic biopsy specimens (both right and left sided) per patient is represented in the graphs by a symbol. Statistical analysis performed using Mann Whitney unpaired nonparametric t tests.* ***b).*** *Stimulated biopsies were co-incubated with PMA 5 µg/ml over the kinetic time-course.*

Thus, the analysis revealed that the primary mediator of differences in superoxide generation by *ex vivo* colonic biopsy specimens is IBD disease activity, particular following stimulation with PMA. The higher levels of superoxide generated in the setting of active disease, are likely reflective of lamina propria infiltration by NOX2-possessing neutrophils and phagocytes (monocytes/macrophages), which have the propensity to generate high levels of superoxide. Interpretation of the results of superoxide production from colonic epithelial biopsies is therefore limited by the inability to control for the multiple sources of superoxide in biopsy specimens.

Thus, in order to meaningfully determine the true superoxide production from colonic epithelial cell in the *NOX1* p.N122H variant patient, analysis of a monoculture of colonic epithelial cells is required.

3.4.10 *NOX1* p.N122H variant patient colonic epithelial organoids

In order to achieve functional analysis of colonic epithelial cells from the *NOX1* p.N122H variant patient, colonic epithelial organoids were cultured from *ex-vivo* biopsy specimens from the *NOX1* p.N122H variant patient, IBD Control 1 patient and a non-inflamed control patient (*Appendix A1*), in collaboration with colleagues at the NIMR (*Figure 3.31*) (262).

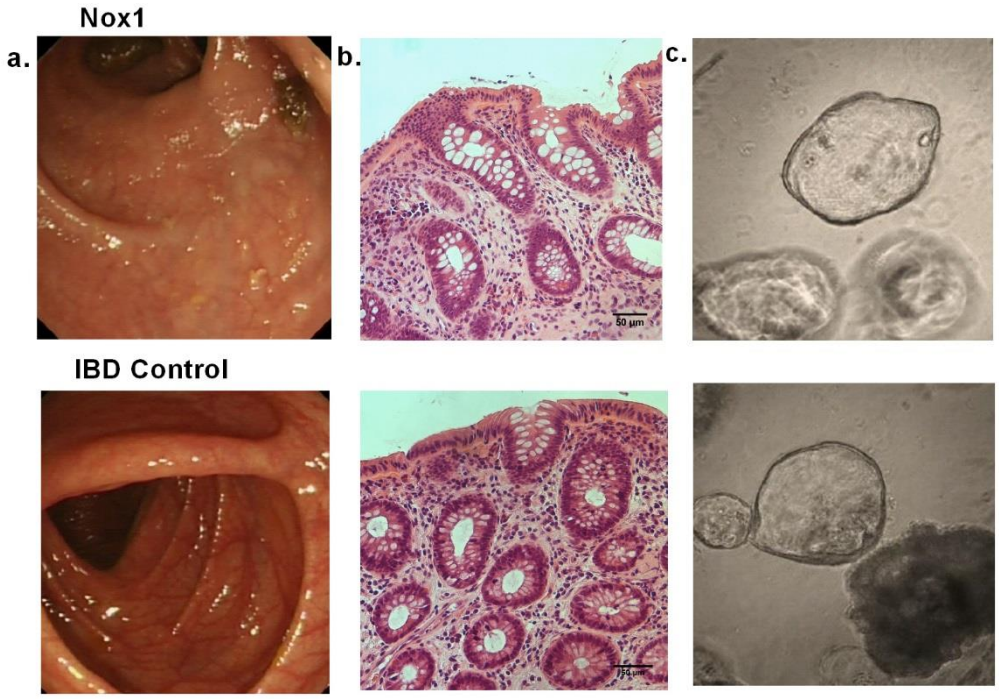

Figure 3.31. Endoscopy, histology, and organoid images from NOX1 p.N122H variant and IBD Control 1 patients. a). *Time point E4 (Colonoscopy 2014). Macroscopic features: quiescent pan-colitis with no active inflammation evident.* ***b).*** *Colonic epithelial biopsy histology (H&E stained) showing quiescent disease without active inflammation.* ***c).*** *Organoids in culture at the cystic phase of growth. Colonic epithelial organoids cultured in collaboration with colleagues at the NIMR (LM, VL).*

3.4.10.1 NOX and DUOX mRNA expression

NOX/DUOX mRNA expression was analysed using qRT-PCR of the cultured organoid colonic epithelial cells from the *NOX1* p.N122H variant patient and the IBD Control 1 patient (*Figure 3.32*). A truncated panel of mRNA expression was analysed given that NOX4 and NOX5 were not shown to be expressed in colonic epithelial biopsies, and NOX3 is only expressed in the human inner ear (157).

There was no difference in NOX1, NOXO1 or NOXA1 mRNA expression between the *NOX1* p.N122H variant patient and the IBD Control 1 patient.

DUOX2 mRNA was highly expressed in the colonic epithelial organoids of the *NOX1* p.N122H variant patient and IBD Control 1 patient; a finding that has previously been reported in the setting of IBD (238).

Minimal NOX2 mRNA expression was measured in the colonic epithelial organoids, confirming the contribution of immune cells in the lamina propria to the increased NOX2 mRNA expression demonstrated in colonic epithelial biopsies.

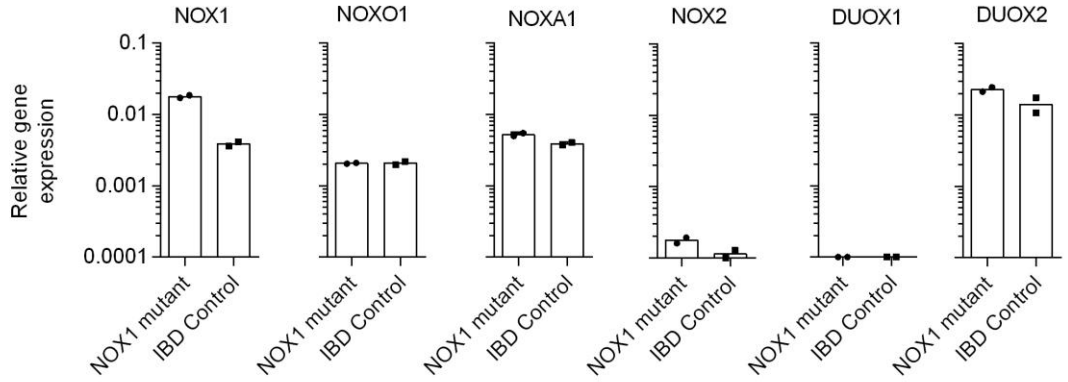

Figure 3.32. NOX and DUOX mRNA expression in NOX1 p.N122H variant colonic epithelial organoids*. Colonic epithelial organoids cultured from the NOX1 p.N122H variant patient and the IBD Control 1 patient were cultured for 8 weeks and trypsinised and harvested as a single cell suspension for analysis. Gene expression was quantified relative to the reference gene (GAPDH) for each sample using the threshold cycle value (Ct). Relative expression was calculated based on the 2(-ΔCt) method. The experiment was performed in duplicates.*

3.4.10.2 Superoxide production

In order to determine the functional significance of the *NOX1* p.N122H variant mutation, a key experiment was to establish whether there was a reduction in superoxide production from the *NOX1* p.N122H variant colonic epithelial organoids (*Figure 3.33*). Colonic epithelial organoids from the IBD Control 1 and a non-inflamed control (*Appendix A1*) were used as comparators.

An L-012 chemiluminescence assay performed on colonic epithelial organoid cells in suspension, demonstrated significantly less superoxide production by the *NOX1* p.N122H variant at baseline, as compared to both the IBD Control 1 and non-inflamed control patients (p=0.03 for both). Furthermore, stimulation with PMA did not augment superoxide production by the *NOX1* p.N122H variant organoids, such that even after stimulation, superoxide production was significantly less than the IBD Control 1 patient at baseline (p=0.03).

The finding that superoxide production from colonic epithelial cells is significantly attenuated, provides evidence that the *NOX1* p.N122H variant disrupts gene function.

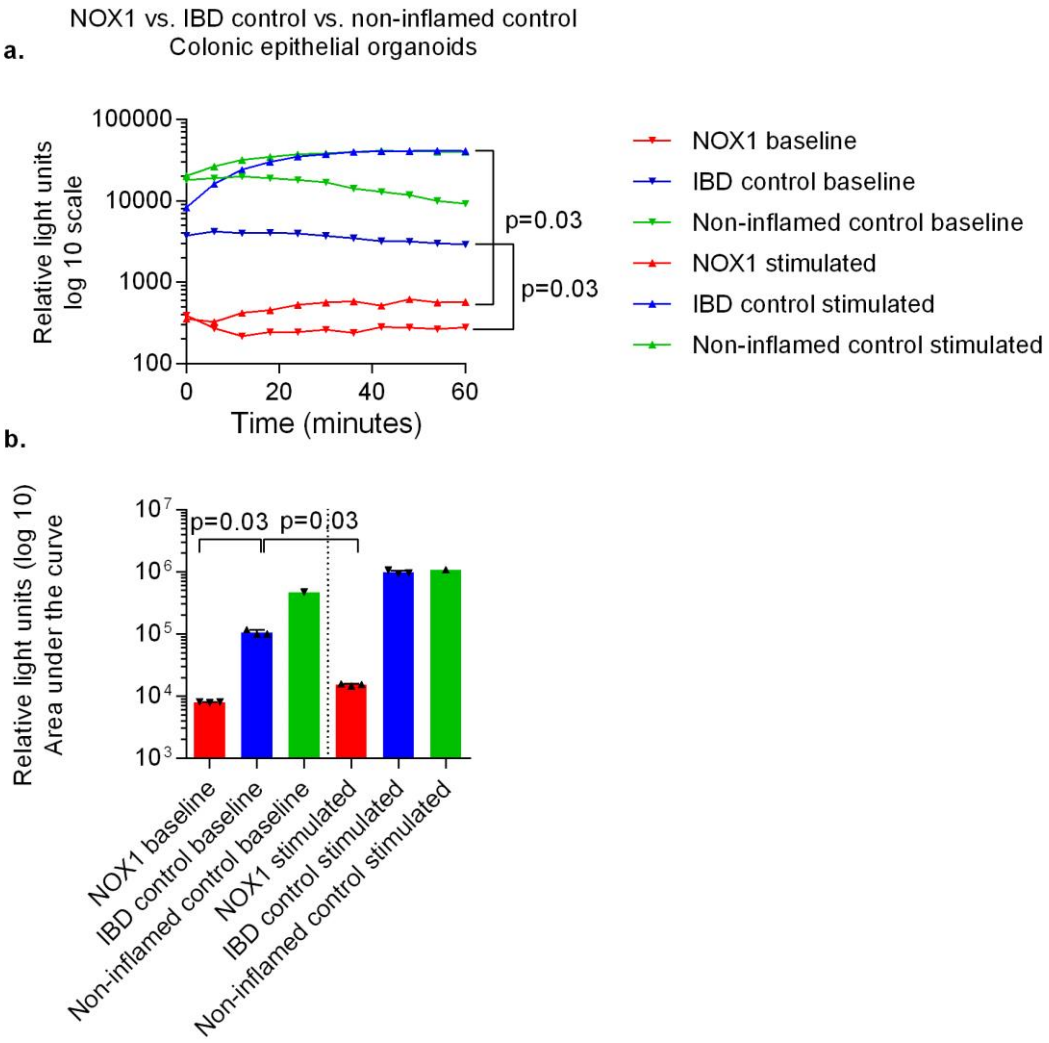

Figure 3.33. Superoxide production from NOX1 p.N122H variant, IBD control 1, and non-inflamed control colonic epithelial organoids. *Colonic epithelial cells in suspension were seeded in a 96 well plate (28,000- 36,500 cells per well).* ***a).*** *L-012 chemiluminescence was plotted as a kinetic curve (RLU) over 60 minutes either unstimulated, or during co-incubation with PMA (5µg/ml).* ***b)****. The AUC of the kinetic plot was calculated. The experiment was performed in triplicates. Results are representative of 2 experiments. NOX1 refers to NOX1 variant patient. Statistical analysis performed using Wilcoxon matched-pairs nonparametric test (not adjusted for multiple comparisons)*

3.4.11 Bacterial killing assays in HT-29 cells

The finding that the *NOX1* p.N122H variant mutation led to a reduction in superoxide production by colonic epithelial cells, led to further experiments to explore the impact of this defect on innate immune function. It was hypothesised that bacterial killing by colonic epithelial cells may be impaired by reduced superoxide production by NOX1. In order to further investigate this hypothesis, bacterial killing experiments were performed using a NOX1 inhibitor in HT-29 cells (*Figure 3.34*).

A gentamicin protection assay was used to assess bacterial killing of intracellular replicating invasive bacteria (*S. typhimurium* and AIEC). An extracellular bacterial killing assay was used to assess bacterial killing of non-invasive bacteria (EcN, *S. aureus*, and *L. rhamnosus*).

Despite optimisation of experimental strategy and multiple trialled protocols, there was no difference in bacterial killing demonstrated following NOX1 inhibition with ML171, in either the gentamicin protection or extracellular bacteria killing assays.

In contrast, a significant reduction in bacterial CFU's was demonstrated following treatment with DPI inhibitor. The hypothesised reason for suppression of bacterial growth following DPI treatment, is that despite thorough washing with PBS following inhibitor treatment, residual DPI has a direct effect on bacterial cells and inhibits bacterial growth.

Thus, these experiments did not reveal an impairment in the killing of either invasive or non-invasive bacterial species following NOX1 inhibition in an HT-29 cell line.

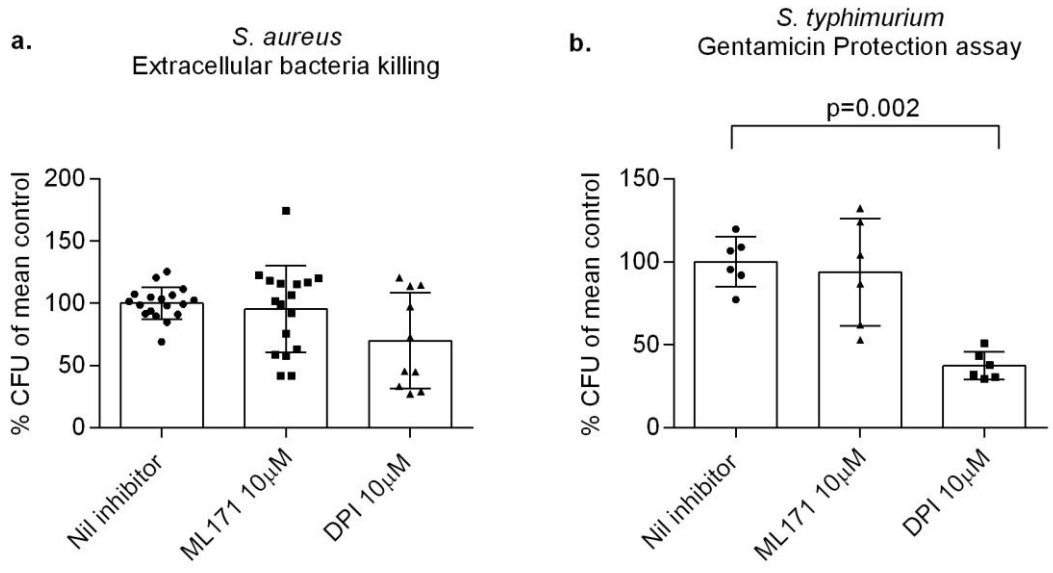

Figure 3.34. Bacterial killing assays in HT-29 cells following inhibitory conditions. a). S. typhimurium gentamicin protection assay. *HT-29 cells were seeded at 1 x10^5 cells per well in a 96 well plate and cultured overnight in tissue culture conditions. The cells were treated with ML171 10 µM or DPI 10 µM for 60 minutes, prior to infection with bacteria (MOI 100) for 2 hours in tissue culture conditions. Following gentamicin treatment (100 µg/mL) for 3 hours, the cell- bacterial lysate was then diluted (1:10, 1:100, or 1:1000) and 10 µL of the diluted lysate (in triplicates) was pipetted by track method onto agar plates. Colony-forming units (CFU) were counted after overnight incubation. Data from MOI 100 and 1:1000 dilution presented. The figure is representative of 3 experiments.* ***b). S. aureus extracellular bacterial killing assay.*** *Pre-treatment with inhibitors as in a). S. aureus infection at 1 and 10 MOI for 5 hours, with preceding centrifugation of bacterial to ensure contact with epithelial cells. The cells were then washed twice with PBS prior to trypsinisation, cell lysis, and plating on agar plates at serial dilutions. Data from MOI 1 and 1:1000 dilution presented. Statistical analysis performed using Mann Whitney unpaired nonparametric tests. Results representative of 5 experiments, performed in collaboration with laboratory colleague (SP).*

3.4.12 Epithelial cell migration assays in HT-29 cells

NOX1-derived superoxide has been shown in cell-line and murine constructs to play a key role in epithelial cell migration and restitution (182, 219, 220, 231). In response to intestinal epithelial injury, NOX1-derived superoxide interacts with redox-sensitive phosphatases to mediate epithelial migration in order to heal the mucosal breach. It was thus hypothesised that epithelial cell migration in the HT-29 cell line would be impaired in the presence of NOX1 inhibition (*Figure 3.35*).

A linear wound in a confluent HT-29 cell culture layer was created in collagen-I coated wells and the migration of HT-29 cells into the wound space analysed after 24 hours in tissue culture conditions. Co-incubation with a NOX1 inhibitor (ML171) or small-molecule inhibitor (RAC1) was performed. Pre-incubation with a non-specific NOX/ROS inhibitor (DPI) was performed.

There was no impairment of HT-29 epithelial cell migration upon treatment with the ML171, nor with the RAC1 inhibitor. Only treatment with DPI was demonstrated to inhibit epithelial cell migration and restitution of the scratch wound, which is likely related to direct inhibition of cellular mitochondrial oxidases. Thus, the hypothesis that NOX1 inhibition would alter epithelial cell migration in the HT-29 cell line was unable to be proven.

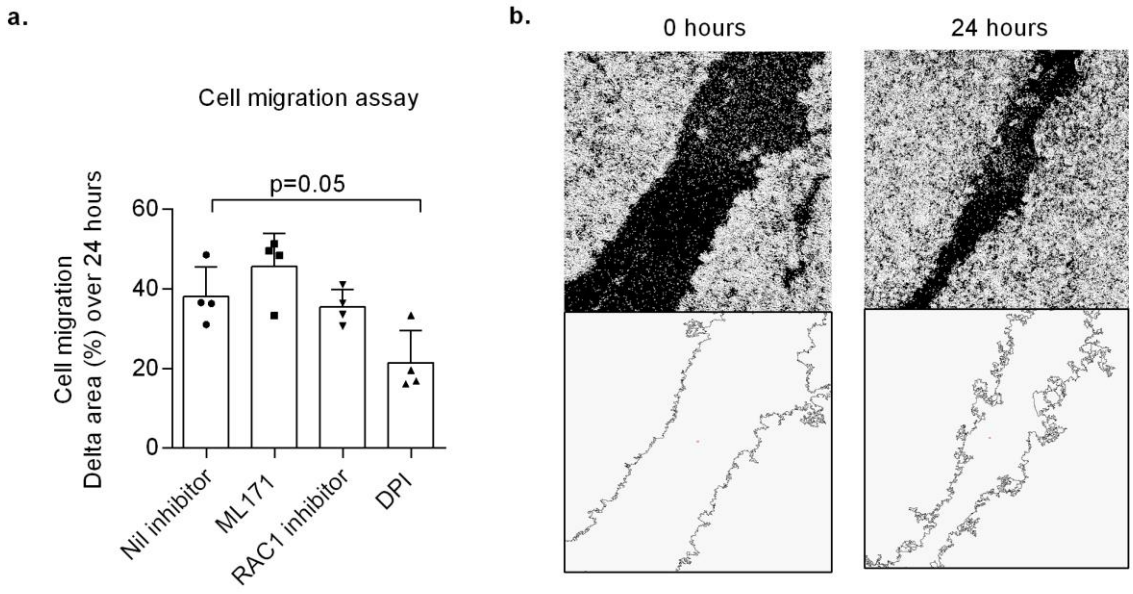

Figure 3.35. HT-29 epithelial cell migration assay. *HT-29 cells cultured until confluent in 24-well collagen-I coated plates. Linear wound in epithelial culture created; analysis of epithelial cell migration into the wound space analysed after 24 hours in tissue culture conditions. Pre-incubation with DPI 10 µM for 60 minutes then wash. Co-incubation with ML171 10 µM and RAC1 inhibitor 100 µM.* ***a).*** *Cell migration into linear epithelial wound expressed as a percentage of wound space occupied by cells at 24 hours compared with 0 hours (delta change, percentage). Experiment performed in duplicates and repeated twice. Each symbol represents mean of 5 images per individual well.* ***b).*** *Representative images taken at 0 hours and 24 hours (200x magnification) reconstructed using ImageJ software. Matching images analysed at time-points using pin-mark as orientation. Outline of linear wound generated and surface area calculated (pixels). Statistical analysis performed using Mann Whitney unpaired nonparametric tests.*

3.4.13 WST-8 assay and cell counting proliferation assays in HT-29 cells

NOX1 was initially coined ‘mitogenic NOX’ due to its putative role in driving cellular proliferation and carcinogenesis (167, 168, 208, 212, 227). Subsequent experiments have shown that NOX1-derived ROS plays an important physiological role in promoting proliferation of intestinal epithelial cells, via interaction with redox sensitive phosphatases such as MAPK and ERK (183, 232). It was hypothesised that inhibition of NOX1 would lead to a reduction in epithelial cell proliferation. In order to test this

hypothesis, assessment of cellular proliferation in HT-29 cells using a WST-8 assay following treatment with inhibitors was performed (*Figure 3.36*).

HT-29 cells were co-incubated with competitive NOX1 inhibitors (ML171) over a 24 time period, whereas pre-incubation with irreversible inhibitors (DPI) was performed. Cell counting using standard technique by haemocytometer was performed in parallel at the 24 hour time point.

Neither the WST-8 assay, nor cell counting, demonstrated any reduction in HT-29 cell proliferation following treatment with the NOX1 inhibitor ML171. In contrast, significantly diminished WST-8 absorbance and cell count was observed following treatment with DPI ($p=0.02$, $p=0.006$, WST-8 and cell count respectively), which was likely mediated by the non-specific inhibition of cellular mitochondrial oxidases by DPI.

Thus, the hypothesis that NOX1 inhibition would reduce HT-29 cellular proliferation was unable to be proven in this experiment.

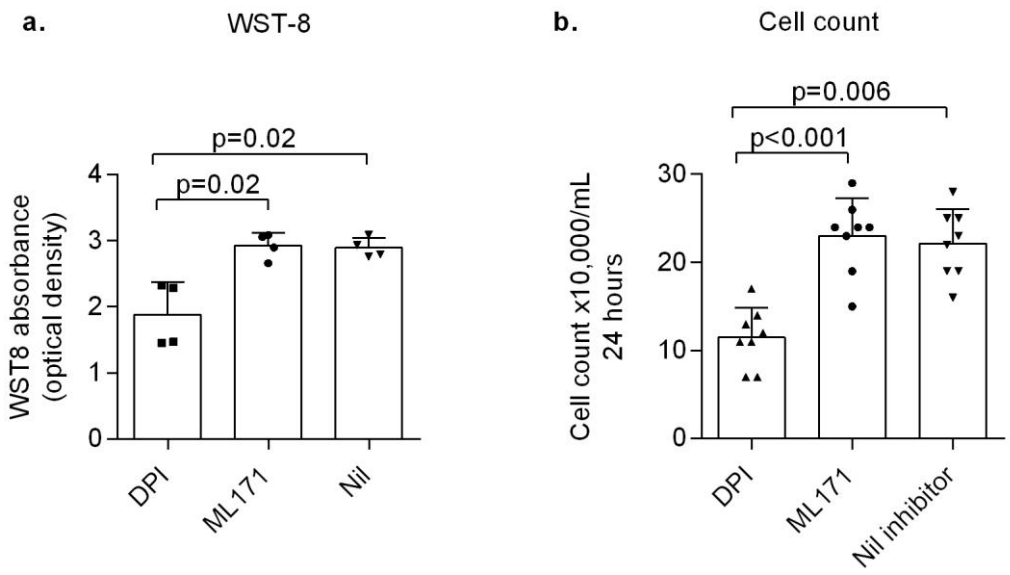

Figure 3.36. WST-8 and haemocytometer counting HT-29 cell proliferation assays. ***a).*** *WST-8 assay. HT-29 cells were seeded at 5 x 10^4 per well in a 96 well plate. After overnight culture in tissue culture conditions, selected wells were treated with inhibitor conditions. ML171 10 µM co-incubated over the 24 time period. Pre-incubation with DPI 10 µM for 60 minutes was performed. After 24 hours in tissue culture conditions, wells were treated with WST-8 (1:10 per well) for 3 hours, following which calorimetric analysis of formazan accumulation was measured by plate-reader absorbance at 460 nm. Experiment performed in duplicates and repeated twice (each symbol represents a result).* ***b).*** *Manual counting of cells was also performed at 24 hours using trypan blue and haemocytometer according to standard technique. 8 haemocytometer quadrants counted for each well. Experiment performed in duplicates and the repeated four times (each symbol represents a result). Statistical analysis performed using Mann Whitney unpaired nonparametric tests.*

3.4.14 Ki67 proliferation index in *NOX1* p.N122H variant patient

Ki67 immunohistochemical staining was performed to assess cellular proliferation in colonic epithelial biopsies from the *NOX1* p.N122H variant patient, IBD controls, and a non-inflamed control (described in *Table 3.14*). The *NOX1* p.N122H variant patient was analysed in both active and quiescent disease states. The Ki67 proliferation index was determined according to standard technique (*Figure 3.37*, *Figure 3.38*) (266, 267).

Patient	Age Gender	Diagnosis	Disease distribution	Disease activity	Medication
***NOX1* p.N122H variant patient** (2013) (Time-point E3)	18, M	UC phenotype	E3	Active	MTX
***NOX1* p.N122H variant patient** (2014) (Time-point E4)	19, M	UC phenotype	E3	Quiescent	ADA
IBD Control 1	24, M	CD	L2	Active	ADA/AZA
IBD Control 2	65, F	UC	E3	Active	5ASA
IBD Control 3	24, M	CD	L3	Quiescent	Nil
Non-inflamed Control	34, F	-	-	-	-

Table 3.14. Characteristics of patients analysed by ki67 proliferation index. *For each patient, 10 longitudinal cut crypts from pan-colonic (left and right colon) biopsy specimens were analysed. Specimens from the patient with the NOX1 p.N122H variant patient were taken during active disease and quiescent disease. Key: Montreal criteria: E3, pan-colonic UC; L2, colonic CD; L3, ileocolonic CD; 5ASA, 5-aminosalycilic acid therapy; ADA, adalimumab; AZA, azathioprine; MTX, methotrexate.*

The ki67 proliferation index revealed similarly increased proliferation indices amongst patients with both active and quiescent IBD, as compared to the non-inflamed control patient ($p<0.001$ both active and quiescent IBD).

During the active phase of disease, both the *NOX1* p.N122H variant patient and patients with active IBD demonstrated significantly increased proliferation compared to the non-inflamed control ($p=0.002$, $p<0.001$, respectively). However, the *NOX1* p.N122H variant patient showed significantly reduced proliferation compared to other patients with active IBD ($p<0.001$). Similarly, during disease quiescence, the *NOX1* p.N122H variant patient demonstrated reduced proliferation compared to quiescent IBD patients ($p=0.03$).

Although the analysed number of patients is small, and it is not possible to control for the confounding effects of disease phenotypes, medications, and age, there seems a trend toward reduced colonic epithelial proliferation in the *NOX1* p.N122H variant patient. However, the most significant influence on cellular proliferation as assessed by ki67 staining, was IBD disease activity. Thus, no reliable conclusion of colonic epithelial cell proliferation in the *NOX1* p.N122H variant patient can be drawn from this experiment.

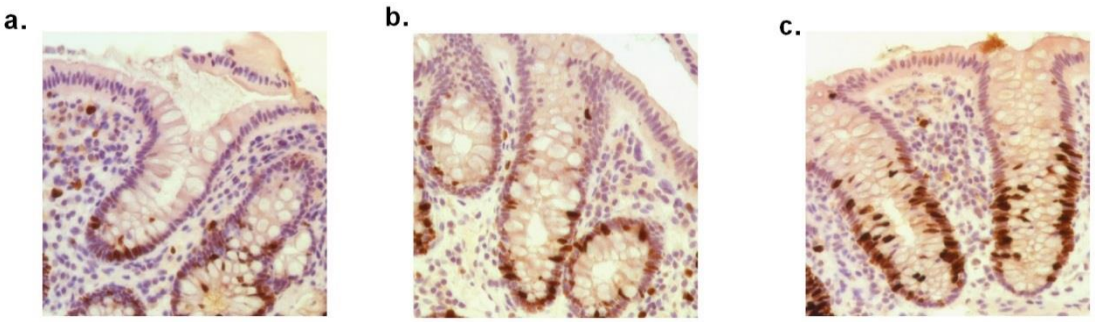

Figure 3.37. Representative images of ki67 stained colonic epithelial biopsies. *The images show longitudinally cut crypts. The ki67 stained cells are dark brown. H&E stain was also used.* ***a).*** *Non-inflamed patient colonic epithelial crypt.* ***b).*** *NOX1 variant patient colonic epithelial crypt (during disease quiescence).* ***c).*** *IBD control colonic epithelial crypt (during disease quiescence). The Ki67 staining was performed by the Histopathology Department at the John Radcliffe Hospital.*

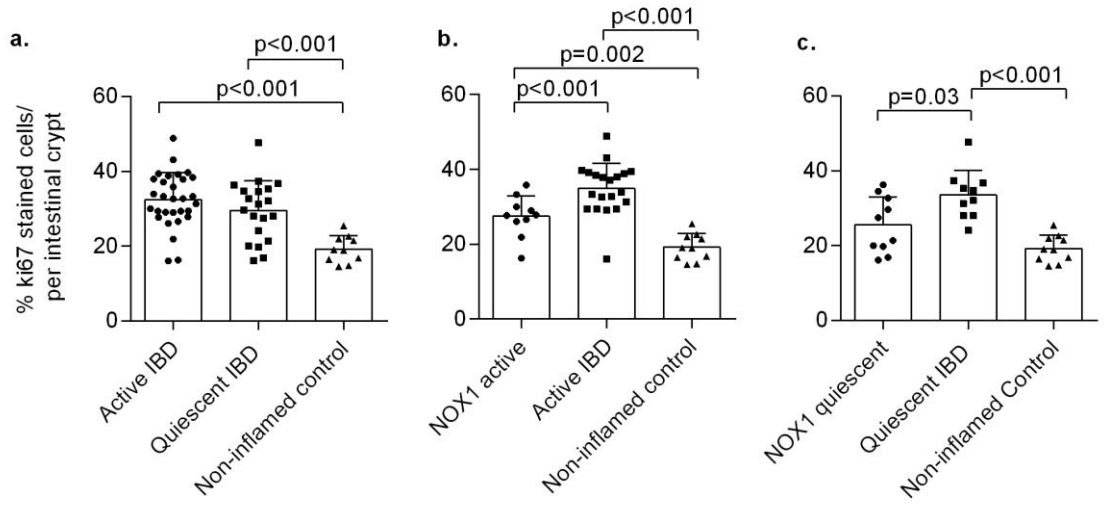

Figure 3.38. Ki67 proliferation index of NOX1 p.N122H variant patient, IBD patients and non-inflamed control. *The patient numbers and characteristics are detailed in Table 3.14. The ki67 proliferation index was calculated from pan-colonic biopsies harvested from each described patient.* ***a).*** *Overall comparison of patients with active IBD, quiescent IBD, and non-inflamed control.* ***b).*** *Comparison between NOX1 p.N122H variant patient and control IBD patients with active disease.* ***c).*** *Comparison between NOX1 p.N122H variant patient and control IBD patients with quiescent disease. Statistical analyses using unpaired nonparametric Mann Whitney test.*

3.4.16 Colonic epithelial goblet cell analysis in *NOX1* p.N122H variant

NOX1 has been shown to influence goblet cell development and function; NOX1 knock-out models show reduced numbers of goblet cells, increased intracellular mucin accumulation, and increased goblet cell apoptosis (221-223). In order to evaluate goblet cells of the colonic epithelium of the *NOX1* p.N122H variant patient, Alcian blue/PAS staining (with nuclear fast red) was undertaken (*Figure 3.39*). The *NOX1* p.N122H variant patient was analysed in both active and quiescent disease states, in addition to colonic biopsies from IBD and non-inflamed control patients described in *Table 3.13*.

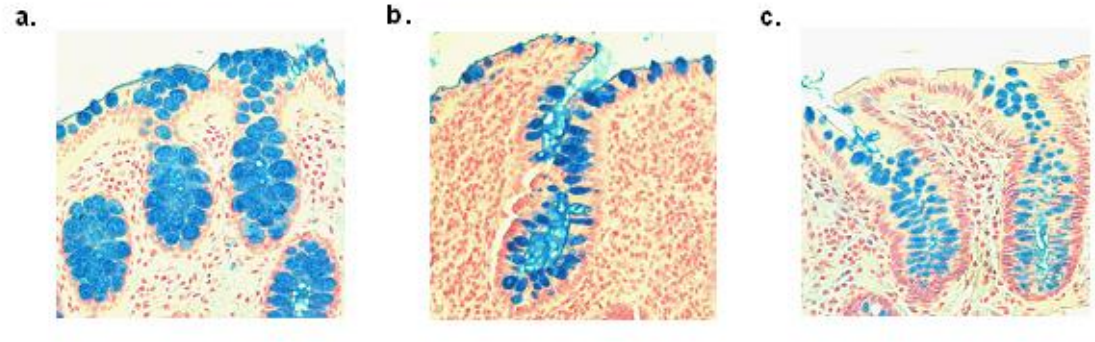

Figure 3.39. Alcian blue/PAS goblet cell staining of NOX1 p.N122H variant patient, IBD control, and non-inflamed control patients. *Alcian blue/PAS/Nuclear fast red colonic epithelial staining.* ***a).*** *Non-inflamed control biopsy showing regular, plump goblet cells lining the colonic epithelial crypt.* ***b).*** *NOX1 p.N122H variant patient biopsy during active disease showing relative paucity of goblet cells and retention of mucin within goblet cells.* ***c).*** *IBD control patient biopsy during active disease showing increased number of goblet cells which are of relatively reduced size having extruded mucin onto the surface epithelium. The Alcian blue/PAS staining was performed in collaboration with colleagues at the Sir William Dunn School of Pathology (RS).*

There was no significant difference in the number of colonic epithelial crypt goblet cells or the average goblet cell area between the IBD patients (either with quiescent or active disease) and non-inflamed controls (all comparisons non-significant) (*Figure 3.40*).

During active disease, goblet cell number was seen to be significantly reduced in the *NOX1* p.N122H variant patient compared to active IBD and non-inflamed controls (p=0.01, p=0.04 respectively), with a concordant increase in goblet cell area compared to the IBD control patients (p=0.02) (*Figure 3.41*). During disease quiescence, there was no significant difference demonstrated between the *NOX1* p.N122H variant patient and either IBD or healthy controls.

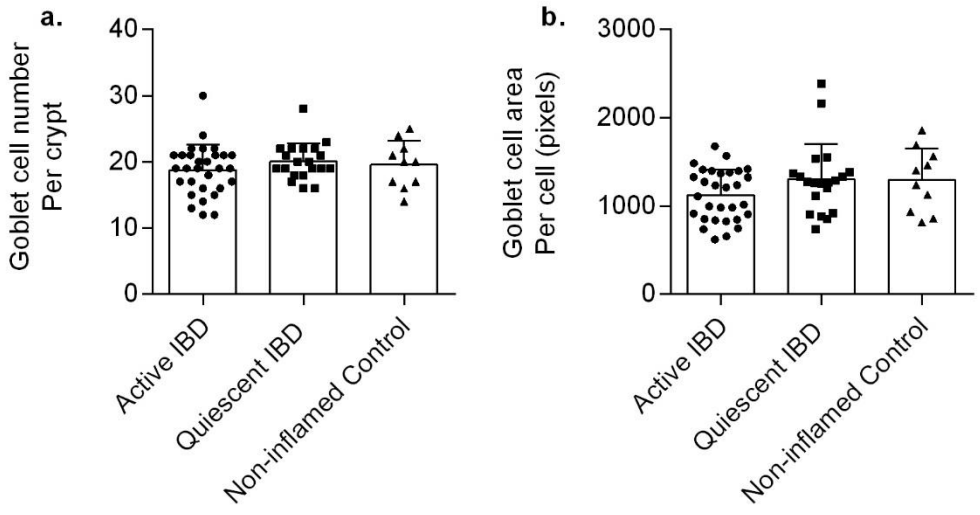

Figure 3.40. Goblet cells of proximal colonic epithelial crypts: analysis stratified by IBD disease activity. *The patient numbers and characteristics are detailed in Table 3.14.* ***a).*** *Manual counting of goblet cells of proximal colonic crypts (defined distance of 300 pixels from the surface epithelium) performed on ten longitudinally cut crypts (representative of pan-colonic biopsies) for each patient.* ***b).*** *Average individual goblet cell area of proximal colonic crypts was calculated.*

In summary, evaluation of colonic epithelial goblet cells amongst a small cohort of IBD patients and non-inflamed controls, suggests a trend toward a reduction in goblet cell number and a concordant increase in goblet cell size in the *NOX1* p.N122H variant patient. However, the largest influence on goblet cell number and size was demonstrated to be IBD disease activity. Thus, no reliable conclusion on the goblet cell number and size in the *NOX1* p.N122H variant patients can be drawn from this experiment.

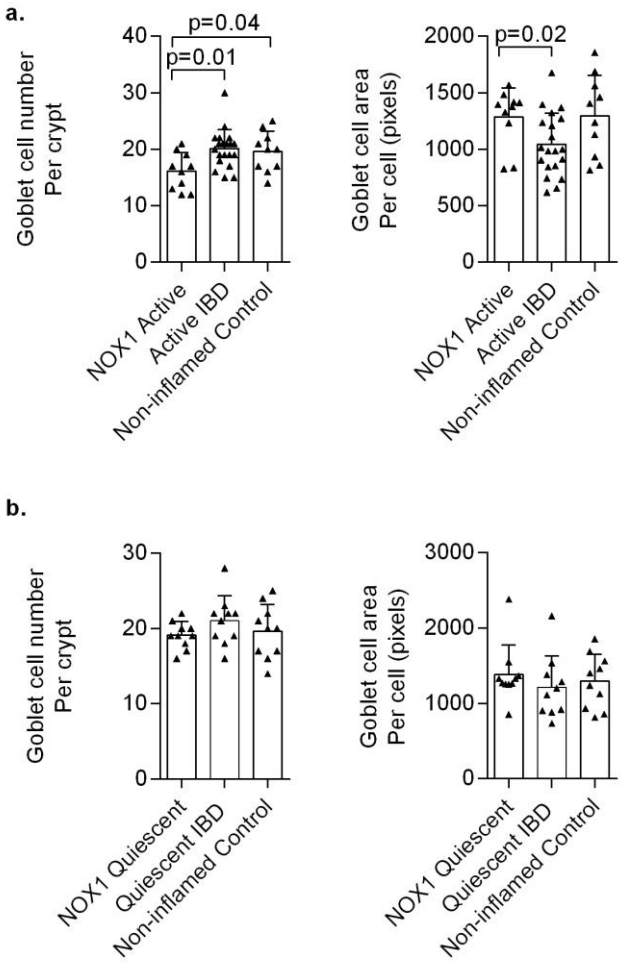

Figure 3.41. Goblet cells in NOX1 p.N122H variant patient, IBD and non-inflamed controls stratified by disease activity. *The patient numbers and characteristics are detailed in Table 3.14. Manual counting of goblet cells of proximal colonic crypts (defined distance of 300 pixels from the surface epithelium) performed on ten longitudinally cut crypts (representative of pan-colonic biopsies) for each patient. Average individual goblet cell area of proximal colonic crypts was calculated as above.* ***a).*** *NOX1 p.N122H variant and IBD controls with active disease.* ***b).*** *NOX1 p.N122H variant and IBD controls with quiescent disease. Statistical analyses using Mann Whitney non-parametric test.*

3.5 DISCUSSION

In this chapter, the investigation of a novel rare variant in the *NOX1* gene in a single patient with very early onset colitis is described, in order to explore the possibility of a causal relationship between the genotype and clinical phenotype. Recent guidelines have proposed that certain criteria be met, in order to establish pathogenic causality of a novel genetic variant for a disease phenotype in a single patient (*Table 3.15*) (273).

The challenges of establishing causality of a rare genetic variant in a single patient are inherent; studies of single patients lack the genetic statistical power of studies amongst multiple patients or families, and penetrance of a mutation cannot definitively be established in a single patient (273). Accordingly, some criteria have stressed the importance of describing multiple cases, so as to avoid the potential consequences of false assignment of pathogenicity of such rare variants for affected patients and their families (274). However, there is increasing recognition of the importance of well-designed studies of novel monogenic defects, particularly in the field of immunology, where such research can yield valuable insight into the pathogenesis of complex disease (273, 275, 276). A monogenic defect provides a natural example of an experimental construct for investigation of a pathway of disease (275).

In order to discuss the progress made in this chapter toward the identifying the functional significance of the *NOX1* p.N122H variant mutation in a single patient with a VEOIBD phenotype, each of the criteria set out in *Table 3.15* are addressed directly.

Casanova Criteria	***NOX1* p.N122H variant**
1.The patient's candidate genotype is monogenic and does not occur in individuals without the clinical phenotype	
1.1 Rare and distinctive phenotype and genotype.	VEOIBD Refractory to conventional therapy
1.2 Family studies demonstrate complete clinical penetrance.	Family pedigree: mother a carrier Penetrance not possible to ascertain from single patient
1.3 Population studies demonstrate that the genotype does not occur in healthy individuals	Variant not identified in UK-IBD genetic consortium screening of IBD patients and healthy controls
2.Experimental studies indicate that the genetic variant impairs or destroys expression or function of gene product	
2.1 Demonstrate expression of the gene and gene product in cells/tissue relevant to the disease pathogenesis	NOX1 mRNA highly expressed in the colonic epithelium.
2.2 Demonstrate abnormal expression of the gene and function of the gene product in relevant cells/tissues.	Diminished superoxide production demonstrated in colonic epithelial organoid monoculture
3. The causal relationship between the candidate genotype and the clinical phenotype must be established via a relevant cellular of animal phenotype	
3.1 A patient-specific cellular (or animal) phenotype should be caused by the mutant allele.	Severe spontaneous early onset colitis in IL-10/NOX1^{dKO} mouse model (223).
3.2 Correct of the phenotypic defect in either the cellular or animal model should be demonstrated by rescue with the wild-type allele	Not yet performed.

Table 3.15. 'Casanova criteria' for attributing a clinical phenotype to a candidate genotype in a single patient. *Adapted from (273).*

3.4.1 *NOX1* p.N122H variant genotype and phenotype

The clinical phenotype of the NOX1 p.N122H variant patient is rare; VEOIBD (IBD diagnosed before the age of 6 years) has an estimated incidence of 4.37 per 100,000 children (10, 25). Of the overall 25% of patients with IBD diagnosed during children, around 15% of these patients are diagnosed in the VEOIBD age group (<4% of IBD overall) (277). In addition to the very early age of onset, the clinical phenotype of the *NOX1* p.N122H variant patient is severe. The *NOX1* p.N122H variant patient presented with failure to thrive and manifest a severe pan-colitis, refractory to conventional IBD

medications, and requiring of biological therapy. Thus, the distinct and severe phenotypic characteristics of the *NOX1* p.N122H variant patient raise the possibility of an underlying monogenic disorder (*Criterion 1.1, Table 3.15*).

Work for this thesis included a family pedigree study of the *NOX1* p.N122H variant patient, performed in order to assess for transmission and clinical penetrance of the genotype. The affected patient carries the candidate hemizygous X-linked mutation (c.A364C), leading to substitution of asparagine for histidine (p.N122H). Sequencing of the patient's mother revealed that she was a heterozygous carrier of the c.A364C substitution mutation, confirming X-linked transmission of the mutation to the male *NOX1* p.N122H variant patient. The *NOX1* p.N122H variant patient has an unaffected sister. This family pedigree demonstrates transmission of the *NOX1* p.N122H variant mutation, however a more detailed maternal family history would be beneficial to investigate for an IBD phenotype in prior male generations (*Criterion 1.2, Table 3.15*).

Outside the context of this thesis, the frequency of the *NOX1* p.N122H variant was further investigated through the genotyping of 6000 IBD patients and non-inflamed controls, collected by the UK-IBD genetics consortium (unpublished data courtesy of supervisor, HU). Furthermore, the Exac Variant Server (http://exac.broadinstitute.org/), spanning 60,706 unrelated individuals sequenced as part of various disease-specific and population genetic studies, was screened. None of the genotyped controls, nor patients with IBD, carried the *NOX1* p.N122H variant, supporting the view that this is an extremely rare genetic variant (*Criterion 1.3, Table 3.15*). The fact that the *NOX1* p.N122H variant is an evolutionarily conserved missense mutation, affecting all isoforms of NOX1, adds further weight of evidence to the significance of the mutation (278). Thus, the *NOX1* p.N122H variant mutation meets *Criterion 1* set out in *Table 3.15*; the affected patient's candidate genotype is monogenic and does not occur in

individuals without the clinical phenotype.

3.5.2 Gastrointestinal tract expression of NOX1 mRNA

In this chapter, it was demonstrated that NOX1 mRNA is highly expressed in the epithelium of the distal gastrointestinal tract, with a gradient of expression from the ileum (intermediate) to the distal colon (high). NOX1 is also expressed along with its functional subunits necessary for activation of the complex (157). This pattern of expression is in keeping with prior literature (168, 204, 211), and parallels density of bacterial colonisation in the gut, implicating a possible role for the NOX1 enzyme in bacterial handling (156). The clinical phenotype of pan-colitis in the *NOX1* p.N122H variant, is thus in keeping with the expression of NOX1 in the colonic epithelium (*Criterion 2.1, Table 3.15*).

Further investigation into NOX1 mRNA expression in the colonic epithelium of patients with IBD compared with non-inflamed controls, revealed a significant reduction in NOX1 expression. However, this difference was not considered biologically relevant, given that an outlying result generated the statistical significance. Thus, reduced NOX1 mRNA expression is not a likely contributor to the pathogenesis of polygenic conventional IBD. The primary difference between IBD patients and non-inflamed controls was upregulation of DUOX2 expression in the setting of active IBD, which is in keeping with established literature (238).

NOX1 mRNA colonic epithelial expression was examined in the *NOX1* p.N122H variant patient via an organoid construct, and there was no difference in the expression of NOX1 (nor its subunits NOXO1 or NOXA1) compared with a matched IBD control, suggesting that the mutation does not affect mRNA stability.

3.5.3 Superoxide generation by NOX1 in the gastrointestinal tract

In order to investigate the functional role of NOX1 in the human colonic epithelium, superoxide production by colonic epithelial biopsies, both from non-inflamed controls, patients with IBD, and the *NOX1* p.N122H variant patient was examined. Amongst non-inflamed control patients, superoxide production from the proximal to the distal gastrointestinal tract correlated with NOX1 mRNA expression. This suggests that NOX1 is the primary source of superoxide in the non-inflamed colonic epithelium. This was confirmed via the use of a NOX1 inhibitor (ML171), which was shown to significantly diminish the formation of reduced formazan precipitate at the epithelial margin of colonic epithelial crypts.

In patients with IBD however, superoxide generation from colonic epithelial biopsies was influenced by the presence of NOX2-expressing phagocytic immune cells in the lamina propria. This was suggested by the enhanced superoxide generation in biopsy specimens from patients with active disease, particularly upon stimulation with PMA. DUOX2 mRNA upregulation in the setting of IBD was a less likely source of enhanced superoxide generation, as the primary product of DUOX2 is hydrogen peroxide, which is not measured using an L-012 chemiluminescence assay.

Given the difficulty with accurately measuring NOX1-derived superoxide from colonic epithelial biopsy specimens in patients with IBD, colonic epithelial organoids were cultured from the *NOX1* p.N122H variant patient, along with IBD and non-inflamed controls. This key experiment demonstrated that the colonic epithelial organoids from the *NOX1* p.N122H variant patient produced significantly less superoxide at baseline, than both IBD and non-inflamed controls. Even upon stimulation with PMA, a potent inducer activation of the NOX1 complex (256), a low level of superoxide was generated

by the *NOX1* p.N122H variant colonic epithelial cells.

Thus, the comparatively reduced superoxide production from the colonic epithelial cells of the *NOX1* p.N122H variant patient was considered evidence of disrupted function of the *NOX1* gene product consequent to the mutation (*Criterion 2.2, Table 3.15*).

3.5.4 Relationship between the *NOX1* p.N122H variant and IBD phenotype

As summarised in *Table 3.16 and Figure 3.43*, there are extensive animal and cell-line data to suggest that NOX1 plays a key role in many physiological and pathological processes in the intestinal epithelium. Such evidence provides a potential link between the *NOX1* p.N122H variant and intestinal inflammation (*Criterion 3.1, Table 3.15).*

NOX1 is an important protagonist in colonic epithelial barrier function and bacterial handling. Upon interaction with commensal microflora, NOX1 has been shown to generate superoxide, which acts on intracellular redox-sensitive phosphatases to mediate anti-inflammatory cellular signalling along with cell migration and proliferation (182, 184, 218-220, 231, 232). NOX1-derived superoxide also influences intestinal epithelial differentiation and goblet cell function (201, 221, 223). Colonic mucus produced by goblets cells provides an important barrier between the intestinal microbiota and the colonic epithelium, maintaining sterility at the epithelial border (64).

A mouse model has demonstrated that mice with an IL-10/NOX1^{dKO} develop spontaneous colitis, which is phenotypically similar to UC (223). The colitic phenotype in the IL-10/NOX1^{dKO} mice was severe and of early onset (6-7 weeks of age). In comparison, IL-10^{KO} mice demonstrated only slight weight loss at 13 weeks of age. Inflammatory cytokine expression was significantly increased in the IL-10/NOX1^{dKO} mice (IL1-β, TNF-α, IL-13, IL-17A, and IFN-β). Furthermore, the IL-10/NOX1^{dKO}

mice demonstrated diminished goblet cell number and function, as well as ER stress, both of which preceded the onset of colitis. Bone marrow chimeric mice were generated and demonstrated that the colitis was inherent to the epithelial cells rather than haematopoietic lineages. Thus, there is an animal model in support of a loss of function *NOX1* mutation being pathogenic. However, it must be acknowledged that the *NOX1* mutation was only pathogenic when in combination with an *IL10* mutation, as the NOX1 ^{KO} mice were the same in all parameters to the wild-type mice (*Criterion 3.1, Table 3.15).*

In summary, there is literature to suggest that NOX1 plays a key role in epithelial barrier function and bacterial handling in the colon. Goblet cell function seems implicitly linked to NOX1-derived superoxide, and a defect in NOX1 may thus compromise the integrity of the colonic mucus layer. Furthermore, diminished superoxide production at the colonic epithelial border in the setting of a NOX1 defect, may reduce the sterility of the usually impervious inner mucus layer, allowing commensal microflora to come into contact with epithelial cells (64). This defect in barrier function may initiate a chronic inflammatory response and IBD-like inflammation. In addition, impairment of the role of NOX1 in promoting cellular proliferation and migration upon interaction with intestinal flora, may further exacerbate the barrier function defect.

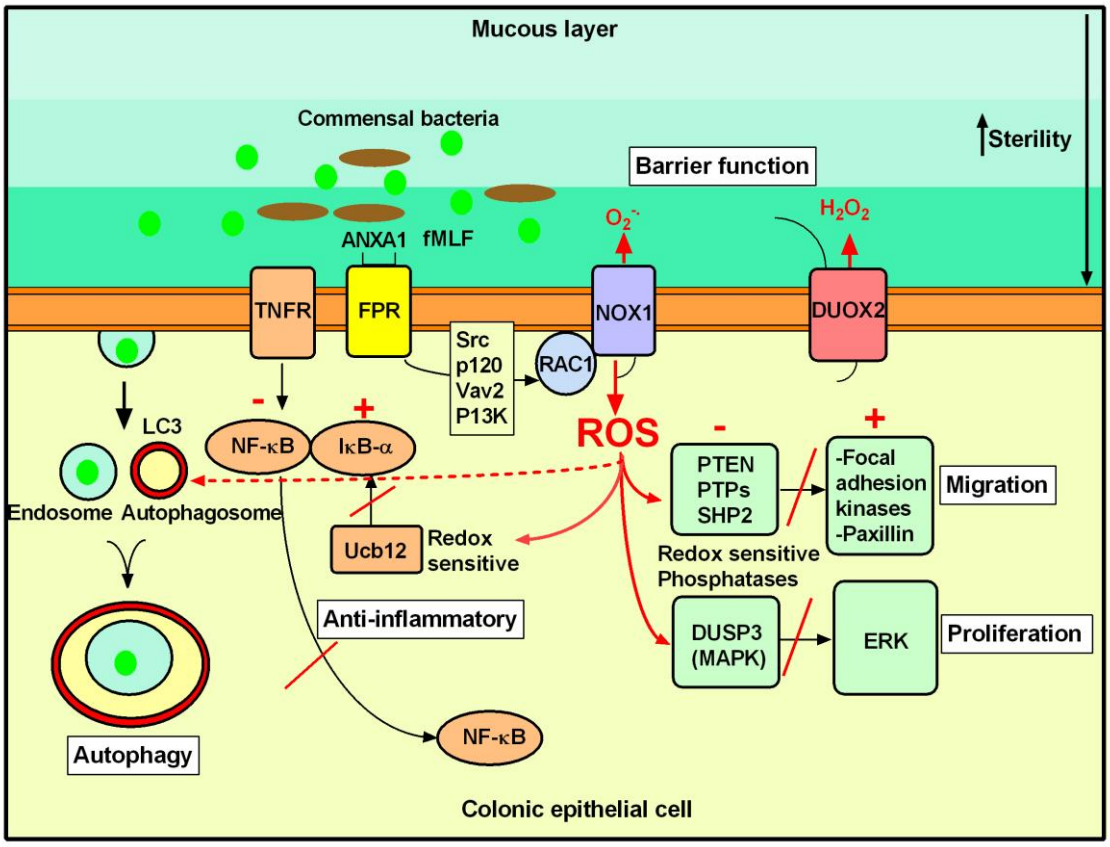

Figure 3.42. Putative functional roles of NOX1-derived ROS in colonic epithelial cells. *The figure provides a mechanistic outline of the physiological roles of NOX1 in colonic epithelial cells; barrier function, migration, proliferation, autophagy, and anti-inflammatory signalling.*

Pathway	Evidence and mechanisms	Key molecules
Bacterial handling and autophagy	-Gradient of NOX1 expression in colon parallels density of bacterial colonisation (168, 204, 211). -Commensal bacteria mediate superoxide generation by NOX1 through innate immune system (FPR receptors) in cell-lines and animal models (179, 182, 184, 218, 230-232) - Recruitment of LC3 to intracellular bacteria inhibited by $p22^{phox}$ siRNA knock-down in epithelial cells. Concordant impairment in autophagy (201).	*Lactobacillus species* FPRs LC3
Epithelial barrier function	-NOX1 is involved in differentiation of progenitor cells into goblet cells (222) -NOX1 knock-out models show reduced goblet cell number and mucin accumulation within goblet cells due to defective autophagy (201, 221, 223).	Pi3K/AKT/Wnt/beta-catenin and Notch1 signalling pathways
Anti-inflammatory role (179)	-Bacterial induced ROS inactivate Ubc12, which normally neddylates the Cul1 subunit of the ubiquitin ligase complex targeting IκB-α for proteosomal degradation. As Iκ*B*-α is no longer targeted for degradation, NF-κ*B* is unable to translocate to the nucleus.	NF-κB Ucb12 IκB-α
Cell proliferation , migration, restitution, and repair (182-184, 219, 220, 231-233)	-Commensal bacteria via FPR receptors induce NOX1 generated superoxide which leads to oxidative inactivation of redox-sensitive tyrosine phosphatases (PTEN, PTP, and SHP-2, DUSP3, and MAPK), leading to increased phosphorylation of focal adhesion kinases (FAK) and ERK, which enhance cell proliferation, migration and wound healing.	*Lactobacillus species* Annexin A1 FAK PTEN PTP MAPK ERK SHP-2 Src, p120, Vav2, P13K

Table 3.16. Summary of putative IBD pathways influenced by NOX1. *The table outlines the key pathways influenced by NOX1 that are relevant to IBD, as well as the key mechanism and involved molecules.*

Beyond reduced superoxide production by *NOX1* p.N122H variant colonic epithelial cells, further exploration of a possible causal relationship between the mutation and the VEOIBD clinical phenotype was performed in this thesis chapter.

Bacterial handling. A role for NOX1 in bacterial handling was investigated using a

NOX1-expressing HT-29 cell line. Bacterial killing of both invasive (*S. typhimurium*) and non-invasive (EcN) bacterial species by HT-29 cells was analysed, following treatment with a NOX1 inhibitor (ML171). There was no difference in bacterial killing mediated by treatment with ML171 in the HT-29 cell-line. The weakness of this experimental strategy are discussed in (*Section 3.5.5*)

Colonic epithelial cell proliferation and migration. Colonic epithelial cell proliferation was assessed by ki67 immuno-reactive staining of colonic epithelial biopsies harvested from the *NOX1* p.N122H variant patient both during active and quiescent disease. Although there was a trend towards a reduced number of proliferating epithelial cells in the *NOX1* p.N122H variant patient compared to IBD and non-inflamed control patients, the primary factor influencing cellular proliferation was disease activity. Thus, no definitive conclusion could be drawn from this experiment, aside from the observation that there is no profound defect in cellular proliferation in the *NOX1* p.N122H variant patient.

Further studies using the HT-29 cell line and a NOX1 inhibitor (ML171) failed to demonstrate any effect of chemical inhibition of NOX1 on epithelial cell migration and proliferation. The weaknesses of these experiments are inherent and are discussed in (*Section 3.5.5).*

Colonic epithelial barrier function. The goblet cell number and structure of the *NOX1* p.N122H variant patient was assessed by staining of mucopolysaccharides with Alcian Blue/PAS. Although there was a trend toward a reduction in goblet cell number in the *NOX1* p.N122H variant patient compared to IBD and non-inflamed control patients, the primary determinant of goblet cell number and size was IBD disease activity. Thus, no reliable conclusion could be drawn from this experiment, aside from the observation

that there was no profound absence of goblet cells in the epithelium of the *NOX1* p.N122H variant patient.

In summary, beyond diminished superoxide production by the colonic epithelial cells of the *NOX1* p.N122H variant patient, a further functional role of NOX1 in putative IBD pathways was not definitely proven in this thesis chapter. However, there is ample evidence from cell-line and animal data to hypothesise that a *NOX1* mutation leading to loss of function may indeed be pathogenic, via epithelial barrier function and bacterial handling defects, thereby predisposing to intestinal inflammation and IBD.

3.4.5 Limitations of experimental strategy

There are important weaknesses of the experimental strategy employed in this chapter that warrant discussion.

HT-29 cell line

The HT-29 cell line was selected for experimental use as it expresses high levels of NOX1 mRNA as well as the necessary subunits (NOXO1 and NOXA1) for activation of the NOX1 complex (234). However, given that it is a colon cancer cell-line, HT-29 cells possess oncogenes (myc, ras, myb, fos, sis, p53, abl, ros, and src), which have a substantial influence cellular growth and differentiation (279, 280). Thus, experimental models using HT-29 cells to assess epithelial cell migration and proliferation in the setting of NOX inhibition have an inherent oncogenic bias, which may have limited capacity for detection of any functional defects.

Colonic epithelial organoids cultured from the *NOX1* p.N122H variant patient are the appropriate cell-line for future experimental work.

NOX1 chemical inhibition

ML171 is a novel competitive small-molecule inhibitor of NOX1, which was chosen for use on the basis of demonstrated specificity of inhibition, cost, and ease of use (254). However, chemical inhibitors of NOX1 are not perfect. Firstly, although ML171 is reported to be specific for NOX1, at higher doses there is demonstrated inhibition of other NOX enzymes (254). Secondly, the duration of ML171 inhibition was shown to be limited over 24 hours at the concentrations used, and a tapering of inhibition may have had an impact on prolonged experiments for bacterial killing, cellular proliferation and cellular migration. Lastly, many of the biological functions of NOX1 relate to intracellular superoxide generation, which may not be completely inhibited by ML171. Thus, the use of a chemical inhibitor limits interpretation of results and may have limited capacity for detection of true functional defects.

The appropriate experimental construct for future work is a NOX1 knock-out model, which may be achieved using CRISPR-Cas 9 technology or short-interfering RNA (siRNA) techniques (281-283).

3.4.6 Conclusions and future directions

In this chapter, examination of a rare *NOX1* p.N122H variant in a single patient with VEOIBD is performed, in order to investigate the possibility of a causal relationship between the genotype and clinical phenotype. Evidence is provided that the *NOX1* p.N122H variant impairs function of the gene product, via demonstration of diminished superoxide production from affected colonic epithelial cells. There is extensive animal and cell-line data to suggest that NOX1 plays a key role in many physiological and pathological processes in the intestinal epithelium including intestinal barrier function

and bacterial handling. Such evidence provides the potential link between the *NOX1* p.N122H variant genotype and the clinical phenotype of intestinal inflammation. The *NOX1* p.N122H variant may thus be considered an 'implicated' genetic variant (274), however, further evidence of causality is required before this variant may be deemed truly pathogenic.

In order to explore a causal link between the *NOX1* p.N122H variant and intestinal inflammation, further experimental work is planned by our group:

- Generating an appropriate NOX1 knock-out cellular phenotype using CRISPR-Cas9 technology with subsequent correction of the cellular phenotype following rescue with the wild-type allele.
- Functional studies in *NOX1* p.N122H variant using primary colonic epithelial organoids.
- Expanding international collaboration in an effort to investigate other patients with *NOX1* loss of function variants.

CHAPTER 4: FINAL DISCUSSION

The experimental work undertaken in thesis was performed with the intent of expanding the current understanding of genetics in UC. Unlike CD, for which key genetic markers have been identified that denote risk not only for susceptibility but for disease phenotype, the role of genetics in UC remains less clear. UC phenotype is poorly explained by polymorphisms associated with risk (7, 14, 102).

This thesis provided the opportunity to explore two distinct aspects of genetics in UC; the influence of polygenic burden in predicting UC disease phenotype, and a possible causal relationship between a rare mutation and a severe early onset colitis phenotype. The key findings and future directions for each body of work are summarised separately.

4.1 Quantifying genetic risk in UC phenotypes (Chapter 2)

4.1.1 Key findings

1. Genetic risk burden, as measured by a GRS model, is enriched amongst UC patients who are diagnosed before the age of 10 years. Although, a higher rate of first degree family history is recognised amongst this group, a higher polygenic risk burden has not been previously shown (27).
2. Genetic burden, as measured by GRS, is enriched amongst patients with ASUC, as compared to those with non-severe UC. This is the first time that a higher polygenic load has been demonstrated in the ASUC cohort. This result is contingent on the robust accuracy of phenotyping within the examined cohort, given that the diagnosis of ASUC requires application of clinical criteria. A prior study has studied the genetics of an ASUC cohort, however in adopting an

association approach for candidate loci, only a single associated polymorphism was identified (127).

3. Although the study was underpowered for analysis of candidate loci, there was a signal that polymorphisms within the IL-10 cytokine signalling pathway may impart risk for ASUC. The significant enrichment of the *IL10* associated SNP rs3024505 in the ASUC cohort, replicates the findings of a key prior genotype-phenotype study in UC for the first time (15).

4.1.2 Therapeutic implications and future directions

The experimental findings implicating defects within the regulatory IL-10 cytokine signalling pathways in patients with ASUC, may have potential therapeutic implications. Administration of IL-10 cytokine to patients with ASUC may be considered, however prior trials using subcutaneous IL-10 in mild-moderate CD have shown very modest effect (284). Further limiting optimism for IL-10 cytokine therapy are its complex and partially pro-inflammatory effects, as well as short half-life (86). Moreover, there is currently no evidence demonstrating diminished IL-10 levels in patients with ASUC.

Deficient immune-regulation by IL-10 and its down-stream mediators, may lead to amplification of the pro-inflammatory activity of other pathways. This may be hypothesised to be a partial explanation for the efficacy observed for TNF-α inhibitor therapy in ASUC (285). Unopposed activity of the IL-23/Th17 pathway, may also be a target for unconventional therapies in ASUC, such as ustekinumab, a monoclonal antibody against the p40 subunit of IL-12/23, shown to be efficacious in moderate to severe CD (286, 287). Other novel therapeutics are also on the horizon, including antagonists of the IL-23 and the IL-23 p19 subunit (288).

The anticipated future plans for this work in this chapter are:

1. To undertake a multivariate analysis including clinical and environmental factors, such as disease extent, age at diagnosis, and smoking status, alongside genetics, so as to generate a more comprehensive model of risk prediction for ASUC. Given that ASUC frequently occurs early in the disease course, the integration of genetic factors (GRS) at the time of diagnosis of UC, together with currently available markers of risk (disease extent, haemoglobin, CRP) is planned (117).
2. To seek out collaborators to undertake a replication study in another group of ASUC patients, so as to validate the findings of enriched GRS and cumulative defects in the IL-10 signalling pathway amongst this group.

4.2 *NOX1* variant in very early onset colitis (Chapter 3)

4.2.1 Key findings

1. In this chapter, for the first time, it is demonstrated that the *NOX1* p.N122H variant impairs function of the gene product. Colonic epithelial cells from the *NOX1* p.N122H variant patient produce less superoxide than matched controls, even upon stimulation. There was no difference in NOX1 mRNA expression in the *NOX1* p.N122H variant colonic epithelial cells, showing that the mutation does not impair stability of the mRNA transcript.
2. Extensive animal and cell-line data suggest a vital role of NOX1 in physiological processes in the colonic epithelium, including epithelial barrier function, migration, proliferation, and autophagy, providing a link between the *NOX1* p.N122H variant and the clinical phenotype of intestinal inflammation.

4.2.2 Therapeutic implications and future directions

The *NOX1* p.N122H variant sheds light on a putative mechanism of intestinal innate immunity; the role of superoxide at the colonic epithelial border in the maintenance of sterility of the inner mucus layer and crypts. It may be hypothesised that such an impairment of bacterial handling was a key contributor to the initiation of colonic inflammation in the affected *NOX1* p.N122H variant patient. Accordingly, antibacterial therapy at the onset of symptoms of intestinal inflammation may have been a useful therapeutic strategy. Such an approach may have restored the balance at the colonic epithelium prior to the establishment of chronic inflammation, beyond which conventional immunomodulatory therapy would be required.

In order to further investigate a causal link between the *NOX1* p.N122H variant and the clinical phenotype of colitis, further experiments are planned.

1. A pivotal experiment is required to demonstrate that diminished superoxide production in colonic epithelial cells harbouring the *NOX1* p.N122H variant leads to inflammation akin to that of IBD. This could be achieved through an animal or cell-line construct. Furthermore, correction of the phenotypic defect induced by the *NOX1* p.N122H variant, would need to be demonstrated by rescue with the wild-type allele. Thus, generating a *NOX1* knock-out cellular phenotype, using CRISPR-Cas9 technology, is a future direction for this work.
2. Studies of genetic defects in single patients lack statistical power and the ability to determine penetrance of the mutation. Thus, a key strategy is to engage in international collaborative efforts to identify other patients with the *NOX1* loss of function mutations.

REFERENCES

1. Cosnes J, Gower-Rousseau C, Seksik P, et al. Epidemiology and natural history of inflammatory bowel diseases. Gastroenterology. 2011;140(6):1785-94.
2. Molodecky NA, Soon IS, Rabi DM, et al. Increasing incidence and prevalence of the inflammatory bowel diseases with time, based on systematic review. Gastroenterology. 2012;142(1):46-54 e42; quiz e30.
3. Burisch J, Jess T, Martinato M, et al. The burden of inflammatory bowel disease in Europe. J Crohns Colitis. 2013;7(4):322-37.
4. Khor B, Gardet A, Xavier RJ. Genetics and pathogenesis of inflammatory bowel disease. Nature. 2011;474(7351):307-17.
5. Knights D, Lassen KG, Xavier RJ. Advances in inflammatory bowel disease pathogenesis: linking host genetics and the microbiome. Gut. 2013;62(10):1505-10.
6. Maloy KJ, Powrie F. Intestinal homeostasis and its breakdown in inflammatory bowel disease. Nature. 2011;474(7351):298-306.
7. Jostins L, Ripke S, Weersma RK, et al. Host-microbe interactions have shaped the genetic architecture of inflammatory bowel disease. Nature. 2012;491(7422):119-24.
8. Parkes M, Cortes A, van Heel DA, et al. Genetic insights into common pathways and complex relationships among immune-mediated diseases. Nat Rev Genet. 2013;14(9):661-73.
9. Uhlig HH. Monogenic diseases associated with intestinal inflammation: implications for the understanding of inflammatory bowel disease. Gut. 2013;62(12):1795-805.
10. Uhlig HH, Schwerd T, Koletzko S, et al. The diagnostic approach to monogenic very early onset inflammatory bowel disease. Gastroenterology. 2014;147(5):990-1007.e3.
11. Brunham LR, Hayden MR. Hunting human disease genes: lessons from the past, challenges for the future. Hum Genet. 2013;132(6):603-17.
12. Manolio TA, Collins FS, Cox NJ, et al. Finding the missing heritability of complex diseases. Nature. 2009;461(7265):747-53.
13. Goyette P, Boucher G, Mallon D, et al. High-density mapping of the MHC identifies a shared role for HLA-DRB1*01:03 in inflammatory bowel diseases and heterozygous advantage in ulcerative colitis. Nature 2015;47(2):172-9.
14. Ananthakrishnan AN, Huang H, Nguyen DD, et al. Differential effect of genetic burden on disease phenotypes in Crohn's disease and ulcerative colitis: analysis of a north american cohort. Am J Gastroenterol. 2014;109(3):395-400.
15. Haritunians T, Taylor KD, Targan SR, et al. Genetic predictors of medically refractory ulcerative colitis. Inflamm Bowel Dis. 2010;16(11):1830-40.
16. Ko Y, Butcher R, Leong RW. Epidemiological studies of migration and environmental risk factors in the inflammatory bowel diseases. World J Gastroenterol. 2014;20(5):1238-47.
17. Ko Y, Kariyawasam V, Karnib M, et al. Inflammatory bowel disease environmental risk factors: a population-based case-control study of Middle Eastern migration to Australia. Clin Gastroenterol Hepatol. 2015.
18. Zhao J, Ng SC, Lei Y, et al. First prospective, population-based inflammatory bowel disease incidence study in mainland of China: the emergence of "western" disease. Inflamm Bowel Dis. 2013;19(9):1839-45.

19. Dignass A, Eliakim R, Magro F, et al. Second European evidence-based consensus on the diagnosis and management of ulcerative colitis part 1: definitions and diagnosis. J Crohns Colitis. 2012;6(10):965-90.
20. Satsangi J, Silverberg MS, Vermeire S, et al. The Montreal classification of inflammatory bowel disease: controversies, consensus, and implications. Gut. 2006;55(6):749-53.
21. Solem CA, Loftus EV, Jr., Tremaine WJ, et al. Correlation of C-reactive protein with clinical, endoscopic, histologic, and radiographic activity in inflammatory bowel disease. Inflamm Bowel Dis. 2005;11(8):707-12.
22. Travis SP, Schnell D, Krzeski P, et al. Developing an instrument to assess the endoscopic severity of ulcerative colitis: the Ulcerative Colitis Endoscopic Index of Severity (UCEIS). Gut. 2012;61(4):535-42.
23. Travis SP, Schnell D, Krzeski P, et al. Reliability and initial validation of the ulcerative colitis endoscopic index of severity. Gastroenterology. 2013;145(5):987-95.
24. Kim B, Barnett JL, Kleer CG, et al. Endoscopic and histological patchiness in treated ulcerative colitis. Am J Gastroenterol. 1999;94(11):3258-62.
25. Benchimol EI, Fortinsky KJ, Gozdyra P, et al. Epidemiology of pediatric inflammatory bowel disease: a systematic review of international trends. Inflamm Bowel Dis. 2011;17(1):423-39.
26. Henderson P, Hansen R, Cameron FL, et al. Rising incidence of pediatric inflammatory bowel disease in Scotland. Inflamm Bowel Dis. 2012;18(6):999-1005.
27. Levine A, Griffiths A, Markowitz J, et al. Pediatric modification of the Montreal classification for inflammatory bowel disease: the Paris classification. Inflamm Bowel Dis. 2011;17(6):1314-21.
28. Muise AM, Snapper SB, Kugathasan S. The age of gene discovery in very early onset inflammatory bowel disease. Gastroenterology. 2012;143(2):285-8.
29. Ekbom A, Helmick C, Zack M, et al. Ulcerative colitis and colorectal cancer. A population-based study. N Engl J Med. 1990;323(18):1228-33.
30. Jakobovits SL, Travis SP. Management of acute severe colitis. Br Med Bull. 2005;75-76:131-44.
31. Bryant RV, Brain O, Travis SP. Conventional drug therapy for inflammatory bowel disease. Scand J Gastroenterol. 2015;50(1):90-112.
32. Dignass A, Lindsay JO, Sturm A, et al. Second European evidence-based consensus on the diagnosis and management of ulcerative colitis part 2: current management. J Crohns Colitis. 2012;6(10):991-1030.
33. Langholz E, Munkholm P, Davidsen M, et al. Changes in extent of ulcerative colitis: a study on the course and prognostic factors. Scand J Gastroenterol. 1996;31(3):260-6.
34. Magro F, Rodrigues A, Vieira AI, et al. Review of the disease course among adult ulcerative colitis population-based longitudinal cohorts. Inflamm Bowel Dis. 2012;18(3):573-83.
35. Truelove SC, Witts LJ. Cortisone in ulcerative colitis; final report on a therapeutic trial. Br Med J. 1955;2(4947):1041-8.
36. Corte CJ, Fernandopulle A, Catuneanu A, et al. Association between the Ulcerative Colitis Endoscopic Index of Severity (UCEIS) and outcomes in acute severe ulcerative colitis. J Crohns Colitis. 2015.
37. Pera A, Bellando P, Caldera D, et al. Colonoscopy in inflammatory bowel disease. Diagnostic accuracy and proposal of an endoscopic score. Gastroenterology. 1987;92(1):181-5.

38. Langholz E, Munkholm P, Davidsen M, et al. Course of ulcerative colitis: analysis of changes in disease activity over years. Gastroenterology. 1994;107(1):3-11.
39. Bryant RV, Winer S, Travis SP, et al. Systematic review: histological remission in inflammatory bowel disease. Is 'complete' remission the new treatment paradigm? An IOIBD initiative. J Crohns Colitis. 2014;8(12):1582-97.
40. Travis SP, Higgins PD, Orchard T, et al. Review article: defining remission in ulcerative colitis. Aliment Pharmacol Ther. 2011;34(2):113-24.
41. Dinesen LC, Walsh AJ, Protic MN, et al. The pattern and outcome of acute severe colitis. J Crohns Colitis. 2010;4(4):431-7.
42. Turner D, Walsh CM, Steinhart AH, et al. Response to corticosteroids in severe ulcerative colitis: a systematic review of the literature and a meta-regression. Clin Gastroenterol Hepatol. 2007;5(1):103-10.
43. Hendriksen C, Kreiner S, Binder V. Long term prognosis in ulcerative colitis--based on results from a regional patient group from the county of Copenhagen. Gut. 1985;26(2):158-63.
44. Odes S, Vardi H, Friger M, et al. Clinical and economic outcomes in a population-based European cohort of 948 ulcerative colitis and Crohn's disease patients by Markov analysis. Aliment Pharmacol Ther. 2010;31(7):735-44.
45. Ananthakrishnan AN. Epidemiology and risk factors for IBD. Nat Rev Gastroenterol Hepatol. 2015;12(4):205-17.
46. Van Limbergen J, Radford-Smith G, Satsangi J. Advances in IBD genetics. Nat Rev Gastroenterol Hepatol. 2014;11(6):372-85.
47. Vermeire S. Review article: genetic susceptibility and application of genetic testing in clinical management of inflammatory bowel disease. Aliment Pharmacol Ther. 2006;24 Suppl 3:2-10.
48. Orholm M, Munkholm P, Langholz E, et al. Familial occurrence of inflammatory bowel disease. N Engl J Med. 1991;324(2):84-8.
49. Yang H, McElree C, Roth MP, et al. Familial empirical risks for inflammatory bowel disease: differences between Jews and non-Jews. Gut. 1993;34(4):517-24.
50. Halme L, Paavola-Sakki P, Turunen U, et al. Family and twin studies in inflammatory bowel disease. World J Gastroenterol. 2006;12(23):3668-72.
51. Halfvarson J, Bodin L, Tysk C, et al. Inflammatory bowel disease in a Swedish twin cohort: a long-term follow-up of concordance and clinical characteristics. Gastroenterology. 2003;124(7):1767-73.
52. Orholm M, Binder V, Sorensen TI, et al. Concordance of inflammatory bowel disease among Danish twins. Results of a nationwide study. Scand J Gastroenterol. 2000;35(10):1075-81.
53. Spehlmann ME, Begun AZ, Burghardt J, et al. Epidemiology of inflammatory bowel disease in a German twin cohort: results of a nationwide study. Inflamm Bowel Dis. 2008;14(7):968-76.
54. Thompson NP, Driscoll R, Pounder RE, et al. Genetics versus environment in inflammatory bowel disease: results of a British twin study. BMJ. 1996;312(7023):95-6.
55. Anderson CA, Boucher G, Lees CW, et al. Meta-analysis identifies 29 additional ulcerative colitis risk loci, increasing the number of confirmed associations to 47. Nat Genet. 2011;43(3):246-52.
56. McGovern DP, Gardet A, Torkvist L, et al. Genome-wide association identifies multiple ulcerative colitis susceptibility loci. Nat Genet. 2010;42(4):332-7.
57. Rivas MA, Beaudoin M, Gardet A, et al. Deep resequencing of GWAS loci identifies independent rare variants associated with inflammatory bowel disease. Nat Genet. 2011;43(11):1066-73.

58. Silverberg MS, Cho JH, Rioux JD, et al. Ulcerative colitis-risk loci on chromosomes 1p36 and 12q15 found by genome-wide association study. Nat Genet. 2009;41(2):216-20.
59. Franke A, Balschun T, Karlsen TH, et al. Replication of signals from recent studies of Crohn's disease identifies previously unknown disease loci for ulcerative colitis. Nat Genet. 2008;40(6):713-5.
60. Cho JH, Brant SR. Recent insights into the genetics of inflammatory bowel disease. Gastroenterology. 2011;140(6):1704-12.
61. Salim SY, Soderholm JD. Importance of disrupted intestinal barrier in inflammatory bowel diseases. Inflamm Bowel Dis. 2011;17(1):362-81.
62. Geremia A, Biancheri P, Allan P, et al. Innate and adaptive immunity in inflammatory bowel disease. Autoimmun Rev. 2014;13(1):3-10.
63. Adolph TE, Tomczak MF, Niederreiter L, et al. Paneth cells as a site of origin for intestinal inflammation. Nature. 2013;503(7475):272-6.
64. Johansson ME, Gustafsson JK, Holmen-Larsson J, et al. Bacteria penetrate the normally impenetrable inner colon mucus layer in both murine colitis models and patients with ulcerative colitis. Gut. 2014;63(2):281-91.
65. Kaser A, Lee AH, Franke A, et al. XBP1 links ER stress to intestinal inflammation and confers genetic risk for human inflammatory bowel disease. Cell. 2008;134(5):743-56.
66. Geremia A, Arancibia-Carcamo CV, Fleming MP, et al. IL-23-responsive innate lymphoid cells are increased in inflammatory bowel disease. J Exp Med. 2011;208(6):1127-33.
67. Hugot JP, Chamaillard M, Zouali H, et al. Association of NOD2 leucine-rich repeat variants with susceptibility to Crohn's disease. Nature. 2001;411(6837):599-603.
68. Ogura Y, Bonen DK, Inohara N, et al. A frameshift mutation in NOD2 associated with susceptibility to Crohn's disease. Nature. 2001;411(6837):603-6.
69. Cooney R, Baker J, Brain O, et al. NOD2 stimulation induces autophagy in dendritic cells influencing bacterial handling and antigen presentation. Nat Med. 2010;16(1):90-7.
70. Van Limbergen J, Stevens C, Nimmo ER, et al. Autophagy: from basic science to clinical application. Mucosal Immunol. 2009;2(4):315-30.
71. Abraham C, Cho J. Interleukin-23/Th17 pathways and inflammatory bowel disease. Inflamm Bowel Dis. 2009;15(7):1090-100.
72. Neurath MF, Finotto S, Glimcher LH. The role of Th1/Th2 polarization in mucosal immunity. Nat Med. 2002;8(6):567-73.
73. Wang J, Anders RA, Wang Y, et al. The critical role of LIGHT in promoting intestinal inflammation and Crohn's disease. J Immunol. 2005;174(12):8173-82.
74. Satsangi J, Welsh KI, Bunce M, et al. Contribution of genes of the major histocompatibility complex to susceptibility and disease phenotype in inflammatory bowel disease. Lancet. 1996;347(9010):1212-7.
75. Yap LM, Ahmad T, Jewell DP. The contribution of HLA genes to IBD susceptibility and phenotype. Best Pract Res Clin Gastroenterol. 2004;18(3):577-96.
76. Liu JZ, Hov JR, Folseraas T, et al. Dense genotyping of immune-related disease regions identifies nine new risk loci for primary sclerosing cholangitis. Nat Genet. 2013;45(6):670-5.
77. Achkar JP, Klei L, de Bakker PI, et al. Amino acid position 11 of HLA-DRbeta1 is a major determinant of chromosome 6p association with ulcerative colitis. Genes Immun. 2012;13(3):245-52.

78. Glocker EO, Kotlarz D, Boztug K, et al. Inflammatory bowel disease and mutations affecting the interleukin-10 receptor. N Engl J Med. 2009;361(21):2033-45.
79. Moran CJ, Walters TD, Guo CH, et al. IL-10R polymorphisms are associated with very-early-onset ulcerative colitis. Inflamm Bowel Dis. 2013;19(1):115-23.
80. Kotlarz D, Beier R, Murugan D, et al. Loss of interleukin-10 signaling and infantile inflammatory bowel disease: implications for diagnosis and therapy. Gastroenterology. 2012;143(2):347-55.
81. Pigneur B, Escher J, Elawad M, et al. Phenotypic characterization of very early-onset IBD due to mutations in the IL10, IL10 receptor alpha or beta gene: a survey of the Genius Working Group. Inflamm Bowel Dis. 2013;19(13):2820-8.
82. Ruel J, Ruane D, Mehandru S, et al. IBD across the age spectrum: is it the same disease? Nat Rev Gastroenterol Hepatol. 2014;11(2):88-98.
83. Dhillon SS, Fattouh R, Elkadri A, et al. Variants in nicotinamide adenine dinucleotide phosphate oxidase complex components determine susceptibility to very early onset inflammatory bowel disease. Gastroenterology. 2014;147(3):680-9.e2.
84. Muise AM, Xu W, Guo CH, et al. NADPH oxidase complex and IBD candidate gene studies: identification of a rare variant in NCF2 that results in reduced binding to RAC2. Gut. 2012;61(7):1028-35.
85. Blaydon DC, Biancheri P, Di WL, et al. Inflammatory skin and bowel disease linked to ADAM17 deletion. N Engl J Med. 2011;365(16):1502-8.
86. Shah N, Kammermeier J, Elawad M, et al. Interleukin-10 and interleukin-10-receptor defects in inflammatory bowel disease. Curr Allergy Asthma Rep. 2012;12(5):373-9.
87. Rigaud S, Fondaneche MC, Lambert N, et al. XIAP deficiency in humans causes an X-linked lymphoproliferative syndrome. Nature. 2006;444(7115):110-4.
88. Wong KK, deLeeuw RJ, Dosanjh NS, et al. A comprehensive analysis of common copy-number variations in the human genome. Am J Hum Genet. 2007;80(1):91-104.
89. Conrad DF, Pinto D, Redon R, et al. Origins and functional impact of copy number variation in the human genome. Nature. 2010;464(7289):704-12.
90. Craddock N, Hurles ME, Cardin N, et al. Genome-wide association study of CNVs in 16,000 cases of eight common diseases and 3,000 shared controls. Nature. 2010;464(7289):713-20.
91. Mokry M, Middendorp S, Wiegerinck CL, et al. Many inflammatory bowel disease risk loci include regions that regulate gene expression in immune cells and the intestinal epithelium. Gastroenterology. 2014;146(4):1040-7.
92. Zheng Y, Josefowicz S, Chaudhry A, et al. Role of conserved non-coding DNA elements in the Foxp3 gene in regulatory T-cell fate. Nature. 2010;463(7282):808-12.
93. Lee JC, Espeli M, Anderson CA, et al. Human SNP links differential outcomes in inflammatory and infectious disease to a FOXO3-regulated pathway. Cell. 2013;155(1):57-69.
94. Ventham NT, Kennedy NA, Nimmo ER, et al. Beyond gene discovery in inflammatory bowel disease: the emerging role of epigenetics. Gastroenterology. 2013;145(2):293-308.
95. Mahid SS, Minor KS, Soto RE, et al. Smoking and inflammatory bowel disease: a meta-analysis. Mayo Clin Proc. 2006;81(11):1462-71.
96. Odes HS, Fich A, Reif S, et al. Effects of current cigarette smoking on clinical course of Crohn's disease and ulcerative colitis. Dig Dis Sci. 2001;46(8):1717-21.
97. Wang MH, Fiocchi C, Zhu X, et al. Gene-gene and gene-environment interactions in ulcerative colitis. Hum Genet. 2014;133(5):547-58.

98. Ananthakrishnan AN, Nguyen DD, Sauk J, et al. Genetic Polymorphisms in Metabolizing Enzymes Modifying the Association Between Smoking and Inflammatory Bowel Diseases. Inflamm Bowel Dis. 2014.
99. Nagalingam NA, Lynch SV. Role of the microbiota in inflammatory bowel diseases. Inflamm Bowel Dis. 2012;18(5):968-84.
100. Elinav E, Strowig T, Kau AL, et al. NLRP6 inflammasome regulates colonic microbial ecology and risk for colitis. Cell. 2011;145(5):745-57.
101. Wu GD, Chen J, Hoffmann C, et al. Linking long-term dietary patterns with gut microbial enterotypes. Science. 2011;334(6052):105-8.
102. Ananthakrishnan AN, Xavier RJ. How does genotype influence disease phenotype in inflammatory bowel disease? Inflamm Bowel Dis. 2013;19(9):2021-30.
103. Abreu MT, Taylor KD, Lin YC, et al. Mutations in NOD2 are associated with fibrostenosing disease in patients with Crohn's disease. Gastroenterology. 2002;123(3):679-88.
104. Adler J, Rangwalla SC, Dwamena BA, et al. The prognostic power of the NOD2 genotype for complicated Crohn's disease: a meta-analysis. Am J Gastroenterol. 2011;106(4):699-712.
105. Annese V, Lombardi G, Perri F, et al. Variants of CARD15 are associated with an aggressive clinical course of Crohn's disease--an IG-IBD study. Am J Gastroenterol. 2005;100(1):84-92.
106. Fowler EV, Doecke J, Simms LA, et al. ATG16L1 T300A shows strong associations with disease subgroups in a large Australian IBD population: further support for significant disease heterogeneity. Am J Gastroenterol. 2008;103(10):2519-26.
107. Cleynen I, Gonzalez JR, Figueroa C, et al. Genetic factors conferring an increased susceptibility to develop Crohn's disease also influence disease phenotype: results from the IBDchip European Project. Gut. 2013;62(11):1556-65.
108. Henckaerts L, Van Steen K, Verstreken I, et al. Genetic risk profiling and prediction of disease course in Crohn's disease patients. Clin Gastroenterol Hepatol. 2009;7(9):972-80.e2.
109. Dubinsky MC, Kugathasan S, Kwon S, et al. Multidimensional prognostic risk assessment identifies association between IL12B variation and surgery in Crohn's disease. Inflamm Bowel Dis. 2013;19(8):1662-70.
110. Chibnik LB, Keenan BT, Cui J, et al. Genetic risk score predicting risk of rheumatoid arthritis phenotypes and age of symptom onset. PLoS One. 2011;6(9):e24380.
111. Karlson EW, Ding B, Keenan BT, et al. Association of environmental and genetic factors and gene-environment interactions with risk of developing rheumatoid arthritis. Arthritis Care Res (Hoboken). 2013;65(7):1147-56.
112. Reinisch W, Reinink AR, Higgins PD. Factors associated with poor outcomes in adults with newly diagnosed ulcerative colitis. Clin Gastroenterol Hepatol. 2015;13(4):635-42.
113. Solberg IC, Lygren I, Jahnsen J, et al. Clinical course during the first 10 years of ulcerative colitis: results from a population-based inception cohort (IBSEN Study). Scand J Gastroenterol. 2009;44(4):431-40.
114. Henriksen M, Jahnsen J, Lygren I, et al. C-reactive protein: a predictive factor and marker of inflammation in inflammatory bowel disease. Results from a prospective population-based study. Gut. 2008;57(11):1518-23.

115. Ho GT, Mowat C, Goddard CJ, et al. Predicting the outcome of severe ulcerative colitis: development of a novel risk score to aid early selection of patients for second-line medical therapy or surgery. Aliment Pharmacol Ther. 2004;19(10):1079-87.
116. Ho GT, Lee HM, Brydon G, et al. Fecal calprotectin predicts the clinical course of acute severe ulcerative colitis. Am J Gastroenterol. 2009;104(3):673-8.
117. Cesarini MC, G.; Ronnblom, A.; Santos, A.; Sjoberg, D.; Parkes, M.; Keshav, S.; Travis, SPL. P079. Predicting the risk of acute severe colitis (ASC) at diagnosis of Ulcerative Colitis (UC): external validation. J Crohns Colitis. 2015;9 Suppl 1:S117-8.
118. Travis SP, Farrant JM, Ricketts C, et al. Predicting outcome in severe ulcerative colitis. Gut. 1996;38(6):905-10.
119. Boyko EJ, Perera DR, Koepsell TD, et al. Effects of cigarette smoking on the clinical course of ulcerative colitis. Scand J Gastroenterol. 1988;23(9):1147-52.
120. Froslie KF, Jahnsen J, Moum BA, et al. Mucosal healing in inflammatory bowel disease: results from a Norwegian population-based cohort. Gastroenterology. 2007;133(2):412-22.
121. Ryan JD, Silverberg MS, Xu W, et al. Predicting complicated Crohn's disease and surgery: phenotypes, genetics, serology and psychological characteristics of a population-based cohort. Aliment Pharmacol Ther. 2013;38(3):274-83.
122. Annese V, Piepoli A, Latiano A, et al. HLA-DRB1 alleles may influence disease phenotype in patients with inflammatory bowel disease: a critical reappraisal with review of the literature. Dis Colon Rectum. 2005;48(1):57-64; discussion -5.
123. Roussomoustakaki M, Satsangi J, Welsh K, et al. Genetic markers may predict disease behavior in patients with ulcerative colitis. Gastroenterology. 1997;112(6):1845-53.
124. Ho GT, Nimmo ER, Tenesa A, et al. Allelic variations of the multidrug resistance gene determine susceptibility and disease behavior in ulcerative colitis. Gastroenterology. 2005;128(2):288-96.
125. Mansfield JC, Holden H, Tarlow JK, et al. Novel genetic association between ulcerative colitis and the anti-inflammatory cytokine interleukin-1 receptor antagonist. Gastroenterology. 1994;106(3):637-42.
126. Iliev ID, Funari VA, Taylor KD, et al. Interactions between commensal fungi and the C-type lectin receptor Dectin-1 influence colitis. Science. 2012;336(6086):1314-7.
127. Radford-Smith GD, J.D.; Lees,C.W.; McGovern, D.P.; Vermeire, S.; International IBD Genetics Consortium, et al Clinical and Molecular Characterization of Medically Refractory Acute, Severe Colitis: Preliminary Results From the International Inflammatory Bowel Disease Genetics Consortium (IIBDGC) Immunochip Study. Gastroenterology. 2013;144:S470.
128. Ho GT, Soranzo N, Nimmo ER, et al. ABCB1/MDR1 gene determines susceptibility and phenotype in ulcerative colitis: discrimination of critical variants using a gene-wide haplotype tagging approach. Hum Mol Genet. 2006;15(5):797-805.
129. Cortes A, Brown MA. Promise and pitfalls of the Immunochip. Arthritis Res Ther. 2011;13(1):101.
130. Trynka G, Hunt KA, Bockett NA, et al. Dense genotyping identifies and localizes multiple common and rare variant association signals in celiac disease. Nat Genet. 2011;43(12):1193-201.
131. Abecasis GR, Altshuler D, Auton A, et al. A map of human genome variation from population-scale sequencing. Nature. 2010;467(7319):1061-73.
132. Shah TS, Liu JZ, Floyd JA, et al. optiCall: a robust genotype-calling algorithm for rare, low-frequency and common variants. Bioinformatics. 2012;28(12):1598-603.

133. Teo YY, Inouye M, Small KS, et al. A genotype calling algorithm for the Illumina BeadArray platform. Bioinformatics. 2007;23(20):2741-6.
134. Lang R, Patel D, Morris JJ, et al. Shaping gene expression in activated and resting primary macrophages by IL-10. J Immunol. 2002;169(5):2253-63.
135. Travis S, Satsangi J, Lemann M. Predicting the need for colectomy in severe ulcerative colitis: a critical appraisal of clinical parameters and currently available biomarkers. Gut. 2011;60(1):3-9.
136. Chen P, Takeuchi F, Lee JY, et al. Multiple nonglycemic genomic loci are newly associated with blood level of glycated hemoglobin in East Asians. Diabetes. 2014;63(7):2551-62.
137. Quaranta M, Burden AD, Griffiths CE, et al. Differential contribution of CDKAL1 variants to psoriasis, Crohn's disease and type II diabetes. Genes Immun. 2009;10(7):654-8.
138. Kole A, Maloy KJ. Control of intestinal inflammation by interleukin-10. Curr Top Microbiol Immunol. 2014;380:19-38.
139. Kuhn R, Lohler J, Rennick D, et al. Interleukin-10-deficient mice develop chronic enterocolitis. Cell. 1993;75(2):263-74.
140. Asano K, Esaki M, Umeno J, et al. Contribution of susceptibility variants at FCGR2A and 13q12 to the risk of relapse among Japanese patients with ulcerative colitis. J Gastroenterol. 2015.
141. Kobayashi T, Steinbach EC, Russo SM, et al. NFIL3-deficient mice develop microbiota-dependent, IL-12/23-driven spontaneous colitis. J Immunol. 2014;192(4):1918-27.
142. Geiger TL, Abt MC, Gasteiger G, et al. Nfil3 is crucial for development of innate lymphoid cells and host protection against intestinal pathogens. J Exp Med. 2014;211(9):1723-31.
143. Seillet C, Rankin LC, Groom JR, et al. Nfil3 is required for the development of all innate lymphoid cell subsets. J Exp Med. 2014;211(9):1733-40.
144. Hedrich CM, Bream JH. Cell type-specific regulation of IL-10 expression in inflammation and disease. Immunol Res. 2010;47(1-3):185-206.
145. Murai M, Turovskaya O, Kim G, et al. Interleukin 10 acts on regulatory T cells to maintain expression of the transcription factor Foxp3 and suppressive function in mice with colitis. Nat Immunol. 2009;10(11):1178-84.
146. Asseman C, Mauze S, Leach MW, et al. An essential role for interleukin 10 in the function of regulatory T cells that inhibit intestinal inflammation. J Exp Med. 1999;190(7):995-1004.
147. Asseman C, Powrie F. Interleukin 10 is a growth factor for a population of regulatory T cells. Gut. 1998;42(2):157-8.
148. Kamada N, Hisamatsu T, Okamoto S, et al. Abnormally differentiated subsets of intestinal macrophage play a key role in Th1-dominant chronic colitis through excess production of IL-12 and IL-23 in response to bacteria. J Immunol. 2005;175(10):6900-8.
149. Smallie T, Ricchetti G, Horwood NJ, et al. IL-10 inhibits transcription elongation of the human TNF gene in primary macrophages. J Exp Med. 2010;207(10):2081-8.
150. Uhlig HH, Powrie F. Mouse models of intestinal inflammation as tools to understand the pathogenesis of inflammatory bowel disease. Eur J Immunol. 2009;39(8):2021-6.

151. Engelhardt KR, Shah N, Faizura-Yeop I, et al. Clinical outcome in IL-10- and IL-10 receptor-deficient patients with or without hematopoietic stem cell transplantation. J Allergy Clin Immunol. 2013;131(3):825-30.
152. Juyal G, Prasad P, Senapati S, et al. An investigation of genome-wide studies reported susceptibility loci for ulcerative colitis shows limited replication in north Indians. PLoS One. 2011;6(1):e16565.
153. Sakurai D, Zhao J, Deng Y, et al. Preferential binding to Elk-1 by SLE-associated IL10 risk allele upregulates IL10 expression. PLoS Genet. 2013;9(10):e1003870.
154. Andersen V, Ernst A, Christensen J, et al. The polymorphism rs3024505 proximal to IL-10 is associated with risk of ulcerative colitis and Crohns disease in a Danish case-control study. BMC Med Genet. 2010;11:82.
155. Wang AH, Lam WJ, Han DY, et al. The effect of IL-10 genetic variation and interleukin 10 serum levels on Crohn's disease susceptibility in a New Zealand population. Hum Immunol. 2011;72(5):431-5.
156. Rada B, Leto TL. Oxidative innate immune defenses by Nox/Duox family NADPH oxidases. Contrib Microbiol. 2008;15:164-87.
157. Bedard K, Krause KH. The NOX family of ROS-generating NADPH oxidases: physiology and pathophysiology. Physiol Rev. 2007;87(1):245-313.
158. Lambeth JD. NOX enzymes and the biology of reactive oxygen. Nat Rev Immunol. 2004;4(3):181-9.
159. Csordas A, Bernhard D. The biology behind the atherothrombotic effects of cigarette smoke. Nat Rev Cardiol. 2013;10(4):219-30.
160. Shiraiwa M, Selzle K, Poschl U. Hazardous components and health effects of atmospheric aerosol particles: reactive oxygen species, soot, polycyclic aromatic compounds and allergenic proteins. Free Radic Res. 2012;46(8):927-39.
161. Kim JH, Jenrow KA, Brown SL. Mechanisms of radiation-induced normal tissue toxicity and implications for future clinical trials. Radiat Oncol J. 2014;32(3):103-15.
162. Nathan C, Cunningham-Bussel A. Beyond oxidative stress: an immunologist's guide to reactive oxygen species. Nat Rev Immunol. 2013;13(5):349-61.
163. Aguirre J, Lambeth JD. Nox enzymes from fungus to fly to fish and what they tell us about Nox function in mammals. Free Radic Biol Med. 2010;49(9):1342-53.
164. Cheng G, Cao Z, Xu X, et al. Homologs of gp91phox: cloning and tissue expression of Nox3, Nox4, and Nox5. Gene. 2001;269(1-2):131-40.
165. Nauseef WM. Assembly of the phagocyte NADPH oxidase. Histochem Cell Biol. 2004;122(4):277-91.
166. Banfi B, Tirone F, Durussel I, et al. Mechanism of Ca2+ activation of the NADPH oxidase 5 (NOX5). J Biol Chem. 2004;279(18):18583-91.
167. Suh YA, Arnold RS, Lassegue B, et al. Cell transformation by the superoxide-generating oxidase Mox1. Nature. 1999;401(6748):79-82.
168. Szanto I, Rubbia-Brandt L, Kiss P, et al. Expression of NOX1, a superoxide-generating NADPH oxidase, in colon cancer and inflammatory bowel disease. J Pathol. 2005;207(2):164-76.
169. Banfi B, Malgrange B, Knisz J, et al. NOX3, a superoxide-generating NADPH oxidase of the inner ear. J Biol Chem. 2004;279(44):46065-72.
170. Paffenholz R, Bergstrom RA, Pasutto F, et al. Vestibular defects in head-tilt mice result from mutations in Nox3, encoding an NADPH oxidase. Genes Dev. 2004;18(5):486-91.
171. Geiszt M, Kopp JB, Varnai P, et al. Identification of renox, an NAD(P)H oxidase in kidney. Proc Natl Acad Sci U S A. 2000;97(14):8010-4.

172. Ha JS, Lee JE, Lee JR, et al. Nox4-dependent H2O2 production contributes to chronic glutamate toxicity in primary cortical neurons. Exp Cell Res. 2010;316(10):1651-61.
173. Banfi B, Molnar G, Maturana A, et al. A Ca(2+)-activated NADPH oxidase in testis, spleen, and lymph nodes. J Biol Chem. 2001;276(40):37594-601.
174. Dupuy C, Virion A, Ohayon R, et al. Mechanism of hydrogen peroxide formation catalyzed by NADPH oxidase in thyroid plasma membrane. J Biol Chem. 1991;266(6):3739-43.
175. Moskwa P, Lorentzen D, Excoffon KJ, et al. A novel host defense system of airways is defective in cystic fibrosis. Am J Respir Crit Care Med. 2007;175(2):174-83.
176. Grasberger H, El-Zaatari M, Dang DT, et al. Dual oxidases control release of hydrogen peroxide by the gastric epithelium to prevent Helicobacter felis infection and inflammation in mice. Gastroenterology. 2013;145(5):1045-54.
177. Segal AW. How neutrophils kill microbes. Annu Rev Immunol. 2005;23:197-223.
178. Lekstrom-Himes JA, Kuhns DB, Alvord WG, et al. Inhibition of human neutrophil IL-8 production by hydrogen peroxide and dysregulation in chronic granulomatous disease. J Immunol. 2005;174(1):411-7.
179. Kumar A, Wu H, Collier-Hyams LS, et al. Commensal bacteria modulate cullin-dependent signaling via generation of reactive oxygen species. Embo j. 2007;26(21):4457-66.
180. Hempel N, Melendez JA. Intracellular redox status controls membrane localization of pro- and anti-migratory signaling molecules. Redox Biol. 2014;2:245-50.
181. Hurd TR, DeGennaro M, Lehmann R. Redox regulation of cell migration and adhesion. Trends Cell Biol. 2012;22(2):107-15.
182. Leoni G, Alam A, Neumann PA, et al. Annexin A1, formyl peptide receptor, and NOX1 orchestrate epithelial repair. J Clin Invest. 2013;123(1):443-54.
183. Kamata H, Honda S, Maeda S, et al. Reactive oxygen species promote TNFalpha-induced death and sustained JNK activation by inhibiting MAP kinase phosphatases. Cell. 2005;120(5):649-61.
184. Wentworth CC, Alam A, Jones RM, et al. Enteric commensal bacteria induce extracellular signal-regulated kinase pathway signaling via formyl peptide receptor-dependent redox modulation of dual specific phosphatase 3. J Biol Chem. 2011;286(44):38448-55.
185. Burdon RH. Superoxide and hydrogen peroxide in relation to mammalian cell proliferation. Free Radic Biol Med. 1995;18(4):775-94.
186. Kamata T. Roles of Nox1 and other Nox isoforms in cancer development. Cancer Sci. 2009;100(8):1382-8.
187. Lim SD, Sun C, Lambeth JD, et al. Increased Nox1 and hydrogen peroxide in prostate cancer. Prostate. 2005;62(2):200-7.
188. Donato AJ, Morgan RG, Walker AE, et al. Cellular and molecular biology of aging endothelial cells. J Mol Cell Cardiol. 2015.
189. Colavitti R, Finkel T. Reactive oxygen species as mediators of cellular senescence. IUBMB Life. 2005;57(4-5):277-81.
190. Sumimoto H, Hata K, Mizuki K, et al. Assembly and activation of the phagocyte NADPH oxidase. Specific interaction of the N-terminal Src homology 3 domain of p47phox with p22phox is required for activation of the NADPH oxidase. J Biol Chem. 1996;271(36):22152-8.

191. Han CH, Freeman JL, Lee T, et al. Regulation of the neutrophil respiratory burst oxidase. Identification of an activation domain in p67(phox). J Biol Chem. 1998;273(27):16663-8.
192. Diebold BA, Bokoch GM. Molecular basis for Rac2 regulation of phagocyte NADPH oxidase. Nat Immunol. 2001;2(3):211-5.
193. Babior BM, Lambeth JD, Nauseef W. The neutrophil NADPH oxidase. Arch Biochem Biophys. 2002;397(2):342-4.
194. Klebanoff SJ, Kettle AJ, Rosen H, et al. Myeloperoxidase: a front-line defender against phagocytosed microorganisms. J Leukoc Biol. 2013;93(2):185-98.
195. Reeves EP, Lu H, Jacobs HL, et al. Killing activity of neutrophils is mediated through activation of proteases by K+ flux. Nature. 2002;416(6878):291-7.
196. Nauseef WM. Biological roles for the NOX family NADPH oxidases. J Biol Chem. 2008;283(25):16961-5.
197. Marks DJ, Miyagi K, Rahman FZ, et al. Inflammatory bowel disease in CGD reproduces the clinicopathological features of Crohn's disease. Am J Gastroenterol. 2009;104(1):117-24.
198. Parkos CA, Allen RA, Cochrane CG, et al. Purified cytochrome b from human granulocyte plasma membrane is comprised of two polypeptides with relative molecular weights of 91,000 and 22,000. J Clin Invest. 1987;80(3):732-42.
199. Parkos CA, Dinauer MC, Jesaitis AJ, et al. Absence of both the 91kD and 22kD subunits of human neutrophil cytochrome b in two genetic forms of chronic granulomatous disease. Blood. 1989;73(6):1416-20.
200. Berendes H, Bridges RA, Good RA. A fatal granulomatosus of childhood: the clinical study of a new syndrome. Minn Med. 1957;40(5):309-12.
201. Huang J, Brumell JH. NADPH oxidases contribute to autophagy regulation. Autophagy. 2009;5(6):887-9.
202. Meissner F, Seger RA, Moshous D, et al. Inflammasome activation in NADPH oxidase defective mononuclear phagocytes from patients with chronic granulomatous disease. Blood. 2010;116(9):1570-3.
203. Banfi B, Maturana A, Jaconi S, et al. A mammalian H+ channel generated through alternative splicing of the NADPH oxidase homolog NOH-1. Science. 2000;287(5450):138-42.
204. Banfi B, Clark RA, Steger K, et al. Two novel proteins activate superoxide generation by the NADPH oxidase NOX1. J Biol Chem. 2003;278(6):3510-3.
205. Cheng G, Lambeth JD. NOXO1, regulation of lipid binding, localization, and activation of Nox1 by the Phox homology (PX) domain. J Biol Chem. 2004;279(6):4737-42.
206. Cheng G, Diebold BA, Hughes Y, et al. Nox1-dependent reactive oxygen generation is regulated by Rac1. J Biol Chem. 2006;281(26):17718-26.
207. Ambasta RK, Kumar P, Griendling KK, et al. Direct interaction of the novel Nox proteins with p22phox is required for the formation of a functionally active NADPH oxidase. J Biol Chem. 2004;279(44):45935-41.
208. Chamulitrat W, Schmidt R, Tomakidi P, et al. Association of gp91phox homolog Nox1 with anchorage-independent growth and MAP kinase-activation of transformed human keratinocytes. Oncogene. 2003;22(38):6045-53.
209. Janiszewski M, Lopes LR, Carmo AO, et al. Regulation of NAD(P)H oxidase by associated protein disulfide isomerase in vascular smooth muscle cells. J Biol Chem. 2005;280(49):40813-9.
210. Oshitani N, Kitano A, Okabe H, et al. Location of superoxide anion generation in human colonic mucosa obtained by biopsy. Gut. 1993;34(7):936-8.

211. Glebov OK, Rodriguez LM, Nakahara K, et al. Distinguishing right from left colon by the pattern of gene expression. Cancer Epidemiol Biomarkers Prev. 2003;12(8):755-62.
212. Laurent E, McCoy JW, 3rd, Macina RA, et al. Nox1 is over-expressed in human colon cancers and correlates with activating mutations in K-Ras. Int J Cancer. 2008;123(1):100-7.
213. Kobayashi S, Nojima Y, Shibuya M, et al. Nox1 regulates apoptosis and potentially stimulates branching morphogenesis in sinusoidal endothelial cells. Exp Cell Res. 2004;300(2):455-62.
214. Konior A, Schramm A, Czesnikiewicz-Guzik M, et al. NADPH oxidases in vascular pathology. Antioxid Redox Signal. 2014;20(17):2794-814.
215. Cui XL, Brockman D, Campos B, et al. Expression of NADPH oxidase isoform 1 (Nox1) in human placenta: involvement in preeclampsia. Placenta. 2006;27(4-5):422-31.
216. Manea A, Raicu M, Simionescu M. Expression of functionally phagocyte-type NAD(P)H oxidase in pericytes: effect of angiotensin II and high glucose. Biol Cell. 2005;97(9):723-34.
217. Choi DH, Kim JH, Lee KH, et al. Role of neuronal NADPH oxidase 1 in the peri-infarct regions after stroke. PLoS One. 2015;10(1):e0116814.
218. Jones RM, Luo L, Ardita CS, et al. Symbiotic lactobacilli stimulate gut epithelial proliferation via Nox-mediated generation of reactive oxygen species. EMBO J. 2013;32(23):3017-28.
219. Babbin BA, Jesaitis AJ, Ivanov AI, et al. Formyl peptide receptor-1 activation enhances intestinal epithelial cell restitution through phosphatidylinositol 3-kinase-dependent activation of Rac1 and Cdc42. J Immunol. 2007;179(12):8112-21.
220. Babbin BA, Laukoetter MG, Nava P, et al. Annexin A1 regulates intestinal mucosal injury, inflammation, and repair. J Immunol. 2008;181(7):5035-44.
221. Patel KK, Miyoshi H, Beatty WL, et al. Autophagy proteins control goblet cell function by potentiating reactive oxygen species production. EMBO J. 2013;32(24):3130-44.
222. Coant N, Ben Mkaddem S, Pedruzzi E, et al. NADPH oxidase 1 modulates WNT and NOTCH1 signaling to control the fate of proliferative progenitor cells in the colon. Mol Cell Biol. 2010;30(11):2636-50.
223. Treton X, Pedruzzi E, Guichard C, et al. Combined NADPH oxidase 1 and interleukin 10 deficiency induces chronic endoplasmic reticulum stress and causes ulcerative colitis-like disease in mice. PLoS One. 2014;9(7):e101669.
224. Mouzaoui S, Djerdjouri B, Makhezer N, et al. Tumor necrosis factor-alpha-induced colitis increases NADPH oxidase 1 expression, oxidative stress, and neutrophil recruitment in the colon: preventive effect of apocynin. Mediators Inflamm. 2014;2014:312484.
225. Kuwano Y, Kawahara T, Yamamoto H, et al. Interferon-gamma activates transcription of NADPH oxidase 1 gene and upregulates production of superoxide anion by human large intestinal epithelial cells. Am J Physiol Cell Physiol. 2006;290(2):C433-43.
226. Kuwano Y, Tominaga K, Kawahara T, et al. Tumor necrosis factor alpha activates transcription of the NADPH oxidase organizer 1 (NOXO1) gene and upregulates superoxide production in colon epithelial cells. Free Radic Biol Med. 2008;45(12):1642-52.

227. Geiszt M, Lekstrom K, Brenner S, et al. NAD(P)H oxidase 1, a product of differentiated colon epithelial cells, can partially replace glycoprotein 91phox in the regulated production of superoxide by phagocytes. J Immunol. 2003;171(1):299-306.
228. Rokutan K, Kawahara T, Kuwano Y, et al. Nox enzymes and oxidative stress in the immunopathology of the gastrointestinal tract. Semin Immunopathol. 2008;30(3):315-27.
229. Kajla S, Mondol AS, Nagasawa A, et al. A crucial role for Nox 1 in redox-dependent regulation of Wnt-beta-catenin signaling. Faseb j. 2012;26(5):2049-59.
230. Kawahara T, Kuwano Y, Teshima-Kondo S, et al. Role of nicotinamide adenine dinucleotide phosphate oxidase 1 in oxidative burst response to Toll-like receptor 5 signaling in large intestinal epithelial cells. J Immunol. 2004;172(5):3051-8.
231. Alam A, Leoni G, Wentworth CC, et al. Redox signaling regulates commensal-mediated mucosal homeostasis and restitution and requires formyl peptide receptor 1. Mucosal Immunol. 2014;7(3):645-55.
232. Swanson PA, 2nd, Kumar A, Samarin S, et al. Enteric commensal bacteria potentiate epithelial restitution via reactive oxygen species-mediated inactivation of focal adhesion kinase phosphatases. Proc Natl Acad Sci U S A. 2011;108(21):8803-8.
233. Sadok A, Bourgarel-Rey V, Gattacceca F, et al. Nox1-dependent superoxide production controls colon adenocarcinoma cell migration. Biochim Biophys Acta. 2008;1783(1):23-33.
234. Perner A, Andresen L, Pedersen G, et al. Superoxide production and expression of NAD(P)H oxidases by transformed and primary human colonic epithelial cells. Gut. 2003;52(2):231-6.
235. El Hassani RA, Benfares N, Caillou B, et al. Dual oxidase2 is expressed all along the digestive tract. Am J Physiol Gastrointest Liver Physiol. 2005;288(5):G933-42.
236. Ha EM, Oh CT, Bae YS, et al. A direct role for dual oxidase in Drosophila gut immunity. Science. 2005;310(5749):847-50.
237. Gerson C, Sabater J, Scuri M, et al. The lactoperoxidase system functions in bacterial clearance of airways. Am J Respir Cell Mol Biol. 2000;22(6):665-71.
238. Haberman Y, Tickle TL, Dexheimer PJ, et al. Pediatric Crohn disease patients exhibit specific ileal transcriptome and microbiome signature. J Clin Invest. 2014;124(8):3617-33.
239. Lipinski S, Till A, Sina C, et al. DUOX2-derived reactive oxygen species are effectors of NOD2-mediated antibacterial responses. J Cell Sci. 2009;122(Pt 19):3522-30.
240. Maghzal GJ, Krause KH, Stocker R, et al. Detection of reactive oxygen species derived from the family of NOX NADPH oxidases. Free Radic Biol Med. 2012;53(10):1903-18.
241. Altenhofer S, Kleikers PW, Radermacher KA, et al. The NOX toolbox: validating the role of NADPH oxidases in physiology and disease. Cell Mol Life Sci. 2012;69(14):2327-43.
242. Nishinaka Y, Aramaki Y, Yoshida H, et al. A new sensitive chemiluminescence probe, L-012, for measuring the production of superoxide anion by cells. Biochem Biophys Res Commun. 1993;193(2):554-9.
243. Zielonka J, Lambeth JD, Kalyanaraman B. On the use of L-012, a luminol-based chemiluminescent probe, for detecting superoxide and identifying inhibitors of NADPH oxidase: a reevaluation. Free Radic Biol Med. 2013;65:1310-4.
244. Oberley LW, Spitz DR. Assay of superoxide dismutase activity in tumor tissue. Methods Enzymol. 1984;105:457-64.

245. Baehner RL, Nathan DG. Quantitative nitroblue tetrazolium test in chronic granulomatous disease. N Engl J Med. 1968;278(18):971-6.
246. Wardman P. Fluorescent and luminescent probes for measurement of oxidative and nitrosative species in cells and tissues: progress, pitfalls, and prospects. Free Radic Biol Med. 2007;43(7):995-1022.
247. Spitz DR, Oberley LW. An assay for superoxide dismutase activity in mammalian tissue homogenates. Anal Biochem. 1989;179(1):8-18.
248. Holland PC, Clark MG, Bloxham DP, et al. Mechanism of action of the hypoglycemic agent diphenyleneiodonium. J Biol Chem. 1973;248(17):6050-6.
249. Li Y, Trush MA. Diphenyleneiodonium, an NAD(P)H oxidase inhibitor, also potently inhibits mitochondrial reactive oxygen species production. Biochem Biophys Res Commun. 1998;253(2):295-9.
250. Wind S, Beuerlein K, Eucker T, et al. Comparative pharmacology of chemically distinct NADPH oxidase inhibitors. Br J Pharmacol. 2010;161(4):885-98.
251. Drummond GR, Selemidis S, Griendling KK, et al. Combating oxidative stress in vascular disease: NADPH oxidases as therapeutic targets. Nat Rev Drug Discov. 2011;10(6):453-71.
252. Tazzeo T, Worek F, Janssen L. The NADPH oxidase inhibitor diphenyleneiodonium is also a potent inhibitor of cholinesterases and the internal Ca(2+) pump. Br J Pharmacol. 2009;158(3):790-6.
253. Gao Y, Dickerson JB, Guo F, et al. Rational design and characterization of a Rac GTPase-specific small molecule inhibitor. Proc Natl Acad Sci U S A. 2004;101(20):7618-23.
254. Gianni D, Taulet N, Zhang H, et al. A novel and specific NADPH oxidase-1 (Nox1) small-molecule inhibitor blocks the formation of functional invadopodia in human colon cancer cells. ACS Chem Biol. 2010;5(10):981-93.
255. Takeya R, Ueno N, Kami K, et al. Novel human homologues of p47phox and p67phox participate in activation of superoxide-producing NADPH oxidases. J Biol Chem. 2003;278(27):25234-46.
256. Yamamoto A, Takeya R, Matsumoto M, et al. Phosphorylation of Noxo1 at threonine 341 regulates its interaction with Noxa1 and the superoxide-producing activity of Nox1. Febs j. 2013;280(20):5145-59.
257. Jones RM, Mercante JW, Neish AS. Reactive oxygen production induced by the gut microbiota: pharmacotherapeutic implications. Curr Med Chem. 2012;19(10):1519-29.
258. von Kleist S, Chany E, Burtin P, et al. Immunohistology of the antigenic pattern of a continuous cell line from a human colon tumor. J Natl Cancer Inst. 1975;55(3):555-60.
259. Gianni D, Bohl B, Courtneidge SA, et al. The involvement of the tyrosine kinase c-Src in the regulation of reactive oxygen species generation mediated by NADPH oxidase-1. Mol Biol Cell. 2008;19(7):2984-94.
260. Geiszt M, Lekstrom K, Witta J, et al. Proteins homologous to p47phox and p67phox support superoxide production by NAD(P)H oxidase 1 in colon epithelial cells. J Biol Chem. 2003;278(22):20006-12.
261. The WGS500 Project. Assessing the clinical utility of whole genome sequencing from 156 cases with diverse disorders. . Nature Genetics. 2015;In press.
262. Sato T, Vries RG, Snippert HJ, et al. Single Lgr5 stem cells build crypt-villus structures in vitro without a mesenchymal niche. Nature. 2009;459(7244):262-5.
263. Barker N, van Es JH, Kuipers J, et al. Identification of stem cells in small intestine and colon by marker gene Lgr5. Nature. 2007;449(7165):1003-7.

264. Livak KJ, Schmittgen TD. Analysis of relative gene expression data using real-time quantitative PCR and the 2(-Delta Delta C(T)) Method. Methods. 2001;25(4):402-8.
265. Berridge MV, Herst PM, Tan AS. Tetrazolium dyes as tools in cell biology: new insights into their cellular reduction. Biotechnol Annu Rev. 2005;11:127-52.
266. Zambon AC. Use of the Ki67 promoter to label cell cycle entry in living cells. Cytometry A. 2010;77(6):564-70.
267. Tang LH, Gonen M, Hedvat C, et al. Objective quantification of the Ki67 proliferative index in neuroendocrine tumors of the gastroenteropancreatic system: a comparison of digital image analysis with manual methods. Am J Surg Pathol. 2012;36(12):1761-70.
268. Halliwell B. Cell culture, oxidative stress, and antioxidants: avoiding pitfalls. Biomed J. 2014;37(3):99-105.
269. Matxain JM, Padro D, Ristila M, et al. Evidence of high *OH radical quenching efficiency by vitamin B6. J Phys Chem B. 2009;113(29):9629-32.
270. Mahfouz MM, Zhou SQ, Kummerow FA. Vitamin B6 compounds are capable of reducing the superoxide radical and lipid peroxide levels induced by H2O2 in vascular endothelial cells in culture. Int J Vitam Nutr Res. 2009;79(4):218-29.
271. Salles N, Szanto I, Herrmann F, et al. Expression of mRNA for ROS-generating NADPH oxidases in the aging stomach. Exp Gerontol. 2005;40(4):353-7.
272. Tiede I, Fritz G, Strand S, et al. CD28-dependent Rac1 activation is the molecular target of azathioprine in primary human CD4+ T lymphocytes. J Clin Invest. 2003;111(8):1133-45.
273. Casanova JL, Conley ME, Seligman SJ, et al. Guidelines for genetic studies in single patients: lessons from primary immunodeficiencies. J Exp Med. 2014;211(11):2137-49.
274. MacArthur DG, Manolio TA, Dimmock DP, et al. Guidelines for investigating causality of sequence variants in human disease. Nature. 2014;508(7497):469-76.
275. Casanova JL, Abel L. The human model: a genetic dissection of immunity to infection in natural conditions. Nat Rev Immunol. 2004;4(1):55-66.
276. Quintana-Murci L, Alcais A, Abel L, et al. Immunology in natura: clinical, epidemiological and evolutionary genetics of infectious diseases. Nat Immunol. 2007;8(11):1165-71.
277. Heyman MB, Kirschner BS, Gold BD, et al. Children with early-onset inflammatory bowel disease (IBD): analysis of a pediatric IBD consortium registry. J Pediatr. 2005;146(1):35-40.
278. Tennessen JA, Bigham AW, O'Connor TD, et al. Evolution and functional impact of rare coding variation from deep sequencing of human exomes. Science. 2012;337(6090):64-9.
279. Huet C, Sahuquillo-Merino C, Coudrier E, et al. Absorptive and mucus-secreting subclones isolated from a multipotent intestinal cell line (HT-29) provide new models for cell polarity and terminal differentiation. J Cell Biol. 1987;105(1):345-57.
280. Phillips TE, Huet C, Bilbo PR, et al. Human intestinal goblet cells in monolayer culture: characterization of a mucus-secreting subclone derived from the HT29 colon adenocarcinoma cell line. Gastroenterology. 1988;94(6):1390-403.
281. Charpentier E, Marraffini LA. Harnessing CRISPR-Cas9 immunity for genetic engineering. Curr Opin Microbiol. 2014;19:114-9.
282. Marraffini LA, Sontheimer EJ. CRISPR interference: RNA-directed adaptive immunity in bacteria and archaea. Nat Rev Genet. 2010;11(3):181-90.

283. Wiedenheft B, Sternberg SH, Doudna JA. RNA-guided genetic silencing systems in bacteria and archaea. Nature. 2012;482(7385):331-8.
284. Fedorak RN, Gangl A, Elson CO, et al. Recombinant human interleukin 10 in the treatment of patients with mild to moderately active Crohn's disease. The Interleukin 10 Inflammatory Bowel Disease Cooperative Study Group. Gastroenterology. 2000;119(6):1473-82.
285. Gibson DJ, Heetun ZS, Redmond CE, et al. An accelerated infliximab induction regimen reduces the need for early colectomy in patients with acute severe ulcerative colitis. Clin Gastroenterol Hepatol. 2015;13(2):330-5.e1.
286. Sandborn WJ, Feagan BG, Fedorak RN, et al. A randomized trial of Ustekinumab, a human interleukin-12/23 monoclonal antibody, in patients with moderate-to-severe Crohn's disease. Gastroenterology. 2008;135(4):1130-41.
287. Sandborn WJ, Gasink C, Gao LL, et al. Ustekinumab induction and maintenance therapy in refractory Crohn's disease. N Engl J Med. 2012;367(16):1519-28.
288. Amiot A, Peyrin-Biroulet L. Current, new and future biological agents on the horizon for the treatment of inflammatory bowel diseases. Therap Adv Gastroenterol. 2015;8(2):66-82.

APPENDIX A1. Phenotypic description of IBD Control 1 patient and non-inflamed control patient.

IBD Control 1 is a 24 year old male with a history of ileocolonic CD diagnosed at the age of 19 years old, who had previously undergone an ileocaecal resection. He was on no medications at the time of the procedure and the colonoscopy was performed for routine postoperative surveillance. Macroscopic colonoscopic findings were of mild ileal inflammation with erythema and several aphthous ulcers (Rutgeert's Score i1). There was no colonic inflammation evident. Biopsies of the ileum revealed mild to moderate inflammatory features consistent with a postoperative recurrence of CD. Colonic biopsies did not reveal active inflammation.

The non-inflamed control patient was a 55 year old female, who underwent a colonoscopy for abdominal symptoms consistent with irritable bowel syndrome. Colonoscopic features were normal, and histological analysis of colonic biopsy specimens was also normal. There were no other confounding medical comorbidities nor family history of gastrointestinal disorders.